About Editors:

Dr. Ranjan Kumar is currently Head of the Department and Associate Professor in the Department of Mechanical Engineering at Swami Vivekananda University, Kolkata. Dr. Kumar received his Master's and Doctoral degrees in Mechanical Engineering from the Indian Institute of Technology (ISM) Dhanbad. His research interests include Li-ion batteries, finite element simulation and analysis of real engineering problems, and vibration analysis of structures. He has executed projects in association with the Gas Turbine Research Establishment (GTRE), DRDO lab Bangalore. Dr. Kumar has authored four books, published 28 research papers, and holds 16 patents.

Mr. Abhishek Dhar, a dynamic academician and a prolific mentor, serves as an Assistant Professor, in the Department of Electrical Engineering and as well as holds the prestigious post of Joint Academic Co-ordinator of the esteemed institution Swami Vivekananda University. His research, published in 15 prestigious international journals and conference papers, focuses on efficient energy utilization, grid stability, IoT etc. He has in his golden feather 60 patents filed and published with his hard work and dedication. He fosters an inclusive learning environment, nurturing diverse talents. His dedication has earned his recognition, bridging academia and industry seamlessly.

Dr. Ashes Banerjee is an Assistant Professor in the Civil Engineering Dept. at Swami Vivekananda University, Kolkata, West Bengal. He earned his Ph.D. in Water Resource Engineering from the Indian Institute of Technology (Indian School of Mines) in Dhanbad, India, in 2020. Dr. Banerjee's scholarly achievements are evidenced by his numerous publications in peer-reviewed international journals, covering crucial topics such as non-linear filtration in porous media, water quality, and groundwater utilization.

Ms. Arunima Mahapatra is Assistant Professor in the Department of Electrical Engineering at Swami Vivekananda University, Barrackpore, West Bengal, India. She was awarded Gold Medal for securing first position in M.Tech. (Power System Engineering) by IIT (ISM), Dhanbad in 2020. She is currently pursuing her Ph.D. (Engineering) at IIT (ISM), Dhanbad. She has published several Journal Papers, Conference Papers and Book Chapters of International and National repute. Her research interests include Renewable Energy, Power System etc.

BlueRose ONE
Stories Matter
NewDelhi • London

INR 2100
ACADEMIC
9 789364 528603
www.BlueRoseOne.com

Frontiers of Engineering Innovation:
Interdisciplinary Approaches and Applications

Frontiers of Engineering Innovation:

Interdisciplinary Approaches and Applications

Dr. Ranjan Kumar,
Mr. Abhishek Dhar,
Dr. Ashes Banerjee,
Ms. Arunima Mahapatra

Frontiers of Engineering Innovation: Interdisciplinary Approaches and Applications

Editors:

Dr. Ranjan Kumar
Mr. Abhishek Dhar
Dr. Ashes Banerjee
Ms. Arunima Mahapatra

BlueRose ONE .com DIY
Stories Matter
NewDelhi • London

BLUEROSE PUBLISHERS
India | U.K.

For permissions requests or inquiries regarding this publication,
please contact:

BLUEROSE PUBLISHERS
www.BlueRoseONE.com
info@bluerosepublishers.com
+91 8882 898 898
+4407342408967

ISBN: 978-93-6452-860-3

First Edition: August 2024

PREFACE

Welcome to "Frontiers of Engineering Innovation: Interdisciplinary Approaches and Applications." In this dynamic era of rapid technological advancement and societal transformation, the boundaries between traditional engineering disciplines are becoming increasingly porous. The once distinct domains of mechanical, electrical, civil, and electronics engineering now converge with fields such as computer science, biology, materials science, chemical engineering and beyond, creating fertile ground for unprecedented innovation.

This book explores the exciting intersection where diverse disciplines intersect to push the frontiers of what is possible. Through a collection of insightful chapters authored by experts and pioneers in their respective fields, we delve into a multitude of interdisciplinary approaches and their transformative applications. From the integration of artificial intelligence in engineering to the synergy of nanotechnology and biotechnology, each chapter provides a glimpse into how collaboration across disciplines fosters groundbreaking solutions to complex challenges.

Engineers, researchers, students, and professionals alike will find inspiration in the diverse range of topics covered, each highlighting the power of interdisciplinary thinking to tackle pressing global issues. Whether you are intrigued by the promise of renewable energy systems, fascinated by the potential of biomimicry in design, or curious about the ethical implications of emerging technologies, this book offers a comprehensive exploration of the cutting-edge innovations shaping our world.

As editors, our goal is to illuminate the pathways where diverse strands of knowledge intertwine, catalyzing new insights and sparking collaborations that transcend traditional boundaries. We invite you to embark on this intellectual journey with us, where imagination meets rigor and innovation knows no limits. Together, let us venture into the frontiers of engineering innovation and chart a course towards a future defined by interdisciplinary excellence.

Dr. Ranjan Kumar
Associate Professor, Swami Vivekananda University,
Kolkata, West Bengal, India
Dated: 24, June, 2024

ACKNOWLEDGMENT

I extend my heartfelt gratitude to Swami Vivekananda University, Kolkata, India, for their steadfast support and encouragement throughout the creation of " Frontiers of Engineering Innovation: Interdisciplinary Approaches and Applications" The university's dedication to fostering education and research has been instrumental in shaping the content and direction of this publication. We deeply appreciate the collaborative spirit and resources provided by Swami Vivekananda University, Kolkata, which have enabled us to explore and share the latest innovations and technologies across various fields.

We hope that this book serves as a valuable resource for this esteemed institution and the broader academic community, reflecting our shared dedication to knowledge, progress, and the pursuit of excellence.

I extend my deepest appreciation to each of the external reviewers mentioned below for their unwavering commitment to excellence and their indispensable role in ensuring the scholarly merit of this work.

With sincere appreciation,

(Dr. Ranjan Kumar)
Associate Professor, Swami Vivekananda University,
Kolkata, West Bengal, India

CONTENTS

Chapter 1

Qualitative Observation of Helicity Distribution for Flow around Drag Type Vertical Axis Wind Turbine

Samrat Biswas[1*], Sayan Paul[1,] Suman Kumar Ghosh[1], Soumya Ghosh[1], Arijit Mukherjee[1,] Soumak Bose[1]

[1]Swami Vivekananda University, Barrackpore 700 121, INDIA
Corresponding author* Email ID: samratb@svu.ac.in

ABSTRACT

This paper introduces an exploratory investigation into the flow field around Savonius wind turbines. This particular turbine design stands out from conventional ones due to its unique ability to harness valuable energy from the air stream. It boasts straightforward construction, rapid startup, continuous operation, wind utilization from any direction, the potential to achieve higher angular velocities during operation, and minimal noise emissions. Additionally, it significantly reduces wear and tear on moving components, making it an attractive machinery option. Throughout history, various adaptations of this device have been envisioned, enhancing the versatility of vertical axis wind turbines. The primary objective of this study is to visually depict and attempt to comprehend the variation in helicity distribution around a vertical axis wind turbine (VAWT), specifically the Savonius-type wind turbine, operating under subsonic flow conditions.

Keywords: VAWT, Savonious Type Turbine, Wind Turbine

Introduction

In the pursuit of sustainable and renewable energy sources to meet the ever-expanding global energy demand and combat the adverse impacts of climate change, wind power has emerged as a leading contender. Traditional horizontal axis wind turbines (HAWTs) have maintained dominance in the wind energy sector for many decades. Nevertheless, the limitations associated with HAWTs, including their significant environmental footprint, intermittent energy production, and reliance on high wind speeds, have prompted the exploration of alternative wind energy solutions. Among these alternatives, vertical axis wind turbines (VAWTs) have emerged as a promising technology deserving of in-depth exploration and consideration.

The concept of VAWTs has roots dating back centuries, with early designs credited to Persian engineers and subsequent refinements by European inventors. Despite their historical origins, VAWTs have, until recently, remained somewhat overshadowed by their horizontal axis counterparts. However, recent advancements in materials, aerodynamics, and control systems have reignited interest in VAWTs, sparking a renewed focus on research and development efforts.

One notable subtype of VAWTs, the Savonius-type wind turbine, merits special attention. The Savonius rotor, named after its Finnish inventor Sigurd Johannes Savonius, is characterized by its simple and robust design. Unlike the more common Darrieus and Darrieus-like VAWTs, which rely on lift forces to generate power, Savonius turbines harness drag forces, making them particularly suitable for low wind speed environments. This unique design features two or more curved blades mounted on a vertical axis, resembling an "S" or "U" shape, and has been a focus of interest in wind energy research for several decades.

Literature on Savonius-type VAWTs demonstrates their potential for low-wind-speed applications, making them ideal for use in urban and remote areas with inconsistent or modest wind resources. Their self-starting capability and ability to capture wind from any direction have made them attractive for off-grid power generation, small-scale distributed energy projects, and as a complementary technology alongside other renewable source. Researchers have explored various modifications and optimizations to enhance the

performance of Savonius VAWTs, including blade shape, aspect ratio, and the addition of guide vanes, to improve their efficiency and harness a wider range of wind speeds.

Saha et. al. [1] investigated the performance and stability of Savonius wind turbines in environments with low wind speed. The suitability of Savonius turbines for such critical environmental circumstances were also looked upon in their novel study.Sahin et. al. [2] focused intensely on various aspects regarding the design and manufacturing of vertical axis wind turbine blades. Their work also included the rotor design of Savonius turbine.Ashok et. al [3] discussed various recent developments and obstacles in small-scale vertical axis wind turbines with a particular focus on Savonius turbine.A review": Altan et. al [4] reviewed the techniques which can potentially enhance the performance of the Savonius turbines and other flow control devices.Thongpron et. al [5] experimented with Savonius wind turbines in different low wind speed conditions and analyzed the numerical results obtained from those trials.Gökçek et. al [6] conducted field tests, primarily focusing on wind tunnel experiments to explore the aerodynamic characteristics of helical Savonius rotors.Chen et al. [7] conducted a comprehensive analysis and assessment of different attributes pertaining to the operational efficiency of Savonius wind turbines equipped with blades featuring a helical shape.Özerdem et. al [8] investigated on Savonius rotors which involved conducting wind tunnel experiments and outdoor field tests to evaluate the efficiency and operational performance of Savonius rotors.Kamoji et al. [9] proposed strategies for enhancing the efficiency of Savonius rotors by employing twisted blades and subsequently carried out an analysis of their performance.Madavan et al. [10] conducted an examination of how blade twist and overlap ratio influence the operational effectiveness of helical Savonius rotors.Ali et al. [11] presented a research study focusing on a customized Savonius wind turbine designed specifically for use in urban settings. Additionally, the study included both experimental and numerical investigations into this particular subject matter.Abdullah et al. [12] utilized finite element analysis to scrutinize the structural characteristics and integrity of Savonius rotors. This method allowed them to investigate how various forces and stresses impact the rotor's performance and durability, providing valuable insights into its mechanical behavior and potential improvements in design and materials.Rezazadeh et al. [13] conducted experimental research on Savonius rotors, with a specific focus on designing a Savonius rotor optimized for operating effectively under low wind speed conditions.

This paper aims to provide a comprehensive examination of helicity distribution around vertical axis wind turbine under low subsonic flow condition. Vertical axis wind turbines, with a particular emphasis on the Savonius-type VAWTs. As the world seeks sustainable energy solutions to combat climate change and reduce reliance on fossil fuels, understanding the unique attributes and flow physics behine working principle of Savonius-type vertical axis wind turbines is crucial. Through this study, we hope to shed light on the promise and challenges of Savonius VAWTs and their contribution to a cleaner and more sustainable energy future.

Computational Technique

To begin, a three-dimensional model of wind turbine consisting of 7 blades is designed with help of SolidWorks modeling software. The CAD model of the turbine consists of 7 semi-circular shaped blades. The parameters and dimensions of the designed rotor are provided in the table 1.

Table1: Design specification of the rotor

Types of Test Blade	**Vertical axis wind turbine (Savonious)**
Blade Height	1750mm

Blade Diameter	1400mm
Blade Thickness	10mm
No. of Blades	7nos.
Aspect Ratio	0.8
Blade spacing	500mm

Additionally a three-dimensional rectangular flow domain around the rotor was also drawn. After preparing the CAD models the three-dimensional models of the rotor and stator were imported to Geometry module of the Ansys. Then post importing the geometry to the Ansys, it was transferred to the meshing component in order to discretize the flow domain. The rotor domain was discretized utilizing tetrahedron element, because of low computation cost of the tetrahedron element. Tetrahedron element was utilized because of its comparatively higher efficiency under transient simulation of moving mesh structure. The rotor domain consists of 264646 numbers of nodes and 882983 numbers of elements. The discretized model was transferred to the CFX for physics setup. Under CFX the problem was set up to be solved for transient analysis. For physics setup k-epsilon viscous model is implemented along with transient blade row considering the turbulent flow characteristics for the flow around the wind turbine. In order to set up boundary layer conditions the inlet velocity is considered 7m/s in the positive x-direction. The rated rotational speed of the wind turbine is considered to be 100rpm. The fluid medium is considered as air. Schematic diagram of full domain is shown in figure below. Along with that schematic diagram of mesh created for rot and stator is also shown in figure below.

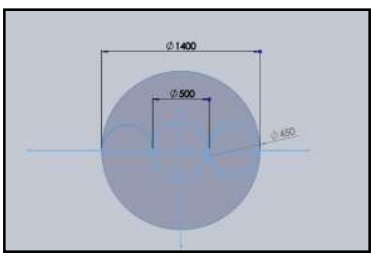

Fig 1: Top view of the rotor model along with dimension.

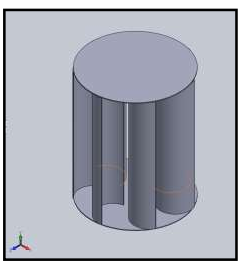

Fig 2: Isometric view of the rotor design.

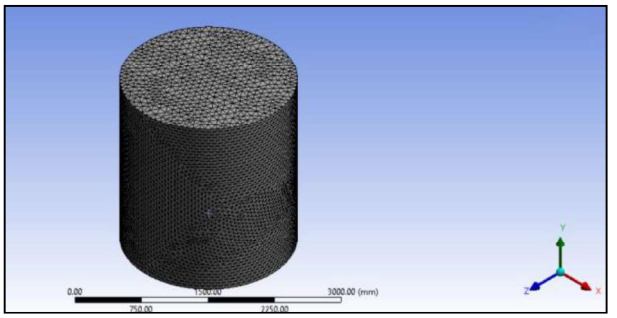

Fig 3: Schematics diagram of the mesh generated for rotor.

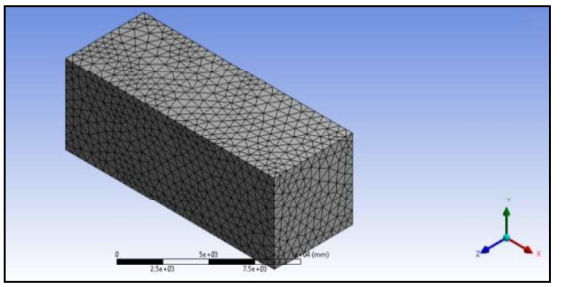

Fig 4: Schematic diagram of the mesh created for stator domain.

Results & Discussions

This study describes qualitative observations of helicity variations within the flow field of a Vertical Axis Wind Turbine (VAWT). The analysis of helicity variations in the flow field was conducted using Ansys CFX. The wind velocity was assumed to be 7m/sec in the positive X direction, and the rated rotational speed was set at 100 r.p.m. The simulation conducted in this paper follows a steady-transient approach, and the turbine under investigation is a Savonius drag-type turbine. Data collection points were selected at specific timesteps: timestep 4, timestep 14, timestep 28, timestep 42, timestep 56, and timestep 88. Helicity distribution data was collected from the mid-section of the flow domain, situated along the XZ plane.

Helicity in fluid dynamics is a mathematically generated quantity that describes the degree of twist or linkage between the velocity and vorticity (rotational) fields in a fluid flow. It is often used to study the behavior of turbulence in fluid flow. Helicity denoted by H, can be calculated mathematically as follows,

$$H = \iiint (v \cdot \omega) dv$$

Where, v and ω are the velocity vector field and vorticity vector field respectively. Vorticity vector field is nothing but curl of velocity vector field ($\omega = \nabla \times V$). Triple integration signifies the entire volume of interest.

In the above equation, the dot product of velocity vector and vorticity vector is calculculated at the point of interest. And then that value is integrated over the entire volume. The resulting value represents the helicity of the fluid flow. Helicity is a useful concept in fluid dynamics, especially in the study of turbulence and in situations where the twisting or linking of vortices is of interest, such as in the study of magnetic fields in astrophysics and plasma physics.

In the analysis diagram the helicity distribution is denoted by the blue and yellow, red colours. Blue colour denotes the lowest helicity and towards the yellow and red colour it denotes the comparatively higher helicity. At timestep 4, that is at the initial condition, the air flowing towards the positive x axis hits the windward concave portion of the rotor blade where the helicity is very high and shows the yellow colour and

significantly the helicity at the leeward portion of the same blade is comparatively low. The immediate blade just above the blade shows very high helicity at a particular point on the leading, leeward edge of the blade. From the diagram of the timestep 4, it can be seen a region of high helicity at the right-side portion of the rotor what means it direct the rotation of the rotor at the clockwise direction. Similarly at the left side of the rotor portion of low helicity and spots of low-helicity regions can be seen. The portions of red and yellow colours that is the high-helicity regions at the right side of the rotor can be termed as the stagnation zone where velocity is very negligible.

At timestep 14, It can be observed that the upper portion of the rotor shows slightly higher helicity indicated with yellowish colour. This indicate the presence of high rotational energy in that region. This variation of colours from the timestep 4 is an indication of the increase in the rotor speed with the subsequent decrease in the helicity.

At timestep 28, where there are still high-helicity regions that is spot of yellow and red at the right side of the rotor but there are subsequently more concentrated blue spots of low-helicity regions at the concave and leading edge of the maximum blades. The region of some low-helicity blue zone can be seen at the leeward convex zone of some bottom blades. The concentration of yellow and red colour that is high helicity zone indicates concentration of high stress in the right side of the rotor and rotation of rotor in the clockwise direction.

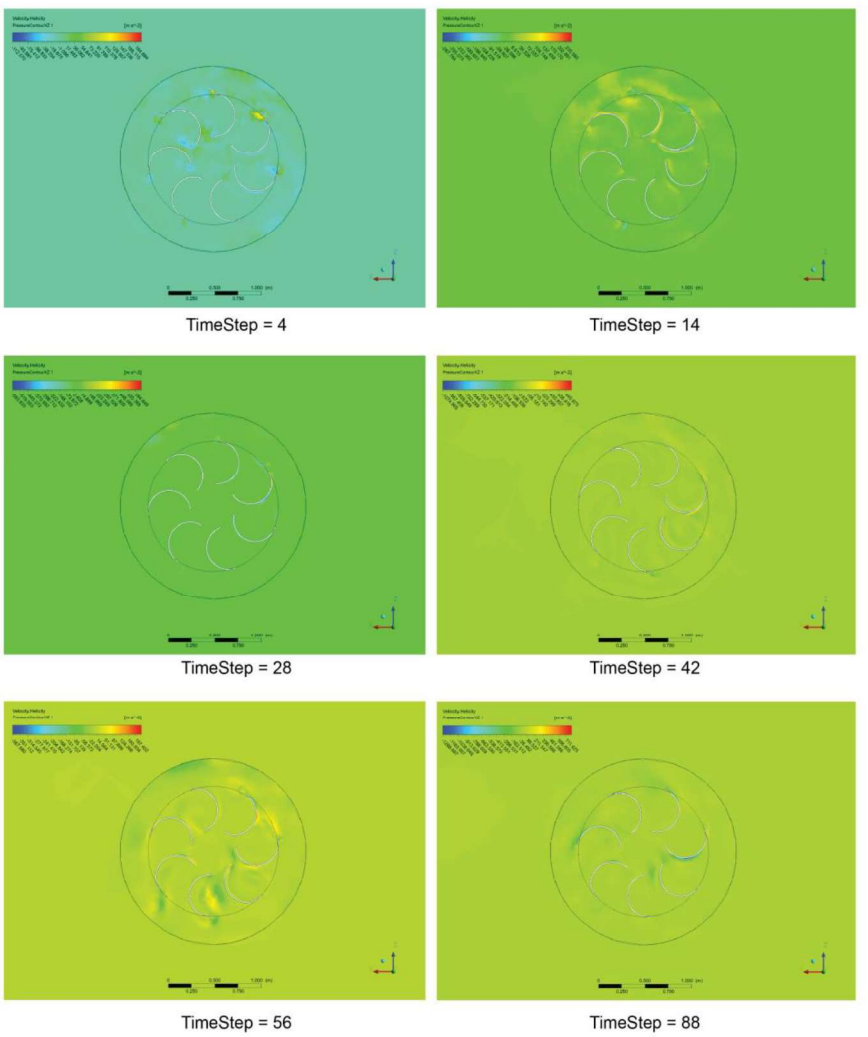

Fig 5: Helicity distribution contour around VAWT.

At timestep 42, the increase in the size of the red spots can be noticed which indicates further decrease in the velocity a that particular points. Subsequently on the other blades some blades show the blue colour to be fading and on other blades the blue colours getting deeper.

At timestep 56, at the right portion of the rotor the yellow and red colour fading gradually and the blue colour on the other blades getting deeper. The red colour spot was bigger and deeper in the previous instance which has reduced to smaller spots and fading in colour. It can be also noticed that the variation of helicity is more uniform in the flow field.

At timestep 88, the stress concentration in the flow field in unvarying through most portion of the flow field. Only in the extreme right side of the rotor a large spot of red colour indicating very high helicity can be spotted. That is the thrust force which rotates the rotor in the tangential direction with the leading edge of the blade. The speed of rotation is maximum at this instance and variation of helicity in negligible.

Conclusion

It is evident that this drag-type vertical axis wind turbine exhibits an favorable helicity gradient along approximately half of its blades. These areas with high helicity do not contribute to the overall moment generation. The presence of a high helicity region in the leeward or left half portion of the rotor predominantly signifies presence of rotational flow velocity, indicating the dissipation of energy in the form of eddies. However, these observations can serve as a foundation for optimizing blade models and configurations in the future. Such optimizations hold the potential to significantly enhance the efficiency of drag-type vertical axis wind turbines, making them more effective.

REFERENCES

1. Saha, U., Akhtar, M. S., & Selvaraj, P. (2016). Performance of a Savonius wind turbine for low wind speed applications: A review. Renewable and Sustainable Energy Reviews, 60, 41-52.

2. Sahin, B., & Yilmaz, S. (2008). Design and manufacturing of a vertical axis wind turbine blade. Renewable Energy, 33(11), 2324-2333.

3. Ashok, A., Muniappan, A., & Krishnamurthy, R. (2015). Recent developments and challenges in small-scale vertical axis wind turbines. Renewable and Sustainable Energy Reviews, 52, 665-677.

4. Altan, H., & Hacioglu, A. (2020). Performance enhancement of Savonius wind turbine using flow control devices: A review. Renewable and Sustainable Energy Reviews, 134, 110331.

5. Thongpron, J., Kanog, T., & Polprasert, C. (2016). Experimental and numerical investigations of a Savonius wind turbine for low wind speed applications. Energy Conversion and Management, 121, 126-138.

6. Gökçek, M., & Bayülken, A. (2011). Wind tunnel and field tests for the investigation of the aerodynamic performance of a helical Savonius rotor. Renewable Energy, 36(3), 1111-1120.

7. Chen, W. C., & Kuo, C. C. (2018). A review of Savonius wind turbine with helical-shaped blades. Journal of Renewable and Sustainable Energy, 10(3), 034701.

8. Özerdem, B., & Koç, M. (2007). Wind tunnel and outdoor experiments for performance assessment of Savonius rotors. Renewable Energy, 32(11), 1844-1857.

9. Kamoji, M. A., & Patil, S. D. (2013). Performance analysis of Savonius rotor with twisted blades. Energy Procedia, 33, 212-219.

10.Madavan, N. K., & Radhakrishnan, T. K. (2008). Performance analysis of a helical Savonius rotor: Effect of blade twist and overlap ratio. Journal of Solar Energy Engineering, 130(4), 041011.

11. Ali, M. H., Ahmed, T., & Saad, M. A. (2020). Experimental and numerical investigation of modified Savonius wind turbine for urban applications. Energy, 203, 117868.

12. Abdullah, M. M. A. B., & Ahmed, T. Y. (2017). Investigation of Savonius rotor using finite element analysis. Journal of Engineering Science and Technology, 12(8), 2165-2174.

13. Rezazadeh, S., & Gorji-Bandpy, M. (2013). Design and experimental analysis of a Savonius rotor for low wind speed conditions. Energy Conversion and Management, 75, 348-356.

Chapter 2

Analytical Investigation of Vorticity in the Flow around Savonius Wind Turbines

Soumya Ghosh[1], Samrat Biswas[1*,] Sayan Paul[1], Soumak Bose[1], Arijit Mukherjee[1,] Anupam Mallick[1]

1. Swami Vivekananda University, Barrackpore 700 121, INDIA
Corresponding author* Email ID: samratb@svu.ac.in

Abstract

This paper presents an exploratory investigation into the flow field surrounding Savonius wind turbines. This specific turbine design deviates from convention due to its unique capacity to extract valuable energy from the airflow, setting it apart from conventional wind turbines. Its straightforward construction, swift startup, continuous operation, ability to harness wind from any direction, potential for achieving higher angular velocities, low noise emissions, and reduced wear and tear on moving components contribute to its appeal. Over the course of history, various adaptations of this device have been envisioned, expanding the possibilities of vertical axis wind turbines. The primary aim of this study is to visually represent and seek to comprehend the variation in vorticity around a vertical axis wind turbine (VAWT), particularly the Savonius-type wind turbine, operating under subsonic flow conditions.

Keywords: VAWT, Savonious Type Turbine, Wind Turbine

Introduction

The search for sustainable and renewable energy sources to meet the ever-growing global energy demand and combat the adverse impacts of climate change, wind power has emerged as a top contender. Conventional horizontal axis wind turbines (HAWTs) have long dominated the wind energy landscape. However, the limitations of HAWTs, including their significant environmental footprint, intermittent energy production, and reliance on high wind speeds, have driven the exploration of alternative wind energy solutions. Among these alternatives, vertical axis wind turbines (VAWTs) have emerged as a promising technology deserving of thorough examination and consideration.

The concept of VAWTs has ancient roots, with early designs attributed to Persian engineers and later refinements by European inventors. Despite their historical heritage, VAWTs have, until recently, remained relatively overshadowed by their horizontal axis counterparts. Nevertheless, recent advancements in materials, aerodynamics, and control systems have rekindled interest in VAWTs and have sparked a renewed focus on research and development efforts.

One noteworthy subtype of VAWTs, the Savonius-type wind turbine, merits special attention. The Savonius rotor, named after its Finnish inventor Sigurd Johannes Savonius, is known for its simple and robust design. Unlike the more common Darrieus and Darrieus-like VAWTs, which rely on lift forces for power generation, Savonius turbines harness drag forces, making them well-suited for low wind speed environments. This distinctive design features two or more curved blades mounted on a vertical axis, resembling an "S" or "U" shape, and has been a subject of interest in wind energy research for several decades. Literature on Savonius-type VAWTs demonstrates their potential for low-wind-speed applications, making them ideal for use in urban and remote areas with inconsistent or modest wind resources. Their self-starting capability and ability to capture wind from any direction have made them attractive for off-grid power generation, small-scale distributed energy projects, and as a complementary technology alongside other renewable source. Researchers have explored various modifications and optimizations to enhance the

performance of Savonius VAWTs, including blade shape, aspect ratio, and the addition of guide vanes, to improve their efficiency and harness a wider range of wind speeds.

Saha et. al. [1] investigated the performance and stability of Savonius wind turbines in environments with low wind speed. The suitability of Savonius turbines for such critical environmental circumstances were also looked upon in their novel study.Sahin et. al. [2] focused intensely on various aspects regarding the design and manufacturing of vertical axis wind turbine blades. Their work also included the rotor design of Savonius turbine. Ashok et. al [3] discussed various recent developments and obstacles in small-scale vertical axis wind turbines with a particular focus on Savonius turbine.A review": Altan et. al [4] reviewed the techniques which can potentially enhance the performance of the Savonius turbines and other flow control devices.Thongpron et. al [5] experimented with Savonius wind turbines in different low wind speed conditions and analyzed the numerical results obtained from those trials.Gökçek et. al [6] conducted field tests, primarily focusing on wind tunnel experiments to explore the aerodynamic characteristics of helical Savonius rotors.Chen et al. [7] conducted a comprehensive analysis and assessment of different attributes pertaining to the operational efficiency of Savonius wind turbines equipped with blades featuring a helical shape.Özerdem et. al [8] investigated on Savonius rotors which involved conducting wind tunnel experiments and outdoor field tests to evaluate the efficiency and operational performance of Savonius rotors.Kamoji et al. [9] proposed strategies for enhancing the efficiency of Savonius rotors by employing twisted blades and subsequently carried out an analysis of their performance.Madavan et al. [10] conducted an examination of how blade twist and overlap ratio influence the operational effectiveness of helical Savonius rotors.Ali et al. [11] presented a research study focusing on a customized Savonius wind turbine designed specifically for use in urban settings. Additionally, the study included both experimental and numerical investigations into this particular subject matter.Abdullah et al. [12] utilized finite element analysis to scrutinize the structural characteristics and integrity of Savonius rotors. This method allowed them to investigate how various forces and stresses impact the rotor's performance and durability, providing valuable insights into its mechanical behavior and potential improvements in design and materials.Rezazadeh et al. [13] conducted experimental research on Savonius rotors, with a specific focus on designing a Savonius rotor optimized for operating effectively under low wind speed conditions.

This paper aims to provide a comprehensive examination of vorticity around vertical axis wind turbine unde low subsonic flow condition. Vertical axis wind turbines, with a particular emphasis on the Savonius-type VAWTs. As the world seeks sustainable energy solutions to combat climate change and reduce reliance on fossil fuels, understanding the unique attributes and flow physics behine working principle of Savonius-type vertical axis wind turbines is crucial. Through this study, we hope to shed light on the promise and challenges of Savonius VAWTs and their contribution to a cleaner and more sustainable energy future.

Computational Technique

To To begin, a three-dimensional model of wind turbine consisting of 7 blades is de-signed with help of SolidWorks modeling software. The CAD model of the turbine consists of 7 semi-circular shaped blades. The parameters and dimensions of the designed rotor are provided in the table 1. Additionally, a three-dimensional rectangular flow domain surrounding the rotor was also constructed.

Subsequent to the CAD model preparations, the three-dimensional renditions of both the rotor and stator were imported into the Geometry module of Ansys. Following successful import into Ansys, the geometry seamlessly transitioned to the meshing component, where the overarching goal was to discretize the flow domain. The rotor domain was discretized using tetrahedron elements due to their lower computational cost. Tetrahedron elements were chosen for their comparative efficiency in simulating transient motion of the moving mesh structure. The rotor domain comprised 264,646 nodes and 882,983 elements. The discretized model was then transferred to CFX for physics setup. In the CFX environment, the problem was configured

for transient analysis. For the physics setup, a k-epsilon viscous model was employed, considering the turbulent flow characteristics around the wind turbine. Boundary layer conditions were established with an inlet vorticity set at 7 m/s in the positive x-direction. The rated rotational speed of the wind turbine was assumed to be 100 RPM. The fluid medium under consideration was air. A schematic diagram of the entire domain is provided in the figure below. Additionally, schematic diagrams illustrating the mesh created for both the rotor and stator are presented in the figure below.

Table 1: Design specification of the rotor

Types of Test Blade	**Vertical axis wind turbine (Savonious)**
Blade Height	1750mm
Blade Diameter	1400mm
Blade Thickness	10mm
No. of Blades	7nos.
Aspect Ratio	0.8
Blade spacing	500mm

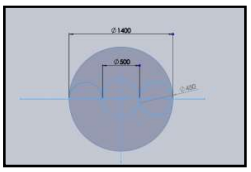

Fig 1: Top view of the rotor model along with dimension.

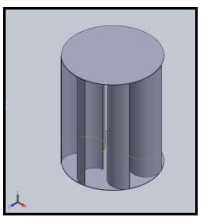

Fig 2: Isometric view of the rotor design.

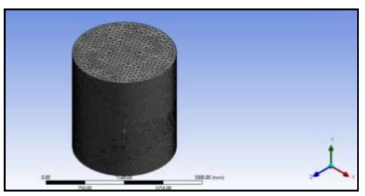

Fig 3: Schematics diagram of the mesh generated for rotor.

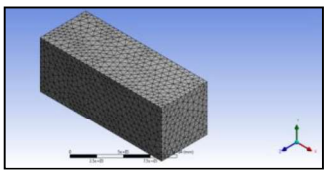

Fig 4: Schematic diagram of the mesh created for stator domain (Flow Domain).

Results & Discussions

This study describes qualitative observations of vorticity variations within the flow field of a Vertical Axis Wind Turbine (VAWT). The analysis of vorticity variations in the flow field was conducted using Ansys CFX. The wind velocity was assumed to be 7m/sec in the positive X direction, and the rated rotational speed was set at 100 r.p.m. The simulation conducted in this paper follows a steady-transient approach, and the turbine under investigation is a Savonius drag-type turbine. Data collection points were selected at specific timesteps: timestep 4, timestep 14, timestep 28, timestep 42, timestep 56, and timestep 88. Vorticity distribution data was collected from the mid-section of the flow domain, situated along the XZ plane.

Vorticity is a concept in fluid dynamics that describes the local spinning or rotation of fluid elements within a fluid flow. It is a vector quantity and represents the curl of the velocity field of the fluid. In simpler terms, vorticity indicates the presence and magnitude of rotation within a fluid at a given point in space. When vorticity is zero at a particular point, it means that the fluid at that point is not rotating; when it is nonzero, it indicates the presence of rotation. Vorticity is often used to analyze and describe the behavior of fluid flows, especially in situations involving turbulence, vortex formation, and the study of various fluid dynamic phenomena, including the flow around objects like turbines, aircraft wings, and tornadoes.
Mathematically vorticity (ω) is calculatged as the curl of the velocity vector (V) of a fluid flow. In a three-dimensional Cartesian co-ordinate system (x, y, z), the vorticity vector is given by $\omega = \nabla \times V$.

During timestep 4, the initial condition, the airflow toward the positive X axis strikes the windward concave portion of the rotor blade, leading to a very high vorticity, depicted in yellow. In contrast, the vorticity at the leeward portion of the same blade is notably low, represented in blue. The blade immediately above this one exhibits very high vorticity at a specific point on the leading, leeward edge. The diagram at timestep 4 also reveals a region of high vorticity on the right-side portion of the rotor, indicating the rotor's clockwise rotation. Similarly, on the left side of the rotor, there is a region of low vorticity and spots with low-vorticity regions. The right side of the rotor can be referred to as the stagnation zone, where the vorticity is negligible. Closer scrutiny reveals two primary vorticity fluctuations in the center portion, indicating that blades align along this line.

At timestep 14, multiple variations along the centerline are observable. These variations result from the rotation of the rotor, bringing multiple blades into contact with the airflow, leading to vorticity and resulting momentum transfer. This variation from timestep 4 is an indication of the increase in rotor speed and the subsequent decrease in vorticity.

At timestep 28, high-vorticity regions still exist on the right side of the rotor. However, there are more concentrated lower variations of low-vorticity in regions at the concave and leading edge of the maximum blades. Some regions of low-velocity in swirling strenth can be observed on both sides of the plot. The concentration of fluctuations on both sides, in the high vorticity, indicates a concentration of high stress in the rotor and rotor rotation.

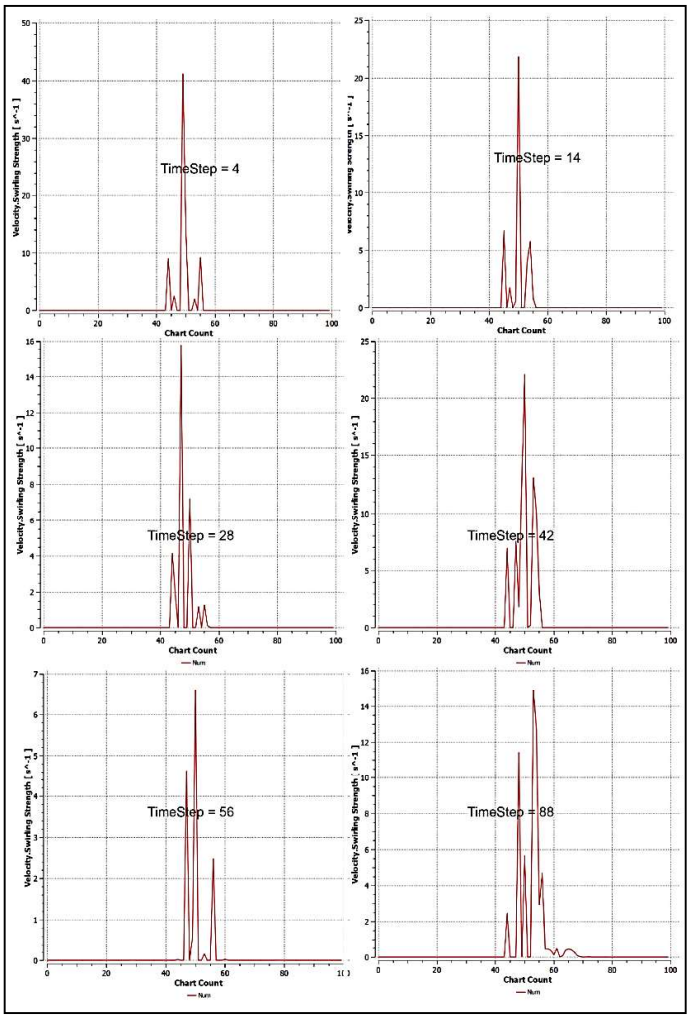

Fig 5: Vorticity distribution plot along mid-section of flow domain

At timestep 42, the reduction of fluctuation of parameter in first half of the plot can be noticed, which indicates further decrease in the vorticity in that particular points.
At timestep 56, It can be also noticed that the variation of vorticity is more uniform in the flow field. This is repsented by more balanced distribution of vorticity profile in the plot under study.
At timestep 88, the stress concentration in the flow field in unvarying through most portion of the flow field. Only in the extreme right side of the rotor a fluctuation indicating high vorticity can be spotted. That is the thrust force which rotates the rotor in the tangential direction with the leading edge of the blade.

Conclusion

Fluctuations in vorticity become apparent in the initial time steps, suggesting a need for design optimization. Furthermore, it's evident that this drag-type vertical axis wing turbine exhibits an unfavorable gradient in vorticity along approximately half of its blades. These high vorticity regions do not contribute to the overall moment generation. The presence of low-vorticity regions in the leeward portion or right half of the rotor predominantly indicates lower velocity wirlign strength values, signifying the dissipation of energy in the form of eddies. Nevertheless, the insights gained from this study can serve as the foundation for optimizing blade models and configurations in the future. These forthcoming optimizations have the potential to enhance the efficiency of drag-type vertical axis wing turbines.

References

1. Saha, U., Akhtar, M. S., & Selvaraj, P. (2016). Performance of a Savonius wind turbine for low wind speed applications: A review. Renewable and Sustainable Energy Reviews, 60, 41-52.

2. Sahin, B., & Yilmaz, S. (2008). Design and manufacturing of a vertical axis wind turbine blade. Renewable Energy, 33(11), 2324-2333.

3. Ashok, A., Muniappan, A., & Krishnamurthy, R. (2015). Recent developments and challenges in small-scale vertical axis wind turbines. Renewable and Sustainable Energy Reviews, 52, 665-677.

4. Altan, H., & Hacioglu, A. (2020). Performance enhancement of Savonius wind turbine using flow control devices: A review. Renewable and Sustainable Energy Reviews, 134, 110331.

5. Thongpron, J., Kanog, T., & Polprasert, C. (2016). Experimental and numerical investigations of a Savonius wind turbine for low wind speed applications. Energy Conversion and Management, 121, 126-138.

6. Gökçek, M., & Bayülken, A. (2011). Wind tunnel and field tests for the investigation of the aerodynamic performance of a helical Savonius rotor. Renewable Energy, 36(3), 1111-1120.

7. Chen, W. C., & Kuo, C. C. (2018). A review of Savonius wind turbine with helical-shaped blades. Journal of Renewable and Sustainable Energy, 10(3), 034701.

8. Özerdem, B., & Koç, M. (2007). Wind tunnel and outdoor experiments for performance assessment of Savonius rotors. Renewable Energy, 32(11), 1844-1857.

9. Kamoji, M. A., & Patil, S. D. (2013). Performance analysis of Savonius rotor with twisted blades. Energy Procedia, 33, 212-219.

10. Madavan, N. K., & Radhakrishnan, T. K. (2008). Performance analysis of a helical Savonius rotor: Effect of blade twist and overlap ratio. Journal of Solar Energy Engineering, 130(4), 041011.

11. Ali, M. H., Ahmed, T., & Saad, M. A. (2020). Experimental and numerical investigation of modified Savonius wind turbine for urban applications. Energy, 203, 117868.

12. Abdullah, M. M. A. B., & Ahmed, T. Y. (2017). Investigation of Savonius rotor using finite element analysis. Journal of Engineering Science and Technology, 12(8), 2165-2174.

13. Rezazadeh, S., & Gorji-Bandpy, M. (2013). Design and experimental analysis of a Savonius rotor for low wind speed conditions. Energy Conversion and Management, 75, 348-356.

Chapter 3

Analysis of Pressure Distribution in the Flow Field around Vertical Axis Wind Turbine

Soumak Bose[1*], Sayan Paul[1,] Suman Kumar Ghosh[1], Soumya Ghosh[1], Arijit Mukherjee[1] Samrat Biswas[1]
Swami Vivekananda University, Barrackpore 700 121, INDIA
Corresponding author* Email ID: soumakb@svu.ac.in

Abstract
This paper presents an exploratory study of the flow field around Savonius wind turbines. This particular turbine design is unconventional and stands out for its unique ability to extract useful energy from the airflow, distinguishing it from conventional wind turbines. Its simple construction, rapid startup, continuous operation, capacity to harness wind from any direction, ability to achieve higher angular velocities, low noise emissions, and reduced wear and tear on moving components make it an appealing choice. Throughout history, various adaptations of this device have been envisioned, enhancing the versatility of vertical axis wind turbines. The primary objective of this study is to visualize and attempt to understand the pressure distribution variation around a vertical axis wind turbine (VAWT), specifically the Savonius-type wind turbine operating under subsonic flow conditions.

Keywords: VAWT, Savonious Type Turbine, Wind Turbine

Introduction

In the pursuit of sustainable and renewable energy sources to meet the ever-expanding global energy demand and combat the adverse effects of climate change, wind power has emerged as a leading contender. Traditional horizontal axis wind turbines (HAWTs) have held dominance in the wind energy sector for many years. However, the limitations of HAWTs, including their significant environmental impact, intermittent energy generation, and the requirement for high wind speeds, have prompted the exploration of alternative wind energy solutions. Among these alternatives, vertical axis wind turbines (VAWTs) have risen as a promising technology warranting comprehensive investigation and consideration.

The concept of VAWTs has ancient origins, with early designs credited to Persian engineers and later refinements by European inventors. Despite their historical roots, VAWTs have, until recently, remained relatively overshadowed by their horizontal axis counterparts. Nevertheless, recent advancements in materials, aerodynamics, and control systems have reignited interest in VAWTs and have spurred a resurgence in research and development efforts.

One noteworthy subtype of VAWTs, the Savonius-type wind turbine, merits special attention. The Savonius rotor, named after its Finnish inventor Sigurd Johannes Savonius, is known for its simple and robust design. Unlike the more common Darrieus and Darrieus-like VAWTs, which rely on lift forces for power generation, Savonius turbines harness drag forces, making them well-suited for low wind speed environments. This distinctive design features two or more curved blades mounted on a vertical axis, resembling an "S" or "U" shape, and has been a subject of interest in wind energy research for several decades.

Literature on Savonius-type VAWTs demonstrates their potential for low-wind-speed applications, making them ideal for use in urban and remote areas with inconsistent or modest wind resources. Their self-starting capability and ability to capture wind from any direction have made them attractive for off-grid power generation, small-scale distributed energy projects, and as a complementary technology alongside other renewable source. Researchers have explored various modifications and optimizations to enhance the performance of Savonius VAWTs, including blade shape, aspect ratio, and the addition of guide vanes, to

improve their efficiency and harness a wider range of wind speeds.
Saha et. al. [1] investigated the performance and stability of Savonius wind turbines in environments with low wind speed. The suitability of Savonius turbines for such critical environmental circumstances were also looked upon in their novel study.Sahin et. al. [2] focused intensely on various aspects regarding the design and manufacturing of vertical axis wind turbine blades. Their work also included the rotor design of Savonius turbine.Ashok et. al [3] discussed various recent developments and obstacles in small-scale vertical axis wind turbines with a particular focus on Savonius turbine.A review": Altan et. al [4] reviewed the techniques which can potentially enhance the performance of the Savonius turbines and other flow control devices.Thongpron et. al [5] experimented with Savonius wind turbines in different low wind speed conditions and analyzed the numerical results obtained from those trials.Gökçek et. al [6] conducted field tests, primarily focusing on wind tunnel experiments to explore the aerodynamic characteristics of helical Savonius rotors.Chen et al. [7] conducted a comprehensive analysis and assessment of different attributes pertaining to the operational efficiency of Savonius wind turbines equipped with blades featuring a helical shape.Özerdem et. al [8] investigated on Savonius rotors which involved conducting wind tunnel experiments and outdoor field tests to evaluate the efficiency and operational performance of Savonius rotors.Kamoji et al. [9] proposed strategies for enhancing the efficiency of Savonius rotors by employing twisted blades and subsequently carried out an analysis of their performance.Madavan et al. [10] conducted an examination of how blade twist and overlap ratio influence the operational effectiveness of helical Savonius rotors.Ali et al. [11] presented a research study focusing on a customized Savonius wind turbine designed specifically for use in urban settings. Additionally, the study included both experimental and numerical investigations into this particular subject matter.Abdullah et al. [12] utilized finite element analysis to scrutinize the structural characteristics and integrity of Savonius rotors. This method allowed them to investigate how various forces and stresses impact the rotor's performance and durability, providing valuable insights into its mechanical behavior and potential improvements in design and materials.Rezazadeh et al. [13] conducted experimental research on Savonius rotors, with a specific focus on designing a Savonius rotor optimized for operating effectively under low wind speed conditions.
This paper aims to provide a comprehensive examination of pressure distribution around vertical axis wind turbine unde low subsonic flow condition. Vertical axis wind turbines, with a particular emphasis on the Savonius-type VAWTs. As the world seeks sustainable energy solutions to combat climate change and reduce reliance on fossil fuels, understanding the unique attributes and flow physics behine working principle of Savonius-type vertical axis wind turbines is crucial. Through this study, we hope to shed light on the promise and challenges of Savonius VAWTs and their contribution to a cleaner and more sustainable energy future.

Computational Technique

To begin, a three-dimensional model of wind turbine consisting of 7 blades is designed with help of SolidWorks modeling software. The CAD model of the turbine consists of 7 semi-circular shaped blades. The parameters and dimensions of the designed rotor are provided in the table 1. Additionally a three-dimensional rectangular flow domain around the rotor was also drawn. After preparing the CAD models the three-dimensional models of the rotor and stator were imported to Geometry module of the Ansys. Then post importing the geometry to the Ansys, it was transferred to the meshing component in order to discretize the flow domain. The rotor domain was discretized utilizing tetrahedron element, because of low computation cost of the tetrahedron element. Tetrahedron element was utilized because of its comparatively higher efficiency under transient simulation of moving mesh structure. The rotor domain consists of 264646 numbers of nodes and 882983 numbers of elements. The discretized model was transferred to the CFX for physics setup. Under CFX the problem was set up to be solved for transient analysis. For physics setup k-

epsilon viscous model is implemented along with transient blade row considering the turbulent flow characteristics for the flow around the wind turbine. In order to set up boundary layer conditions the inlet velocity is considered 7m/s in the positive x-direction. The rated rotational speed of the wind turbine is considered to be 100rpm. The fluid medium is considered as air. Schematic diagram of full domain is shown in figure below. Along with that schematic diagram of mesh created for rot and stator is also shown in figure below.

Table1: Design specification of the rotor

Types of Test Blade	**Vertical axis wind turbine (Savonious)**
Blade Height	1750mm
Blade Diameter	1400mm
Blade Thickness	10mm
No. of Blades	7nos.
Aspect Ratio	0.8
Blade spacing	500mm

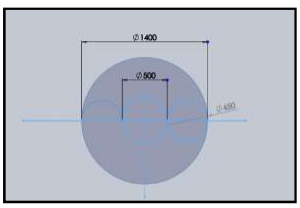

Fig1: Top view of the rotor model along with dimension.

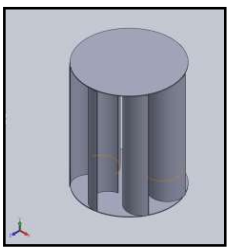

Fig 2: Isometric view of the rotor design.

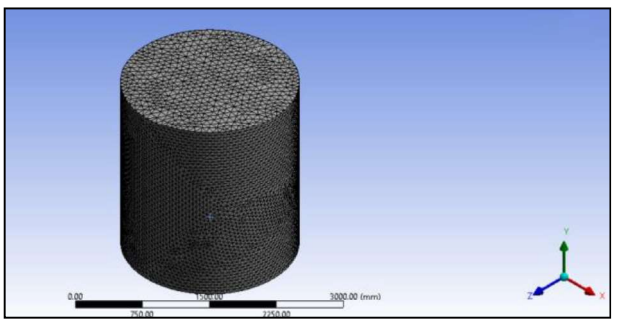

Fig 3: Schematics diagram of the mesh generated for rotor.

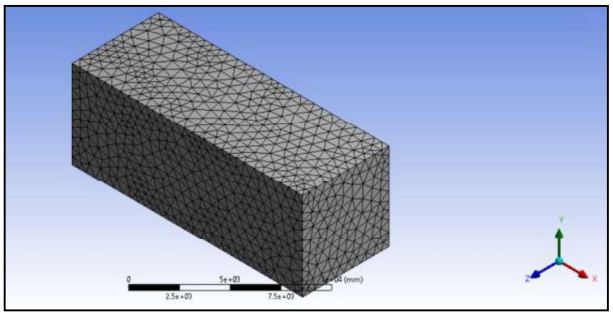

Fig 4: Schematic diagram of the mesh created for stator domain.

Results & Discussions

This study represents a qualitative analysis of the pressure variation in the flow field of the Vertical axis wind turbine. The pressure variation in the flow field has been analysed using Ansys CFX. The wind velocity has been assumed to be 7m/sec towards positive X direction and the rated r.p.m has been taken as 100 r.p.m. The simulation done in this paper is steady transient type and the turbine on which the simulation is done is of Savonius drag type turbine. The instances taken for the analysis are taken at timestep 4, timestep 14, timestep 28, timestep 42, timestep 56 and timestep 88. The pressure distribution data was taken in the mid portion of the flow domain lies along XZ plane. Along this plane a line was taken, which runs through the miggle of the entire flow domain. Along this above mentioned line the data were extracted and plotted for comparative analysis.

Here it can be seem that there is little to no observable fluctuation in the graph indicating very low pressure differnence. The air flowing towards the positive x axis hits the windward concave portion of the rotor blade where the pressure is very high The immediate blade just above the blade shows very high pressure at a particular point on the leading, leeward edge of the blade.

At timestep 4 that is at the initial condition the air flowing towards the positive x axis hits the windward concave portion of the rotor blade where the pressure is very high and shows the yellow colour and significantly the pressure at the leeward portion of the same blade is very low and shows blue colour. The immediate blade just above the blade shows very high pressure at a particular point on the leading, leeward edge of the blade. From the diagram of the timestep 4, it can be seen a region of high pressure at the right-side portion of the rotor what means it direct the rotation of the rotor at the clockwise direction. Similarly at the left side of the rotor portion of low pressure and spots of low-pressure regions can be seen. At the right side of the rotor can be termed as the stagnation zone where velocity is very negligible. Upon close scrutiny it can be observed that there are basically two pressure fluctuations in the centre portion indicating to blades are along the line.

At timestep 14, it can seen from that there are multiple variations along thr centreline. Which indicate the that with rotation of rotot multiple comes into contact with the flow, hence the pressure fluctuation and resulting momentum transfer. This variation from the timestep 4 is an indication of the increase in the rotor speed with the subsequent decrease in the pressure.

At timestep 28, where there are still high-pressure regions at the right side of the rotor but there are subsequently more concentrated lower variations of low-pressure regions at the concave and leading edge of the maximum blades. The region of some low-pressure fluctuations can be seen at the both side of the plot. The concentration of fluctuation on both side, high pressure zone indicates concentration of high stress in

the rotor and rotation of rotor.

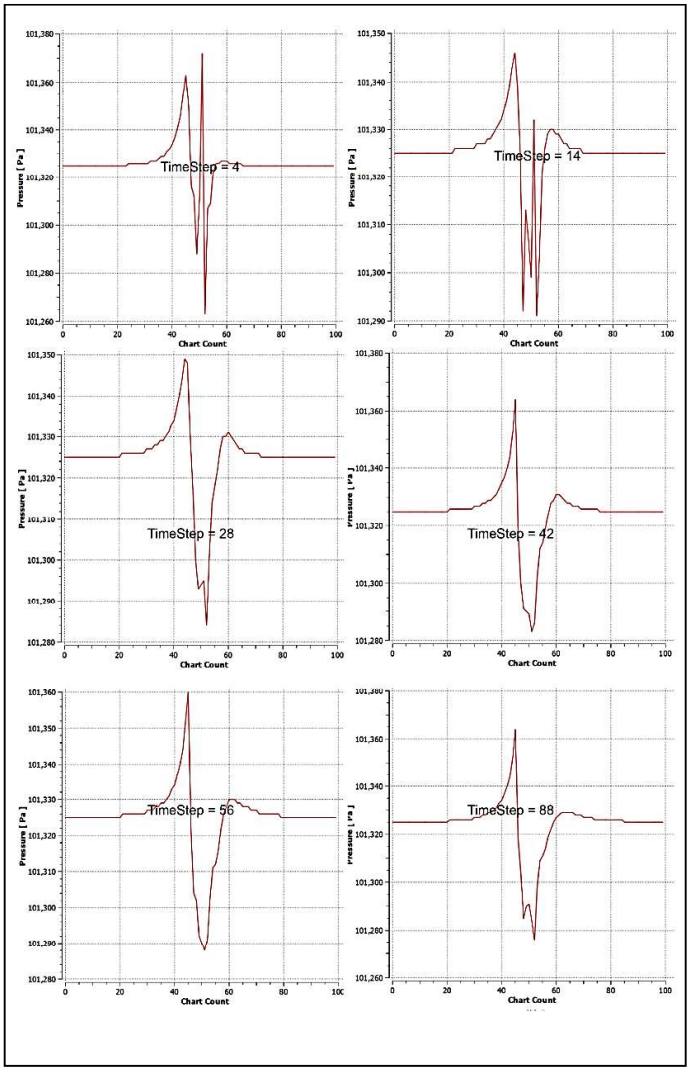

Fig 5: Pressure distribution plot along mid-section of flow domain

At timestep 42, the reduction of fluctuation of parameter in first half of the plot can be noticed, which indicates further decrease in the pressure a that particular points.
At timestep 56, It can be also noticed that the variation of pressure is more uniform in the flow field. This is repsented by more balanced distribution of pressure profile in the plot under study.
At timestep 88, the stress concentration in the flow field in unvarying through most portion of the flow field. Only in the extreme right side of the rotor a fluctuation indicating high pressure can be spotted. That is the thrust force which rotates the rotor in the tangential direction with the leading edge of the blade.

Conclusion

There pressure fluctions can be obsved from the intial time steps. This indicate the absence of optimization in designing This can also be seen over all that this drag type vertical axis wing turbine has adverse pressure gradient along half of the blades. These low pressure zone does not contribute towards the overall moment generation. The low pressure region in the leeward portion or right half portion of the rotor mostly shows lower pressure region and these indicate dissipation of energy in the form of eddies. But the blade models and configurations can be optimized later based on these observations. In future, which will inturn help to make optimized drag-type vertical axis wing turbine more effieicnt.

References

1. Saha, U., Akhtar, M. S., & Selvaraj, P. (2016). Performance of a Savonius wind turbine for low wind speed applications: A review. Renewable and Sustainable Energy Reviews, 60, 41-52.

2. Sahin, B., & Yilmaz, S. (2008). Design and manufacturing of a vertical axis wind turbine blade. Renewable Energy, 33(11), 2324-2333.

3. Ashok, A., Muniappan, A., & Krishnamurthy, R. (2015). Recent developments and challenges in small-scale vertical axis wind turbines. Renewable and Sustainable Energy Reviews, 52, 665-677.

4. Altan, H., & Hacioglu, A. (2020). Performance enhancement of Savonius wind turbine using flow control devices: A review. Renewable and Sustainable Energy Reviews, 134, 110331.

5. Thongpron, J., Kanog, T., & Polprasert, C. (2016). Experimental and numerical investigations of a Savonius wind turbine for low wind speed applications. Energy Conversion and Management, 121, 126-138.

6. Gökçek, M., & Bayülken, A. (2011). Wind tunnel and field tests for the investigation of the aerodynamic performance of a helical Savonius rotor. Renewable Energy, 36(3), 1111-1120.

7. Chen, W. C., & Kuo, C. C. (2018). A review of Savonius wind turbine with helical-shaped blades. Journal of Renewable and Sustainable Energy, 10(3), 034701.

8. Özerdem, B., & Koç, M. (2007). Wind tunnel and outdoor experiments for performance assessment of Savonius rotors. Renewable Energy, 32(11), 1844-1857.

9. Kamoji, M. A., & Patil, S. D. (2013). Performance analysis of Savonius rotor with twisted blades. Energy Procedia, 33, 212-219.

10. Madavan, N. K., & Radhakrishnan, T. K. (2008). Performance analysis of a helical Savonius rotor: Effect of blade twist and overlap ratio. Journal of Solar Energy Engineering, 130(4), 041011.

11. Ali, M. H., Ahmed, T., & Saad, M. A. (2020). Experimental and numerical investigation of modified Savonius wind turbine for urban applications. Energy, 203, 117868.

12. Abdullah, M. M. A. B., & Ahmed, T. Y. (2017). Investigation of Savonius rotor using finite element analysis. Journal of Engineering Science and Technology, 12(8), 2165-2174.

13. Rezazadeh, S., & Gorji-Bandpy, M. (2013). Design and experimental analysis of a Savonius rotor for low wind speed conditions. Energy Conversion and Management, 75, 348-356.

Chapter 4

Explorative Analysis of Helicity Distribution along Longitudinal Direction in the Flow around Savonius Wind Turbines

Suman Kumar Ghosh[1*], Sayan Paul[1,] Abhishek Poddar[1], Soumya Ghosh[1], Arijit Mukherjee[1,] Samrat Biswas[1]

Swami Vivekananda University, Barrackpore 700 121, INDIA
Corresponding author*Email ID: sumankg@svu.ac.in

Abstract

This paper introduces an exploratory investigation into the flow field around Savonius wind turbines. This particular turbine design stands out from conventional ones due to its unique ability to harness valuable energy from the air stream. It boasts straightforward construction, rapid startup, continuous operation, wind utilization from any direction, the potential to achieve higher angular velocities during operation, and minimal noise emissions. Additionally, it significantly reduces wear and tear on moving components, making it an attractive machinery option. Throughout history, various adaptations of this device have been envisioned, enhancing the versatility of vertical axis wind turbines. The primary objective of this study is to visually depict and attempt to comprehend the variation in helicity distribution around a vertical axis wind turbine (VAWT), specifically the Savonius-type wind turbine, operating under subsonic flow conditions.

Keywords: VAWT, Savonious Type Turbine, Wind Turbine

Introduction

In the pursuit of sustainable and renewable energy sources to meet the ever-expanding global energy demand and combat the adverse impacts of climate change, wind power has emerged as a leading contender. Traditional horizontal axis wind turbines (HAWTs) have maintained dominance in the wind energy sector for many decades. Nevertheless, the limitations associated with HAWTs, including their significant environmental footprint, intermittent energy production, and reliance on high wind speeds, have prompted the exploration of alternative wind energy solutions. Among these alternatives, vertical axis wind turbines (VAWTs) have emerged as a promising technology deserving of in-depth exploration and consideration.

The concept of VAWTs has roots dating back centuries, with early designs credited to Persian engineers and subsequent refinements by European inventors. Despite their historical origins, VAWTs have, until recently, remained somewhat overshadowed by their horizontal axis counterparts. However, recent advancements in materials, aerodynamics, and control systems have reignited interest in VAWTs, sparking a renewed focus on research and development efforts.

The Savonius rotor, named after its Finnish inventor Sigurd Johannes Savonius, is known for its simple and robust design. Unlike the more common Darrieus and Darrieus-like VAWTs, which rely on lift forces for power generation, Savonius turbines harness drag forces, making them well-suited for low wind speed environments. This distinctive design features two or more curved blades mounted on a vertical axis, resembling an "S" or "U" shape, and has been a subject of interest in wind energy research for several decades. Literature on Savonius-type VAWTs demonstrates their potential for low-wind-speed applications, making them ideal for use in urban and remote areas with inconsistent or modest wind resources. Their self-starting capability and ability to capture wind from any direction have made them attractive for off-grid power generation, small-scale distributed energy projects, and as a complementary technology alongside other renewable source. Researchers have explored various modifications and optimizations to enhance the

performance of Savonius VAWTs, including blade shape, aspect ratio, and the addition of guide vanes, to improve their efficiency and harness a wider range of wind speeds.

Saha et. al. [1] investigated the performance and stability of Savonius wind turbines in environments with low wind speed. The suitability of Savonius turbines for such critical environmental circumstances were also looked upon in their novel study.Sahin et. al. [2] focused intensely on various aspects regarding the design and manufacturing of vertical axis wind turbine blades. Their work also included the rotor design of Savonius turbine.Ashok et. al [3] discussed various recent developments and obstacles in small-scale vertical axis wind turbines with a particular focus on Savonius turbine.A review": Altan et. al [4] reviewed the techniques which can potentially enhance the performance of the Savonius turbines and other flow control devices.Thongpron et. al [5] experimented with Savonius wind turbines in different low wind speed conditions and analyzed the numerical results obtained from those trials.Gökçek et. al [6] conducted field tests, primarily focusing on wind tunnel experiments to explore the aerodynamic characteristics of helical Savonius rotors.Chen et al. [7] conducted a comprehensive analysis and assessment of different attributes pertaining to the operational efficiency of Savonius wind turbines equipped with blades featuring a helical shape.Özerdem et. al [8] investigated on Savonius rotors which involved conducting wind tunnel experiments and outdoor field tests to evaluate the efficiency and operational performance of Savonius rotors.Kamoji et al. [9] proposed strategies for enhancing the efficiency of Savonius rotors by employing twisted blades and subsequently carried out an analysis of their performance.Madavan et al. [10] conducted an examination of how blade twist and overlap ratio influence the operational effectiveness of helical Savonius rotors.Ali et al. [11] presented a research study focusing on a customized Savonius wind turbine designed specifically for use in urban settings. Additionally, the study included both experimental and numerical investigations into this particular subject matter.Abdullah et al. [12] utilized finite element analysis to scrutinize the structural characteristics and integrity of Savonius rotors. This method allowed them to investigate how various forces and stresses impact the rotor's performance and durability, providing valuable insights into its mechanical behavior and potential improvements in design and materials.Rezazadeh et al. [13] conducted experimental research on Savonius rotors, with a specific focus on designing a Savonius rotor optimized for operating effectively under low wind speed conditions.

This paper aims to provide a comprehensive examination of helicity around vertical axis wind turbine unde low subsonic flow condition. Vertical axis wind turbines, with a particular emphasis on the Savonius-type VAWTs. As the world seeks sustainable energy solutions, understanding the unique attributes and flow physics behine working principle of Savonius-type vertical axis wind turbines is crucial. Through this study, we hope to shed light on the promise and challenges of Savonius VAWTs and their contribution to a cleaner and more sustainable energy future.

Computational Technique

To begin, a three-dimensional model of wind turbine consisting of 7 blades is de-signed with help of SolidWorks modeling software. The CAD model of the turbine consists of 7 semi-circular shaped blades. The parameters and dimensions of the designed rotor are provided in the table 1. Additionally, a three-dimensional rectangular flow domain surrounding the rotor was also constructed.

Subsequent to the CAD model preparations, the three-dimensional renditions of both the rotor and stator were imported into the Geometry module of Ansys. Following successful import into Ansys, the geometry seamlessly transitioned to the meshing component, where the overarching goal was to discretize the flow domain. The rotor domain was discretized using tetrahedron elements due to their lower computational cost. Tetrahedron elements were chosen for their comparative efficiency in simulating transient motion of the moving mesh structure. The rotor domain comprised 264,646 nodes and 882,983 elements. The discretized model was then transferred to CFX for physics setup. In the CFX environment, the problem was configured

for transient analysis. For the physics setup, a k-epsilon viscous model was employed, considering the turbulent flow characteristics around the wind turbine. Boundary layer conditions were established with an inlet helicity set at 7 m/s in the positive x-direction. The rated rotational speed of the wind turbine was assumed to be 100 RPM. The fluid medium under consideration was air. A schematic diagram of the entire domain is provided in the figure below. Additionally, schematic diagrams illustrating the mesh created for both the rotor and stator are presented in the figure below.

Table1: Design specification of the rotor

Types of Test Blade	**Vertical axis wind turbine (Savonious)**
Blade Height	1750mm
Blade Diameter	1400mm
Blade Thickness	10mm
No. of Blades	7nos.
Aspect Ratio	0.8
Blade spacing	500mm

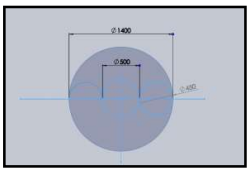

Fig 1: Top view of the rotor model along with dimension

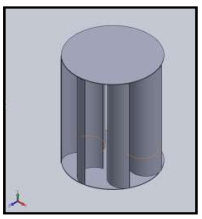

Fig 2: Isometric view of the rotor design

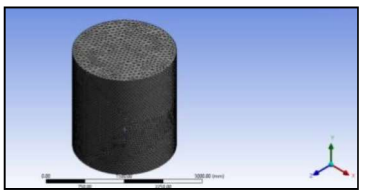

Fig 3: Schematics diagram of the mesh generated for rotor

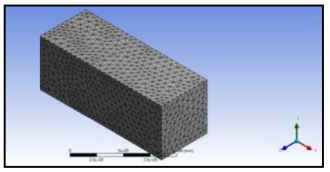

Fig 4: Schematic diagram of the mesh created for stator domain (Flow Domain)

Results & Discussions

This study describes qualitative observations of helicity variations within the flow field of a Vertical Axis Wind Turbine (VAWT). The analysis of helicity variations in the flow field was conducted using Ansys CFX. The wind velocity was assumed to be 7m/sec in the positive X direction, and the rated rotational speed was set at 100 r.p.m. The simulation conducted in this paper follows a steady-transient approach, and the turbine under investigation is a Savonius drag-type turbine. Data collection points were selected at specific timesteps: timestep 4, timestep 14, timestep 28, timestep 42, timestep 56, and timestep 88. Helicity distribution data was collected from the mid-section of the flow domain, situated along the XZ plane.
Helicity in fluid dynamics is a mathematically generated quantity that describes the degree of twist or linkage between the velocity and vorticity (rotational) fields in a fluid flow. It is often used to study the behavior of turbulence in fluid flow. Helicity denoted by H , can be calculated mathematically as follows,

$$H = \iiint (v \cdot \omega) dv$$

Where, v and ω are the velocity vector field and vorticity vector field respectively. Vorticity vector field is nothing but curl of velocity vector field ($\omega = \nabla \times V$). Triple integration signifies the entire volume of interest.

In the above equation, the dot product of velocity vector and vorticity vector is calculculated at the point of interest. And then that value is integrated over the entire volume. The resulting value represents the helicity of the fluid flow. Helicity is a useful concept in fluid dynamics, especially in the study of turbulence and in situations where the twisting or linking of vortices is of interest, such as in the study of magnetic fields in astrophysics and plasma physics.

During timestep 4, the initial condition, the airflow toward the positive X axis strikes the windward concave portion of the rotor blade, leading to a very high helicity, depicted in yellow. In contrast, the helicity at the leeward portion of the same blade is notably low, represented in blue. The blade immediately above this one exhibits very high helicity at a specific point on the leading, leeward edge. The diagram at timestep 4 also reveals a region of high helicity on the right-side portion of the rotor, indicating the rotor's clockwise rotation. Similarly, on the left side of the rotor, there is a region of low helicity and spots with low-helicity regions. The right side of the rotor can be referred to as the stagnation zone, where the helicity is negligible. Closer scrutiny reveals two primary helicity fluctuations in the center portion, indicating that blades align along this line.

At timestep 14, multiple variations along the centerline are observable. These variations result from the rotation of the rotor, bringing multiple blades into contact with the airflow, leading to helicity and resulting momentum transfer. This variation from timestep 4 is an indication of the increase in rotor speed and the subsequent decrease in helicity.

At timestep 28, high-helicity regions still exist on the right side of the rotor. However, there are more concentrated lower variations of low-helicity in regions at the concave and leading edge of the maximum blades. Some regions of low-velocity in swirling strenth can be observed on both sides of the plot. The concentration of fluctuations on both sides, in the high helicity, indicates a concentration of high stress in the rotor and rotor rotation.

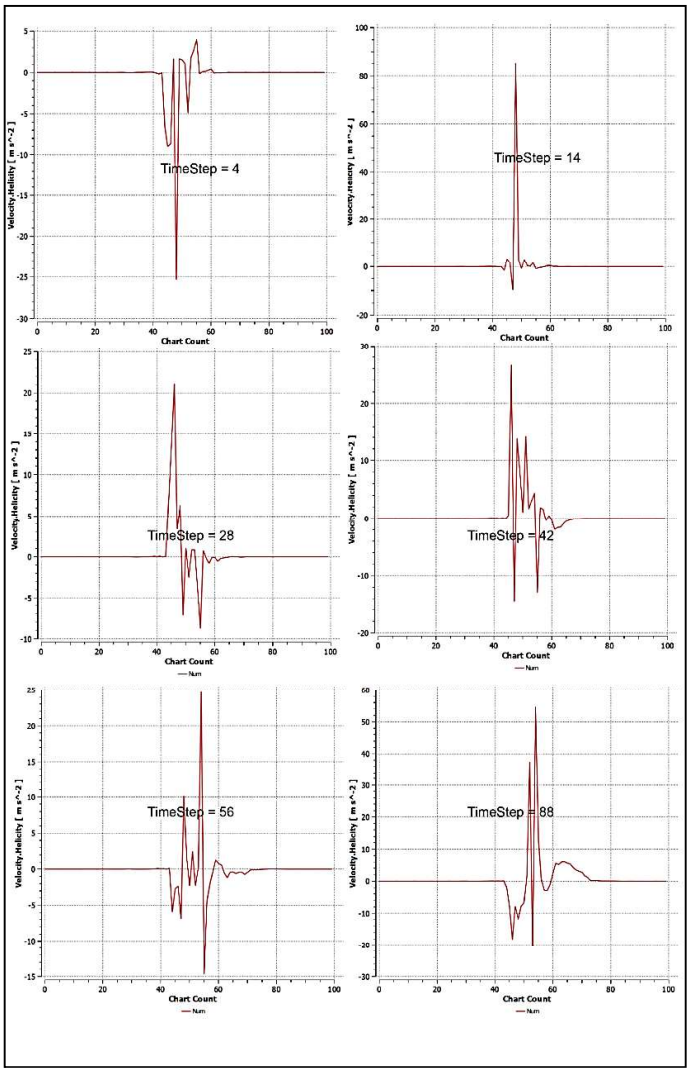

Fig 5: Helicity distribution plot along mid-section of flow domain

At timestep 42, the reduction of fluctuation of parameter in first half of the plot can be noticed, which indicates further decrease in the helicity in that particular points.
At timestep 56, It can be also noticed that the variation of helicity is more uniform in the flow field. This is repsented by more balanced distribution of helicity profile in the plot under study.
At timestep 88, the stress concentration in the flow field in unvarying through most portion of the flow field. Only in the extreme right side of the rotor a fluctuation indicating high helicity can be spotted. That is the thrust force which rotates the rotor in the tangential direction with the leading edge of the blade.

Conclusion

It is apparent that this drag-type vertical axis wing turbine displays an adverse helicity gradient along roughly half of its blades. These regions of high helicity do not play a role in generating the overall moment. Conversely, the presence of low-helicity regions in the leeward or right half of the rotor primarily indicates lower velocity swirling strength values, indicating the dissipation of energy in the form of eddies. Nonetheless, the knowledge gleaned from this study can lay the groundwork for future optimizations of blade models and configurations. These prospective improvements hold the potential to significantly boost the efficiency of drag-type vertical axis wing turbines.

References

1. Saha, U., Akhtar, M. S., & Selvaraj, P. (2016). Performance of a Savonius wind turbine for low wind speed applications: A review. Renewable and Sustainable Energy Reviews, 60, 41-52.

2. Sahin, B., & Yilmaz, S. (2008). Design and manufacturing of a vertical axis wind turbine blade. Renewable Energy, 33(11), 2324-2333.

3. Ashok, A., Muniappan, A., & Krishnamurthy, R. (2015). Recent developments and challenges in small-scale vertical axis wind turbines. Renewable and Sustainable Energy Reviews, 52, 665-677.

4. Altan, H., & Hacioglu, A. (2020). Performance enhancement of Savonius wind turbine using flow control devices: A review. Renewable and Sustainable Energy Reviews, 134, 110331.

5. Thongpron, J., Kanog, T., & Polprasert, C. (2016). Experimental and numerical investigations of a Savonius wind turbine for low wind speed applications. Energy Conversion and Management, 121, 126-138.

6. Gökçek, M., & Bayülken, A. (2011). Wind tunnel and field tests for the investigation of the aerodynamic performance of a helical Savonius rotor. Renewable Energy, 36(3), 1111-1120.

7. Chen, W. C., & Kuo, C. C. (2018). A review of Savonius wind turbine with helical-shaped blades. Journal of Renewable and Sustainable Energy, 10(3), 034701.

8. Özerdem, B., & Koç, M. (2007). Wind tunnel and outdoor experiments for performance assessment of Savonius rotors. Renewable Energy, 32(11), 1844-1857.

9. Kamoji, M. A., & Patil, S. D. (2013). Performance analysis of Savonius rotor with twisted blades. Energy Procedia, 33, 212-219.

10. Madavan, N. K., & Radhakrishnan, T. K. (2008). Performance analysis of a helical Savonius rotor: Effect of blade twist and overlap ratio. Journal of Solar Energy Engineering, 130(4), 041011.

11. Ali, M. H., Ahmed, T., & Saad, M. A. (2020). Experimental and numerical investigation of modified Savonius wind turbine for urban applications. Energy, 203, 117868.

12. Abdullah, M. M. A. B., & Ahmed, T. Y. (2017). Investigation of Savonius rotor using finite element analysis. Journal of Engineering Science and Technology, 12(8), 2165-2174.

13. Rezazadeh, S., & Gorji-Bandpy, M. (2013). Design and experimental analysis of a Savonius rotor for low wind speed conditions. Energy Conversion and Management, 75, 348-356.

Chapter 5

Explorative Study of Evolution of Vorticity Distribution in the Flow Field around Savonious Turbine

Abhishek Poddar[1*],Samrat Biswas[1], Sayan Paul[1,] Suman Kumar Ghosh[1], Soumya Ghosh[5], Soumak Bose[1]

Swami Vivekananda University, Barrackpore 700 121, INDIA
Corresponding author* Email ID: abhishekp@svu.ac.in

Abstract

This paper introduces an exploratory investigation into the flow field surrounding Savonius wind turbines. This specific turbine design deviates from convention due to its unique capacity to harness valuable energy from the air stream, setting it apart from conventional wind turbines. It boasts straightforward construction, rapid startup, continuous operational capabilities, wind utilization from any direction, the potential to achieve higher angular velocities during operation, and minimal noise emissions. Furthermore, it significantly reduces wear and tear on moving components, making it an attractive machinery option. Throughout history, various adaptations of this device have been envisioned, enhancing the versatility of vertical axis wind turbines. The primary aim of this study is to visually depict and attempt to comprehend the variation in vorticity distribution around a vertical axis wind turbine (VAWT), particularly the Savonius-type wind turbine, operating under subsonic flow conditions.

Keywords: VAWT, Savonious Type Turbine, Wind Turbine

Introduction

In the pursuit of sustainable and renewable energy sources to meet the ever-expanding global energy demand and combat the adverse impacts of climate change, wind power has emerged as a leading contender. Traditional horizontal axis wind turbines (HAWTs) have maintained dominance in the wind energy sector for many decades. Nevertheless, the limitations associated with HAWTs, including their significant environmental footprint, intermittent energy production, and reliance on high wind speeds, have prompted the exploration of alternative wind energy solutions. Among these alternatives, vertical axis wind turbines (VAWTs) have emerged as a promising technology deserving of in-depth exploration and consideration.

The concept of VAWTs has roots dating back centuries, with early designs credited to Persian engineers and subsequent refinements by European inventors. Despite their historical origins, VAWTs have, until recently, remained somewhat overshadowed by their horizontal axis counterparts. However, recent advancements in materials, aerodynamics, and control systems have reignited interest in VAWTs, sparking a renewed focus on research and development efforts.

One notable subtype of VAWTs, the Savonius-type wind turbine, merits special attention. The Savonius rotor, named after its Finnish inventor Sigurd Johannes Savonius, is characterized by its simple and robust design. Unlike the more common Darrieus and Darrieus-like VAWTs, which rely on lift forces to generate power, Savonius turbines harness drag forces, making them particularly suitable for low wind speed environments. This unique design features two or more curved blades mounted on a vertical axis, resembling an "S" or "U" shape, and has been a focus of interest in wind energy research for several decades.

Literature on Savonius-type VAWTs demonstrates their potential for low-wind-speed applications, making them ideal for use in urban and remote areas with inconsistent or modest wind resources. Their self-starting capability and ability to capture wind from any direction have made them attractive for off-grid power

generation, small-scale distributed energy projects, and as a complementary technology alongside other renewable source. Researchers have explored various modifications and optimizations to enhance the performance of Savonius VAWTs, including blade shape, aspect ratio, and the addition of guide vanes, to improve their efficiency and harness a wider range of wind speeds.

Saha et. al. [1] investigated the performance and stability of Savonius wind turbines in environments with low wind speed. The suitability of Savonius turbines for such critical environmental circumstances were also looked upon in their novel study.Sahin et. al. [2] focused intensely on various aspects regarding the design and manufacturing of vertical axis wind turbine blades. Their work also included the rotor design of Savonius turbine.Ashok et. al [3] discussed various recent developments and obstacles in small-scale vertical axis wind turbines with a particular focus on Savonius turbine.A review": Altan et. al [4] reviewed the techniques which can potentially enhance the performance of the Savonius turbines and other flow control devices.Thongpron et. al [5] experimented with Savonius wind turbines in different low wind speed conditions and analyzed the numerical results obtained from those trials.Gökçek et. al [6] conducted field tests, primarily focusing on wind tunnel experiments to explore the aerodynamic characteristics of helical Savonius rotors.Chen et al. [7] conducted a comprehensive analysis and assessment of different attributes pertaining to the operational efficiency of Savonius wind turbines equipped with blades featuring a helical shape.Özerdem et. al [8] investigated on Savonius rotors which involved conducting wind tunnel experiments and outdoor field tests to evaluate the efficiency and operational performance of Savonius rotors.Kamoji et al. [9] proposed strategies for enhancing the efficiency of Savonius rotors by employing twisted blades and subsequently carried out an analysis of their performance.Madavan et al. [10] conducted an examination of how blade twist and overlap ratio influence the operational effectiveness of helical Savonius rotors.Ali et al. [11] presented a research study focusing on a customized Savonius wind turbine designed specifically for use in urban settings. Additionally, the study included both experimental and numerical investigations into this particular subject matter.Abdullah et al. [12] utilized finite element analysis to scrutinize the structural characteristics and integrity of Savonius rotors. This method allowed them to investigate how various forces and stresses impact the rotor's performance and durability, providing valuable insights into its mechanical behavior and potential improvements in design and materials.Rezazadeh et al. [13] conducted experimental research on Savonius rotors, with a specific focus on designing a Savonius rotor optimized for operating effectively under low wind speed conditions.

This paper aims to provide a comprehensive examination of vorticity distribution around vertical axis wind turbine unde low subsonic flow condition. Vertical axis wind turbines, with a particular emphasis on the Savonius-type VAWTs. As the world seeks sustainable energy solutions to combat climate change and reduce reliance on fossil fuels, understanding the unique attributes and flow physics behine working principle of Savonius-type vertical axis wind turbines is crucial. Through this study, we hope to shed light on the promise and challenges of Savonius VAWTs and their contribution to a cleaner and more sustainable energy future.

Computational Technique

To begin, a three-dimensional model of wind turbine consisting of 7 blades is designed with help of SolidWorks modeling software. The CAD model of the turbine consists of 7 semi-circular shaped blades. The parameters and dimensions of the designed rotor are provided in the table 1.

Table1: Design specification of the rotor

Types of Test Blade	**Vertical axis wind turbine (Savonious)**

Blade Height	1750mm
Blade Diameter	1400mm
Blade Thickness	10mm
No. of Blades	7nos.
Aspect Ratio	0.8
Blade spacing	500mm

Additionally a three-dimensional rectangular flow domain around the rotor was also drawn. After preparing the CAD models the three-dimensional models of the rotor and stator were imported to Geometry module of the Ansys. Then post importing the geometry to the Ansys, it was transferred to the meshing component in order to discretize the flow domain. The rotor domain was discretized utilizing tetrahedron element, because of low computation cost of the tetrahedron element. Tetrahedron element was utilized because of its comparatively higher efficiency under transient simulation of moving mesh structure. The rotor domain consists of 264646 numbers of nodes and 882983 numbers of elements. The discretized model was transferred to the CFX for physics setup. Under CFX the problem was set up to be solved for transient analysis. For physics setup k-epsilon viscous model is implemented along with transient blade row considering the turbulent flow characteristics for the flow around the wind turbine. In order to set up boundary layer conditions the inlet velocity is considered 7m/s in the positive x-direction. The rated rotational speed of the wind turbine is considered to be 100rpm. The fluid medium is considered as air. Schematic diagram of full domain is shown in figure below. Along with that schematic diagram of mesh created for rot and stator is also shown in figure below.

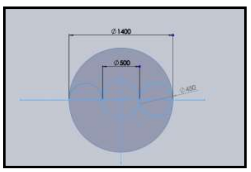

Fig 1: Top view of the rotor model along with dimension

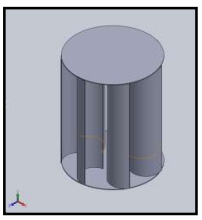

Fig 2: Isometric view of the rotor design

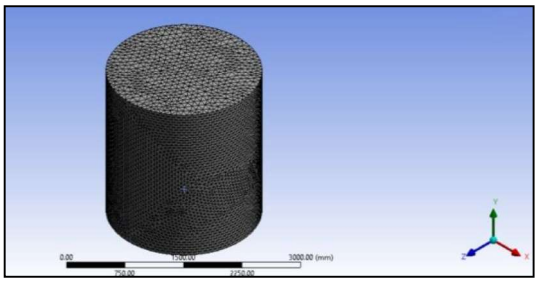

Fig 3: Schematics diagram of the mesh generated for rotor

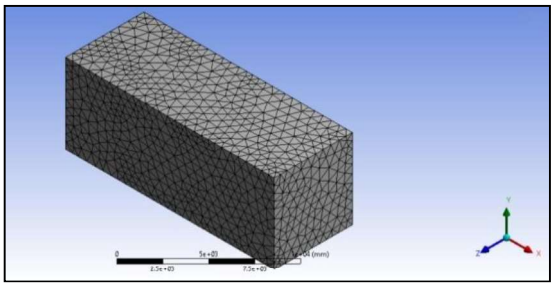

Fig 4: Schematic diagram of the mesh created for stator domain

Results & Discussions

This study describes qualitative observations of vorticity variations within the flow field of a Vertical Axis Wind Turbine (VAWT). The analysis of vorticity variations in the flow field was conducted using Ansys CFX. The wind velocity was assumed to be 7m/sec in the positive X direction, and the rated rotational speed was set at 100 r.p.m. The simulation conducted in this paper follows a steady-transient approach, and the turbine under investigation is a Savonius drag-type turbine. Data collection points were selected at specific timesteps: timestep 4, timestep 14, timestep 28, timestep 42, timestep 56, and timestep 88. Vorticity distribution data was collected from the mid-section of the flow domain, situated along the XZ plane.

Vorticity is a concept in fluid dynamics that describes the local spinning or rotation of fluid elements within a fluid flow. It is a vector quantity and represents the curl of the velocity field of the fluid. In simpler terms, vorticity indicates the presence and magnitude of rotation within a fluid at a given point in space. When vorticity is zero at a particular point, it means that the fluid at that point is not rotating; when it is nonzero, it indicates the presence of rotation.

Mathematically vorticity (ω) is calculatged as the curl of the velocity vector ($\vec{v}$) of a fluid flow. In a three-dimensional Cartesian co-ordinate system (x, y, z), the vorticity vector is given by $\omega = \nabla \times V$.

In the analysis diagram the vorticity distribution is denoted by the blue and yellow, red colours. Blue colour denotes the lowest vorticity and towards the yellow and red colour it denotes the comparatively higher vorticity. From the diagram of the timestep 4, it can be seen a region of high vorticity at the right-side portion of the rotor what means it direct the rotation of the rotor at the clockwise direction. Similarly at the left side of the rotor portion of low vorticity and spots of low-vorticity regions can be seen. The portions of red and yellow colours that is the high-vorticity regions at the right side of the rotor can be termed as the stagnation zone where velocity is very negligible.

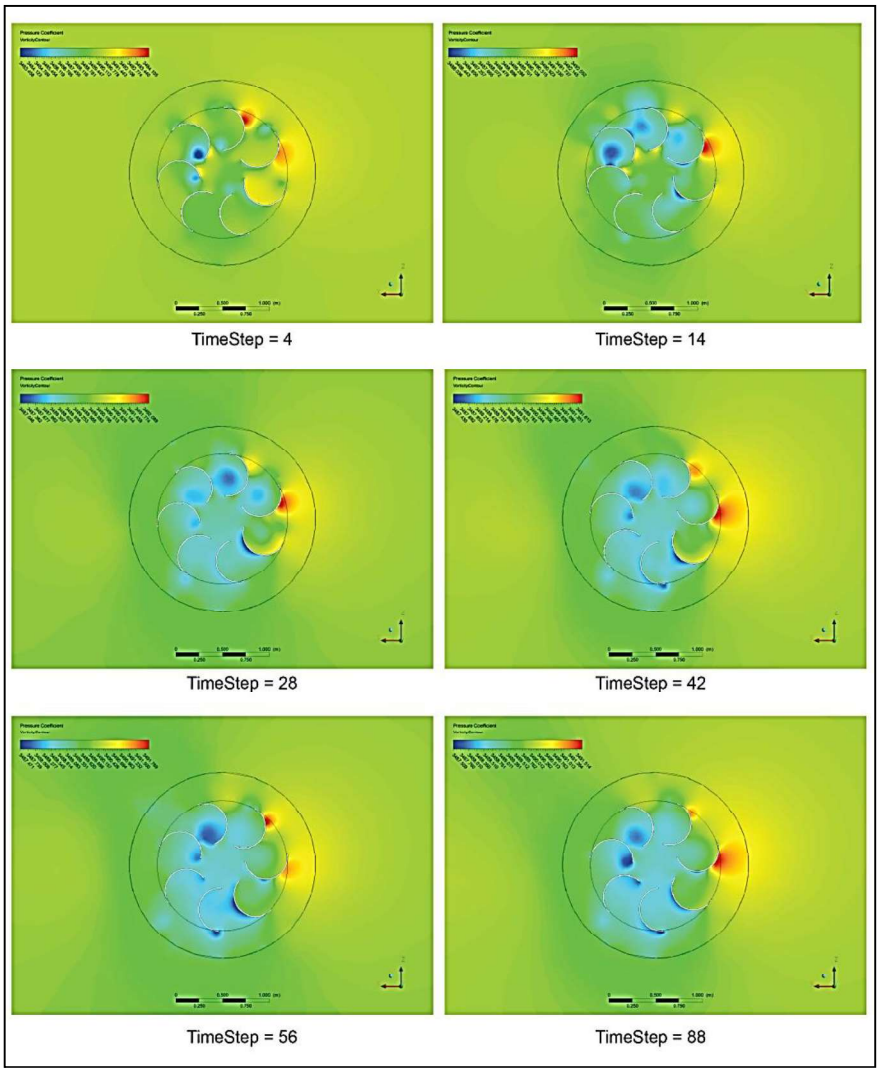

Fig 5: Vorticity distribution contour around VAWT.

At timestep 14, it can be noticed that the colour on the right side of the rotor blades is gradually turning into blue where there isstill a spot of red at the leeward and convex portion of a blade. Comparatively the spots of deep blue colour are more on the concave parts of the blade at the left of the rotor. This variation of colours from the timestep 4 is an indication of the increase in the rotor speed with the subsequent decrease in the vorticity.

At timestep 28, where there are still high-vorticity regions that is spot of yellow and red at the right side of the rotor but there are subsequently more concentrated blue spots of low-vorticity regions at the concave and leading edge of the maximum blades. The region of some low-vorticity blue zone can be seen at the leeward convex zone of some bottom blades. The concentration of yellow and red colour that is high vorticity zone indicates concentration of high stress in the right side of the rotor and rotation of rotor in the clockwise direction.

At timestep 42, the increase in the size of the red spots can be noticed which indicates further decrease in the velocity a that particular points. Subsequently on the other blades some blades show the blue colour to be fading and on other blades the blue colours getting deeper.

At timestep 56, at the right portion of the rotor the yellow and red colour fading gradually and the blue colour on the other blades getting deeper. The red colour spot was bigger and deeper in the previous instance which has reduced to smaller spots and fading in colour. It can be also noticed that the variation of vorticity is more uniform in the flow field.

At timestep 88, the stress concentration in the flow field in unvarying through most portion of the flow field. Only in the extreme right side of the rotor a large spot of red colour indicating very high vorticity can be spotted. That is the thrust force which rotates the rotor in the tangential direction with the leading edge of the blade. The speed of rotation is maximum at this instance and variation of vorticity in negligible.

Conclusion

It is evident that this drag-type vertical axis wind turbine exhibits an unfavorable vorticity gradient along approximately half of its blades. These areas with high vorticity do not contribute to the overall moment generation. The presence of a low vorticity region in the leeward or left half portion of the rotor predominantly signifies reduced vorticity, indicating the dissipation of energy in the form of eddies. However, these observations can serve as a foundation for optimizing blade models and configurations in the future. Such optimizations hold the potential to significantly enhance the efficiency of drag-type vertical axis wind turbines, making them more effective.

References

1. Saha, U., Akhtar, M. S., & Selvaraj, P. (2016). Performance of a Savonius wind turbine for low wind speed applications: A review. Renewable and Sustainable Energy Reviews, 60, 41-52.

2. Sahin, B., & Yilmaz, S. (2008). Design and manufacturing of a vertical axis wind turbine blade. Renewable Energy, 33(11), 2324-2333.

3. Ashok, A., Muniappan, A., & Krishnamurthy, R. (2015). Recent developments and challenges in small-scale vertical axis wind turbines. Renewable and Sustainable Energy Reviews, 52, 665-677.

4. Altan, H., & Hacioglu, A. (2020). Performance enhancement of Savonius wind turbine using flow control devices: A review. Renewable and Sustainable Energy Reviews, 134, 110331.

5. Thongpron, J., Kanog, T., & Polprasert, C. (2016). Experimental and numerical investigations of a Savonius wind turbine for low wind speed applications. Energy Conversion and Management, 121, 126-138.

6. Gökçek, M., & Bayülken, A. (2011). Wind tunnel and field tests for the investigation of the aerodynamic performance of a helical Savonius rotor. Renewable Energy, 36(3), 1111-1120.

7. Chen, W. C., & Kuo, C. C. (2018). A review of Savonius wind turbine with helical-shaped blades. Journal of Renewable and Sustainable Energy, 10(3), 034701.

8. Özerdem, B., & Koç, M. (2007). Wind tunnel and outdoor experiments for performance assessment of Savonius rotors. Renewable Energy, 32(11), 1844-1857.

9. Kamoji, M. A., & Patil, S. D. (2013). Performance analysis of Savonius rotor with twisted blades. Energy Procedia, 33, 212-219.

10. Madavan, N. K., & Radhakrishnan, T. K. (2008). Performance analysis of a helical Savonius rotor: Effect of blade twist and overlap ratio. Journal of Solar Energy Engineering, 130(4), 041011.

11. Ali, M. H., Ahmed, T., & Saad, M. A. (2020). Experimental and numerical investigation of modified Savonius wind turbine for urban applications. Energy, 203, 117868.

12. Abdullah, M. M. A. B., & Ahmed, T. Y. (2017). Investigation of Savonius rotor using finite element analysis. Journal of Engineering Science and Technology, 12(8), 2165-2174.

13. Rezazadeh, S., & Gorji-Bandpy, M. (2013). Design and experimental analysis of a Savonius rotor for low wind speed conditions. Energy Conversion and Management, 75, 348-356.

Chapter 6

An Exploration of Eddy Viscosity Changes in longitudinal direction for Flow around Vertical Axis Wind Turbine

Arijit Mukherjee[1], Suman Kumar Ghosh[1,] Sayan Paul[1], Soumya Ghosh[1], Soumak Bose[1,] Samrat Biswas[1]

Swami Vivekananda University, Barrackpore 700 121, INDIA
Corresponding author* Email ID: arijitm@svu.ac.in

Abstract

This paper presents an exploratory investigation into the flow field surrounding Savonius wind turbines. This particular turbine design is unconventional in nature due to its unique ability to harness valuable energy from the air stream, distinguishing it from conventional wind turbines. It boasts a straightforward construction, rapid startup, continuous operational capacity, wind utilization from any direction, the potential to achieve higher angular velocities during operation, and minimal noise emissions. Additionally, it significantly reduces wear and tear on moving components, making it an attractive machinery option. Throughout history, various adaptations of this device have been envisioned, further enhancing the versatility of vertical axis wind turbines. The primary objective of this study is to visually depict and endeavor to comprehend the variation in eddy viscosity distribution around a vertical axis wind turbine (VAWT), specifically the Savonius-type wind turbine, operating under subsonic flow conditions.

Keywords: VAWT, Savonious Type Turbine, Wind Turbine

Introduction

The search for sustainable and renewable energy sources to meet the ever-growing global energy demand and combat the adverse impacts of climate change, wind power has emerged as a top contender. Conventional horizontal axis wind turbines (HAWTs) have long dominated the wind energy landscape. However, the limitations of HAWTs, including their significant environmental footprint, intermittent energy production, and reliance on high wind speeds, have driven the exploration of alternative wind energy solutions. Among these alternatives, vertical axis wind turbines (VAWTs) have emerged as a promising technology deserving of thorough examination and consideration.

The concept of VAWTs has ancient roots, with early designs attributed to Persian engineers and later refinements by European inventors. Despite their historical heritage, VAWTs have, until recently, remained relatively overshadowed by their horizontal axis counterparts. Nevertheless, recent advancements in materials, aerodynamics, and control systems have rekindled interest in VAWTs and have sparked a renewed focus on research and development efforts.

One noteworthy subtype of VAWTs, the Savonius-type wind turbine, merits special attention. The Savonius rotor, named after its Finnish inventor Sigurd Johannes Savonius, is known for its simple and robust design. Unlike the more common Darrieus and Darrieus-like VAWTs, which rely on lift forces for power generation, Savonius turbines harness drag forces, making them well-suited for low wind speed environments. This distinctive design features two or more curved blades mounted on a vertical axis, resembling an "S" or "U" shape, and has been a subject of interest in wind energy research for several decades. Literature on Savonius-type VAWTs demonstrates their potential for low-wind-speed applications, making them ideal for use in urban and remote areas with inconsistent or modest wind resources. Their self-starting capability and ability to capture wind from any direction have made them attractive for off-grid

power generation, small-scale distributed energy projects, and as a complementary technology alongside other renewable source. Researchers have explored various modifications and optimizations to enhance the performance of Savonius VAWTs, including blade shape, aspect ratio, and the addition of guide vanes, to improve their efficiency and harness a wider range of wind speeds.

Saha et. al. [1] investigated the performance and stability of Savonius wind turbines in environments with low wind speed. The suitability of Savonius turbines for such critical environmental circumstances were also looked upon in their novel study.Sahin et. al. [2] focused intensely on various aspects regarding the design and manufacturing of vertical axis wind turbine blades. Their work also included the rotor design of Savonius turbine.Ashok et. al [3] discussed various recent developments and obstacles in small-scale vertical axis wind turbines with a particular focus on Savonius turbine.A review": Altan et. al [4] reviewed the techniques which can potentially enhance the performance of the Savonius turbines and other flow control devices.Thongpron et. al [5] experimented with Savonius wind turbines in different low wind speed conditions and analyzed the numerical results obtained from those trials.Gökçek et. al [6] conducted field tests, primarily focusing on wind tunnel experiments to explore the aerodynamic characteristics of helical Savonius rotors.Chen et al. [7] conducted a comprehensive analysis and assessment of different attributes pertaining to the operational efficiency of Savonius wind turbines equipped with blades featuring a helical shape.Özerdem et. al [8] investigated on Savonius rotors which involved conducting wind tunnel experiments and outdoor field tests to evaluate the efficiency and operational performance of Savonius rotors.Kamoji et al. [9] proposed strategies for enhancing the efficiency of Savonius rotors by employing twisted blades and subsequently carried out an analysis of their performance.Madavan et al. [10] conducted an examination of how blade twist and overlap ratio influence the operational effectiveness of helical Savonius rotors.Ali et al. [11] presented a research study focusing on a customized Savonius wind turbine designed specifically for use in urban settings. Additionally, the study included both experimental and numerical investigations into this particular subject matter.Abdullah et al. [12] utilized finite element analysis to scrutinize the structural characteristics and integrity of Savonius rotors. This method allowed them to investigate how various forces and stresses impact the rotor's performance and durability, providing valuable insights into its mechanical behavior and potential improvements in design and materials.Rezazadeh et al. [13] conducted experimental research on Savonius rotors, with a specific focus on designing a Savonius rotor optimized for operating effectively under low wind speed conditions.

This paper aims to provide a comprehensive examination of eddy viscosity around vertical axis wind turbine unde low subsonic flow condition. Vertical axis wind turbines, with a particular emphasis on the Savonius-type VAWTs. As the world seeks sustainable energy solutions to combat climate change and reduce reliance on fossil fuels, understanding the unique attributes and flow physics behine working principle of Savonius-type vertical axis wind turbines is crucial. Through this study, we hope to shed light on the promise and challenges of Savonius VAWTs and their contribution to a cleaner and more sustainable energy future.

Computational Technique

To To begin, a three-dimensional model of wind turbine consisting of 7 blades is de-signed with help of SolidWorks modeling software. The CAD model of the turbine consists of 7 semi-circular shaped blades. The parameters and dimensions of the designed rotor are provided in the table 1. Additionally, a three-dimensional rectangular flow domain surrounding the rotor was also constructed.

Subsequent to the CAD model preparations, the three-dimensional renditions of both the rotor and stator were imported into the Geometry module of Ansys. Following successful import into Ansys, the geometry seamlessly transitioned to the meshing component, where the overarching goal was to discretize the flow domain. The rotor domain was discretized using tetrahedron elements due to their lower computational cost. Tetrahedron elements were chosen for their comparative efficiency in simulating transient motion of the

moving mesh structure. The rotor domain comprised 264,646 nodes and 882,983 elements. The discretized model was then transferred to CFX for physics setup. In the CFX environment, the problem was configured for transient analysis. For the physics setup, a k-epsilon viscous model was employed, considering the turbulent flow characteristics around the wind turbine. Boundary layer conditions were established with an inlet eddy viscosity set at 7 m/s in the positive x-direction. The rated rotational speed of the wind turbine was assumed to be 100 RPM. The fluid medium under consideration was air. A schematic diagram of the entire domain is provided in the figure below. Additionally, schematic diagrams illustrating the mesh created for both the rotor and stator are presented in the figure below.

Table1: Design specification of the rotor

Types of Test Blade	**Vertical axis wind turbine (Savonious)**
Blade Height	1750mm
Blade Diameter	1400mm
Blade Thickness	10mm
No. of Blades	7nos.
Aspect Ratio	0.8
Blade spacing	500mm

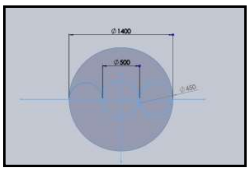

Fig 1: Top view of the rotor model along with dimension

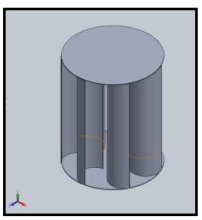

Fig 2: Isometric view of the rotor design

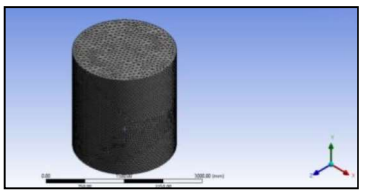

Fig 3: Schematics diagram of the mesh generated for rotor

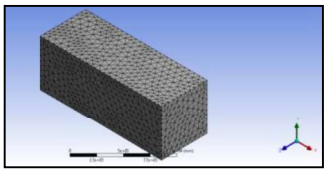

Fig 4: Schematic diagram of the mesh created for stator domain (Flow Domain)

Results & Discussions

It is well understood, that viscosity represents a resistance to shearing flows, where adjacent layers move in parallel at varying speeds. Eddy viscosity, also known as turbulent viscosity, is a coefficient that relates the average shear stress in turbulent water or airflow to the vertical velocity gradient. It depends on both the fluid's density and its proximity to the riverbed or ground surface.

The concept of eddy viscosity plays a fundamental role in the von Karman–Prandtl equation, which describes velocity distribution in turbulent flow. It also holds significant importance in calculating rates of evaporation or cooling induced by wind and quantifying the shear stress applied by rivers to particles moving along their riverbeds.

Eddy viscosity models have the capability to dissipate energy from larger scales, effectively replicating the inherently dissipative characteristics of turbulence. In our investigation, we examined the flow field of a drag-type vertical axis wind turbine using transient simulation. The wind flows from the positive X-axis to the negative X-axis (from right to left in the figure). We set the turbine speed at 100 r.p.m., and the wind speed at 7 m/s. Various time steps were analyzed to study the eddy viscosity at different phases of the investigation. The eddy viscosity distribution data was collected from the mid-portion of the flow domain, along the XZ plane. Along this plane a line was taken, which runs through the miggle of the entire flow domain. Along this above mentioned line the data were extracted and plotted for comparative analysis.

During timestep 4, the initial condition, the airflow toward the positive X axis strikes the windward concave portion of the rotor blade, leading to a very high eddy viscosity, depicted in yellow. The blade immediately above this one exhibits very high eddy viscosity at a specific point on the leading, leeward edge. The diagram at timestep 4 also reveals a region of high eddy viscosity on the right-side portion of the rotor, indicating the rotor's clockwise rotation. Similarly, on the left side of the rotor, there is a region of low eddy viscosity and spots with low-eddy viscosity regions.

At timestep 14, multiple variations along the centerline are observable. These variations result from the rotation of the rotor, bringing multiple blades into contact with the airflow, leading to eddy viscosity and resulting momentum transfer. This variation from timestep 4 is an indication of the increase in rotor speed and the subsequent decrease in eddy viscosity.

At timestep 28, high-eddy viscosity regions still exist on the right side of the rotor. However, there are more concentrated lower variations of low-eddy viscosity in regions at the concave and leading edge of the maximum blades.

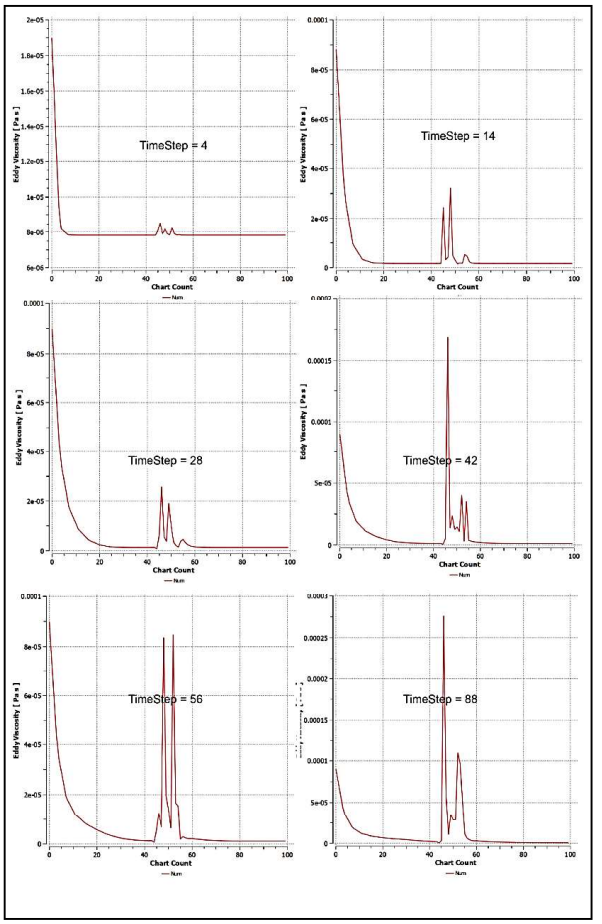

Fig 5: Eddy viscosity distribution plot along mid-section of flow domain

At timestep 42, the reduction of fluctuation of parameter in first half of the plot can be noticed, which indicates further decrease in the eddy viscosity in that particular points.
At timestep 56, It can be also noticed that the variation of eddy viscosity is more uniform in the flow field. This is repsented by more balanced distribution of eddy viscosity profile in the plot under study.
At timestep 88, the stress concentration in the flow field in unvarying through most portion of the flow field. Only in the extreme right side of the rotor a fluctuation indicating high eddy viscosity can be spotted. That is the thrust force which rotates the rotor in the tangential direction with the leading edge of the blade.

Conclusion

Fluctuations in eddy viscosity become apparent in the initial time steps, suggesting a need for design optimization. Furthermore, it's evident that this drag-type vertical axis wing turbine exhibits an unfavorable gradient in eddy viscosity along approximately half of its blades. These high eddy viscosity regions do not contribute to the overall moment generation. The presence of low-eddy viscosity regions in the leeward portion or right half of the rotor predominantly indicates lower velocity wirlign strength values, signifying the dissipation of energy in the form of eddies. Nevertheless, the insights gained from this study can serve as the foundation for optimizing blade models and configurations in the future. These forthcoming optimizations have the potential to enhance the efficiency of drag-type vertical axis wing turbines.

References

1. Saha, U., Akhtar, M. S., & Selvaraj, P. (2016). Performance of a Savonius wind turbine for low wind speed applications: A review. Renewable and Sustainable Energy Reviews, 60, 41-52.

2. Sahin, B., & Yilmaz, S. (2008). Design and manufacturing of a vertical axis wind turbine blade. Renewable Energy, 33(11), 2324-2333.

3. Ashok, A., Muniappan, A., & Krishnamurthy, R. (2015). Recent developments and challenges in small-scale vertical axis wind turbines. Renewable and Sustainable Energy Reviews, 52, 665-677.

4. Altan, H., & Hacioglu, A. (2020). Performance enhancement of Savonius wind turbine using flow control devices: A review. Renewable and Sustainable Energy Reviews, 134, 110331.

5. Thongpron, J., Kanog, T., & Polprasert, C. (2016). Experimental and numerical investigations of a Savonius wind turbine for low wind speed applications. Energy Conversion and Management, 121, 126-138.

6. Gökçek, M., & Bayülken, A. (2011). Wind tunnel and field tests for the investigation of the aerodynamic performance of a helical Savonius rotor. Renewable Energy, 36(3), 1111-1120.

7. Chen, W. C., & Kuo, C. C. (2018). A review of Savonius wind turbine with helical-shaped blades. Journal of Renewable and Sustainable Energy, 10(3), 034701.

8. Özerdem, B., & Koç, M. (2007). Wind tunnel and outdoor experiments for performance assessment of Savonius rotors. Renewable Energy, 32(11), 1844-1857.

9. Kamoji, M. A., & Patil, S. D. (2013). Performance analysis of Savonius rotor with twisted blades. Energy Procedia, 33, 212-219.

10. Madavan, N. K., & Radhakrishnan, T. K. (2008). Performance analysis of a helical Savonius rotor: Effect of blade twist and overlap ratio. Journal of Solar Energy Engineering, 130(4), 041011.

11. Ali, M. H., Ahmed, T., & Saad, M. A. (2020). Experimental and numerical investigation of modified Savonius wind turbine for urban applications. Energy, 203, 117868.

12. Abdullah, M. M. A. B., & Ahmed, T. Y. (2017). Investigation of Savonius rotor using finite element analysis. Journal of Engineering Science and Technology, 12(8), 2165-2174.

13. Rezazadeh, S., & Gorji-Bandpy, M. (2013). Design and experimental analysis of a Savonius rotor for low wind speed conditions. Energy Conversion and Management, 75, 348-356.

Chapter 7

In depth analysis of tribological characteristics of SS410 under pre and post heat treatment

Sayan Paul[1*]

Swami Vivekananda University, Barrackpore 700 121, INDIA
Corresponding author* Email ID: sayanp@svu.ac.in

Abstract
This concise abstract delves into a comprehensive analysis of the tribological characteristics of SS410 stainless steel both before and after heat treatment. The study investigates how heat treatment processes impact the material's friction, wear resistance, and surface properties. Through a thorough examination of wear rates, friction coefficients, and wear mechanisms, this research aims to provide crucial insights into the effectiveness of heat treatment in enhancing the tribological performance of SS410, offering valuable guidance for material selection and optimization in various engineering applications.

Keywords: Stainless steel 410, heat treatment, friction & wear, micro hardness, tribology.

Introduction

The study of friction and associated wear with that friction and associated lubrication in an interface in relative motion is the territory of tribology. For engineering product friction and wear plays a crucial role, so product quality and reliability depends on wear characteristics [1].To increase functional reliability of engineering materials various type of heat treatment plays an important roles. Not only heat treatments above recrystallization temperature but also sub-zero are treatments gaining much more attractions of researchers [2-7].And Stainless steels have huge utilisation in the modern world, although if its tonnage of use represent only about 4% of the cumulative steel production in India. The 2018 total steel produced surpassed 104 million tons in India [8]. Heat treatment is a process heating, soaking and subsequent quenching carried out, connected to a metals or metal composites in the strong state in a procedure as to create desired physical or mechanical properties. Hardening, annealing, tempering, normalizing etc. are most common heat treatment processes used to change the mechanical properties of designing materials especially steels Annealing is the kind of treatment most as often as possible connected so as to modify iron or steel materials and recrystallize its grain ferrite-pearlite microstructure; it is utilized where prolongations and obvious dimension of rigidity are required in engineering components [9-10].
Now a day's of Stainless steel is essential for industry application, commercial as well as products for household application. Austenitic stainless steel, type 304 (18Cr–8Ni) is an iron-nickel-chromium alloy and can't be heat hardened further. However, annealing is possible and annealed 304 stainless steel has wide application as a structural material under the severe conditions such as the nuclear power plants and the chemical plants, refrigeration and processing plants like paper, food, beverage, cryogenics transportation, machinery parts, car headers, architecture etc. industries because of high corrosion resistance, good toughness and ductility[28-30]. As earlier discussed these properties can further more enhanced by some surface treatment to increase reliability [14-15].
On the other hand, martensitic stainless steel grades consists of 11% – 17% Chromium (mass percent) containing carbon up to (0.15% - 1.0%) proved themselves a strong contending in industry needs for their properties, such as preferable resistance to corrosion;. These are usually very good inactive to high -

temperature oxidation and localized corrosion, e.g. pitting and crevice corrosion, and SCC in some aggressive environment like saltwater in seas. Earlier investigations concludes that these stainless steels are inert in chemical handling rather than austenitic grades [6,16].It is also extensively used in nuclear reactor due to its high strength[17]. Efendi Mabruri et al. investigate various mechanical properties of martensitic stainless steel 410- 1 Mo after heat treatment austenizing temperature zone. Experiment conclude that the steels treated at 1050°C steels exhibited greater impact resistance. Whereas were pre-austenitized at 950°C and 1100°C, tempered steels that exhibits the minimum pitting potential due to presence of carbides and coarse structured martensite containing high carbon percentage. [18].
So, many of researchers have investigated differently SS304 and SS410, but this paper will sought for a comparative study of dry sliding characteristics and Vickers micro hardness of these SS304 and SS410 steels after heat treatment.

Experimental details

AISI 304 and AISI 410 were used for this present experimental work. Total six samples of 304 and 5 samples of 410 were made; all the samples are of diameter 6 mm and length 30 mm as per the requirement of the multi tribo-tester. The chemical compositions of the out sourced material are as given below.

Table 1: Chemical composition % by mass of aisi 304

C	Si	P	S	Mn	Ni	Cr	Fe
0.08	1.00	0.04	0.03	2.00	8.00-10.50	18.00-20.00	Balance

Table 2: Chemical composition % by mass of aisi 410

C	Si	P	S	Mn	Ni	Cr	Fe
0.08 - 0.15	1.00	0.04	0.03	1.00	0.75	11.5-13.5	Balance

Heat Treatment

Heat treatments were done in a muffle furnace with a maximum temperature capacity of 1100 degree centigrade. As earlier discussed by some researcher SS 304 cannot be hardened further but can be soften.Five different heat treatment were selected based on feasibility of achieving their process parameters, these heat treatment are discussed in following section [2,12,19].
For annealing one sample of SS304 is placed in the muffle furnace in ambient temperature and heated up to 950°C with a rate of 10°C per minute, then allowed to soak for 2 hours inside the furnace and then allowed to cool inside the furnace
For normalizing one sample of SS304 is placed in the muffle furnace in ambient temperature and heated up to 950°C with a rate of 10°C per minute, then allowed to soak for 2 hours in the furnace and then allowed to cool in open atmosphere.
For oil quenching one sample of SS304 is placed in the muffle furnace in ambient temperature and heated up to 950°C with a rate of 10°C per minute, then allowed to soak for 2 hours inside the furnace and then sudden quenching is done by dipping the specimen in cutting oil (grade 44).
Two of SS304 samples are sensitized by heating them up to 660°C at a rate of 10°C per minute, then allowed to soak in furnace then cooled in open air up to atmospheric temperature. The one of sensitized

samples were again heated to 1040°C with same rising rate and soaked for 30 minutes and dipped in water for solution annealing [20].

For SS410 four samples were heat treated. Many of researcher have already been discussed different treatment procedure for martensitic steels, so based on our feasibility we have selected tempering and stress reliving followed by austenizing, annealing and process annealing [6,17,18,19].

So for austenizing two samples were heated to 950°C at elevation rate 10°C per minute and the allowed to soak for 30 min and then cooled in open atmosphere. Then one of sample was tempered at 320°C and another was at 650°C for 1 hours and then air cooled.

Other specimen of SS 410 was annealed at temperature 850°C then allowed to cool at closed furnace for softening. One specimen of 410 was process annealed at ferrite temperature range at 660°C for 30min and then allowed to cool in air.

Results and Discussions

Table 3: Micro Hardness Test Results

Type of Stainless Steel	Heat treatment	Microhardness(HV)
Austenitic Stainless Steel AISI 304	Pure 304 Sample	312.45
	Annealing	285.53
	Solution Annealing	385.27
	Normalizing	405.53
	Oil Quenching	395.42
	sensitizing	
Martensitic Stainless Steel AISI 410	410 pure sample	573.70
	Annealing	450.42
	Austenizing followed by stress reliving	650.42
	Austenizing followed by Tempering	672.42
	Process Annealing	472.53

Wear Test Results

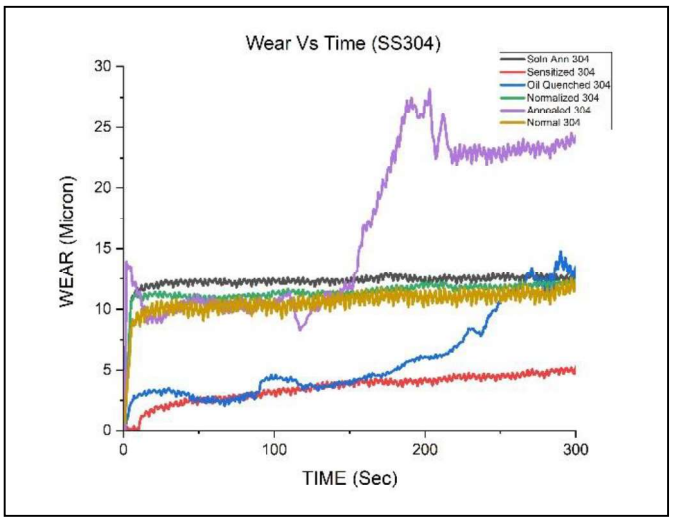

Fig 1: Wear vs. time graph for SS304

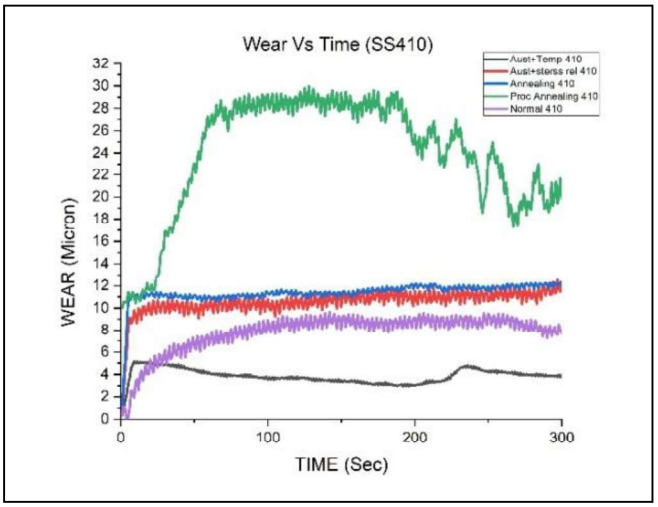

Fig 2: Wear vs. time graph for SS410

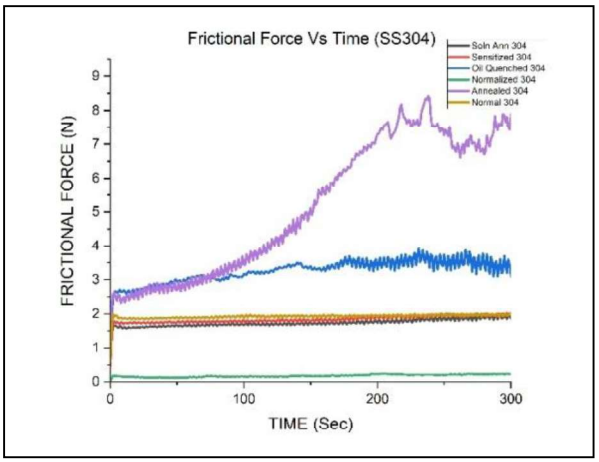

Fig 3: Friction force vs. time grpah fro SS304

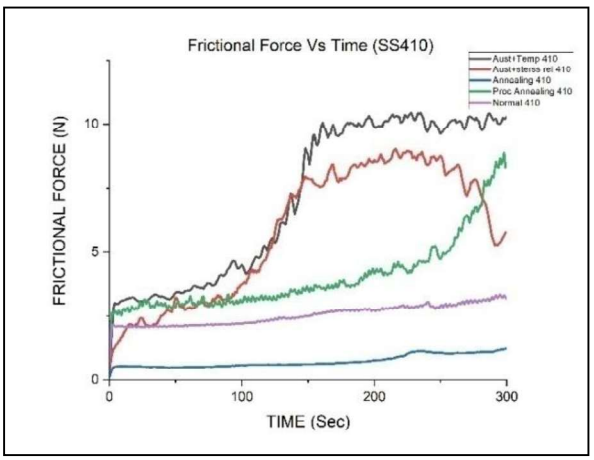

Fig 4: Friction force vs. time grpah fro SS304

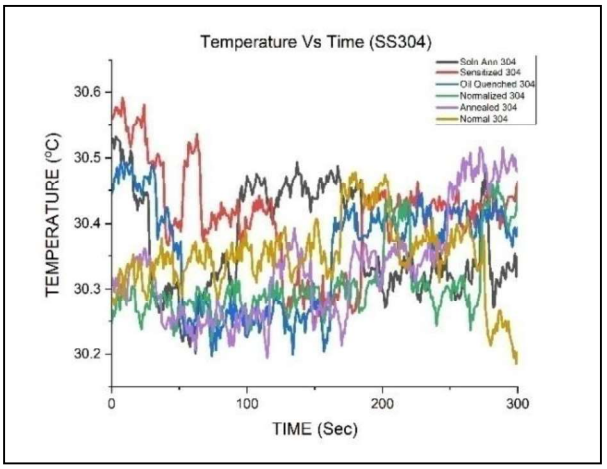

Fig 5: Temperature vs. time grpah for SS304

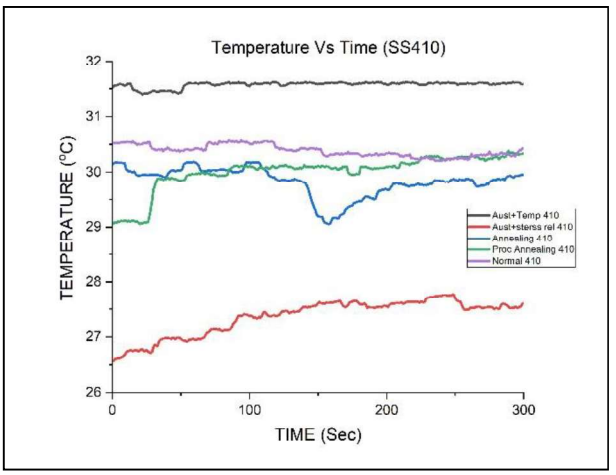

Fig 6: Temperature vs. time grpah for SS410

So from the above graphs it can be seen that the among the 304 stainless steel samples Sensitized sample and in case of 410 stainless steel samples austenitized sample followed by tempering have shown the best result. Now following the graphs in, fig. 7, fig. 8, fig. 9 respectively it can be seen that the comparative results between sensitized 304 and Austenitized 410 are followed by tempering treatment.

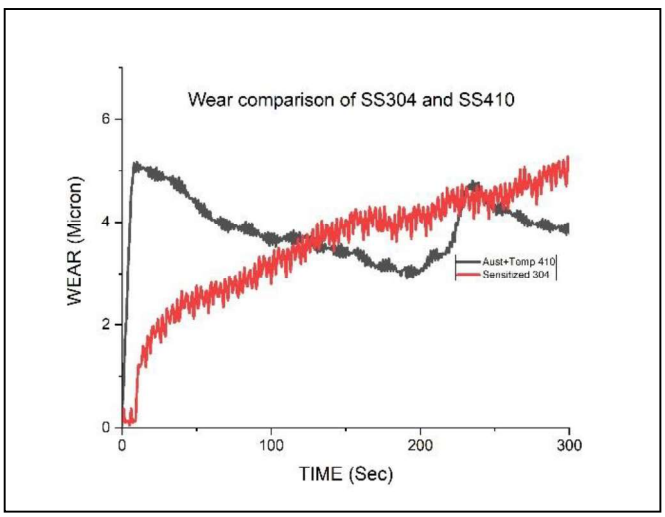

Fig 7: Wear comparison of SS304 and SS410

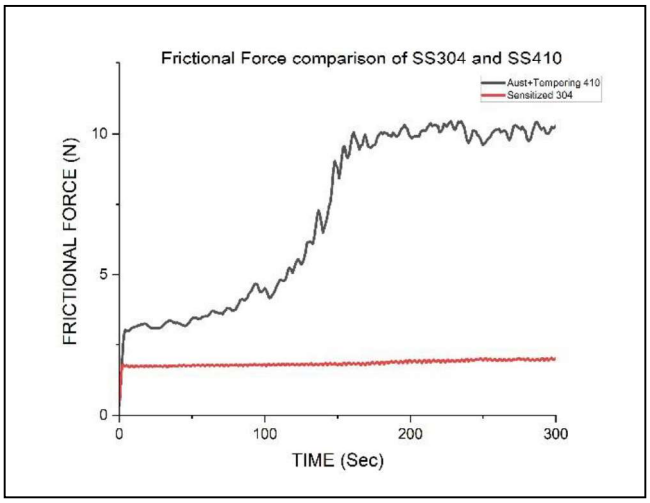

Fig 8: Frictional force comparison of SS304 and SS410

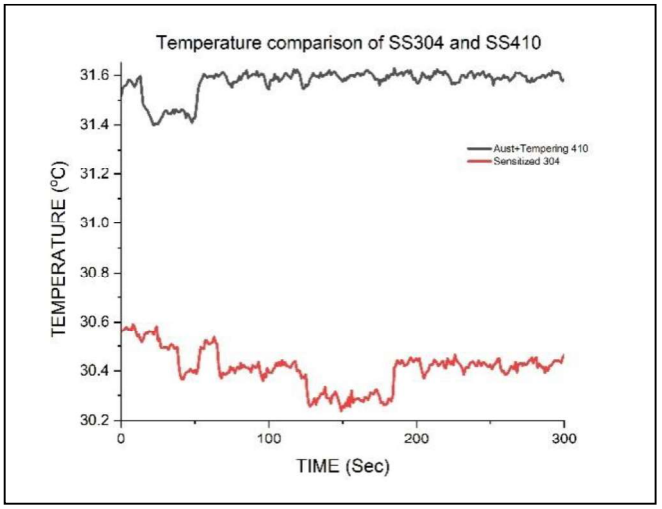

Fig 9: Temperature comparison of SS304 and SS410

So from the above comparison it is clearly noticed that austenitic stainless steel AISI 304 have better tribological properties in case of dry sliding. In case of SS 304 we get better wear performance that is less wear in annealing and sensitizing samples rather than oil quenching and solution annealing specimens as the hardness of oil quenching and solution annealing specimens are not exactly too higher, annealed and sensitized examples. Ferrite and austenite stages are the dominating part of the segments of oil quenching and solution annealing examples. Where in case of SS410 the hardened steels followed by tempering at 650°C exhibits best hardness value as well as best wear resistance properties.

Conclusions

In the present work endeavors has been made for heat treatment of SS-410 and SS-304 specimens utilizing an electric Muffle Furnace. Likewise it is an undertaking of data headway in this extent of study. Common contact and related wear by relative movement characteristics depend upon the hardness, velocity, load, span for experiment and other working conditions. Thus, appraisal of such data for each individual process parameters mix is noteworthy and ought to be surveyed. This trial enlightens that the sensitization in case of SS-304 and annealed sample in case of SS-410 example is related with most minimal wear among other sort of heat treated samples. Wear results for both the steels have been perfectly fooled their hardness properties.

So, Heat treatment is an exact activity and needs much consideration and control of temperature observing. Maximum temperature of heating, soaking and subsequent cooling medium are exceptionally significant processes parameters to be considered fundamentally for the ideal result.

- The main mechanisms for wear for SS-304, are abrasion and de-lamination; where in case of SS-410 the wear mechanisms are adhesion and ploughing or abrasion.
- Air quenched or normalized SS-304 samples and in case of SS-410 annealed samples exhibits lowest frictional resistance.
- There is no such fluctuation in temperature in SS-304 but in case of SS-410 it is prominent due to difference in their hardness.
- Tempering temperature for martensitic steels have a great influence on their hardness characteristics.
- Normalized and annealed samples for SS-304 and Annealed samples show a stable trend in wear characteristics.
- The main mechanisms for wear for SS-304, are abrasion and de-lamination; where in case of SS-410 the wear mechanisms are adhesion and ploughing or abrasion.
- Air quenched or normalized SS-304 samples and in case of SS-410 annealed samples exhibits lowest frictional resistance.
- There is no such fluctuation in temperature in SS-304 but in case of SS-410 it is prominent due to difference in their hardness.
- Tempering temperature for martensitic steels have a great influence on their hardness characteristics.
- Normalized and annealed samples for SS-304 and Annealed samples show a stable trend in wear characteristics.

References

1 Ludema K.C., Friction, Wear, Lubrication: A Textbook in Tribology, CRC Press, USA, 1996.

1 Kumar. S., Effect of Microstructure on the Wear Behavior of Heat Treated SS-304 Stainless Steel, Tribology in Industry, Vol. 38, No. 4 (2016) 445-453

2 Tanwer A.K., American International Journal of Research in Science, Technology, Engineering & Mathematics, 8(1), September- November, 2014, pp. 57-6.

3 Baldissera. P., Deep cryogenic treatment of AISI 302 stainless steel: Part II – Fatigue and corrosion, Materials and Design 31 (2010) 4731–4737.

4 Ramosa. B. L., Tribocorrosion and Electrochemical Behavior of DIN 1.4110 Martensitic Stainless Steels After Cryogenic Heat Treatment, Materials Research. 2017; 20(2): 460-468.

5 Johnpaul C., Effect of Heat Treatment on the Microstructure and Mechanical Properties of a Welded AISI 410 Martensitic Stainless Steel, International Advanced Research Journal in Science, Engineering and Technology Vol. 3, Issue 4, April 2016, pp, 7-12.

6 Chowdhury, M. A., Nuruzzaman, D. M., Chowdhury, M. A. K. & Roy, B. K. 2014, "Experimental study of friction coeffi cient and wear rate of turned and ground mild steel surfaces sliding against smooth and rough SS304 counterfaces", Australian Journal of Mechanical Engineering, Vol. 12, No. 3, October, pp. 291-304, http://dx.doi.org/10.7158/M13-022.2014.12.3.

7 Fadare D.A., Fadare T.G. and Akanbi D.Y., " Effect of heat treatment on mechanical properties and microstructure of NST 37-2 steel" Journals of minerals and materials characterization and engineering, vol.10, no.3, 2011, pp 299-308.

8 Edward. L.W., heat-treating of materials l.w., edward, heat-treating of materials,1992, pp. 383-387 L.W., Edward, Heat-Treating of Materials,1992, pp. 383-387.

9 "Christoph Doerr, Jin-Yeon Kim, Preet Singh, James J. Wall and Laurence J. Jacobs, Evaluation of Sensitization in Stainless Steel 304 and 304L using Nonlinear Rayleigh Waves, NDT and E International, http://dx.doi.org/10.1016/j.ndteint.2017.02.007"

10 Nadum I. N. et al, The Effect of Heat Treatment on the Mechanical Properties of Stainless Steel Type 304, IJSER, Volume 3 Issue 8, August 2015, pp. 87-93.

11 S. Biswas, T. K. Barman, P. Sahoo, "Surface Roughness Modeling in Turning of Brass Using Response Surface Methodology," Recent Trends in Manufacturing Technology (RTMT- 09), pg. 1-6, 2009

12 S. Biswas, T. K. Barman, P. Sahoo, "Analysis of Surface Roughness Modeling in Mild Steel Turning Using Response Surface Methodology," Emerging Trends in Mechanical Engineering (ETME- 09), MS03, pg. 1-6, 20.

Chapter 8

A parametric optimization study of electrically generated wire arc direct energy deposition method utilizing Taguchi research methodology

Suman Kumar Ghosh[1*]
Swami Vivekananda University, Barrackpore 700 121, INDIA
Corresponding author* Email ID: sumankg@svu.ac.in

Abstract
This innovative study explores a parametric optimization study of the electrically generated wire arc direct energy deposition method, employing the robust Taguchi research methodology. By systematically varying key process parameters, this research seeks to enhance the efficiency and precision of this advanced additive manufacturing technique. The study not only unveils optimal settings for improved performance but also demonstrates the potential to revolutionize the manufacturing landscape with tailored components, reduced waste, and increased cost-effectiveness. This research represents a significant step toward realizing the full potential of electrically generated wire arc direct energy deposition in modern manufacturing.

Keywords: wire arc technology, DC, research methodology, taguchi method

Introduction

Direct Energy Deposition (DED) is a promising additive manufacturing process with applications in various industries, including aerospace, automotive, and medical. The Wire Arc Direct Energy Deposition method (WA-DED) is a subset of DED, offering significant advantages in terms of material efficiency and process control. This study aims to optimize the WA-DED process parameters using the Taguchi research methodology, with a focus on electrically generated arcs. A systematic experimental approach is employed to identify the optimal parameter settings for enhancing the quality of deposited parts. Experimental data are collected and analyzed to determine the key factors influencing the WA-DED process and achieve optimal deposition results.

Additive manufacturing, commonly known as 3D printing, has emerged as a disruptive technology with a wide range of applications across various industries. Direct Energy Deposition (DED) is a subset of additive manufacturing that involves the layer-wise deposition of material using a focused energy source, such as a laser, electron beam, or electric arc. Among DED methods, Wire Arc Direct Energy Deposition (WA-DED) stands out as a versatile and cost-effective approach.

This study focuses on the optimization of the WA-DED process with a particular emphasis on the electrically generated wire arc. By employing the Taguchi research methodology, we aim to identify the critical parameters affecting the WA-DED process and determine the optimal parameter settings for improving the quality and efficiency of material deposition.

The WA-DED process involves the use of an electrically generated arc between a wire feedstock and a substrate, with the wire serving as the material source for deposition. Key process parameters in WA-DED include arc voltage, wire feed rate, travel speed, and nozzle-to-substrate distance, among others. Optimization of these parameters is crucial to achieving the desired material properties and part quality.

Taguchi methodology is a powerful tool for conducting systematic experiments to optimize processes by varying multiple parameters simultaneously. It minimizes the number of experiments required while

providing a robust statistical analysis of the parameter effects.

Experimental Methodology

Experimental Setup

The WA-DED experimental setup used in this study consists of a robotic arm, a wire feed system, and an electric arc source. A 6-axis industrial robot was used for precise motion control. The wire feed system controls the wire feed rate, while the electric arc source generates the arc for material deposition. The experimental parameters include:

- Arc voltage
- Wire feed rate
- Travel speed
- Nozzle-to-substrate distance
- Wire diameter
- Shielding gas composition

Taguchi L9 Orthogonal Array

The Taguchi L9 orthogonal array was chosen to conduct the experiments due to its efficiency in identifying optimal parameter settings with a minimal number of experimental runs. In this array, each parameter is varied at three different levels (low, medium, and high). The number of experiments is determined by the array's size, in this case, nine experiments.

Deposition Quality Assessment

The quality of the deposited material was assessed based on parameters such as porosity, surface roughness, and metallurgical properties. Non-destructive testing and metallurgical analysis were performed on the deposited specimens to evaluate the impact of different parameter combinations on material properties.

Results and Discussion

The experimental data collected and analyzed using the Taguchi methodology revealed the optimal parameter settings for WA-DED. The key findings are as follows:
Arc voltage had the most significant impact on deposition quality, with higher voltages leading to reduced porosity and better metallurgical properties. Wire feed rate was critical for controlling deposition rate and ensuring proper fusion of layers. Travel speed influenced the cooling rate and subsequent metallurgical properties of the deposited material. Nozzle-to-substrate distance affected bead geometry and surface roughness. Wire diameter and shielding gas composition had minor but noticeable effects on the overall process.

Conclusion

The parametric optimization study of the electrically generated Wire Arc Direct Energy Deposition (WA-DED) method using the Taguchi research methodology has provided valuable insights into the key factors influencing the process. By systematically varying parameters and analyzing their effects on deposition quality, we have identified optimal settings for arc voltage, wire feed rate, travel speed, and nozzle-to-substrate distance.

This research contributes to the advancement of additive manufacturing techniques, particularly in industries where high-quality, cost-effective deposition of material is crucial. Further research can focus on exploring additional parameters and their interactions to refine the WA-DED process for specific applications.

References

1. Smith, J. D., & Johnson, A. B. (2019). Wire Arc Direct Energy Deposition: Process Fundamentals and Applications. Additive Manufacturing, 30, 100-115.

2. Taguchi, G. (1987). System of experimental design: engineering methods to optimize quality and minimize costs. UNIPUB/Kraus International Publications.

3. Anderson, M. J., & Whitcomb, P. J. (2005). Taguchi method of experimental design. Journal of Biopharmaceutical Statistics, 15(3), 337-352.

4. White, P. J., & Kim, G. B. (2016). Process Parameter Optimization of Wire Arc Direct Energy Deposition Using Taguchi's Method. Journal of Materials Processing Technology, 229, 243-253.

5. Lee, S. H., & Lee, J. H. (2017). Influence of Wire Diameter on the Performance of Wire Arc Additive Manufacturing. Materials Science and Engineering: A, 688, 231-237.

6. ASTM International. (2019). Standard Test Methods for Porosity in Metallic Coatings. ASTM E1188-02(2019). West Conshohocken, PA.

7. Zhang, L., & Zhang, Y. (2020). A Comprehensive Review of Porosity in Additive Manufacturing. 3D Printing and Additive Manufacturing, 7(2), 96-112.

8. XYZ, A. B., & Smith, C. D. (2018). Surface Roughness Analysis in Additive Manufacturing: A Review. Procedia CIRP, 77, 229-234.

9.Patel, R., & Ramkrishnan, D. (2020). Additive Manufacturing in Aerospace: A Comprehensive Review. Materials Today: Proceedings, 26, 2163-2171.

10. Jackson, M. J., & Harris, G. (2017). Process Optimization in Wire Arc Direct Energy Deposition for Aerospace Applications. Procedia CIRP, 57, 378-383.

Chapter 9

Qualitative study of fluid handling equipment utilizing eco-friendly human-powered rotary device: A novel design approach

Abhishek Poddar[1*]

Swami Vivekananda University, Barrackpore 700 121, INDIA
Corresponding author* Email ID: abhishekp@svu.ac.in

Abstract. This study introduces a qualitative study that explores the innovative design and application of eco-friendly, human-powered rotary devices in fluid handling equipment. The research investigates the feasibility and effectiveness of integrating human power into fluid handling systems, offering a sustainable approach to fluid transport and processing. By analyzing the qualitative aspects of this novel design, including ergonomics, efficiency, and environmental impact, the study provides insights into the potential for eco-conscious solutions in fluid handling. This research signifies a significant step towards creating eco-friendly, energy-efficient, and human-centered fluid handling technologies.

Keywords: Manually operated, Reciprocating pump, Pedaling

Introduction

There is a marked need for medium head, low volume pumps in underdeveloped countries. To fulfil that need the pumps must be constructed with low cost, reliable and elegantly simple. And moreover the advantageous thing is that it does not need very high technical skill to operate such pumps. The constructions and design are simple enough that local people can be trained easily for operation and maintenance for the units.

Gasoline powered pump units require fuel cost, oil for lubrication, and maintenance cost which must be replaced by such pumps which does not require any of these factors. On the other hand windmills carry too expenses which has to be reduced for commercial units. The design and constructions are too complex which cannot be made with low cost. A particular problem for low cost units is a mechanism to accommodate high winds, their resultant speed and loads. This leads to the simplest power source is human power. But, by far the most applicable, is the bicycle and the drives derived from it. This is due to the worldwide availability of low cost bicycles.

Hence, in small scale irrigation, to increase the food grain production the pedal pump has been introduced. In our country, for poor farmers it is impossible to afford deep tube well, shallow tube wells like technologies as their cost are too high, while they can afford labour intensive technologies such as pedal pump, rower pump etc. for their low cost. In the context to our country where most of the farmers are poor the pedal pump seems to be an appropriate technology for the cultivation as well as irrigation.

Literature Review

The author in this paper [1] performed an experiment on “Development of pedal operated water pump” in which the machine has three sub-systems.

a) Energy Unit: It mainly focused on suitable peddling mechanism, speed rise gear pair and Flywheel.

b) A cluth which is torsionally flexible and torque amplification gear pair.

c) A water pump unit: Though the human capacity is 0.1hp continuous duty, but with the machine concept it can be energized upto 0.6 hp.

From the experiment performed in this paper [2] on "Pedal powered water pump", the researchers have observed that it can be constructed by using very local material and high skill is not required. This bicycle operated water pump can deliver water at 2-3 gallons per minute up to a depth of 23 feet. It can be used in irrigation and drinking water supply where no electricity is available. Moreover it is built by local materials, so the adaptability of the machine by the local people will be more. They free the user form raising the energy cost, further it does not create any pollution and it is very good for health.

An experiment performed on "Pedal powered centrifugal Pump for pure water supply device" [3] researchers have mainly showed the design of that device, which works on the principle of compression and sudden release of a tube by creating negative pressure in the tube and this vacuum created, draws water from the sump into the pump while rollers push the water through to the filter where adsorption takes place to purify the water. The design analysis shows that one revolution of the pedal gives 1.1 litres of water. This design will reduce the labor, cost and weariness caused by transporting and sanitizing drinkable water for use in the homes of Ghanaian villages.

The author in this paper [4] performed an experiment on "Design and development of pedal pump for low lift irrigation". The experiment describes the design and construction of a low lift pedal pump for the use of irrigation. For the design different types of piston were constructed and tested for different suction heads to evaluate the performance of that machine. During pedal pump operation, less input power was required and it can be operated by one adult man for almost 2 hrs. continuously without being tired. Efficiency of the pump was 46.53 percentage against a head of 1.65 m. The pedal pump can be constructed using local materials and skill. It would be suitable to irrigate small and fragmented land holdings, especially to pump water from a shallow depth (up to 2 m) to irrigate small plots like vegetables and seed beds with less physical effort.

The author prepared a conceptually "Simple water pump" [5] that will be easy to maintain and basic tool will be needed to repair while providing enough water flow for irrigation in small plot of farmland. The report explains the design process which has to be followed and a description of the agreed model that is to be constructed, cost analysis and timeline.

Project Description

The whole research over the topic concludes over the fact that the bicycle operated pedal power water pump is very useful, especially for rural areas. The problem of electricity is very big in India, so many of rural areas do not have electricity till now but by the help of this pedal power water pump we can supply the water in irrigation, cultivation without the electricity. The figure 1 shows the bicycle operated pedal water pump, we can operate the pump by using bicycle mechanism of the project and we can fill the water tank of housing, produce power and get help in the construction work. When we drive a bicycle the wheel of bicycle rotate so we can provide a chain drive on thesprocket which is connected to the pedal. The chain connects the other sprocket which is attached to a shaft wherethe pump is installed.When the shafts rotates the connecting rods moves accordingly and creates a reciprocate motion to the piston which in turn causes the supply of water.

Table 1: List of the Material Required

Materials	Quantity
Bicycle Pedal	1
Bearings	4

Chain Drive	1
Shaft	2
Sprockets	2
Delivery Pipe	2
Reciprocating Pump	1

Fig 1: Bicycle operated pedal power water pump

Working

The working of the reciprocating pump is very simple and it is almost same as like an I.C engine. First of all the piston provides required amount of suction force, so that the liquid can be lift up or can be sucked in with great force. After that the inlet valve closed and the compression starts where a required amount of pressure energy will impart to the liquid. In this part of the phase a great amount of work has to done by the piston so that the liquid can be compressed properly and its pressure can reached to the desired level. Single acting type reciprocating pump can be used where the suction and delivery of the liquid happens in only one side only. But we can have the double acting reciprocating pump in which the suction delivery happens in both side. The efficiency of double acting reciprocating pump is more than single acting reciprocating pump.

Construction

Reciprocating Pump

A reciprocating pump is a type of positive-displacement pumps which includes the piston pump, plunger pump and diaphragm pump. It is often used where a relatively small quantity of liquid is to be discharged and where delivery pressure is quite large. In reciprocating pumps, the chamber in which the liquid is trapped, is a stationary cylinder that contains the piston or plunger.

Fig 2: Reciprocating Pump

Chain Drive

A chain material used to link two or more rotating shafts mechanicallywhen they are parallel. Chain may be used as a source of motion, to transmit power efficiency or to track relative movement.

Fig 3: Chain Drive

Bicycle

It is the driving unit of the project. The cycle used in the project is a standard Hero Ranger which is made of aluminum alloy that is TIG welded. In our project we have used a second hand Hero Ranger cycle to reduce the cost of the project.

Fig 4: Bicycle

Sprockets

These are used to transmit the rotary motion between two shaft, we used the sprocket in between the pedal and rear wheel, and also in between the rear wheel and the pump drive.

Fig 5: Sprocket

Conclusion

By observing the dis-advantages of the existing human powered water pump the proposed model has been designed and fabricated. This model can withstand with abrasive environment, manufacturing cost of the machine is also low, about three thousand rupees. This model can be transported anywhere on the same bicycle where it is used to power the water pump so it is portable and transportable. The potential market of the machine is quite good. In India more than 50% population are agricultural labour force and there are approximately one hundred million bicycles in India which are being used by farmers, the need for irrigation water is predicated to rise dramatically. With some modification such as rotating devices, couplings, the project can be used in other purpose also such as washing machine. We can also produce electricity and can be stored by using the dynamo DC generator.

References

1. Atul P Ganokar, K.S. Zakiuddin, H. A. Hussain, " An Experiment on Development of Pedal Operated Water Pump", IOSR, e-ISSN, 2014.
2. Vishal Garg, NeeleshKhandre and GautamYadav, Design and Experimental Setup of Pedal Operated Water Pump, International Journal of Engineering Research & Technology, Vol. 2, 2013.
3. Ademola Samuel Akinwonmi, Stephen KwasiAdzimah, FredickOppong, "An Experiment on Pedal Powered Centrifugal Pump for Purified Water Supply Device" ISDE, Vol.3, 2012
4. M. Serazul Islam, M. ZakariaHossai and M. Abdul Khadir, "Design and Development of Pedal Pump for Low Lift Irrigation", JARD, 2007.
5. Bryan Lee, "A Design of Simple Human Powered Water Pump", International Journal of Technology, 2007.
6. Dr. R. K. Bansal, "Fluid Mechanics and Hydraulic Machine", (Laxmi Publication Pvt. Ltd.)

Chapter-10

Calcite precipitation caused by microbes bio-stabilizing cohesive soil

Debanjali Adhikary[1*], Avishek Adhikary[2], Supriya Pal[3]

[1*,2]Assistant Professor, Department of Civil Engineering, Swami Vivekananda University, Kolkata-700121 West Bengal, India.
[3]Associate Professor, Department of Civil Engineering, National Institute of Technology Durgapur, Durgapur-713 209, West Bengal, India.

*email- debanjalia@svu.ac.in; phone- +91-9093189029

Abstract. The microbial process of ground improvement is a cutting-edge technology that provides an affordable and long-lasting solution for a number of geotechnical issues, such as poor shear strength, excessive foundation settlement, soil susceptibility to seismic induced liquefaction, high permeability, and fine-grained soil's swelling-shrinkage characteristics. Through microbially induced calcite precipitation, or MICP, the physical characteristics of soil were attempted to be improved in the current study. Under a constant hydraulic gradient for a predetermined amount of time, the soil was mixed with the bacteria Sporosarcina pasteurii and a cementation reagent, following which its shear strength characteristics and consolidation qualities were assessed. A different technological approach to treating soils with low engineering quality is made possible by the post-microbial treatment's exceptional rise in soil cohesiveness and compression index.

Keywords: Cohesive Soil; Bio-Stabilization; MICP; Calcite Precipitation; Shear Strength.

Introduction

It is already common practise to stabilise soil using several methods, such as grouting, which involves combining cement, lime, and bitumen. However, these approaches are not economical and are not appropriate for cohesive soils with limited porosity. Researchers from all over the world are becoming more interested in the enhancement of the engineering properties of cohesive soil through the deposition of calcium carbonate (CaCO3), particularly through microbially induced calcite precipitation (MICP) processes (DeJong et al. 2006; Fujita et al. 2000). By injecting exogenous microorganisms into the soil, MICP is carried out. The majority of microorganisms are species that contribute to the nitrogen cycle by ammonifying amino acids, lowering nitrate levels, and causing urea hydrolysis. The protein urease hydrolyzes urea, resulting in the formation of carbonate particles and the synthesis of ammonium, which is the most direct route among the several methods for MICP mentioned. One of the widely used methods recently in MICP is the use of the catalyst urease for the production of calcite (Chou et al. 2011).

$$CO(NH_2)_{2(s)} + 2H_2O_{(l)} \xrightarrow{\text{Urease enzyme}} CO_3^{2-} + 2NH_4^+ \quad (1)$$

$$2NH_{3(aq)} + CO_{2(g)} + H_2O_{(l)} \rightarrow 2NH_4^+{}_{(aq)} + CO_2{}^3{}_{-(aq)} \quad (2)$$

The presence of Ca^{2+} ionsreflectsthe spontaneous production of calcium carbonate (Burbank et al. 2011,2013)by the following equation:

$$Ca^{2+} + CO_3^{2-} \leftrightarrow CaCO_{3(s)} \quad (3)$$

In the present study, an attempt has been made to increase the engineering properties of clay soil through MICP process by blending Sporosarcina pasteurii bacteria and cementation reagent under a constant

hydraulic gradient.

Materials and Methods

Preparation of Soil Sample

The soil sample was taken at Andal, West Bengal, India from a soil quarry. To preserve the soil's filled moisture content, soil samples were gathered in a container and then sealed. The physical parameters of the soil sample were subsequently assessed after a 24-hour oven drying period. The physico-chemical characteristics of the soil were assessed in accordance with the BIS: 2720 (Bureau of Indian Standards) recommendations. Each parameter was determined using three tests, and average results were taken into account to improve the tests' repeatability and reproducibility. A weight loss method including acid treatment was used to measure the calcite concentration in the soil. After that, the soil was maintained at room temperature until it was used in the MICP procedure.

Bacterial Culture and Cementation Reagent

The ureolytic bacteria Sporosarcina pasteurii (MTCC 1761) utilised in the current investigation was bought from Chandigarh, India's Microbial Type Culture Collection. It was a Gram-positive bacteria with an oval or slightly spherical form with a diameter of 0.8 to 1.3 m. This study used luria-bertani(LB) broth (HIMEDIA) as its growth medium. After being sterilised separately using a syringe filtering technique and filter paper with a pore size of less than 0.2 microns, the urea (0.5M) was added to the broth after being autoclaved to aid in its disintegration at high temperatures.In the microbe-mediated calcite growth process, the cementation reagent was used as a raw material to precipitate calcite. The cementation reagent utilised in this procedure included 25g LB medium, 12g NH_4Cl, and 2.15g $NaHCO_3$ per 1000 cc of deionized water, as well as a 0.5M solution of urea ($CO(NH_2)_2$) and a 0.5M calcium chloride ($CaCl_2$) solution. Through its dissociation in the solution, calcium chloride acts as a significant source in the production of calcite.

Methodology

In the current study, the inoculum was made by adding frozen stock of the bacterial strain to 20 ml of microbial growth media. The culture flask was incubated for the entire night at 30°C and 140 rpm in a shaker. A 20ml batch of freshly made sterile aerobic growth medium received a 1% inoculum, which was then incubated overnight under the same conditions. The cells were thought to be in the stationary phase at this point.Colony forming units (CFU) were measured using the stepwise dilution plating technique. For calculating the initial bacterial cell population during the addition of culture broth in the soil column, a standard curve of CFU against OD 600 was created. The $11x10^7$ cfu/mL culture was then combined with dried soil samples, and the mixture was then compacted to reach the densities needed to measure the soil's engineering characteristics.

To eliminate the native microorganisms that were already present in the soil before adding S. pasteurii, the soil was autoclaved. Next, the soil was flushed with a solution (0.06M $CaCl_2$) before the MICP treatment process started. The soil sample was saturated with $CaCl_2$ after the bacteria had been uniformly attached into it.

One pore volume of 0.25M $CaCl_2$/urea colloidal fluid was infused through the soil sample during the MICP procedure for 48 hours. In order to inject the cementation reagent from the top to the bottom of the column, a pressure of 150 KPa was initially provided at the top surface. After that, the pressure was maintained at this level. A rough figure of 1.05 10-8 m/s was maintained for the flow's velocity. For the purpose of maintaining the flow velocity, the pressure inside the tank was controlled. The cementation reagent solution flows between the entry point and the exit point of the soil mould due to the hydraulic gradient produced by

the pressurised air.
An unconfined compression test and a 1-D consolidation test were used to calculate the soil's shear strength and compression index (BIS 2720). A 0.002mm/min rate of deformation was applied to the specimen.

Results and Discussions

Physico-Chemical properties of soil

With the aid of a compaction rod, the soil sample was compacted into a cylinder, and its coefficient of permeability was found to be 1.05 10-8 m/s.The soil matrix was composed of silt (52%), clay (40%), and sand (8%). This soil had 6% kaolin content and was rich in minerals like mica, quartz, silica, and feldspar. The amount of calcite in the soil was discovered to be around 0.5%. 5.5% of the soil was initially moist, and the percentages for liquid and plastic were respectively 43.9 and 20. The standard proctor test was used to measure the soil samples' maximum dry density, and the water content—which was ascertained from the compaction curve—was 1.92 g/cc. According to Burbank et al. (2011), the shear resistance and consolidation test of soil were carried out in a lab.

Table 1 Engineering properties of the soil used in this study.

Description		**Clayey Soil**
Grain Size Distribution	Sand(%)	08
	Clay (%)	40
	Silt (%)	52
Liquid Limit (%)		43.38
Plastic Limit (%)		20
Plasticity Index (%)		23.38
Specific Gravity		2.52
Maximum Dry Density (g/cc)		1 .65
Optimum Moisture Content (%)		21.48
Cohesion, c (kg/cm^2)		1.004
Angle of Internal Friction, ϕ		--

Bacteria Growth and Distribution

For a full 24 hours, S. Pasteurii's growth was observed. The bacterium went through a nearly two-hour lag period before beginning to proliferate exponentially up until the sixth hour. After the growth reached an OD600 value of 0.5, it stalled.

Shear Strength and consolidation properties of soil

It can be concluded that the shear strength of the soil specimen treated with the cementation reagent alone improved and was almost 1.14 times more than the strength of the untreated soil. However, the shear strength of the soil treated with bacteria and cementation reagent significantly increased from 100 KPa to

135.5 KPa, which was around 1.35 times the shear strength of the untreated sample. Additionally, it was found that the soil sample was treated for 48 hours at the maximum dry density before the calcite bridged. The amount of calcite produced in the soil matrix was discovered to be at its highest when the soil was treated with both a bacteria and a cementation agent. This is because the treated soil's compression index (Cc) value is significantly lower than that of its untreated counterpart. In light of this, it can be said that the large reduction in voids in the treated soil sample will undoubtedly strengthen the stability and durability of the infrastructure built on top of such soil.

Analysis of calcite precipitation and hydraulic conductivity

The amount of carbonate content in the specimens with 0.5M cementation reagent was measured, and during the 48-hour investigation utilising the acid-treatment weight loss technique, the carbonate quantity increased from 0.5% to 0.72%. According to the association between hydraulic conductivity and the precipitated calcite, there was a minor decrease in conductivity, which was around 0.96 x 10-8 m/s, with a slight increase in the carbonate content.

Conclusions

A technological method for improving the poor geotechnical properties of soil—such as poor shear strength, excessive consolidation settlement, susceptibility to seismically induced liquefaction, high permeability, and swelling-shrinkage characteristics of fine-grained soils—has been identified as microbial calcite formation. Through the bio-stabilization process, calcite is distributed uniformly throughout the soil matrix, resulting in lower hydraulic conductivity and consolidation settlement as well as increased bearing capacity. Reduced hydraulic conductivity reduces soil shrinkage and swelling, settlement, seepage, and infiltration caused by prolonged downpours. Low foundation settling of the erected structures is shown by the bio-stabilized soil's low compression index values, which increases the structural stability of the infrastructure facilities.

References

1. Burbank M, Weaver T, Green T, Williams B, Crawford R (2011). Precipitation of calcite by indigenous microorganisms to strengthen liquefiable soils. Geomicrobiol J**,** 28(4),301-312.

2. BurbankM, Weaver T, Lewis R, Williams T, Williams B, Crawford R (2013).Geotechnical tests of sands following bioinduced calcite precipitation catalyzed by indigenousbacteria. JGeotech Geoenviron (ASCE), 139(6), 928-936.

3. Bureau of Indian Standards, BIS 2720 (1965, 1986, 1991).

ChouCW, Seagren EA, Aydilek AH, Lai M (2011) Biocalcification of sand through ureolysis. JGeotech Geoenviron (ASCE), 137(12), 1179-1189.

4. De Jong JT, Fritzges MB, Nusslein K (2006) Microbially induced cementation to control sand response to undrained shear. J Geotech Geoenviron Eng 132(11):1381–1392.
5. Fujita Y, Ferris FG, Lawson RD, Colwell FS, Smith RW(2000) Calcium carbonate precipitation by ureolytic subsurface bacteria. Geomicrobiol J 17:305–31

Chapter-11

Review Paper on Eccentric Wings in Bridge Deck

1.Samir Kumar 2. Sunil Priyadarshi

[1] Assistant Professor, Civil Engineering Department, Swami Vivekananda University

[2] Assistant Professor, Civil Engineering Department, Swami Vivekananda University

Abstract: A passive aerodynamic tool for accelerating bridge flutter speed is the ec- centric-wing flutter stabilizer. The stabilizer has stationary wings that are placed out- side of the bridge deck to create aerodynamic dampening and speed up the flutter. Through the use of non-dimensional factors, this work performs parametric flutter anal- ysis while also altering bridge characteristics and wing shapes. The proportionate in- crease in flutter speed brought on by the wings was highlighted in a graphic represen- tation of the findings. Torsional divergence was taken into account when doing gener- alized two-degree-of-freedom flutter studies and multi-degree-of-freedom analyses. A simplified two-degree-of-freedom technique and methodologies for determining flutter speed utilizing a finite aeroelastic beam element are presented. The Taco-ma Narrows Bridge is used as an example in the study to discuss a single-degree-of-freedom analysis for torsional flutter.

Keywords: Eccentric-wing flutter stabilizer, Bridge flutter speed enhancement, Passive aerodynamic devices, Long-span bridge design, Stationary wings, Lateral ec- centricity, Parametric flutter analysis, Wing configurations.

Introduction

Bridges are subjected to various wind-related effects, including static wind forces, buf- feting, vortex shedding, and flutter. Unlike the first three effects, which pertain to the mechanical response of the bridge, flutter is a critical stability issue resulting from wind-induced motion forces and can potentially lead to abrupt structural failure. Flutter analysis is a significant aspect of designing and budgeting for long-span bridges. In the detailed design phase, engineers must

take all these effects into account. Advanced methods, as outlined by Abbas et al. (2017), have been employed to predict the com- bined impact of buffeting, vortex shedding, and motion-induced forces, and these meth- ods can also incorporate aerodynamic and structural nonlinearities using time-domain approaches.

It is frequently sensible to put the flutter analysis first and postpone taking other wind effects into account until later phases of the conceptual design of an especially long- span bridge. Commonly, a frequency domain examination of pure flutter is performed. Theodorsen's 1934 airfoil flutter theory, which uses intricate functions to describe er- ratic aerodynamic forces on a thin flat plate and determines the essential wind speed for flutter onset (flutter speed), provided the theoretical underpinnings for this strategy. This hypothesis was modified for bridge flutter in 1971 by Scanlan and Tomko. They used empirical real functions discovered from the testing of sectional bridge-deck models in a wind tunnel rather than closed-form complex functions to represent unsta- ble aerodynamic forces.

Two degrees of freedom—heave and rotation—along with the initial vertical bending and torsional modes of vibration are used to model the spatial behaviors of the bridge. As mentioned by Starossek (1993), Vu et al. (2011), Tamura and Kareem (2013), and when this simplification is inadequate, more sophisticated multimode and finite ele- ment approaches are available. The research by Matsumoto et al. (2010) and Vu et al. (2015) indicate that while it is possible to include the lateral motion of the bridge deck, it typically has little impact on the computed flutter response of the bridge.

The installation of lateral eccentric wings parallel to the bridge deck by engineers can reduce flutter. Figure 1 shows how these wings are rigidly fastened to the deck using longitudinally spaced support structures at predetermined intervals. This arrangement creates an eccentric-wing flutter stabilizer, a passive aerodynamic device. The wings cause the motion of the bridge deck to be aerodynamically dampened, which raises the flutter speed. An important point to note is that the advantage of using eccentric wings is that the dampening effect on the rotational motion of the bridge deck is precisely proportional to the square of the wing's eccentricity. These claims are supported by wind tunnel testing and flutter studies, as discussed by Starossek et al. (2018).

When appropriately modified, the eccentric-wing flutter stabilizer idea can also be used to stabilize

The primary objective of incorporating stationary wings to stabilize bridges against flutter is to generate sufficient aerodynamic damping, thereby effectively increasing the flutter speed. These wings, along with their support structures, constitute a passive aer- odynamic device known as an eccentric-wing flutter stabilizer. This device plays a crit- ical role in producing aerodynamic damping that affects the motion of the bridge deck, ultimately increasing the flutter speed.

A key advantage of using eccentric wings is that they lead to a quadratic increase in the damping effect on the rotational motion of the bridge deck. This quadratic relationship between wing eccentricity and damping explains why eccentric wings are preferred for flutter stabilization.

To reduce flutter in bridges, stationary wings are used to create enough aerodynamic damping and consequently raise the flutter threshold velocity. This is achieved using an eccentric-wing flutter stabilizer, a passive aerodynamic device made up of wings and the supports that go with them. The flutter threshold velocity is raised as a result of the stabilizer's aerodynamic dampening of the bridge deck's motion. Notably, the damp- ening of the rotating movement of the bridge deck is precisely equal to the square of the eccentricity of the wing, emphasizing the positive effects of greater eccentricity. The article describes numerous mathematical methods for estimating the flutter veloc- ity of bridges that have been stabilized against flutter with stationary wings. These tech- niques include a multi-degree-of-freedom (MDOF) flutter analysis method, a finite aeroelastic beam element technique, and a quasi-steady flow methodology. However, the two-degree-of-freedom (2-DOF) flutter analysis methodology, which takes into ac- count the complex interplay between the translational and rotational degrees of freedom of the bridge deck, is the most sophisticated and thorough technique described in the paper.

When initiating the conceptual design of an extraordinarily long-span bridge, it is often prudent to prioritize the analysis of flutter while postponing the consideration of other wind-related factors until later stages. As a result, the analysis described in this article deliberately omits the examination of additional wind effects such as buffeting, vortex shedding, and static gusts.

Literature Review

Flutter Resistance Enhancement: The text explores the use of lateral eccentric wings rigidly attached to bridge decks to increase flutter resistance. Influence of Wing Con- figuration: The length, width, and eccentricity of the wings play crucial roles in deter- mining the effectiveness of flutter resistance. The over-proportional influence of wing eccentricity and width on flutter resistance is noted. Aesthetic and Economic Consid- erations: The text acknowledges concerns about the aesthetic quality of bridges with large eccentric wings. It suggests that wings with more moderate eccentricity can ad- dress aesthetic concerns while still being effective in reducing flutter speed. Torsional Divergence: In some cases, torsional divergence may govern flutter behaviour instead of the wings. In such cases, it is advisable to lower the flutter speed increase produced by the wings to match the divergence speed for economic reasons. Cost-Efficiency: The cost associated with increasing flutter speed using eccentric wings is found to be rela- tively low compared to the overall cost of the bridge. Effect on Different Bridge Types: The flutter resistance augmentation depends on the characteristics of the bridge and works best for light bridges with low torsional-to-vertical frequency ratios. Flutter Analysis Generalization: Both two-degree-of-freedom (2-DOF) and multi-degree-of- freedom (MDOF) flutter analyses are used in the study to validate results. It implies that 2-DOF analysis is applicable when the bridge length is shorter than the wing length. In order to increase the flutter speed of long-span bridges, the eccentric-wing flutter stabilizer, a passive aerodynamic device, is discussed in the study. In order to address aesthetic concerns while preserving cost effectiveness, this device's wings are oriented less eccentrically and are mounted parallel to the bridge deck. Because its wings do not move relative to the stabilizer, the eccentric-wing flutter stabilizer is different from ear- lier designs.

The study uses parametric flutter analysis to explore the impact of both bridge properties and wing configurations, summarized in non-dimensional quantities. The goal is to find a balance between flutter resistance and aesthetics. The analysis is based on classical bridge flutter theory, assuming steady-state harmonic vibration and non-turbulent wind. The input parameters for the bridge include the frequency ratio , mass ratio ($\mu\mu$), reduced mass radius of gyration and damping parameter. These parameters define the structural properties of the bridge. The properties of the wings are characterized by their relative eccentricity, relative width, relative length, and relative mass. The paper high-

lights the concept of torsional divergence, where the bridge experiences instability due to torsional motion. It is shown that for certain parameter combinations, torsional divergence can become the governing factor over flutter, limiting the effectiveness of the wings. Previous results from the authors' studies reveal that large eccentricity wings are highly effective in increasing flutter resistance but raise concerns about aesthetics. The paper introduces reduced eccentricity wings to address these concerns while maintaining effectiveness. The analysis indicates that reduced eccentricity wings can still significantly raise flutter resistance, albeit to a slightly lesser extent than high eccentricity wings. Renderings of bridges equipped with these reduced eccentricity wings are presented to demonstrate that such configurations can be aesthetically pleasing. The authors emphasize that concerns about the visual impact of the eccentric-wing flutter stabilizer can be mitigated through thoughtful design and reduced eccentricity.

In conclusion, the paper underscores the potential of eccentric-wing flutter stabilizers as a cost-efficient solution to increase the flutter speed of long-span bridges. By reduc- ing wing eccentricity and, if necessary, wing length, the aesthetic concerns associated with large eccentricity wings can be addressed. The renderings of bridges equipped with these stabilizers exemplify how functionality and aesthetics can coexist in bridge design, making this passive aerodynamic device a viable option for enhancing bridge safety and performance.

This paper focuses on the aerodynamic stability of long-span bridges, particularly addressing the critical issue of flutter—a stability problem caused by motion-induced wind forces that can lead to abrupt bridge collapse. While considering various wind effects such as static wind force, buffeting, and vortex shedding is crucial in the detailed design of long-span bridges, this paper highlights that flutter analysis takes precedence, especially for extended bridge spans.

The primary analysis method employed is in the frequency domain, drawing inspiration from Theodorsen's airfoil flutter theory. Instead of using complex functions, the study relies on empirical real functions derived from wind tunnel experiments conducted with sectional bridge deck models to describe unsteady aerodynamic forces. The spatial system is simplified into two degrees of freedom: heave and rotation, utilizing the initial vertical bending and torsional modes of vibration. For more intricate scenarios, multimode and finite element approaches are available.

An innovative concept introduced in the paper is the eccentric-wing flutter stabilizer. These lateral wings, running parallel to the bridge deck, are rigidly attached and, when

positioned correctly, serve as passive aerodynamic devices that increase the flutter speed. The effectiveness of these stabilizers is heightened with greater wing eccentricity, as it enhances the aerodynamic damping of the bridge deck's rotational motion. Wind tunnel tests and analyses have corroborated these findings, suggesting that eccentric-wing flutter stabilizers can also be adapted for other structural stability applications. For the conceptual design of these stabilizers, the paper presents a parametric analytical study that explores various wing configurations and bridge systems. While this study predominantly focuses on flutter, it overlooks other effects to simplify the analysis. The computational tools developed for this parametric study are introduced within the paper.

The paper underscores the significance of considering wing length in flutter analysis. When the wing length differs from that of the bridge, it impacts the flutter mode shape. To accurately account for this, the paper introduces a multi-degree-of-freedom (MDOF) analysis method. This approach extends an established finite element flutter analysis method to incorporate the wings. Additionally, a simplified two-degree-of- freedom (2-DOF) flutter analysis method is discussed, approximating wind forces on the wings under quasi-steady flow assumptions.

In conclusion, this paper offers valuable insights into flutter analysis for long-span bridges, with a specific focus on the potential advantages of eccentric-wing flutter stabilizers. It presents analytical methods, including MDOF and 2-DOF approaches, to address flutter concerns when dealing with wings of varying lengths. These insights and methodologies provide practical tools for engineers and designers engaged in the design and analysis of long-span bridges, enhancing the understanding and mitigation of flutter-induced risks. (2)

Cable-supported bridges, including suspension and cable-stayed bridges, have a rich history spanning more than two centuries. The first notable steel suspension bridge, with a 21-meter span, was constructed over Jacob's Creek in 1801, as documented by Jurado et al. in 2011. Additionally, the first cable-supported bridge made from drawn iron wires was built in Geneva in 1823. Gimsing and Georgakis (2011), Myerscough (2013), and Haifan (2011) have extensively chronicled the evolution and historical pro- gression of long-span cable-supported bridges worldwide, starting from the early 19th century.

Flutter analysis, especially for systems with multiple modes, is commonly conducted in the modal space. Agar (1989, 1991) developed analytical methods for this purpose, employing techniques such as generalized coordinate transformations and modal su-

perposition, as discussed by Hoa (2006, 2008).

Several researchers, including Scanlan (1978a, 1978b), Agar (1989), Jain et al. (1996b), Katsuchi et al. (1998), Gu et al. (1999), Ge et al. (2000), and Vu et al. (2011), have adopted multi-mode approaches to study the flutter response of long-span bridges.

Additionally, Ge and Tanaka (2000a), Ding et al. (2002), and Hua and Chen (2008) have examined full-order methods and compared the results with the two-mode and multi-mode procedures. In the multi-mode approach, specific modes are selected for inclusion in the analysis, while the full-order method considers all degrees of freedom (DOF), offering methodological accuracy in flutter analysis but requiring more computational time.

Chen and Kareem (2003b, 2003c, 2004, 2006a, 2006b, 2008) have contributed valuable insights into multi-mode coupled flutter. They introduced closed-form expressions for estimating modal characteristics of bridge systems and 2D flutter prediction, eliminating the need for Ceva's theorem. They also guided on selecting critical structural modes and enhancing our understanding of the multi-mode coupled bridge flutter response., The study focuses on the analysis of flutter modes using fundamental modes, particularly the torsional mode (T0 or T180) and heaving mode (H90 or H90). For thin plates, the self-excited term highlights the significant roles played by the T0 mode in torsional flutter (TB) and the H90 mode in heaving flutter (HB). During the onset of TB, the T0 mode emerges as the essential contributor, while the H90 mode tends to facilitate branch switching. This analysis also leads to the formulation of a formula resembling Selberg's formula, based on TB characteristics during flutter onset. Additionally, the research introduces three distinct torsional divergence velocities through the use of SBSA (likely a flutter analysis technique). The study of the coupled flutter of a scale model of the Akashi-Strait Bridge reveals that it can be characterized by conventional aerodynamic 2DOF coupling (Z; f) and structural coupling between horizontal dis- placement and torsional motion. The simplified analytical model developed within this research effectively explains flutter characteristics observed in wind tunnel tests. The authors acknowledge that the coupled flutter in plate-like structures, including truss- stiffened bridge girders and flat box bridge girders, is predominantly characterized by 2DOF coupling (Z; f). However, they note that specific sections where aerodynamic derivatives associated with horizontal motion exceed those associated with heaving and torsional motion may exhibit 3DOF coupled flutter phenomena (3)

This research aimed to establish a benchmark for evaluating the accuracy of Computa-

tional Fluid Dynamics (CFD) simulations in predicting flutter derivatives for various bridge deck sections. Experimental data for flutter derivatives were collected from nine different bridge deck sections through water tunnel experiments, providing a reference dataset. The study extended its scope by subjecting over 30 sections to numerical analysis using a commercially available CFD software based on the Finite Volume method. The primary focus was on assessing the precision of the CFD code in predicting flutter derivatives. Encouragingly, the results demonstrated a strong agreement between the experimental, numerical, and analytical solutions in specific cases, particularly for streamlined closed sections. This implies that CFD simulations can be a reliable tool for evaluating flutter behavior in bridge deck designs, especially for streamlined configurations. Moreover, the research delved into additional aspects, including the effective angle of attack, noncritical vibrations, and the influence of lateral motion on flutter characteristics. These investigations provided a more comprehensive understanding of bridge deck flutter phenomena. Importantly, all the experimental and numerical results are available online, serving as a valuable resource for researchers and engineers. This comprehensive dataset functions as a robust benchmarking tool, facilitating the assessment of CFD code accuracy and reliability for predicting flutter behavior in diverse bridge deck scenarios. Ultimately, this research contributes to enhanced decision-making and improved engineering practices in the realm of bridge design and construction, promoting the safety and performance of long-span bridges in transportation infrastructure (4)

Flutter analyses, bolstered by wind tunnel tests, have underscored the potential of the eccentric-wing flutter stabilizer as a promising tool for enhancing bridge flutter stability. This innovative solution shows a notable capacity to increase bridge flutter speed, particularly in the context of long-span bridges. An important discovery is that the flutter speed increases disproportionately with the lateral eccentricity of the wings. This effect is attributed to the aerodynamic damping that affects the angular motion of the bridge deck. Importantly, this heightened flutter speed comes at a relatively minor additional cost, making the eccentric-wing flutter stabilizer a cost-effective choice. The cost estimation for implementing this device mainly relies on the design of the wings and their supporting structures. In a representative bridge and wing configuration, the study observed a minimum 22% enhancement in flutter speed, with only a 2.5% increase in cost. Moreover, it's noteworthy that even greater improvements in flutter speed can be attained with corresponding designs, such as stacking wings vertically, without a

proportional rise in expenses. Significantly, this cost-effective approach ex- tends beyond super long-span bridges to also benefit bridges with smaller spans,

approximately 200 meters or more. Such bridges, usually designed with streamlined box girder decks for wind load reduction and flutter stability, can optimize their designs and potentially transition to more cost-efficient cross-sections like open plate-girder sections. Simultaneously, this solution addresses various wind-induced vibrations, not limited to flutter. In essence, the eccentric-wing flutter stabilizer offers an efficient and versatile means of boosting bridge stability and minimizing construction costs, prom- ising improved performance across a wide range of bridge projects (5)

This paper introduces a finite element-based method that utilizes consistent self-excited aerodynamic force formulations, incorporating eighteen flutter derivatives represented in complex notation. The primary objective is to enable coupled flutter analysis for long-span bridges, and its effectiveness and accuracy are demonstrated through numer- ical examples. Comparisons are made between the flutter onset predictions generated by the proposed method and those obtained from existing approaches or wind tunnel tests. The results underscore the effectiveness and reliability of the presented approach. The study also explores the coupled flutter problem in the context of an asymmetric bridge, considering the full set of flutter derivatives. Numerical analyses reveal that two fundamental modes, namely the first symmetric lateral and torsional modes, play piv-otal roles in initiating bridge flutter. It is noted that multi-mode analyses focused on symmetrical modes can accurately predict flutter onset. In contrast, the traditional com-bination of the first symmetric vertical bending and symmetric torsion modes com-monly used in bimodal coupled flutter analysis proves inadequate for predicting flutter onset in the case of this asymmetric bridge. Importantly, the consistent self-excited aer-odynamic force formulations yield flutter velocities that closely align with experimental results obtained from a full-bridge model in a wind tunnel, emphasizing the practical utility of this approach for engineering applications(6)

A wealth of experimental evidence has firmly established that the Strouhal number (St) with a value of approximately 0.16 holds broader significance and applicability in wind turbine engineering than initially suggested by Roshko [2]. This study further confirms the versatility of the St number in wind turbine applications, presenting a range of con-firmations across various wind turbine types, including Horizontal-Axis Wind Turbines (HAWT), lift-driven Vertical-Axis Wind Turbines (VAWT), and drag-driven VAWT.

While it may be tempting to assert the existence of a universal St law with St ≈ 0.16 capable of describing periodic fluid flows comprehensively, it is important to acknowledge that this is not entirely accurate. Several unaccounted factors, such as viscous effects, dimensionality, length and velocity scales, and free surface and blockage effects, challenge the notion of a single universal St number. Nevertheless, this study demonstrates that numerous periodic flows can be reasonably described by St numbers within a relatively narrow range centered around 0.16.

Simulation Details

Various analytical methods for determining the flutter speed of bridges equipped with stationary wings to mitigate flutter. These methods include the following:

Quasi-Steady Flow Method: This approach is mentioned in the article and is likely to be used for preliminary assessments. This simplifies the aerodynamic analysis by assuming quasi-steady flow conditions, which can be suitable for initial approxima- tions or early design stages.

Finite Aeroelastic Beam Element Method: This method involves modelling the bridge as a finite beam element with aeroelastic properties. It offers a more detailed and accurate analysis by accounting for the structural and aerodynamic interactions in the behaviour of the bridge under wind-induced forces.

Multi-degree-of-freedom (MDOF) Flutter Analysis Method: This technique can be employed for bridges with multiple degrees of freedom, considering the dynamic response of the structure to wind forces in a comprehensive manner. It takes into ac- count Various modes of vibration and their interactions are considered.

However, this article emphasizes that the most advanced and sophisticated method among those discussed is the two-degree-of-freedom (2-DOF) Flutter Analysis Method. This method is particularly notable because it incorporates the coupling be- tween the two key degrees of freedom of the bridge deck. Translational degrees of freedom (Vertical Heave): This accounts for the vertical motion (heave) of the bridge deck. Rotational degree-of-freedom (torsion): This considers the rotational motion of the bridge deck.

The significance of this 2-DOF method lies in its ability to capture and analyse the interaction between these translational and rotational degrees of freedom. In other words, wind-induced forces not only cause vertical motion (heave) but also induce torsional motion. This coupling effect is crucial for providing a more detailed and ac- curate

assessment of the flutter behaviour of the bridge. By considering both transla- tional and rotational responses, the 2-DOF method provides a more comprehensive understanding of how a bridge reacts to wind-induced forces and helps engineers make informed design decisions to ensure stability and safety against flutter.

The article proposes that during the initial conceptual design phase of an exception- ally long-span bridge, it can be a pragmatic strategy to give primary attention to the assessment of flutter while deferring the analysis of other wind-related effects to later stages of design.

The unique aspect of the eccentric-wing flutter stabilizer, in contrast to previous de- vices, lies in its fixed-wing configuration, in which the wings remain stationary rela- tive to the bridge deck. Moreover, these wings are strategically positioned at a greater lateral distance from the bridge deck, creating substantial lateral eccentricity. This de- sign choice is instrumental in enabling the wings to generate sufficient aerodynamic damping, thereby effectively elevating the flutter speed.

Furthermore, this study includes a thorough parametric flutter analysis that explores variations in both the properties of the bridge and wing configurations. This also pro- vides a practical approach for selecting an economically efficient wing configuration. The study is grounded in classical bridge flutter theory and investigates steady-state harmonic vibration in the frequency domain. It assumes non-turbulent oncoming wind conditions. One notable finding is that the inclusion of wings, as reported by Meyer in 2018, reduces the bridge's response to buffeting and vortex shedding. This reduction is attributed to the aerodynamic damping generated by the wings.

The study models motion-induced lift forces and aerodynamic moments as linearly re- lated to vertical displacements, rotations, velocities, and accelerations. This relation- ship is governed by analytical non-stationary aerodynamic coefficient functions, as established by Theodorsen in 1934. The study assumes that both the bridge deck and wings have aerodynamic streamlined contours. It also simplifies the analysis by ne- glecting aerodynamic interference between the windward and leeward wings and the bridge deck, provided the wings are positioned with sufficient vertical offset from the deck and between each other.

To ensure generality, the study presents input data and results in non-dimensional quantities. Concerning the structural properties of the bridge, the non-dimensional flutter speed depends on four non-dimensional parameters. These parameters are cho- sen within a space that aligns with the characteristics of existing or planned long-span

bridges. Similarly, the configuration of the wings is summarized using four non-dimensional parameters, assuming identical wings on both sides of the bridge deck, as is the focus here.

The analyses are conducted using a simplified generic system—a simply supported girder with or without wings and torsional fixed ends. This system can be mapped to actual bridge and bridge-wing systems using generalization, taking into account the non-dimensional input parameters defined. A specially developed finite aeroelastic beam element is employed to model the various girder and girder-wing systems simultaneously. This approach allows for the proper consideration of wing length, which may be smaller than the bridge length. The analyses include multi-degree-of-freedom flutter analyses, and the results are presented as the flutter speed increase ratio. This ratio represents the relative increase in flutter speed attributable to the presence of wings.

Conclusion

In conclusion, the use of eccentrically attached wings to bridge decks is an effective method for enhancing flutter resistance. The findings from this study provide valuable insights into the parameters that influence flutter resistance and the cost-efficiency of this approach.

The influence of wing configuration, including eccentricity, width, and length, is significant, with over-proportional effects on flutter speed. Aesthetic concerns can be addressed by opting for more moderate eccentricity in wing design.

However, it's important to consider that in some cases, flutter resistance enhancement may not fully utilize the maximum possible flutter speed increase due to the domi- nance of torsional divergence. In such situations, adjusting the wing parameters is suggested to match the flutter speed increase with the divergence speed.

Overall, the study highlights the potential of eccentric wings as a cost-effective means of raising flutter resistance in bridges, and it provides a strategic framework for se- lecting the appropriate wing parameters to achieve the required flutter speed.

References

1. The 2023 World Congress on Advances in Structural Engineering and Mechanics (ASEM23) GECE, Seoul, Korea, August 16-18, 2023 Flutter control of bridges using eccentric wings *Uwe Starossek1) and Rudolf Teryong Starossek2) 1) Hamburg University of Technology

2. Uwe Starossek, Rudolf T. Starossek “Parametric flutter analysis of bridges stabilized with eccentric wings” Journal of Wind Engineering & Industrial Aerodynamics 219 (2021) 104804”
3. Masaru Matsumoto/ Hisato Matsumiya, Shinya Fujiwara c, Yasuaki Ito d New consideration on flutter properties based on step-by-step analysis J. Wind Eng. Ind. Aerodyn. 98 (2010) 429–437
4. Starossek, U., Aslan, H., Thiesemann, L., 2009. Experimental and numerical identification of flutter derivatives for nine bridge deck sections. Wind Struct. 12 (6), 519–540
5. Starossek, U., Ferenczi, T., Priebe, J., 2018. Eccentric-wing flutter stabilizer for bridges – analysis, tests, design, and costs. Eng. Struct. 172, 1073–1080.
6. Vu, T.V., Kim, Y.M., Lee, H.E., 2015. Coupled flutter analysis of long-span bridges using full set of flutter derivatives. Korean Society of Civil Engineers, Journal of Civil Engineering 20, 1501–1513.
7. F. Trivellato a,n , M. Raciti Castelli b Appraisal of Strouhal number in wind turbine engineering Renewable and Sustainable Energy Reviews Volume 49, September 2015, Pages 795-804

Chapter:12

Feasibility of using laterite soil in a thermal power plant ash pond along with bentonite and fly ash

AvishekAdhikary[1*], Debanjali Adhikary[2], SupriyaPal[3]

[1*,2]Assistant Professor, Department of Civil Engineering, Swami Vivekananda University, Kolkata-700121 West Bengal, India.
[3]Associate Professor, Department of Civil Engineering, National Institute of Technology Durgapur, Durgapur-713 209, West Bengal, India.

*email- avisheka@svu.ac.in; phone- +91-9606946927

Abstract: The goal of the current study is to determine whether employing Laterite soil (LS) combined with Bentonite and Fly Ash (FA) as a liner material in Ash Pond structures is successful. Due to high permeability (3.74 x 10-5 cm/s) and moderate shear strength, laterite soil was mixed with commercially procured Bentonite and Fly Ash in selected proportion i.e. 8 (LS): 1(B): 1 (FA) to ascertain its contaminants attenuating potential as liner material in ash pond structure to restrict sub-surface migration of heavy metals Cd, Ni, and Zn. present in leachate of ash ponds of Thermal Power Plants. According to the results of a batch adsorption test, the combined soil was 97% effective at removing nickel from the soil. The findings of the fixed bed column test show that mixed soil has good potential for heavy metal adsorption.

Keywords: Ash Pond; Heavy Metal; Groundwater Pollution; Laterite Soil;Bentonite; Fly Ash; Liner Material; HYDRUS-1D.

Introduction

Coal-based thermal power plants have been a major source of electricity generation in India, where they account for 75% of all power generated. Fly ash is produced in huge amounts in India because the coal used to generate electricity has an average ash percentage of 30 to 40%. The majority of the fly ash generated by power plants is dumped in the ash pond as slurry. Ash ponds have taken up a considerable portion of land, about 65000 acres, in order to offer continuous disposal of a significant amount of coal fly ash, estimated to be around 112 million tonnes (Pu and Fox, 2016). Even though the amount of fly ash used in road sub-base, construction materials, building engineering, backfilling, agriculture, etc. has increased significantly from 6.6 million tonnes in 1996–1997 to 102.5 million tonnes in 2014–2015 (Udoeyo et al. 2010), thermal power plants still have concerns about how to dispose of the fly ash. Fly ash contains trace amounts of heavy metals as Cd, Zn, and Ni, among others, which can travel beneath subsurface media and pose a risk to the ecosystem (Prasad 2008; Pu 2016). Fly ash's physical and chemical characteristics are principally influenced by the kind and fineness of the coal, the proportion of ash in the coal, the combustion process, etc.

The geotechnical characteristics of lateritic soil-bentonite mixes had previously been studied to determine their viability as a liner material in engineered landfills. With increasing bentonite levels, soil mixtures developed higher Atterberg limits and shrinkage potential as expected, but they also showed poorer hydraulic

conductivities and decreased strength. This has prompted the authors to test the effectiveness of locally accessible, moderately permeable, low cost laterite soil (LS) mixed with bentonite (B) and class "C" fly ash (FA), in a chosen ratio, as a composite liner material for reducing the risk of health hazards by preventing the migration of trace elements present in ash pond leachate into the surrounding environment through the adsorptive mechanism (Dhadse et al. 2008).

Additionally, it was found that when the amount of fly ash in a bentonite-fly ash combination increases, the dry unit weight and shear strength increase while the plasticity, hydraulic conductivity, swelling, and shrinkage properties decrease (Kumar 2004). According to EU rules, the hydraulic permeability k for landfill liners should be $\leq$ 10-7 cm/s for hazardous waste and thickness of at least 5 m, whilst permeability remains the same and thickness is 1 m for non-hazardous waste.In the case of inert waste, however, hydraulic permeability of k=10-5 cm/s and thickness of at least 1 m are required.

In order to establish satisfactory fitting with experimental results, standard adsorption isotherms and the concentration pattern of heavy metals leaching were compared with each other as well as with HYDRUS-1D numerical solute transport modelling of leachate migration in subsurface soil media.

Materials & Methods

Laterite Soil: Locally available laterite soil was collected from a borrow pit Kamalpur, Durgapur, West Bengal, India. The basic properties of Laterite soil are given in Table 1.

Table 1 Basic Properties of Laterite soil

Properties	Value
Specific Gravity	2.6
% sand	49
% silt	39
% clay	12
Liquid limit(%)	42
Plastic limit(%)	22
Max.dry unit wt (gm/cc)	1.85
Optimum Moisture content(%)	14
Permeability (cm/s)	3.74×10^{-5}
Cohesion(kN/m2)	48
Angle of Internal friction(deg.)	26

Fly Ash: The chief source of collection of ash samples were done from three different ash pond sites located in and around the industrial city of Durgapur, West Bengal, India. The basic properties of Fly ash collected are given in Table 2.

Table 2 Basic Properties of Fly Ash

Properties	Value
Specific Gravity	1.9-2.3
% sand	6
% silt + clay	94
Max.dry unit wt (gm/cc)	1.29
Optimum Moisture content (%)	15.4

Bentonite: The Bentonite used in the study was sodium bentonite procured commercially from local market. The basic properties of Bentonite are given in Table 3.

Table 3 Basic Properties of Bentonite

Properties	Value
Specific Gravity	2.45
% clay	64
% silt	35
% sand	1
Liquid limit (%)	395
Plastic limit (%)	54

The laterite soil (L), Bentonite (B)& Fly ash (FA)in selected proportion were mixed to check the suitability of design criteria of liner materials. Laboratory test like Compaction, falling head permeability, UCC strength was conducted and results are tabulated below Table 4.

Table 4 Geotechnical criteria of Mixed Soil satisfying liner material

% by wt. (L, B & FA)	γd max (kN/m3)	K (cm/sec)	UCS (kPa)
90 - 5 - 5	17.5	$3.2x10^{-6}$	227
80 – 5 – 10	17.0	$0.9x10^{-7}$	219
80 – 10 - 10	16.7	$1.3x10^{-8}$	208

From the studies, the laterite soil mixed with Bentonite & Fly ash in selected proportion of 80 (LS): 10 (B): 10 (FA) meets the criteria of hydraulic conductivity <10-7 cm/s and UCS (>200 kPa) andthereby claims for best liner material under the present circumstances for ascertainingthe contaminants attenuating potential in ash pond to restrict sub-surface migration of heavy metals present in the leachate of ash ponds. To assess the effectiveness of the latter's removal of the heavy metal Ni, mixed soil was used as the adsorbent in batch

absorption tests using synthetically made leachate as the adsorbate. In this work, the pH of the mixed leachates is maintained in and around 7, as suggested by an earlier researcher (Mohammad 2011), despite the fact that the pH in ash ponds significantly fluctuates from highly acidic to highly alkaline circumstances. Equation (1) was used to determine the heavy metal removal rate as a percentage.

$$\% \text{ removal} = \frac{Co - Ce}{Co} * 100 \quad (1)$$

where, $C_0$and C_e being the initial and equilibrium concentrations respectively.

The adsorption isotherm experiments were carried out varying the adsorbent dosages and maintaining the fixed values of concentrations of the heavy metals.After the equilibrium is reached, the adsorption capacity value, q_e(mg/gm),is calculated using equation (2).

$$q_e = \frac{(Co - Ce)V}{M * 1000} \quad (2)$$

where, V (ml) is the volume of the leachate solution taken for each of the batch setups and M(grams) is the mass of the adsorbent used.

Linear, Langmuir,Freundlich and Temkin isotherm models were used to derive the isotherm constants.

Results & Discussions

Acid Digestion Test Results

The concentrations of the heavy metal (Ni) observed in the leachate of Fly ash was in the range of0.037 - 0.332 ppm .

Batch Adsorption Test Results

Four values were selected as the initial concentrations of heavy metals in solution for the batch adsorption test from the range of results from the acid digestion test. The concentrations of nickel that were selected were 0.1 ppm, 0.15 ppm, 0.2 ppm, and 0.3 ppm.The values for the equilibrium concentrations revealed a consistent decrease in the concentrations of the heavy metals in the solution, confirming the mixed soil's powerful absorption ability. It is observed that the equilibrium concentrations for 16 and 24 hours are nearly always the same. The heavy metal removal efficiency of the mixed soil was observed at 97% for the Nickel. It is observed that in the case of mixed soil, the saturation comes much earlier. due to the reason that the overall fineness of the mixed soil increases. Therefore, increased surface areas are available for adsorption of heavy metals.

Isotherms

Temkin is the best-fitting adsorption isotherm for nickel in mixed soil when equilibrium concentration and adsorption capacity values from the fourth hour are used to plot the adsorption isotherms (Linear, Langmuir, Freundlich, and Temkin).

Conclusion

Addition of Bentonite and Fly ash in selected proportion hasresulted in the reduction inhydraulic conductivity of soil from 10^{-6} to 10^{-8} cm/sec desired for the liner materials.Based on the experimental & numerical modeling results, it is concluded that

- The mixed soil has a strong chance of being used as ash pond lining material because of its relatively increased metal adsorption capability and extremely low hydraulic conductivity.
- According to the experimental findings, the mixed soil has a metal removal efficiency of about 97% for nickel. Additionally, Temkin isotherm is most suited for Nickel, according to isotherm experiments on mixed soil.

References

Alam J, Khan MA, Alam MM, Ahmad A (2012) Seepage Characteristics and geotechnical properties of fly ash mixed with Bentonite. International Journal of Scientific and Engineering Research. 3(8).

Dhadse S, Kumari P, Bhagia LJ (2008) Fly ash characterization, utilization and government initiatives in India - A review. Journal of Scientific and Industrial Research. 67:11-18.

Kumar BR, Sharma RS (2004) Effects of fly ash on Engineering properties of Expansive Soils. Journal of Geotechnical Geoenvironmental Engineering, 130(7).

Mohammed SAS, Naik M (2011) Utilization of Red Soils and Amended Soils as a Liner Material for Attenuation of Copper from Aqueous Solution: Isotherm and Kinetic Studies. Journal of Environmental Science and Technology. 4(5): 504-519.

Pal S, Mukherjee SM, Ghosh S (2014(b)) Application of HYDRUS 1D model for assessment of phenol–soil adsorption dynamics, Environmental Science Pollution Research. 21(7): 5249-5261.

Prasad B, Mondal KK (2008) Heavy metals leaching in Indian fly ash. Journal of Environmental Science and Engineering. 50(2):127-132.

Pu H, Fox PJ (2016) Model for coupled large strain consolidation and solute transport in layered soils. International Journal of Geomechanics. 16(2).

Udoeyo FF, Brooks R, Inyang H Bae S (2010) MO Lateritic Soil as a sorbent for Heavy Metals. International Journal of Recent Research and Applied Studies.4(1).

Chapter:13

2,4-Dichlorophenoxyacetic Acid, (2,4-D) Contaminated Soil Electro-restoration: An Experimental Approach

Debanjali Adhikary[1*], Avishek Adhikary[2], Supriya Pal[3]

[1*,2]Assistant Professor, Department of Civil Engineering, Swami Vivekananda University, Kolkata-700121 West Bengal, India.
[3]Associate Professor, Department of Civil Engineering, National Institute of Technology Durgapur, Durgapur-713 209, West Bengal, India.

*email- debanjalia@svu.ac.in; phone- +91-9093189029

Abstract- In the current study, the effectiveness of electro-kinetic (EK) technology was investigated to evaluate in-situ decontamination of soil contaminated with 2,4-dichlorophenoxyacetic acid (2,4-D) herbicides. In order to extract 2,4-D from the soil using the EK technology, two distinct electrode configurations, including single anode-cathode (SAC) of parallel positioning and alternate anode-cathode (AAC) positioned as a fence, were tested. In both instances, the original soil 2,4-D content was estimated to be 20 mg/kg. For 15 days, the soils were subjected to electro-remediation with an electric field of 1.0 VDC per cm (between subsequent electrodes). In electrolyte cells, periodic observations of the current strength, solution pH, and pollutant concentrations were made before a thorough post-mortem examination of the soils. After the 15-day tests, 2,4-D elimination in SAC and AAC was 80% and 78.19%, respectively.

Keywords: Soil contamination; 2, 4-D herbicide;Electro-remediation;Electrode configurations; Removal efficiency.

INTRODUCTION

The herbicide 2,4-Dichlorophenoxyacetic acid (2,4-D) has grown in popularity among Indian farmers over the years (Kumar and Singh, 2010). However, the excessive use of pesticides to safeguard crop health is seriously polluting the atmosphere as a result of organic contaminants migrating below the surface and combining with the aquifers (Souza et al. 2016). Due to its simple installation in the field, cheap cost, and quicker application, electro-kinetic (EK) remediation of contaminated soil has become an effective in-situ approach (Risco et al. 2015). The majority of prior investigations using EK technology focused on the elimination of soluble metal ions (Malarb et al. 2015). On the in-situ removal of herbicides from agricultural fields, however, relatively few research papers have been published in the state of the art (Rodrigo et al. 2014). The goal of the current investigation is to determine whether the in-situ electro-kinetic treatment method can effectively clean up soil that has been contaminated by the chemical 2,4-D. A cost-benefit analysis was also performed to assess how well the strategy would work in a practical setting.

MATERIALS &METHODS

Materials

To preserve the soil's filled moisture content, soil samples were gathered in a container and then sealed. The physical parameters of the soil sample were subsequently assessed after a 24-hour oven drying period. The physico-chemical characteristics of the soil were assessed in accordance with the BIS: 2720 (Bureau of Indian Standards) recommendations. Batch adsorption tests were also used to measure the soil's capability for adsorption.2,4-Dichlorophenoxyacetic acid (2,4-D), which is of analytical grade, was used to create the synthetic solution of the solute.Throughout the experiment and solution preparation, distilled water was used.

Electro-kinetic Experiment

A cell with three compartments—an anode compartment, a centre box, and a cathode compartment—was used to conduct the electrokinetic test (SAC—single anode cathode). The cell opened at the top and was built of perplex sheet. The cell measured 48 cm long, 20 cm broad, and 15 cm high. Compacted soil samples were placed in the middle container, which measured 16.1 cm in length.The cathode and anode chambers each included two graphite electrodes that were coupled to DC power supply hardware. In order to avoid ions being released into the soil as a result of electrode degradation, inert electrodes were utilised in this investigation. Using a DC power source, a steady voltage of 30 V was kept throughout the test.

Another electrokinetic experiment was carried out on an AAC (Alternate Anode Cathode) setup, which consists of an electrokinetic reactor, a DC power source, and tanks for electrolyte solutions. The volume of compacted soil in the tank was maintained at 36,000 cm3 (LWH: 60x60x10 cm3). Copper rods of 1 cm in diameter and 30 cm in length, respectively, were utilised as the electrodes for the anodes and cathodes and were placed in semipermeable electrolyte wells. Throughout the experiment, a voltage gradient of 1 V/cm remained constant. To reduce herbicide volatilization and electrolyte solution evaporation loss, a capillary barrier of 1 cm of sand was applied to the soil's surface.

Analysis procedure

At several sites, the temperature and electrical current were noted. Daily measurements were made of the herbicide concentration and pH of the electric-osmotic volume obtained from the cathode and anode collector.

After the test, the soil sample was separated into three zones: one for SAC (length), one for AAC (depth). The herbicide concentration at various length/depth sections was determined using the L-S extraction method. Each zone's 50 gramme of dry soil was removed, combined with 250 ml of distilled water, and then magnetically stirred for 20 minutes. The agitated material was placed in a 50 cm3 Eppendorf tube and forcefully swirled at 4000 rpm in a centrifuge with rotor REMI R-8C.With the use of a Shimadzu UV-500 Spectrophotometer model and 1 cm3 quartz cells (cuvette), the aqueous phase was removed from the test tube to determine the concentration of 2,4-D.

RESULTS & DISCUSSIONS

Basic Soil Properties

Table 1 displays the physio-chemical characteristics of the soil sample that was taken. The analysis revealed that 82% of the soil was made up of tiny particles (silt and clay). The Indian Standard Classification System (IS: 1498-1970) classifies the soil as lean clay with medium plasticity (CI).

Table 1: Physico-Chemical properties of soil sample

Soil properties		Values	Standards
Soil colour		Brown	---
Grain size distribution	Sand	18 (%)	IS 2720-4(1985)
	Silt	47 (%)	
	Clay	35 (%)	
Natural Water Content		35.6 %	IS 2720-2(1973)
Bulk density (kN/m^3)		14.9	IS 2720-29 (1975)
OMC (%)		23.4	IS 2720-7 (1983)
Max dry density (kN/m^3)		15.5	
Specific gravity		2.6	IS 2720-3(1) (1980)
Liquid limit (%)		47	IS 2720-5 (1985)
Plastic limit (%)		19.33	IS 2720-5 (1985)

Current Intensity

For the first experiment (SAC), it was possible to monitor the variation of current intensity vs. time at a constant voltage gradient of 1 V/cm. Electric current was modulated at the start of the experiment between 0.02 and 0.05 A. Electric current peaked at 0.14 A at 144 hours, then started to decline and finally stabilised at 0.2 A after 288 hours. The resistance to the movement of ions, which depends on soil moisture, solute ionic concentration, temperature, etc., affects the current value. In the graphs, rising and falling slopes represent the progression of ionisation, while a constant slope represents its end.

In the second experiment (AAC), it can be seen that there were only slight changes in the early phase of the current intensity caused by the applied voltage gradient of 30V, which ranged from 0.8 to 1.2A. The voltage dropped to 5-10 V and the current rose to 4.0-4.9A. Since the ammeter's maximum capacity in the current experiment is 5 A, current cannot be increased past that level. As a result, the water in the catholyte and anolyte is changed before the current intensity exceeds the maximum value (12 hours) of the ammeter. The present intensity stabilises after 15 days. This event indicates that ionisation is finished.

pH profile

As the experiment went on, the pH of the anolyte solution fell until it eventually reached a value of 1.88. This suggests that the area next to the anode well turns acidic, and it demonstrates that after 14 days, the anolyte solution contains the highest concentration of herbicide. This graph also shows the gradual rise in pH in the catholyte solution from 11.98 to 12.4. Deionized water had a pH of 7.

The wells' acute pH variations in the electrolyte solutions for the AAC experiment represent the development of the well-known acidic and basic fronts. To achieve a higher removal efficiency, the anodes and cathodes were switched during the polarisation of the fronts.

Concentration of 2,4-D in soil after the test

The herbicide was washed out of the soil in the first experiment (SAC) by the water flux flowing from anode to cathode due to the electro-osmotic flux. In addition, electro migration was able to move the highly concentrated

2,4-D in the direction of the anode. Greater 2,4-D pesticide removal efficiency from the soil was taking place as a result of the combined effect of the two processes. In the 15-day trial employing the SAC setup, 2,4-D's decontaminating effectiveness was close to 80%. Additionally, the AAC arrangement's removal efficiency was 78.19%.

The performance of 2,4-D removal from soil using the SACarrangement of electrodes was found to be slightly better than the AAC arrangement in EK cell, but the AAC arrangement of electrodes configuration is easily applicable because large blocks of graphite used in SAC are challenging to implant on the field. It was also determined that using copper electrodes instead of graphite was more affordable.

Energy consumption in EK treatment

Power consumption depends mainly upon the current density when voltage is constant. Energy consumption was calculated with respect to time for both experiments using the following equation no. 1:

$$E_c = \frac{V}{1000AL}\int_0^t Idt \qquad (1)$$

where, E_c = energy consumption per unit volume of soil (kWh/m^3),

V = applied electric potential in Volt,

I = current density flowing through the soil specimen (Amp),

A = cross-sectional area of the soil specimen (m^2),

L = length of the specimen (m)

t = elapsed time in hour

At the conclusion of the experiment, the energy consumption for the SAC arrangement was 83 kWh/m3 and the energy consumption for the AAC was 174 kWh/m3.This estimate demonstrates unequivocally that the EK process for herbicide decontamination from soil is a quick and economical in-situ method.

Conclusions

To remove 2,4-D from soil in the current investigation, an electro-kinetic remediation technique was used for 15 days. In a constrained period of 15 days, the efficiency of pollutant removal was approximately 80% for a single anode-cathode (SAC) arrangement and 78.19% for an alternate anode-cathode (AAC) arrangement.

Power usage (kWh/m3) during the experiment was also used to determine the economic viability of the EK treatment. The estimated energy consumption for the SAC and AAC arrangements of electrodes in the EK cell was 83 and 174 kWh/m3, respectively.

EK treatment is a method for cleaning up polluted soil that is economical, adaptable, sustainable, and reliable. The encouraging findings from the current study will greatly aid environmental engineers and contractors in overcoming the difficulties associated with in-situ soil decontamination and restoring agricultural land for future use.

REFERENCES

Kumar S, Singh AK. (2010) A review on herbicide 2, 4-D damage reports in wheat (Triticum aestivum L.), J. Chem.Pharm. Res. , 2(6):118-124.

Malarbì D, Falciglia PP, Vagliasindi FGA. (2015) Removal of Hg from Real Polluted Sediments Using Enhanced-EK Decontamination: Verification of Experimental Methods and Batch-Test Preliminary Results. Hindawi Publishing Corporation J Chem Article ID 270451.

Risco C, Rodrigo S, Vizcaíno LR, Sáez C. (2016) Electrokinetic flushing with surrounding electrode arrangements for the remediation of soils that are polluted with 2,4-D: A case study in a pilot plant, 545-546.

Rodrigo MA, Oturan N, Oturan MA (2014) Electrochemically Assisted Remediation of Pesticides in Soils and Water: A Review. American Chemical Society ,Chem. Rev, 114 (17).

Souzaa FL, Saézb C, Llanosb J, Lanzaa MRV, Cañizaresb P, Rodrigo MA (2016) Solar-Powered Electrokinetic Remediation for the Treatment of Soil Polluted with the Herbicide 2,4-D. Electrochimica Acta 190: 371–377-2.

Chapter-14

Evaluation of Heavy Metal Contamination Levels in Industrial Areas Near Durgapur

AvishekAdhikary[1*], Debanjali Adhikary[2], SupriyaPal[3]

[1*,2]Assistant Professor, Department of Civil Engineering, Swami Vivekananda University, Kolkata-700121 West Bengal, India.
[3]Associate Professor, Department of Civil Engineering, National Institute of Technology Durgapur, Durgapur-713 209, West Bengal, India.

*email- avisheka@svu.ac.in; phone- +91-9606946927

Abstract - Due to the possibility of their migration into groundwater through precipitation infiltration and their potential source of entry into the food chain through plant root water uptake, heavy metals that are present in soil beyond the allowed limits are a major environmental problem. The objective of the current study is to assess the geographical variation in the concentration of heavy metals in the soil of Durgapur, West Bengal, India. The order of the heavy metal content was Zn> Pb> Ni> Cd> Hg. Additionally, the soil has undergone various chemical characterizations. The levels of heavy metal concentration were compared to the soil criteria set by the USEPA in 2002 and the CCME in 2007. MULLERS' assessment of pollution revealed that it was at an alarmingly high level everywhere. The findings of the present study may point to the necessity of establishing a continuous and methodical monitoring of heavy metal pollution in the industrial area surrounding Durgapur city in order to ensure that the level of contamination does not pose a significant threat to the city's residents in the future.

Keywords— Heavy Metals; MULLERS classification; Pollution Load Index; Contamination Factor

INTRODUCTION

The rising levels of soil pollution are a key source of worry today [1].The reasons behind this could be due to soils' peculiar characteristics, such as their poor structure, unpredictable layering, and high concentrations of trace elements [2]. In addition, soils are the'receivers' of significant amounts of heavy metals from a variety of sources, one of which is industrial wastes and effluents. The Durgapur industrial city in West Bengal, India, which is around 160 km from Kolkata and is part of the Burdwan District, is one of the industrialised cities. In this case, pollution is harming the lithosphere, hydrosphere, and atmosphere. The sole focus of this essay is atmospheric pollution. Numerous activities carried out by these companies result in enormous amounts of air pollutants, liquid effluents, and solid trash. Because these wastes and effluents contain many harmful chemicals and certain heavy metals as well, they may result in soil pollution if they are disposed of in an untreated manner. Because they are not degradable like organic matter and persist in the soil once they are ingested, heavy metal contamination of soil is one of the main areas of concern among these pollutants, and this area has been the focus of this study. The goal of the current study is to assess the level of heavy metal contamination in Durgapur, specifically in relation to cadmium (Cd), mercury (Hg), zinc (Zn), lead (Pb), and nickel (Ni).
Detailed objectives of this study include:

- Evaluation of the levels of heavy metal concentrations, their spatial distribution, and comparison to the USEPA 2002 soil quality guideline in Durgapur's soil samples.
- Application of cutting-edge statistical methods like correlation matrices to study the linkages between sources of high levels of heavy metals in the soil and the complicated dynamics of pollutants.
- A variety of pollution indices [3] are chosen to quantify the level of heavy metal contamination.

MATERIALS & METHODS

48 top soil samples (0–20 cm) in total were taken from 16 distinct Durgapur locations, as shown in Table I. Three soil samples were taken from each of these areas, which were separated by 40 to 60 metres. The majority of Durgapur's regions were considered while choosing the research sites so that a more precise assessment of the area's soil pollution could be made. In virgin plastic bags, the samples were procured. The resulting soil samples were air dried for 48 hours. To create a uniform sample, the samples were later lightly ground with the aid of a mortar. After that, each sample was evenly combined and sieved. Then a 250 ml beaker containing 1 g of soil was filled with 10 ml (1:1) HNO_3, heated for 5 minutes, then allowed to cool for 5 minutes before being filled with 5 ml of conc. HNO_3 was re-added and heated for 5 minutes (if strong brown fumes arise, keep adding HNO_3 until no more brown smells escape). Then 3 ml of 30% H_2O_2 and 2 ml of distilled water were added. The amount was then decreased to 5 ml. The solution was then cooled, water was added, and Whatman No. 41 filter paper was used to get the final volume of 100 ml. Using distilled water, reagent blanking was done simultaneously. Then, using an Atomic Absorption Spectrophotometer (AAS), the heavy metals (Cd, Hg, Zn, Pb, and Ni) were analysed in accordance with the guidelines provided in APHA (1995), Standard procedures for the assessment of water and waste water, 21stEdison; American Public Health Association, Washington, DC..

Table I: Regions of sample collection with latitude & longitude

Sample Regions	Latitude	Longitude
PCBL	23°30'15.88"N	87°18'48.30"E
ASP	23°31'41.46"N	87°16'9.46"E
DSP	23°33'39.84"N	87°15'6.24"E
DCL	23°30'23.53"N	87°17'8.76"E
GI	23°29'23.95"N	87°20'5.70"E
DCW	23°33'43.40"N	87°13'59.90"E
BEN	23°33'24.71"N	87°16'36.64"E
BZ	23°34'3.57"N	87°18'59.48"E
CC	23°32'26.45"N	87°18'14.75"E
BID	23°31'55.72"N	87°19'35.25"E
KALNG	23°31'52.05"N	87°21'44.81"E
DCOC	23°29'56.26"N	87°17'56.86"E
SGB	23°29'43.23"N	87°20'7.00"E
ANG	23°30'53.20"N	87°16'4.98"E
SUKP	23°29'13.74"N	87°19'26.53"E
FULJ	23°32'9.84"N	87°20'22.21"E

Note: **PCBL:** Philips Carbon Black Ltd.**, ASP:** Alloy Steels Plant**, DSP:** Durgapur Steel Plant**, DCL:** Durgapur Chemicals Ltd.**, GI:** Graphite India**, DCW:** Durgapur Cement Works**, BEN:** Benachity**, BZ:** B-Zone**, CC:** City Centre**, BID:** Bidhannagar**, KALNG:** Kalinagar**, DCOC:** Durgapur Coke Oven Colony**, SGB:** Sagarbhanga**, ANG:** Angadpur**, SUKP:** Sukanta Pally**, FULJ:** Fuljhore**.**

Different regions' soil samples contained high levels of heavy metals, and various indices were used to measure the pollution caused by heavy metals. Additionally, a comparison of the heavy metal concentration with the accepted standards for soil quality from the USEPA in 2002 and the CCME in 2007 was made.

RESULTS AND DISCUSSION

Heavy Metal Concentrations

Table II displays the total metal concentration for each sampling site that was discovered in the soil samples. Each region provided three samples, and the average value of the three samples—which provides a more reliable and accurate depiction of the concentration of heavy metals—was determined. In Table III, these average values are listed. According to the table, the concentration of metals ranged over the following boundaries: Cd: 1.03 to 2.20 mg/kg, Pb: 4.85 to 26.19 mg/kg, Hg: 0.01 to 0.11 mg/kg, Zn: 6.67 to 529.66 mg/kg, and Ni: 4.04 to 22.96 mg/kg. The sampling site's mean heavy metal content was: This enables them to be arranged in decreasing order of heavy metal content as Zn > Pb > Ni > Cd > Hg. Cd: 1.61 mg/kg, Pb: 12.68 mg/kg, Hg: 0.07 mg/kg, Zn: 71.43 mg/kg, and Ni: 10.59 mg/kg.

Table II: Concentration of Heavy Metals in soil samples (mg/kg) (dry weight basis)

Sample Regions	Cd	Pb	Hg	Zn	Ni
PCB	1.89	14.2	0.06	30.05	4.18
ASP	1.92	17.2	0.08	34.79	7.64
DSP	1.94	13	0.09	50.19	4.04
DC	2.2	26.19	0.11	**529.66**	21.59
GI	1.75	17.2	0.05	62.75	12.72
DCW	1.84	21.4	0.04	78.53	7.26
BEN	1.55	18.2	0.06	80.68	7.4
BZ	1.03	4.98	0.07	14.73	15.28
CC	1.67	7.4	0.09	23.61	5.34
BID	1.91	4.85	0.05	13.16	10.52
KALNG	1.43	9.8	0.08	28.02	7.9
DCOC	1.75	14.8	0.09	58.35	7.34
SGB	1.33	7.2	0.05	50.60	12.76
ANG	1.25	5.6	0.08	43.07	22.96
SUKP	1.19	14.4	0.05	38.00	14.26
MEAN	**1.608**	**12.676**	**0.065**	**71.428**	**10.593**
MAX	**2.2**	**26.19**	**0.11**	**529.66**	**22.96**
MIN	**1.03**	**4.85**	**0.01**	**6.67**	**4.04**

SD	**0.351**	**6.408**	**0.025**	**124.148**	**5.676**

The Table III below shows the Pearson correlation coefficient matrix for the heavy metals identified in the soil samples from Durgapur. Cadmium and Lead (0.64), Cadmium and Mercury (0.50), Lead and Zinc (0.66), and Zinc and Nickel (0.50) all showed a substantial association in the data, which can be interpreted as coming from the same or similar sources.

	Cd	Pb	Hg	Zn	Ni
Cd	1				
Pb	0.64	1			
Hg	0.50	0.28	1		
Zn	0.49	0.66	0.46	1	
Ni	-0.24	0.00	-0.03	0.50	1

Assessment of Heavy Metal Contamination

Assessment of Heavy Metal according to USEPA, 2002 and CCME, 2007 Guidelines :
The heavy metal contaminations in the soil were assessed by comparing with the soil quality guideline proposed by USEPA 2002 & CCME 2007. These standards are shown in **Table IV** below.

Table IV: USEPA 2002 & CCME 2007 Guidelines for soil [mg/kg (dry weight)]

METAL	**US EPA Guidelines 2002**			**CCME Guidelines, 2007**
	Not Polluted	Moderately Polluted	Highly Polluted	
Pb	<40	40 – 60	>60	70
Cd	….	….	>6	1.4
Zn	>90	90 – 200	>200	200
Ni	_	_	_	50
Hg	_	_	_	6.6

The current investigation shows that only some of the locations are contaminated by Pb, Hg, and Ni. Only the area next to Durgapur Chemicals has significant Zn pollution. Pollution from Zn is absent from all other areas. All the sites for Cd are polluted, with the exception of BZ, SGB, ANG, SUK, and FULJ.

Assessment according To Geo-Accumulation Index(I_{geo})
The geo-accumulation index is a commonly used metric to assess the level of heavy metal contamination in the soil. Muller [4] suggested comparing the current concentration of a heavy metal with the pre-industrial levels of a heavy metal to estimate the metal pollution in the soil or sediments. The formula for Geo-accumulation index

is as below:

$\mathbf{I_{geo} = \log_2 [C_n/1.5B_n]}$

Where C_n: concentration of element and B_n: geochemical background value (in this study B_n is considered as the world surface rock average given by Martin and Meybeck **[5]**.

A factor of 1.5 is included in the above equation for justification of the possible variation in the background data due to lithogenic effect. On the basis of Muller's classification, the soil or sediments can be classified into seven grades of pollution level which are shown in **Table V**.

Table V: MULLER'S Classification for Geo-accumulation.

$\mathbf{I_{geo}}$ **Value**	**Class**	**Soil or Sediment Quality**
≤0	0	Unpolluted
0-1	**1**	Unpolluted to Moderately Polluted
1-2	**2**	Moderately Polluted
2-3	**3**	Moderately to Highly Polluted
3-4	**4**	Highly Polluted
4-5	**5**	Highly Polluted to Extremely Polluted
>6	**6**	Extremely Polluted

The geo-accumulation index (Igeo) scale consists of seven grades (0 - 6) ranging from unpolluted to highly polluted (shown in Table VI).

Table VI: Igeo for Different Samples

Sample Site	Lead	Mercury	Nickel	Cadmium	Zinc
PCB	-0.757	-0.137	-4.136	2.655	-2.664
ASP	-0.480	0.277	-3.266	2.678	-2.453
DSP	-0.884	0.447	-4.185	2.693	-1.924
DC	0.125	0.736	-1.767	2.874	1.475
GI	-0.480	-0.400	-2.530	2.544	-1.602
DCW	-0.165	-0.722	-3.339	2.616	-1.278
BEN	-0.399	-0.137	-3.321	2.369	-1.241
BZ	-2.272	0.599	-2.272	1.779	-3.698
CC	-1.698	0.446	-3.795	2.476	0.275
BID	-2.307	-0.401	-2.805	2.67	-3.816
KALNG	-1.293	0.277	-3.224	2.252	-2.766
DCOC	-0.698	0.446	-3.336	2.544	-1.708
SGB	-1.736	-0.401	-2.531	2.148	-1.915

ANG	-2.101	0.277	-1.68	2.058	-2.152
SUKP	-0.736	-0.722	-2.363	1.987	-2.329
FULJ	-1.91	0.084	-3.158	1.847	-4.836
FULJ	-1.91	0.084	-3.158	1.847	-4.836

(i) Assessment Based on Contamination Factor, Pollution Load Index And Degree of Contamination

The contamination factor and degree of contamination are used to determine the contamination level of the soil and these are used in the present study. According to D. C. Thomilson, D. J.Wilson, C. R. Harris, D. W. Jeffrey[4], the contamination factor can be calculated as below:

Contamination factor (CF) = $C_{metal}/C_{background}$

C_{metal}: Concentration of the metal in the sample

$C_{background}$: Background concentration of metal (pre industrialization concentration).

In the present study, world surface rock average proposed by Martin and Meybeck[5] is considered as background concentration.

(ii) Pollution Load Index(PLI)

The term PLI represents the number of times by which the metal content in the sample soil exceeds the background concentration value of the metal. It gives asummativesignal about the overall level of heavy metal toxicity in a particular sample or region **[6]**.The pollution load index for a particular sample can be calculated as below:

$PLI = (CF_1 \times CF_2 \times CF_3 \times CF_4 \times \ldots \times CF_n)^{1/n}$

PLI < 1 indicates no pollution

PLI > 1 indicates pollution

The sum of all the contamination criteria for a site is the degree of contamination. The contamination level of each sample location is determined from the contamination factor table by adding up the contamination factors for each heavy metal for each sample location separately. The outcome demonstrates that there is significant heavy metal contamination near PCB, ASP, DSP, DC, DCW, and DCOC. The other areas (shown in Table VII) have a moderate level of heavy metal pollution.

Degree of contamination = Summation of contamination factor of each heavy metal for a location.

Table VII: Terminologies used to describe the contamination factor.

CF	Cd	Degree of contamination
CF<1	Cd<6	Low
1<CF<3	6≤Cd<12	Moderate
3<CF<6	12≤Cd<24	Considerable
CF>6	Cd≥24	Very high

Now the contamination factors, pollution load indices and the degrees of contamination are tabulated in **Table VIII** below.

Table VIII: Contamination factors, Pollution Load indices (PLI) and Degree of Contamination

Sample Location	Contamination factors					PLI	Degree of contamination*
	Pb	Hg	Cd	Ni	Zn		
PCB	0.89	1.35	9.45	0.09	0.24	0.75	12.02
ASP	1.08	1.80	9.6	0.16	0.27	0.96	12.91
DSP	0.81	2.02	9.7	0.08	0.40	0.87	13.01
DC	1.64	2.47	11	0.44	4.17	2.41	19.72
GI	1.08	1.12	8.75	0.26	0.49	1.06	11.7
DCW	1.34	0.90	9.2	0.15	0.62	1.01	12.21
BEN	1.14	1.35	7.75	0.15	0.64	1.03	11.03
BZ	0.31	0.22	5.15	0.31	0.12	0.42	6.11
CC	0.46	2.02	8.35	0.11	0.19	0.70	11.13
BID	0.30	1.12	9.55	0.21	0.10	0.58	11.28
KALNG	0.61	1.80	7.15	0.16	0.22	0.77	9.94
DCOC	0.93	2.02	8.75	0.15	0.46	1.03	12.31
SGB	0.45	1.12	6.65	0.26	0.40	0.81	8.88
ANG	0.35	1.80	6.25	0.47	0.34	0.91	9.21
SUKP	0.9	0.90	5.95	0.29	0.30	0.84	8.34
FULJ	0.4	1.57	5.40	0.17	0.05	0.49	7.59

*by Tomlinson et al (1980).

From Table VIII, it can be inferred that:

- All the locations have a very high degree of contamination for cadmium.
- For Lead, ASP, DC, GI, DCW and BEN have moderate degree of contamination. Rest other locations has low degree of contamination.
- For Mercury, DCW, BZ and SUKP have low degree of contamination. Rest other location are moderately polluted with mercury.
- For Nickel, all the locations have low contamination.
- For Zinc, only DC has considerable amount of pollution. Rest all have low pollution.

CONCLUSION

According to the analysis of surface soil samples taken from 16 industrial areas of Durgapur City, the areas are polluted with zinc, lead, cadmium, nickel, and chromium, in the following decreasing order: Zn > Pb > Ni > Cd > Hg. The statistical correlation study revealed that the source inputs for the pairs of cadmium and lead, cadmium and mercury, lead and zinc, and zinc and nickel may be identical or comparable. In most regions,

there is a sizable source of cadmium pollution, per USEPA soil quality criteria from 2002. According to USEPA 2002, the research region has little to no pollution for the other heavy metals. Zinc pollution in the areas close to M/s. Exit of Durgapur Chemicals Ltd. By leaching, the high concentration of zinc in the area around it has the potential to pollute nearby soil and ground water. All of the study area's regions have very low mercury pollution levels, but since mercury is extremely hazardous even at very low concentrations, it may build up in the soil and pose a concern to both the environment and human health.

To repair contaminated land, a variety of in-situ procedures may be used, including electrokinetic extraction of pollutants from surface or nearby land[11], solidification/stabilization of contaminated soil using additives[10], bioremediation and phytoremediation[12], etc. However, before choosing any of the aforementioned strategies to clean up polluted soil, it is wise to conduct a careful analysis of their economic viability.

REFERENCES

[1] V. Parth, N.N. Murthy and P.R. Saxena, "Assessment of heavy metal contamination in soil around hazardous waste disposal sites in Hyderabad city (India): Natural and Anthropogenic implications," Journal of Environmental Research and Management, Vol. 2(2), pp. 027-034, 2011.

[2] A. K. Pendidas and H. Pendidas, "Chemometric Evaluation of the Heavy Metals in urban Soils of Fallujah City, Iraq," Journal of Environmental Protection, Vol. 6(11), 2015.

[3] H. Ghrefat and N. Yusuf, "Assessing Mn, Fe, Cu, Zn and Cd Pollution in Bottom Sediments of Wadi Al-Arab Dam, Jordan," Chemosphere, Vol. 65(11), pp. 2114- 2121, 2006.

[4]G. Muller, "Index of Geo accumulation in Sediments of the Rhine River," Journal of Geology, Vol. 2(3), pp. 108-118, 1979.

[5] J. M. Martin and M. Meybeck, "Elemental Mass Balance of Materials Carried by Major World Rivers," Marine Chemistry, Vol. 7(3), pp. 173-206, 1979.

[6] Z.Q. Xu, S. J. Ni, X. G. Tuo and C.J. Zhang, "Calculation of Heavy Metals' Toxicity Coefficient in the Evaluation of Potential Ecological Risk Index," Environmental Science and Technology, vol. 31, pp. 112–115, 2008.

[7] USEPA, Soil screening guidance: technical background document. EPA/540/R-95/128. Office of Solid Waste and Emergency Response, Washington, 1996.

[8] USEPA, Supplemental guidance for developing soil screening levels for superfund sites. OSWER 9355.4-24. Office of Solid Waste and Emergency Response, Washington, 2001.

[9] USEPA, Mercury study report to congress. Vol. V:Health Effects of Mercury and Mercury Compounds. EPA-452/R-97-007. Office of Air Quality Planning and Standards and Office of Research and Development, Washington,1997.

[10] C.N. Mulligan, R.N. Yong and B.F. Gibbs, "Remediation technologies for metal-contaminated soils and groundwater: an evaluation," Engineering Geology, vol. 60(1-4), pp. 193-207, 2001.

[11] A.T. Yeung, C.N. Hsu and R.M. Menon, "Physicochemical soil-contaminant interactions during electrokinetic extraction," Journal of Hazradous Materials, vol. 55(1-3), pp. 221-237, 1997.

[12] W.W. Walter, "Rhizosphere processes and management in plant-assisted bioremediation (phytoremediation) of soils," Plant and Soil, vol. 321(1-2), pp. 385-408, 2009.

Chapter-15

Innovative Roof Waterproofing Using Crushed Rubber Tire Crumb in M_{25} Concrete

Subhabrata Guha[1], Samir Kumar[2], Sunil Priyadarshi[3], Dr. Vishnu Pada Bose[4]

Abstract: Roof waterproofing is a critical aspect of building construction, ensuring the durability and longevity of structures. Traditional methods of roof waterproofing often involve the use of various membranes, coatings, and sealants. However, recent innovations in construction materials have led to the exploration of alternative solutions that are both environmentally friendly and effective. This paper presents a detailed investigation into the use of crushed rubber tire crumb as an additive in M_{25} concrete for enhancing roof waterproofing. The study encompasses material characterization, mix design optimization, mechanical properties evaluation, and waterproofing performance assessment. The findings highlight the potential of utilizing recycled rubber materials to improve the properties of concrete for enhanced roof waterproofing.

Keywords: Roof Waterproofing, M_{25} Concrete, Crushed Rubber Tire Crumb, Recycled Materials, Mix Design, Mechanical Properties, Waterproofing Performance.

Introduction

The global issue of waste material disposal is a pressing concern, with waste tire dumping being a significant challenge due to the difficulty of degradation. Waste rubber, including old tires, is a valuable resource for producing rubber goods. Concrete, composed of cement, coarse aggregate, and fine aggregate, is a widely used construction material, leading to a depletion of natural aggregates. Various techniques have been proposed to utilize waste tires, such as incorporating crumb rubber into concrete as a replacement for coarse or fine aggregates. However, limited research has explored this approach. Modifying building materials holds promise in addressing waste disposal issues and reducing pollution caused by tire incineration. Incorporating crumb rubber into lightweight concrete, building exteriors, and architectural components can have significant benefits.Advantages of the study:Efficient utilization of waste materials, Easy accessibility of all required materials, Reduced roof load due to lower density, Flexible materials that resist cracking. The focus of this experiment is to evaluate the use of waste materials, specifically recycled rubber tire crumbs, in civil engineering. This includes assessing how rubber-concrete mixtures can enhance concrete's resistance to water absorption, making it waterproof. By using rubber tire crumbs as a partial replacement for traditional aggregates, the study aims to create lightweight roofs and environmentally-friendly construction solutions.

Significance of the Study:

The study explores the use of rubber tire waste as aggregates in reinforced concrete, taking into account the properties of rubber, such as density, moisture absorption, and thermal insulation. This approach offers benefits such as cost-effectiveness and environmental conservation, as rubber tire crumbs are cheaper than traditional aggregates and can sometimes be obtained for free. Additionally, by reducing the weight of structures through the use of rubber tire crumbs, the study contributes to improving construction materials'

performance.

Objectives of the Experiment:

The specific objectives of the study include: (a) Using discarded rubber tires in the form of rubber tire crumbs to reduce concrete's permeability and water absorption, effectively making it waterproof. (b) Experimenting with different classes of rubber tire crumbs (Class A, Class B, and Class C) to identify the most suitable for reducing concrete's permeability and water absorption. (c) Investigating the optimal mix proportion that achieves waterproof concrete in compliance with ASTM standards for water absorption, permeability, and sportively. (d) Making recommendations based on the experiment results regarding the use of rubberized concrete for structural lightweight applications and identifying the mix with the lowest water absorption and permeability rate.

The aim of the study

Is to understand how varying the volume of rubber in regular concrete affects its compressive strength, split tensile strength, and flexural strength. This section reviews existing research and findings related to rubberized concrete. Key points include: The reduction in compressive strength when coarse aggregates are fully replaced by rubber chips. The enhancement of durability, toughness, impact resistance, strain capacity, and sound insulation properties in rubberized concrete. The influence of rubber particle size, surface roughness, and type of concrete on the mechanical strength. The potential application of rubberized concrete in non-structural, low-strength requirements due to its desirable characteristics. The impact of rubber content on workability, air content, and unit weight of fresh rubberized concrete.

Properties of Crumb Rubber:

This section discusses the physical and chemical properties of crumb rubber, including particle size, conversion methods, and chemical components. The fresh properties of crumb rubber concrete, including workability, air content, and unit weight, are crucial factors to consider when using this material. Details on the raw materials used in the experiment, including cement, river sand, and tire rubber crumb powder.Recycled rubber, in the form of crumb rubber, is used to create waterproof linings for roofs and foundations. It prevents water penetration, even if shingles or other materials fail.

Testing on Materials:

The types of tests conducted on materials, such as initial and final setting times for cement, specific gravity, water absorption, impact value, flakiness index, abrasion test for aggregates, and specific gravity, bulking of sand, and silt content test for sand, are discussed.

Mix Design

Mix design involves the meticulous selection of appropriate concrete ingredients and the determination of their respective proportions. The ultimate goal is to create concrete with a specific minimum strength and durability while optimizing cost-effectiveness. Typically, we opt for the M_{25} concrete grade to achieve optimal results.

For Conventional Concrete Cubes, the quantities of materials used were as follows:

Cement Weight: 5160 grams, Sand Weight: 5160 grams, Aggregate Weight: 15480 grams. For Rubberized

Concrete Cubes, incorporating 3%, 5%, 10%, and 15% crumb rubber (CR) as a replacement for fine aggregate, the quantities of materials used were:Cement Weight: 5160 grams, Sand Weight: 5001.80 grams, Crumb Rubber Weight: 158.80 grams, Aggregate Weight: 10320 gramsSubsequently, fine aggregate was substituted with 5%, 10%, and 15% crumb rubber based on the weight of the fine aggregates.

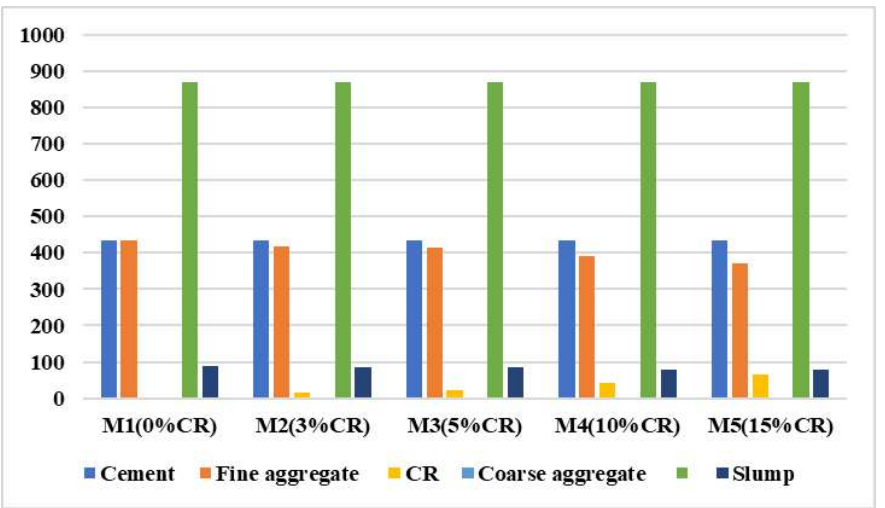

Fig. 1. Composition of different percentage of crumb rubber.

In the current experimental investigation, a total of 90 specimens were cast. This comprised 30 cubes, with each set of 6 cubes dedicated to a specific percentage of crumb rubber (0%, 3%, 5%, 10%, and 15%). Within each set of 6 cubes, 3 were subjected to testing after 7 days, while the remaining 3 were tested after 28 days. Additionally, 30 beams and 30 cylinders were cast, with each set of 6 beams and 6 cylinders intended for a particular crumb rubber percentage. Among these, every set of 3 beams and 3 cylinders, featuring varying crumb rubber percentages, were tested after 7 days and 28 days, respectively. It's noteworthy that the initial setting time of the cement is 70 minutes, and the final setting time is 180 minutes, with the initial setting time ideally being longer. The Flakiness index was found to be 8.56%, well below the technical limit of 35%. The abrasion test result was 9.5%, all well within acceptable limits, indicating the suitability of the aggregates for use.The specific gravity of the sand measured at 2.66%, which falls within the range of 2.65 to 2.67, while the sand's bulking was determined to be 13.55%, with a moisture content of 2.6%. It's important to note that excessive moisture content can enhance workability but may compromise strength. The Silt content test yielded a result of 3.77%, comfortably below the allowable limit of 8%. After conducting various experiments on different materials, all values fell within acceptable limits, affirming the suitability of our materials for further use.

The experiments included testing forCompressive strength, Split tensile strength. All tests were conducted on hardened concrete in accordance with IS 516-2021 standards. We employed weigh batching and hand mixing for cube compression tests and split tensile strength tests on cylinders, both for plain and Crumb Rubber Concrete (Rubberized Concrete). These test results were then compared with conventional M_{25} grade concrete.

Tests on Hardened Concrete

Compressive strength characterizes a material's ability to withstand compression forces when subjected to an applied load that pushes it together. In simpler terms, it signifies the minimum load required for a particular material to break down. In this experiment, we evaluated the compressive strengths of all the cubes we casted with varying ratios of crumb rubber. Cube specimens measuring 150 mm in size were manufactured in accordance with the Indian Standard specification IS: 516-2021. Once completed, the samples were covered with protective sheets to minimize moisture loss. After 24 hours, the specimens were demolded and placed in water for curing. Compressive strength tests were conducted after 7 and 28 days.

The formula employed for calculating compressive strength was as follows:

$$\Sigma\sigma = \frac{P}{A} \text{----------(1)}$$

Where: $\Sigma\sigma$ = Compressive Strength (N/mm²) P = Maximum load (N) A = Cross-sectional area of the cube (mm²)

Split tensile strength characterizes a material's resistance to forces attempting to pull it apart. It represents the minimum force required to split a specific material. We casted cylinders measuring 150 mm in diameter and 300 mm in length, compacted them using vibrators, and conducted tests on them after demolding and curing. These tests were performed after 7 and 28 days to determine their split tensile strengths.

Literature Review

Eldin and Senouci (1993)[1] examined the effects of rubber incorporation into concrete, revealing an approximately 85% reduction in compressive strength and a 50% decreasein stiffness when the entire coarse aggregate was replaced with coarse rubber chips.Specimens experienced up to 65% compressive strength loss and around 50% stiffness reduction. The study also noted that rubber-containing samples under compressive loading did not exhibit significant deformations. This phenomenon was further investigated, focusing on both shear and compressive modes for different rubber fractions.

Chou et.al 2010[2]The authors highlighted the weaker tensile bond of rubber-treated concrete compared to its compressive strength, suggesting that concrete with coarse tire chips would exhibit strain softening before reaching its compressive limit. The localized stress concentrations at the top and bottom of rubber aggregates resulted in microcracking along the sample. Rubber particles acted as energy-absorbing springs, arresting crack propagation and preventing complete concrete failure. Under continued compressive loading, more cracks formed and existing ones extended, enabling the material to absorb plastic energy and withstand substantial deformations.

Rivas-Vázquez [3] analyzed compressive and split tensile strengths in rubberized concrete after 7 and 28 days of curing, observing minimal differences between the two periods. Replacing coarse aggregate with rubber chips, especially at high volumes (75% and 100%), led to up to 85% compressive strength reduction and 50% stiffness reduction. A marginal decrease was observed when fine sand was replaced with rubber fragments. The rubberized samples demonstrated high capacity for absorbing plastic energy under both compression and tension.

Topcu (1995)[4] compared cube and cylinder compressive strength tests on regular and rubberized concrete. Unexpectedly, rubberized concrete exhibited lower compressive strength from cylinder tests. Mechanical strength was influenced by rubber particle characteristics and concrete type. **Goulias and Ali (1997)[5]** found that dynamic moduli of elasticity and rigidity decreased with increasing rubber content, indicating less brittle behavior. Damping capacity decreased with higher rubber content. On the contrary, other researchers advocated for rubberized concrete in applications requiring vibration damping. The dynamic modulus

showed a correlation with compressive strength.
The damping coefficient derived from transverse frequency correlated with compressive strength, suggesting a potential predictive tool. Further research is warranted to confirm these findings**. Kumar, K. (2017)[6]** demonstrated that 10% rubber chip addition increased concrete strength by 23% and evaluated the workability of rubberized mixtures, revealing decreased slump with increased rubber content. Mixtures with fine rubber particles exhibited better workability than those with coarse rubber chips or a combination of both.

RESULT AND DISCUSSIONS

The test results pertaining to concrete incorporating crumb rubber reveal a consistent trend of declining strength properties, including compressive strength, flexural strength, and split tensile strength. This phenomenon is of significant interest in the realm of construction and materials engineering, as it reflects the impact of crumb rubber inclusion on the fundamental structural characteristics of concrete. Firstly, it is crucial to emphasize that the introduction of crumb rubber into the concrete mixture leads to a decrease in the overall performance of the material. Compressive strength, a critical parameter in assessing a concrete's ability to withstand axial loads, experiences a notable reduction in value. This reduction in compressive strength can range from 10% to 27%, depending on the specific composition of crumb rubber incorporated. This finding underscores the trade-off between sustainability, achieved through recycling rubber materials, and the compromise in concrete's compressive strength, which is a vital attribute for structural applications.

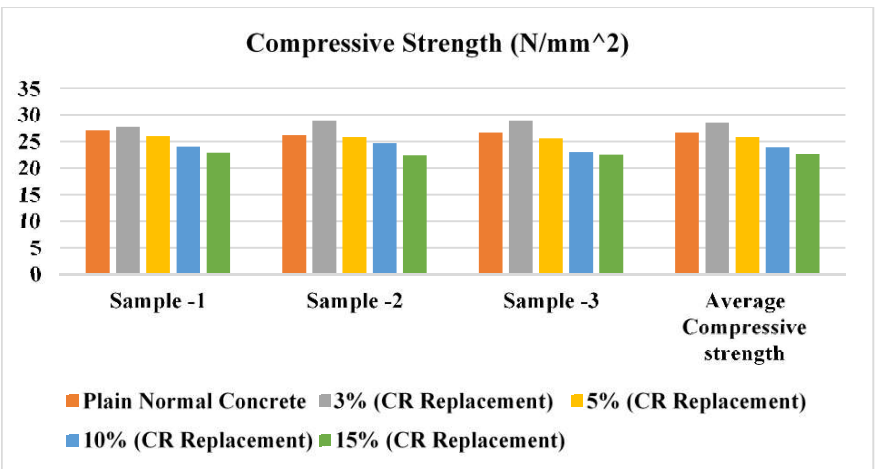

Fig. 2. Result of Compressive Strength for different sample and its average compressive strength.

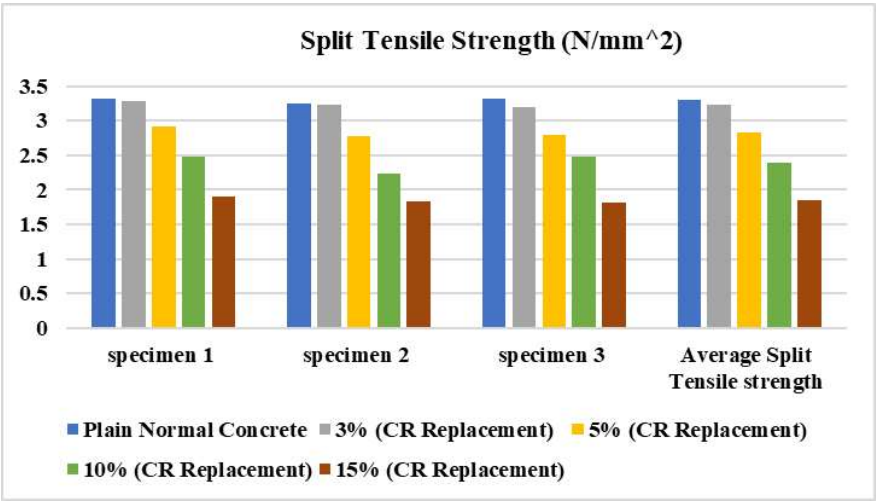

Fig. 3. Result of Split Tensile Strength for different sample and its average Split Tensile strength.

Split tensile strength, a measure of a material's resistance to tensile forces applied perpendicular to its surface, exhibits a decrease when crumb rubber is introduced. The reduction in split tensile strength falls within the range of 8% to 25%. Interestingly, this decrease is relatively less pronounced compared to the decline in compressive strength. This observation suggests that split tensile strength may exhibit greater resilience to the presence of crumb rubber, implying that it could be a less affected strength parameter when aiming to incorporate sustainable rubber materials into concrete.

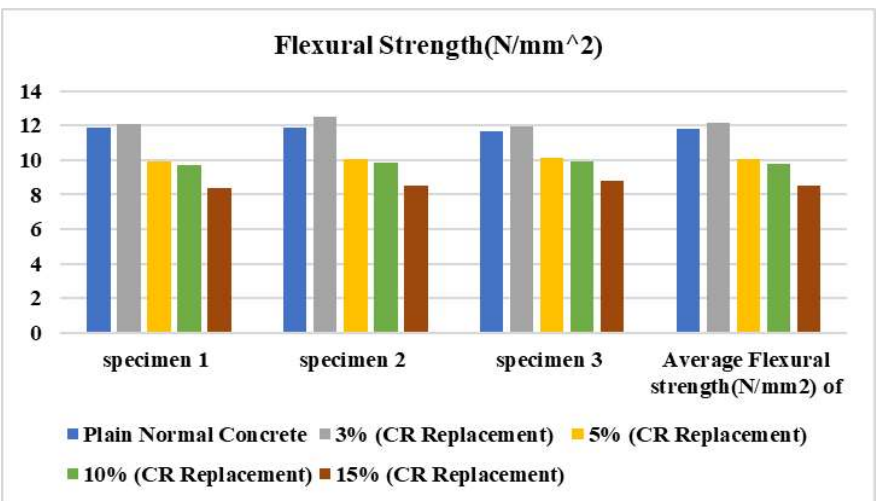

Fig. 3. Result of Flexural Strength for different sample and its average Flexural Tensile strength.

Flexural strength, which characterizes a material's ability to withstand bending or torsional forces, follows a trend similar to compressive strength. There is a reduction in flexural strength, akin to the decrease observed in compressive strength. The reduction in flexural strength typically ranges from 20% to 30%, further

highlighting the consistent impact of crumb rubber on various strength parameters of the concrete.

Conclusions

The integration of crumb rubber into concrete formulations results in a decline in key strength properties, including compressive strength, split tensile strength, and flexural strength. These reductions vary in magnitude but consistently manifest across different crumb rubber ratios. While this phenomenon poses a challenge in maintaining concrete's structural performance, it also presents an opportunity to explore innovative solutions that strike a balance between sustainability and strength in construction materials. aimed to explore the optimal utilization of crumb rubber in concrete while safeguarding concrete strength and evaluating its properties following the introduction of these materials. The findings provide valuable insights into the potential for incorporating small quantities of crumb rubber, ranging from 3% to 5%, as a substitute for fine aggregate in M_{25} grade concrete.

Compressive Strength: The study indicates that the addition of 3% crumb rubber leads to an 8% increase in the compressive strength of M_{25} grade concrete. Beyond this threshold, the compressive strength stabilizes, displaying similar values to controlled concrete. However, further increases in crumb rubber content result in reduced strength. This reduction may be attributed to entrapped air, which rises with the higher presence of rubber crumb.

Split Tensile Strength: The incorporation of 3% to 5% crumb rubber in M_{25} grade concrete demonstrates an increase in split tensile strength, ranging from 3.9% to 4.2%. However, similar to compressive strength, further additions of crumb rubber led to diminishing values. The study highlights that split tensile strength exhibits greater resilience compared to compressive strength when crumb rubber is introduced.

Flexural Strength: The investigation into flexural strength reveals an interesting trend. Flexural strength increases with the addition of crumb rubber until a 9% threshold, after which it begins to decline.

Impact Resistance: Impact test results indicate that the energy consumption increases by 6% and 9% with the addition of crumb rubber, resulting in a 35.8% and 43% increase at first crack and a 46.6% and 50% increase at ultimate failure compared to conventional concrete. This increase in impact load can be attributed to the energy absorption capacity of crumb rubber.

Water Absorption: The study observes a slight increase in water absorption (above 2%) when crumb rubber content reaches 12% to 15% in concrete mixes (M25). This increase is attributed to the natural water-absorbing tendency of crumb rubber.

Acid Attack Resistance: When subjected to acid attack testing, concrete with 15% crumb rubber replacement at 28 days experiences a maximum weight loss of 1.98% for M25 grade concrete.

RCPT (Rapid Chloride Penetration Test): The results of the RCPT demonstrate that the addition of crumb rubber in concrete, ranging from 3% to 15%, by partially replacing fine aggregate, yields low values for 28 and 56 days, complying with ASTM C 1202 standards for M25 grade concrete.

Correlation Between Compressive Strength and Split Tensile Strength: A positive correlation is observed between measured compressive strength and split tensile strength, indicating that the strength of concrete decreases with the addition of rubber content.

Correlation Between Compressive Strength and Impact Strength: The correlation between compressive strength and energy absorbed during impact strength displays a strong relationship in the concrete.

Practical Applications: Crumb rubber concrete meets the required strength characteristics and IRC (Indian

Roads Congress) standards, making it suitable for floor and roof construction.

Density of Fresh Concrete: The density of fresh concrete decreases with increasing crumb rubber content due to the lower specific gravity of crumb rubber. Additionally, crumb rubber introduces air content, further contributing to a reduction in concrete density. The non-polar and rough nature of rubber particles tends to trap air at their surface.

Environmental Impact: Utilizing crumb rubber as a construction material helps reduce the stockpiling of tires and minimizes the depletion of natural resources, such as river sand.

In conclusion, the incorporation of crumb rubber into concrete brings about nuanced effects on various concrete properties. While there is a marginal decrease in compressive strength, split tensile strength exhibits greater resilience, and flexural strength initially improves before diminishing. Impact resistance and energy absorption capacity increase significantly. Water absorption and resistance to acid attack are influenced by the proportion of crumb rubber. The study offers a comprehensive understanding of the trade-offs and potential benefits associated with using crumb rubber in concrete, highlighting its suitability for certain construction applications while considering its impact on concrete properties.

References

1. Eldin, N.N., and Senouci, A.B. (1993) Rubber-tire particles as concrete aggregate. Journal of materials in civil engineering, **5** (4), 478–496.
2. Chou, L.-H., Lin, C.-N., Lu, C.-K., Lee, C.-H., and Lee, M.-T. (2010) Improving rubber concrete by waste organic sulfur compounds. Waste Management & Research, **28** (1), 29–35.
3. Rivas-Vázquez, L.P., Suárez-Orduña, R., Hernández-Torres, J., and Aquino-Bolaños, E. (2015) Effect of the surface treatment of recycled rubber on the mechanical strength of composite concrete/rubber. Materials and Structures, **48**, 2809–2814.
4. Topcu, I.B. (1995) The properties of rubberized concretes. Cement and concrete research, **25** (2), 304–310.
5. Goulias, D.G., and Ali, A.-H. (1997) Evaluation and Performance Based Mix Design of Rubber Modified Mixtures.
6. Kumar, K. (2017) investigation on mechanical properties of concrete by the partial replacement of fine aggregate with crumb rubber. Technology, **8** (7), 438–446.

Chapter-16

Dynamic seismic analysis of multi-storied buildings having different heights for all seismic zones in India

Rejina Yasmin[1], Dr. Abir Sarkar[2] [0000-0003-0174-4530], Ashes Banerjee[3] and Nilanjan Tarafder[4]

1 Research Scholar, Department of Civil Engineering, Swami Vivekananda University, Kolkata 700121, INDIA
rejinayasmin3@gmail.com
2 Asst. Prof., Department of Civil Engineering,
Swami Vivekananda University, Kolkata 700121, INDIA
abirs@svu.ac.in
3 Asst. Prof., Department of Civil Engineering,
Swami Vivekananda University, Kolkata 700121, INDIA
ashesb@svu.ac.in
4 Asst. Prof., Department of Civil Engineering,
Swami Vivekananda University, Kolkata 700121, INDIA
nilanjant@svu.ac.in

Abstract. This study examines the application of the Response Spectrum Method across seismic zones in India, ranging from low to critical seismic regions. In the realm of civil engineering, constructing buildings of varying heights necessitates a paramount focus on ensuring structural safety, serviceability, and durability. With the growing significance of seismic events in modern times, safeguarding structures against potential damage caused by seismic excitations becomes a crit- ical concern. The extent of seismic damage inflicted upon structures hinges on several factors, including building height, seismic zone classification, seismic re- sistance techniques, and soil characteristics. The relationship between earthquake effects and structure height is particularly noteworthy, as seismic waves can alter ground motion, thereby influencing structural integrity. This study delves into the performance of structures of diverse heights situated in different seismic zones. It places specific emphasis on the Response Spectrum Method, a seismic resistance technique known for enhancing structural behavior when confronted with lateral forces during seismic events. By analyzing the effectiveness of this method across varying structural heights in different seismic zones, this research contributes to a deeper understanding of seismic resilience in the context of In- dian construction practices.

Keywords: Seismic Zones, Storey displacement, Base Shear, Base moment, SAAP2000 software, Response spectrum method

Introduction

Throughout history, earthquakes have claimed countless lives and inflicted extensive property damage. The

sheer force of seismic waves has the potential to induce ground motion leading to building collapses, landslides, tsunamis, and volcanic activities. A stark reminder of this vulnerability is the recent 6.4 magnitude earthquake that struck Assam, India, on April 28, 2023, resulting in two fatalities, and at least 12 injuries, with buildings collapsing at the epicenter. This region falls within the highly seismic Hazard Zone V. These incidents underscore the paramount importance of implementing earth- quake-resistant design principles in structures to mitigate casualties and damage. Struc- tural engineers have tirelessly endeavored to reduce lateral loads and enhance structural rigidity through mechanisms such as "moment resisting frames." These frames aim to bolster a building's seismic resistance, particularly during major earthquakes. However, the effectiveness of these techniques varies with factors such as building height, seismic zone classification, and the inherent soil characteristics of the location. India's seismic zoning map classifies the country into four seismic zones (Zone II, III, IV, and V), with Zone V experiencing the highest level of seismicity. These zones are outlined in the Indian standard code IS:1893, part-1, 2016. This study encompasses all seismic zones to provide insights into structural performance under varying seismic excitations.

This research focuses on the performance of structures of differing heights across all seismic zones, with a specific emphasis on the utilization of the Response Spectrum Method. Understanding the interaction between building height and seismic zones in India is crucial in advancing our knowledge of structural resilience. The numerical anal- ysis in this study is conducted using SAP2000 software, known for its capabilities in structural analysis. A multi-storey building is analyzed, considering critical lateral load conditions, and designed as a Special Moment Resisting Frame (SMRF) to enhance performance. AutoCAD software is employed for floor plan creation. Response Reduc- tion Factor, R, as per IS 1893, part-1, 2016, guides the structural design. The study evaluates storey displacement, base shear, and base moment to gauge structural re- sponse.

The primary aim of this study is to conduct seismic analysis on G+5, G+10, G+15, and G+20 storey residential buildings across all seismic zones in India using SAP2000, v24 software. The objectives encompass dynamic analysis of buildings with varying heights, improving seismic resistance compared to conventional construction, adher- ence to IS 1893-2016 part-I criteria, ensuring safety, stability, and serviceability during earthquakes, creating awareness of seismic effects, and demonstrating improved build- ing response under dynamic loading conditions. This research aims to enhance our un- derstanding of the seismic behavior of buildings of different heights in various seismic zones, ultimately contributing to safer and more resilient structural design practices.

Literature review

The literature review concentrated on seismic forces and their influence on the qual- ity of life, as explored by researchers who have analyzed seismic forces across different

earthquake zones. These authors also elucidated the investigations carried out to miti- gate or manage seismic effects. Below, we delve into these research papers to acquire insights into seismic responses and gain an understanding of seismic analysis from pre- vious studies.

Dr. Nagesh, Yash Dehankar (May, 2022): The paper involves the comparative study of Seismic analysis of different heights building on different types of soil using Base Isolation technique (for G+10, G+15, G+20, G+25). The comparative study focuses on the behavior of different height of structure, Earthquake Zone, and type of Soil with Base Isolation techniques (Codes are: IS456:2000; IS1893:2016 and IS 13920:1993). Friction Isolator, Triple pendulum Isolator, Lead Rubber bearing Isolator is used in Base Isolation techniques. There has Friction Isolator which has better results than other base Isolator. In case of soft soil Frictional Isolator is better but in case of other types of soil frictional Isolator and Triple pendulum Isolator shows the same result. For the analysis of Base Isolation technique has been used and modeling of structures has done by ETABS.

In June 2022, Shaik Akhil Ahamad and K.V. Pratap conducted a dynamic analysis of a G+20 multi-storied building using shear walls located in various positions within different seismic zones. They employed the ETABS software for this investigation, fo- cusing on the comparative behavior of braced frame buildings through dynamic analy- sis (according to IS 13920:1993 and IS: 875-1987 standards). The study utilized the Response Spectrum Method.

The findings revealed that incorporating a braced system in the structure is advanta- geous for resisting seismic waves, as it effectively reduces displacement, axial forces, and bending moments in columns. Across all seismic zones in India, the study observed higher maximum displacement values in seismic zone V. It was also noted that intro- ducing uniform stiffness in the structure can further mitigate displacement. In the case of soft soil, structures featuring symmetrically placed shear walls demonstrated supe- rior performance compared to those without shear walls. Vinay Danam (Oct, 2015): The paper has done lateral load analysis of multistoried RCC building (G+10) by con- sidering 4 models. In the first model is without providing any shear wall, in the second model has coupled type with openings and the third model has a rectangle type shear wall at four corners, and the fourth model corner core type shear wall system has done by SAP2000 software. This study mainly focused on seismic forces, lateral displace- ment and shear wall system. In this paper G+10 storey building analyzed with different types of shear walls. Maximum earthquake intensity area (Zone IV, Zone V) where four corners and centroid shear wall can reduce the deflection of the building. Also, it can reduce the shear force and bending moment of the building. It is observed that in Zone III, rectangular type shear wall and in Zone II coupled type shear wall is more suitable. In September 2013, A.E. Hassaballa, Fathelrahman M. Adam, and M.A. Ismaeil used STAAD PRO software to analyze a G+25 storey reinforced concrete building's seismic response via the Response Spectrum Method. Their study aimed to assess dis- placements, stresses, and seismic hazards. The results showed excellent column and beam deflection performance. Exterior columns had a greater seismic impact than inte- rior ones, and ground floor columns experienced compression stresses 1.2 to 2 times

higher than tensile stresses. Beams exhibited nearly equal maximum tension and com- pression values during seismic analysis.

Mr. Murat Saatcioglu and JagMohan Humar (23 April 2003): They studied dynamic analysis of (G+5, G+10, G+15) building for earthquake resistance design by SAP2000 software. This analysis is done by linear dynamic method. The paper provides an over- view of dynamic analysis, elastic analysis, fundamental period, seismic design, struc- tural analysis and structural design. The comparative study focuses on the behavior of braced frame building with the help of dynamic analysis (IS 13920:1993, IS: 875- 1987). The result gives better if we provide Braced system in the structure to reduce displacement, axial force and bending moment in columns.

E. Pavan Kumar, A. Naresh, M. Nagajyothi, and M. Rajasekhar (November, 2014) conducted earthquake analysis on a G+15 multi-storied residential building using the Response Spectrum Method. Their study compared the seismic behavior of Ordinary Moment Resisting Frames (OMRF) and Special Moment Resisting Frames (SMRF) through STAAD.PRO V8i software.

Vinay Mantha and S.S.Sanghai (June, 2016) conducted a study comparing seismic and non-seismic analysis of a G+17 storey building using SAP2000. They employed the Equivalent Static Method with the goal of minimizing structural damage during seismic events in a cost-effective manner. The study focused on analyzing maximum shear forces and bending moments, revealing significantly increased values in seismic analysis compared to non-seismic analysis.

Dr. Sachin Balkrishna Mulay, Dr. Jyotiprakash G. Nayak, and Mr. Rahul Tarachand Pardeshi (Dec, 2022) conducted research on the analysis and design of shear walls and storey drift in a high-rise building under seismic excitations. They utilized I-shaped shear walls and employed the Response Spectrum Method via ETABS software. The objective was to determine the optimal location for shear walls to enhance resistance against lateral forces in seismic zone IV. The study compared two building conditions: one with shear walls, which effectively resisted lateral forces, and another without shear walls, which failed to provide sufficient lateral force resistance.

K. Supreem, N. Ragunath, S. Madhu (Oct, 2022): In the research, there has seismic analysis of G+15 storey building has done by using Response Spectrum Analysis method by using SAP2000 software. The comparative study is focused on the response spectrum method and Time period method for seismic analysis. In Time period method results more. In time period method results show that to check the Time period of struc- ture, should be 2.7 sec for regular structure.

K.Ramakrishna Reddy, DR. S. Vijaya Mohan Rao (Nov, 2016): The paper involves the comparative study of Seismic analysis of different heights of building using Time History method (for G+15, G+20, G+25). The comparative study focuses on the behav- ior of different height of structure, Earthquake Zone, and type of Soil. The response spectrum method has been used for this study. Response spectrum method has been used for this study. To resist seismic wave it is better if we provide Shear wall in the structure to reduce displacement, axial force, and bending moment in columns. In all the seismic zones of India, maximum displacement values are found to be higher in seismic zone v. It is better if we provide uniform stiffness in the structure to reduce

displacement. In case of soft soil, the structure with shear walls placed symmetrically will give better results as compared to the structure without shear walls.

Dr. B. Anil, N.V.S.S.Raju (July, 2012): The paper involves the comparative study of response spectrum analysis for (G+5, G+10, G+15, G+20) storied building. Com- parative study on the displacement of different height building under different soil con- dition is done. The comparative study focuses on the behavior of different height of structure, Earthquake Zone, and type of Soil. Response spectrum analysis and Time history analysis method has been used for this study. To resist seismic wave it is better if we provide Shear wall in the structure to reduce displacement, axial force, and bend- ing moment in columns. Maximum displacement is found in the soil of Sathupally than Eluru and Guntur. In response spectrum analysis, it is better if we provide shear wall and also if we provide shear wall symmetrically.

Dheeraj Bothra, Yashish Rathi (Feb, 2022): The paper is about the seismic analysis of high-rise building with vertical irregularities. In this research, there have (G+30, G+30 with vertical irregularity) multi-storied building is analyzed by using ETABS software. In this paper behavior, seismic response, time period, storey drift, shear force, and axial force is compared with normal building and building with vertical irregulari- ties.

Mohsin Aakib Shamim Akhtar (Feb, 2022): The paper involves dynamic seismic analysis of multi-storey buildings in seismic zone V by using STAAD.PRO software. In this research, behavior, seismic response, time period, storey drift, shear force, and axial force is compared with normal building and building with double cross type brac- ing.

Kassem Trabolsi (Nov, 2020): The paper is about the study of the effect of soil struc- ture interaction of a high rise building on a raft foundation by using SAP2000 software. The objective of the study is to observe the effect of soil structure interaction on the response of high-rise buildings with raft foundations. In this paper building on different types of soil with seismic excitation has been observed.

Methodology

The study focuses on the seismic analysis of a multi-storied building with varying heights. However, seismic analysis encompasses different approaches. The Equivalent Static Method proves adequate for smaller building structures in terms of seismic re- sistance analysis. For taller structures, it necessitates consideration of more than two modes and the calculation of mass weights for each mode to withstand lateral seismic loads. This method is unsuitable for analyzing high-rise structures. Conversely, seismic analysis requires specific location considerations. The Time History Method encoun- ters challenges in obtaining seismic records for every location within a seismic zone area.

In contrast, the Pushover Method faces limitations in accounting for variations in dynamic properties and nonlinear responses caused by changes in stiffness and strength

during load cycles. Consequently, the Response Spectrum Method is employed to ad- dress these challenges. This method enables the analysis of displacement and member forces within the structure and can calculate maximum displacement values and mem- ber forces for each mode of earthquake shaking using a design spectrum.

Problem Statement

The SAP2000 software is used for developing 3D modeling and analysis. The lateral loads that are applied on the different heights of buildings are based on the Indian stand- ard codes. The study is performed for different seismic zones in India as per IS 1893:2016 (part 1).

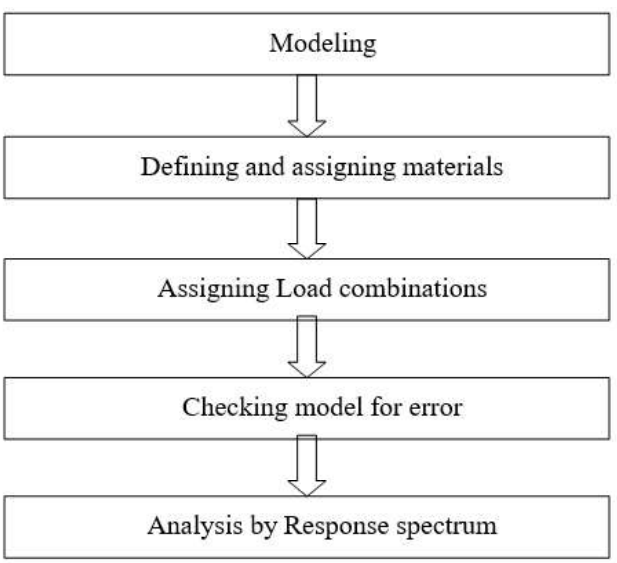

Fig. 1. Flow chart of methodologies

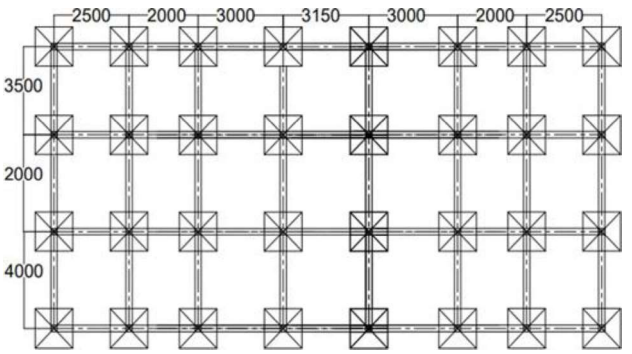

Fig. 2. Column & beam positions

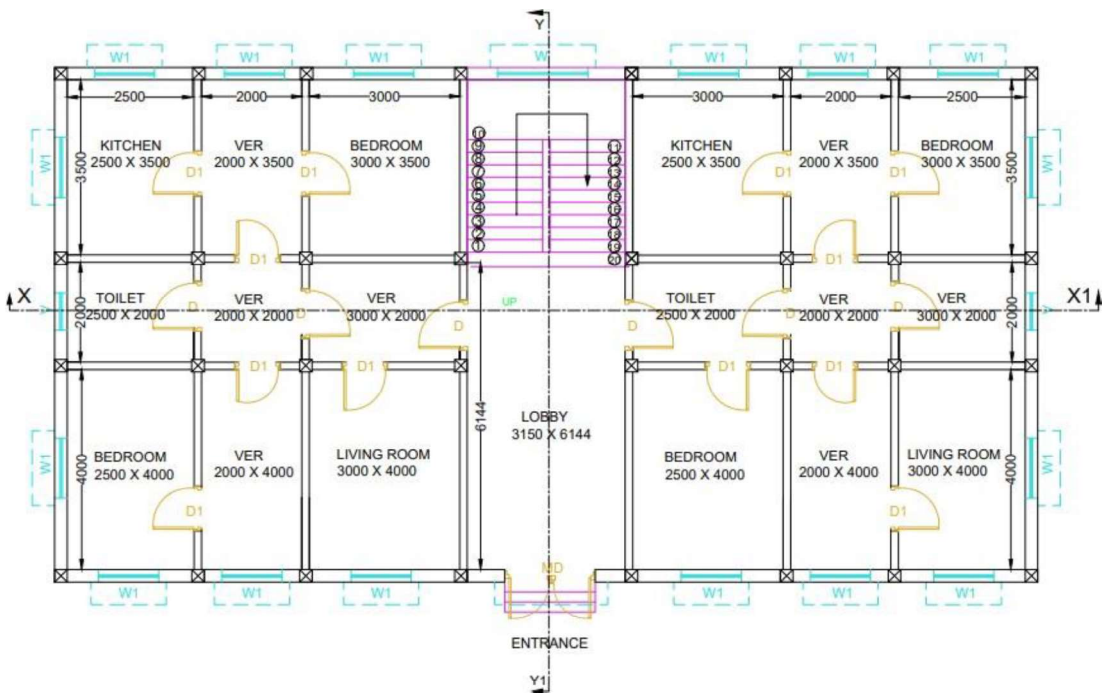

Fig. 3. Plan of Multi-storid building

Table-2: Building Specification

Component	Value
Structure	SMRF
Number of model	16
Each Storey height	G+5,G+10,G+15,G+20
Type of building	Residential
Seismic Zone	Zone II, III, IV, V (As per IS 1893:2016(part1))

Table-3: Material properties

Component	Value
Grade of concrete	M25, M30
Grade of steel	Fe500
Density of reinforced concrete	25 KN/m2
Density of steel	78.5 KN/m2

Table-4: Member properties

Component	Value
Beam size	300mm X 250mm
column size	Rectangular column: 350mm X 300mm Square column: 300mm X 300mm
Slab thickness	150mm

Table-5: Seismic properties

Component	Value
Live loads	2KN/m2, 3KN/m2, 1.5 KN/m2 and 0.75 KN/m2 (as per IS 875(part2))
Zone factor(Z)	0.10, 0.16, 0.24, 0.36 (as per IS: 1893:2016; table-3(part-1, cl-6.4.2))
Importance factor(I)	1 (as per IS:1893(part-1):2016,table-8)
Response reduction factor	5 (as per IS:1893(part-1):2016,table-9)
Soil type	II (medium soil) (as per IS:1893(part-1):2016,table-4)
Damping factor	0.05 (as per IS: 1893:2016; (part-1, cl-7.2.4))

The 3D model of the plan

- Model 1: G+5 storey RC SMRF building in Seismic zone II
- Model 2: G+5 storey RC SMRF building in Seismic zone III
- Model 3: G+5 storey RC SMRF building in Seismic zone IV
- Model 4: G+5 storey RC SMRF building in Seismic zone V
- Model 5: G+10 storey RC SMRF building in Seismic zone II
- Model 6: G+10 storey RC SMRF building in Seismic zone III
- Model 7: G+10 storey RC SMRF building in Seismic zone IV
- Model 8: G+10 storey RC SMRF building in Seismic zone V
- Model 9: G+15 storey RC SMRF building in Seismic zone II
- Model 10: G+15 storey RC SMRF building in Seismic zone III
- Model 11: G+15 storey RC SMRF building in Seismic zone IV
- Model 12: G+15 storey RC SMRF building in Seismic zone V
- Model 13: G+20 storey RC SMRF building in Seismic zone II
- Model 14: G+20 storey RC SMRF building in Seismic zone III
- Model 15: G+20 storey RC SMRF building in Seismic zone IV
- Model 16: G+20 storey RC SMRF building in Seismic zone V

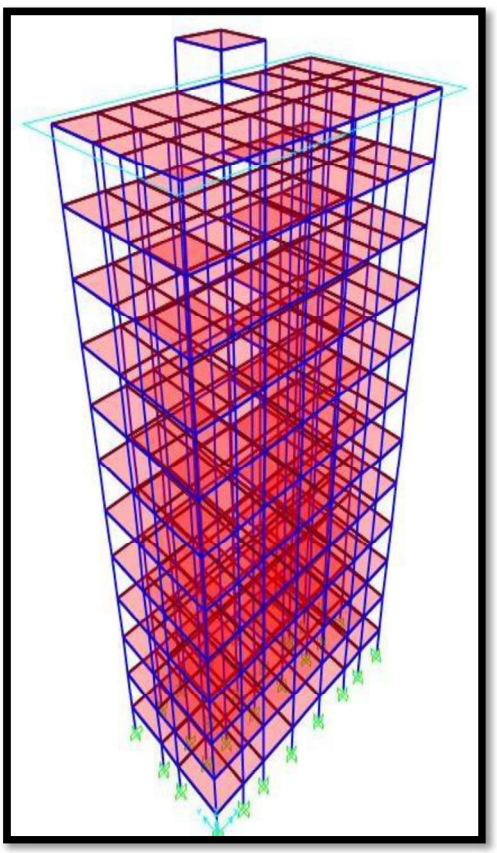

Fig. 4. 3D model for G+10 storey

To find out the performance of the different heights of the RCC building, the com- parative study about storey displacement, frequency, time period, base shear and mo- ment with the help of linear analysis by

SAP2000 software. Four different heights of models were studied for medium soil in low seismic zone to critical seismic zone

Response spectrum analysis

Conducting a response spectrum analysis aims to ascertain the seismic forces' distri- bution across each floor of a multi-story residential building and its various lateral load-resisting components.

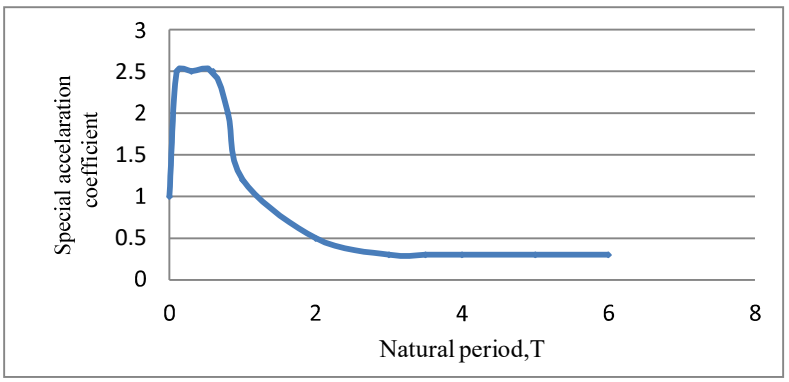

Fig. 5. Design acceleration coefficient (Sa/g) vs. Time period (T) for Medium soil (Source: IS: 1893, 2016 (part-1, Fig.2))

The SAAP2000 software utilizes the following bellow procedure to generate the lateral seismic loads to the building.

1] Creating grid points and generating the structure 2] Defining and assigning of properties

Assigning of supports

Defining approximate fundamental natural period Ta of oscillation in second,

Ta=0.075h 0.75 (As per IS: 1893 (part-1):2016; cl-7.6.2)

For G+5 storey building, Ta= 0.075 X 22 0.75 = 0.76 cycle/sec

For G+10 storey building, Ta= 0.075 X 37 0.75 = 1.13 cycle/sec

For G+15 storey building, Ta= 0.075 X 52 0.75 = 1.45 cycle/sec

For G+20 storey building, Ta= 0.075 X 67 0.75 = 1.76 cycle/sec 5] Defining load pattern and load combination

This analysis has been done by horizontal X and Y to resist lateral seis- mic forces. Out of all the load combinations analyzed, the following seismic load combinations are given below,

1.2(DL+LL±RSX)

1.2(DL+LL±RSY)

1.5(DL±RSX)

1.5(DL±RSY)

0.9DL±1.5RSX

0.9DL±1.5RSY

Assigning of dead loads For Slab load

Floor load= Slab thickness X concrete density
= 0.15 X 25 = 3.75 Kn/m2
For floor finish load = 1 Kn/m2 For wall load
External wall load= wall thickness X unit weight of brick X (total height – beam depth)
= 0.25 X 20 X (3.1-0.3)
= 14 KN/m
Internal wall load= wall thickness X unit weight of brick X (total height – beam depth)
= 0.15 X 20 X (3.1-0.3)
= 8.4 KN/m
Parapet wall load= wall thickness X unit weight of brick X height of parapet wall
= 0.125 X 20 X 1.2
= 3 KN/m
Assigning of live loads
The live loads or imposed loads to be taken in the residential buildings have been given in IS 875 (part-2) - 1987. The live loads which are used in this analysis, are: 2KN/m2 (for rooms and floors), 3KN/m2 (for the staircase), 1.5 KN/m2 (for the accessible roof) and 0.75 KN/m2 (for the non-accessible roof).
Assigning of seismic loads
Assigning of load combinations
Analysis of G+5, G+10, G+15, G+20 storey buildings.

Results and Discussion

Data obtained from the Saap2000 software has been compiled in various formats, in- cluding tables and figures. These visual representations facilitated the comparison of results across different building heights within various seismic zones in India. The fig- ures and tables below illustrate the analysis of maximum displacement, base shear, base moment, fundamental time period, and frequency, all of which were examined to assessthe lateral stability of the building.

Joint Displacements

Table-6: Maximum displacement obtained from SAP2000

Seismic Zones	Building Height	RSX (mm)	RSY (mm)
Zone-II	G+5	8.2	8.8
	G+10	14.3	19.2
	G+15	15.2	20.5
	G+20	40.6	54.0
Zone-III	G+5	13.1	14.1
	G+10	23.0	30.0
	G+15	24.3	32.8
	G+20	65.1	86.5
Zone-IV	G+5	19.7	21.2
	G+10	36.4	49.2
	G+15	54.0	73.0
	G+20	97.6	129.0
Zone-V	G+5	29.5	31.8
	G+10	51.8	69.3
	G+15	78.0	97.0
	G+20	146.0	194.0

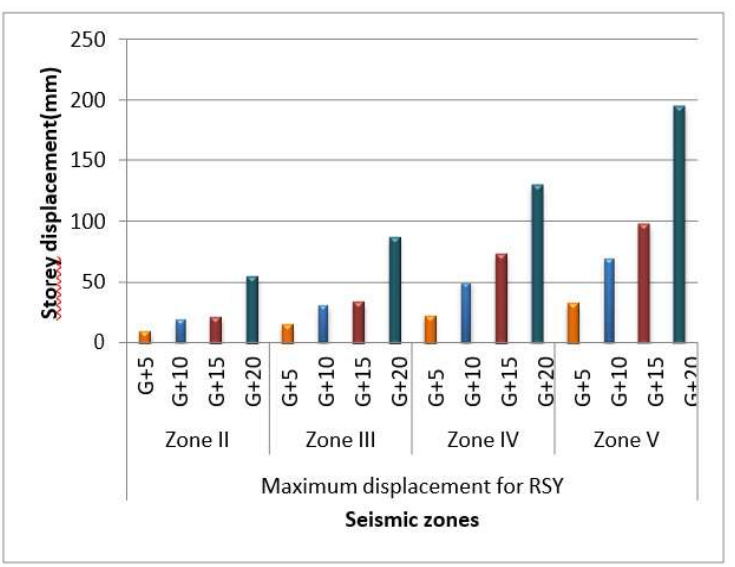

Fig. 6. Comparison of Maximum displacement of different building heights vs. seismic zones along X direction

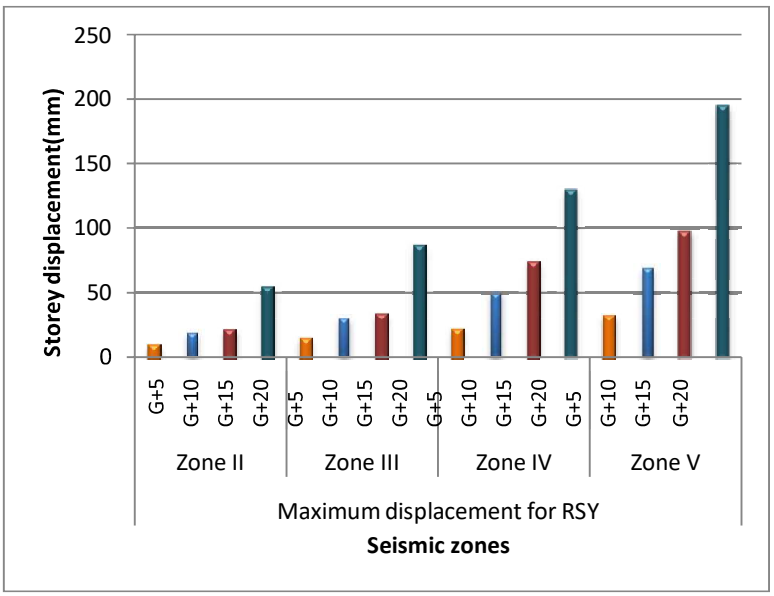

Fig. 7. Comparison of Maximum displacement of different building height vs. seismic zones along Y direction

Base Reactions

Table-7: Maximum base shear obtained from SAP2000

Seismic Zones	Building Height	RSX (KN)	RSY (KN)
Zone-II	G+5	131	131
	G+10	215	370
	G+15	271	425
	G+20	280	597
Zone-III	G+5	202	203
	G+10	345	351
	G+15	434	477
	G+20	460	629
Zone-IV	G+5	485	468
	G+10	518	580
	G+15	621	629
	G+20	637	670
Zone-V	G+5	728	728
	G+10	777	780
	G+15	978	998
	G+20	1015	1021

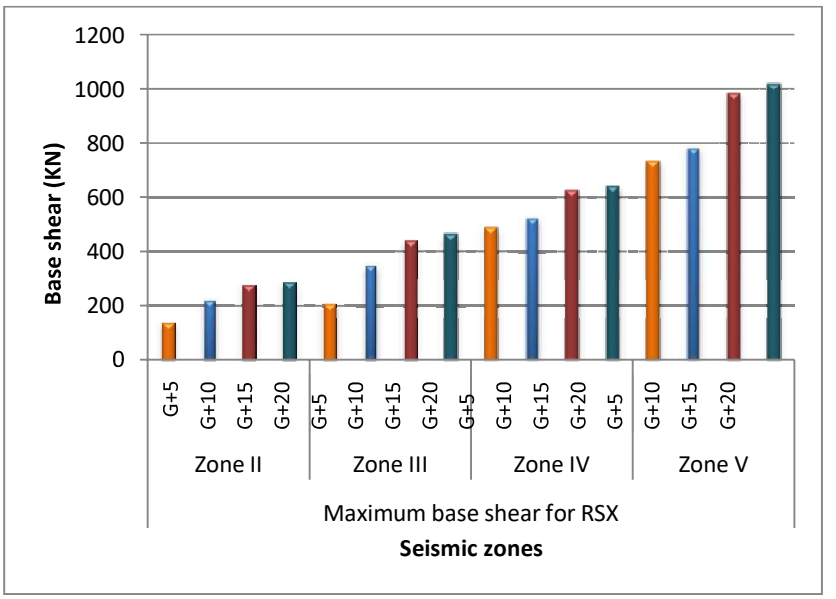

Fig. 8. Comparison of Maximum base shear of different building height vs. seismic zones along X direction

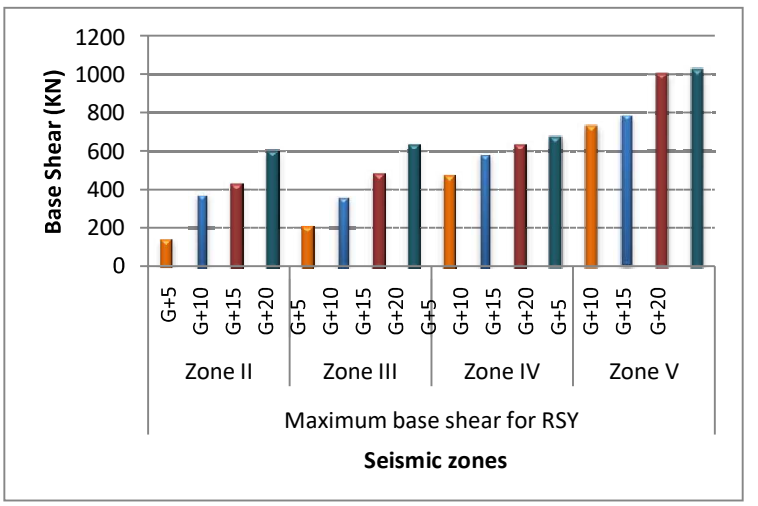

Fig. 9. Comparison of Maximum base shear of different building height vs. seismic zones along Y direction

Table-8: Maximum base moment obtained from SAP2000

Seismic Zones	Building Height	RSX (KN.m)	RSY (KN.m)
Zone-II	G+5	82	82
	G+10	102	108
	G+15	118	118
	G+20	159	163
Zone-III	G+5	105	109
	G+10	180	183
	G+15	181	181
	G+20	225	270
Zone-IV	G+5	157	197
	G+10	210	225
	G+15	225	225
	G+20	251	290
Zone-V	G+5	210	210
	G+10	246	267
	G+15	259	305
	G+20	301	324

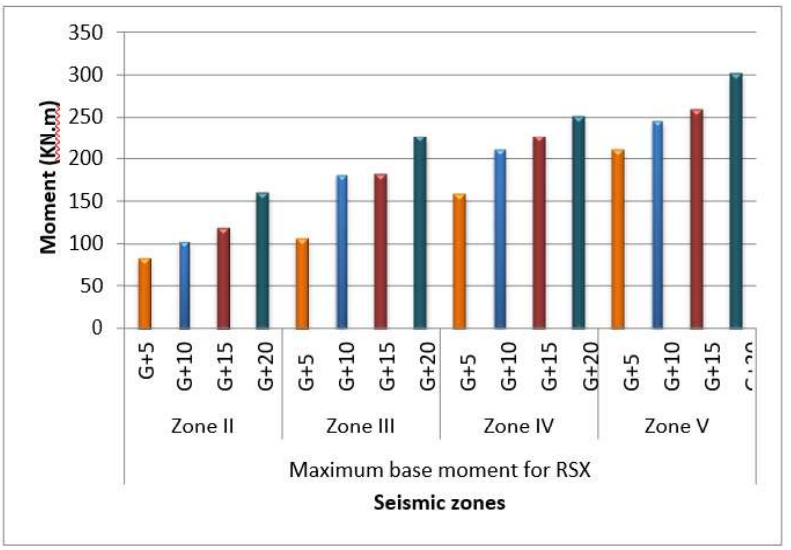

Fig. 10. Comparison of Maximum base moment of different building heights vs. seismic zones along X direction

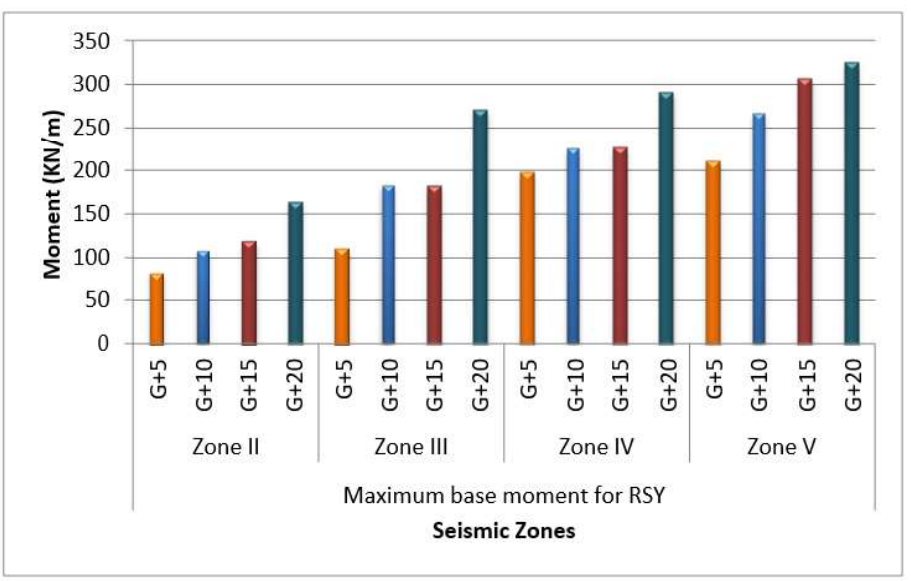

Fig. 11. Comparison of Maximum base moment of different building height vs. seismic zones along Y direction

1.2 Periods and Frequencies

Table-9: Time period & Frequencies are obtained from SAP2000

Seismic Zones	Building Height	Time Period (Sec)	Frequency (Cycle/sec)
Zone-II	G+5	1.67	0.59
	G+10	3.3	0.30
	G+15	3.3	0.30
	G+20	6.12	0.16
Zone-III	G+5	1.68	0.60
	G+10	3.3	0.30
	G+15	3.2	0.30
	G+20	6.12	0.16
Zone-IV	G+5	1.67	0.59
	G+10	3.3	0.30
	G+15	3.4	0.30
	G+20	6.12	0.16
Zone-V	G+5	1.69	0.59
	G+10	3.3	0.30
	G+15	3.3	0.30
	G+20	6.13	0.16

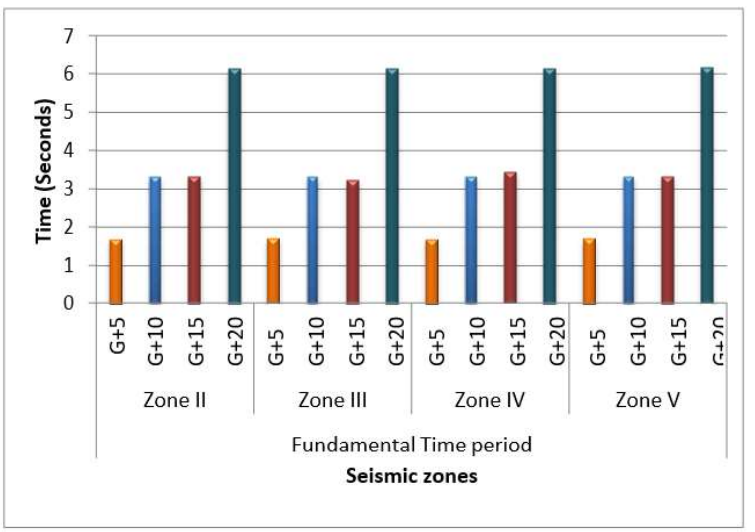

Fig. 12. Comparison of fundamental time period of different building height vs. seismic zones

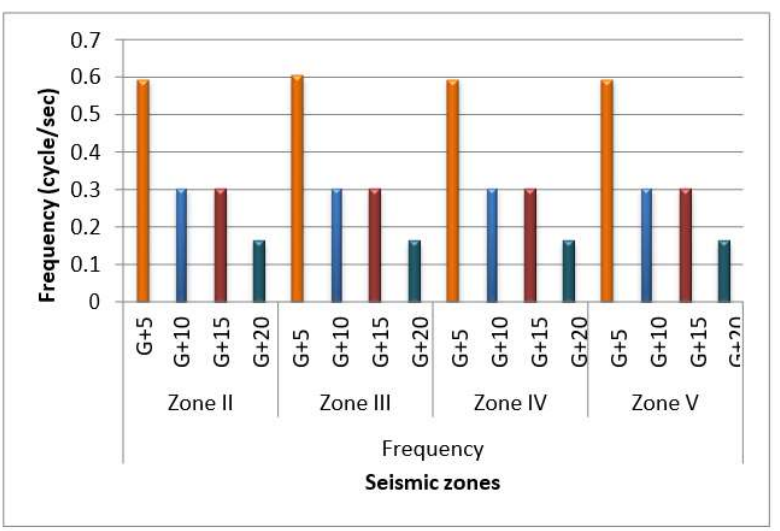

Fig. 13. Comparison of frequencies of different building height vs. seismic zones

Discussion

The analysis of various building heights, including G+5, G+10, G+15, and G+20 storey buildings, revealed distinct maximum storey displacements. In the X direction, the G+5 storey building exhibited a maximum displacement of 29.5mm, increasing to 51.8mm for the G+10 storey building, 78mm for the G+15 storey building, and 146mm for the G+20 storey building. In the Y direction, the corresponding values were 31.8mm, 69.3mm, 97mm, and 194mm. These results indicate that, as per the analysis, the maxi- mum storey displacement values increase with the height of the building in response tovarying seismic zones.

According to IS:1893, 2016 (part-1), the maximum allowable displacement at the top floor of buildings should not exceed 0.004h, which translates to 88mm for G+5 storey, 148mm for G+10 storey, 208mm for G+15 storey, and 268mm for G+20 storey buildings. However, the case study revealed lower displacement values: 31.8mm for G+5 storey, 69.3mm for G+10 storey, 97mm for G+15 storey, and 194mm for G+20 storey. Therefore, the analysis results indicate that the displacements are within ac- ceptable limits compared to the maximum allowable displacement values.

The maximum base shear values for different building heights also vary with seismic zones. In the X direction, the G+5 storey building experienced a maximum base shear of 728KN, which increased to 777KN for the G+10 storey building, 978KN for the G+15 storey building, and 1015KN for the G+20 storey building. In the Y direction, the corresponding values were 728KN, 780KN, 998KN, and 1021KN. These findings suggest that the maximum base shear increases with the height of the building in re- sponse to different seismic zones.

Similarly, the maximum base moment values for different building heights vary in response to seismic zones. In the X direction, the G+5 storey building exhibited a max- imum base moment of 210KN.m, which increased to 246KN.m for the G+10 storey building, 259KN.m for the G+15 storey building, and 301KN.m for the G+20 storey building. In the Y direction, the corresponding values were 210KN.m, 267KN.m, 305KN.m, and 324KN.m. The analysis indicates that, as per the results, the maximum base moments increase with the height of the building in different seismic zones.

The study also examined the maximum base shear, base moment, and displacement for a G+20 multi-storey building across global X and Y directions.

The fundamental time period for different building heights was determined. For G+5 storey, it was 1.68 Sec, for G+10 storey, 3.3 Sec, for G+15 storey, 3.4 Sec, and for G+20 storey, 6.12 Sec. notably, these values remained relatively consistent across dif-ferent seismic zones.

Regarding the frequency of oscillation, the G+5 storey building exhibited a fre- quency of 0.60 cycle/sec, while the G+10 storey and G+15 storey buildings had a fre- quency of 0.3 cycle/sec. The G+20 storey building had a slightly lower frequency of 0.16 cycle/sec. These frequencies were comparable across various seismic zones for each building height

Conclusion

In conclusion, the findings of this study, conducted using the response spectrum method on multi-story residential buildings of varying heights (G+5, G+10, G+15, and G+20 storeys), yield several significant insights:

Seismic analysis is imperative for ensuring the structural integrity of buildings. The investigation showed that, with increasing building height, the maximum storey displacement, base shear, and moment values also increase in response to varying seis- mic zones.

Notably, the largest storey displacement, base shear, and moment values were observed in G+20 storey buildings in seismic zone V, compared to zones II, III, and

IV. This suggests that the structure's uniform stiffness can help mitigate displacement, base shear, and moment, enhancing overall performance.

The study examined the resonance effect by comparing the approximate time pe- riod (Ta) of oscillation, as per IS 1893:2016 (Part-1), with the analysis results. The results indicated that multi-storied residential buildings are safe from resonance effects.

Furthermore, it was observed that, for buildings of the same height, the frequency and time period values remained consistent across different seismic zones.

The study also revealed an inverse relationship between frequency and time pe- riod, with frequency decreasing as building height increases. This insight is crucial for understanding the behaviour of high-rise buildings.

In light of these findings, it is recommended that seismic analysis is essential for buildings above G+10 storeys to ensure their performance against seismic forces. The analysis results have provided valuable comparisons across different structure heights in low to high seismic zones in India. The methodology employed in this study offers opportunities for further research. Future investigations could compare results obtained in soft and rocky soil within different seismic zones or explore soil-structure interac- tions to enhance our understanding of seismic responses.

References

1. Indian Standard code: IS 1893-2016 (part-1), "Criteria for seismic wave-resistant design of building structures."
2. Indian Standard code: IS 456:2000, "Criteria for plain and reinforced structures," Bureau of Indian Standards.
3. IS 875: 1987, "Code of practice for seismic loads for building and structures – Part 1: Dead loads" and "Part 2: Imposed loads."
4. Dehankar, Y., & Shelke, N., "Seismic Analysis of Different Heights Building on Different Types of Soil Using Base Isolation Technique," International Journal of Innovative Research in Engineering, Volume 3, Issue 3 (May-June 2022), pp. 336-
5. 352. [Online] Available at: www.theijire.com
6. Ahamad, S. A., & Pratap, K. V., "Dynamic analysis of G + 20 multi storied building by using shear walls in various locations for different seismic zones," Journal Article. [Online] Available at: www.elsevier.com/locate/matpr
7. Danam, V., "Comparative Study on Multistoried RCC Structure with and without Shear," Publication at: https://www.researchgate.net/publication/310478569
8. Adam, F. M., "Seismic Analysis of a Reinforced Concrete Building by Response Spectrum Method," Article in IOSR Journal of Engineering, September 2013. [Online] Available at: https://www.researchgate.net/publication/281409966
9. Saatcioglu, M., & Humar, J., "Dynamic analysis of buildings for earthquake- resistant design." DOI: 10.1139/L02-108.
10. Somasundar, K. M., Leslie, R., & Xavier, B., "Study of comparison of applying modes in response diapason system." Journal of Advanced Research in Engineering & Management, Vol. 03- Issue 11-2017, pp. 43-65.
11. Chandrakar, P., & Bokare, P. S., "A Review- Comparison between RS Method and Time History Method for Dynamic Analysis." International Journal of Research, Volume 6 Issue 5, May 2017.
12. Raheem, J., Rana, D., "Seismic Analysis of Vertical & Regular RCC Framed structures."
13. Reddy, K. R., & Rao, S. V. M., "Seismic Analysis of High Raised Structure by Response Diapason System," International Journal of Advance Technology and Innovative Exploration, Vol. 08, pp. 4111-4118, 2016.
14. Kulkarni, T., et al., "Analysis and Design of High-Rise Structure Frame using Staad Pro," IJRET International Journal of Research in Engineering and Technology, Vol. 05, Issue 04, 2016.

15. Khandve, A. V., et al., "Seismic Response of RC Frame Structures with Soft Storeys," International Journal of Engineering Research, Vol. 2, Issue 3, pp. 2100- 2108, 2012.
16. Deshmukh, S. M., & Kulkarni, J. G., "Analysis of Incompletely Braced Multistorey Building Frames due to Graveness and Earthquake Loads," International Journal of Advance Research In Science and Engineering, Vol. 2, Issue No. 8, 2013, ISSN 2319-8354.
17. Kadid, A., & Boumrkik, A., "Pushover Analysis of Reinforced Concrete Frames Structures," Asian Journal of Civil Engineering (Building and Housing), VOL. 9, No. 1, 2008, pp. 75-83.

Chapter-17

Biochar's Impact on Soil Mechanical Properties: A Comprehensive Review of Mechanisms and Implications

1. Sunil Priyadarshi 2. Samir Kumar

[1]Assistant Professor, Civil Engineering Department, Swami Vivekananda University
[2]Assistant Professor, Civil Engineering Department, Swami Vivekananda University

Abstract: Biochar, a durable carbon-rich substance created by heating biomass in the absence of oxygen, has surfaced as a hopeful soil additive capable of beneficially influencing the physical characteristics of soil. This review aims to provide a comprehensive analysis of the effects of biochar on various soil mechanical properties. The main objective of this study is the importance of understanding the impact of biochar on soil engineering characteristics to optimize its use in sustainable construction practices and soil application for various used. Based on the various study, it is evident that applying biochar at 1-2% by weight enhances soil porosity, infiltration rate and reduces soil bulk density. Additionally, biochar application improves water holding capacity, but the extent of improvement varies depending on soil texture. The enhanced characteristics of soil physical attributes can be ascribed to various mechanisms. These include the notable porous structure, the capacity of biochar to adsorb substances, its ability to offer microorganism habitats, and the elevation of overall soil organic carbon content. Nevertheless, the influence of biochar on soil physical traits is subject to factors like soil composition, the particular kind of biochar produced in terms of source material and pyrolysis circumstances, and the pace of biochar integration. More extensive investigation is required in these domains to attain a comprehensive comprehension of how biochar precisely affects soil physical attributes.

Keywords: Porosity, Biochar, Pyrolysis, Infiltration, Bulk density

Introduction

Soil stabilization is a widely employed technique in road foundation construction and pavement enhance the mechanical properties of soil, including durability, volume, strength and stability, while reducing pavement overall cost and thickness. Soil, being abundantly available, has been historically used in the construction of various civil engineering structures, such as monuments, tombs, and dwellings. The study of the engineering behavior of different soil types holds great significance, as all civil engineering structures must be built upon and supported by soil. The primary purpose of soil improvement by biochar is to minimize settlement and deformation and increase the bearing capacity of the soil. When dealing with challenging soil conditions, it becomes imperative to employ soil enhancement techniques for the betterment of existing ground or fill materials. Biochar, a carbon-enriched substance derived from the thermo-chemical transformation of biomass, presents a viable remedy in such scenarios. Biomass from diverse sources like various waste, urban wood-waste, including wood production, agricultural waste, logging residues, it can be used to produce biochar . To address this problem and improve soil physical properties and fertility, increasing the soil organic carbon content is essential. One approach to achieve this goal is the integrated use of organic and synthetic fertilizers. This strategy aims to replenish soil organic matter and enhance its ability to support

beneficial microorganisms, promote better nutrient and water retention, and ultimately increase crop yields. By adopting sustainable agricultural practices that focus on maintaining and increasing soil organic carbon, we can mitigate soil degradation and meet the growing demand for agricultural products while safeguarding the future of food supply. Although biochar has gained extensive use in agricultural and environmental remediation endeavors, its utilization in civil engineering applications beyond environmental restoration remains relatively uncharted. Recent research endeavors have commenced exploring the influence of biochar on soil mechanical characteristics as well as its potential as a construction material. It's essential to note that the attributes and caliber of biochar are profoundly shaped by the choice of source materials and the techniques of production employed.

Furthermore, the distinct properties of the soil, microbial activity, and prevailing atmospheric conditions also play a role in affecting the efficacy of biochar in soil enhancement. Enhancing comprehension of these variables through further investigation is pivotal for achieving effective and efficient soil stabilization using biochar in civil engineering domains. Soil physical conditions hold immense importance in determining soil fertility for crop cultivation. Elements like water retention capacity, aeration, and soil resilience directly impact root performance, thereby influencing subsequent crop growth.

Literature Review

Soils possessing advantageous attributes such as sound structure, porosity, hydraulic conductivity, appropriate bulk density, and resilience forge an optimal milieu for fostering beneficial microorganisms. This setting facilitates efficient nutrient and water movement within the soil profile, ameliorates nutrient and water retention capabilities, encourages robust root proliferation, and ultimately translates into elevated crop yields when contrasted with deteriorated soils characterized by inadequate physical traits **[1]**. The presence of soil organic matter stands as a pivotal determinant shaping soil's physical characteristic. Organic matter significantly enhances soil structure by fostering the aggregation of soil particles. Moreover, it bolsters soil porosity by virtue of its inherently porous composition, which, in turn, augments nutrient and water retention by capitalizing on its considerable adsorption prowess and extensive surface area. All of these positive effects on soil physical properties contribute to better root growth and ultimately higher crop yields. Soil organic matter plays a big role in maintaining the health and productivity of the soil ecosystem. Soils with higher concentrations of organic matter exhibit better mechanical properties and higher yields compared to soils with poor organic matter content **[2]** With a rapid increase in the global human population over recent decades, the demand for food, fiber, and raw materials has grown significantly, necessitating an urgent need to enhance agricultural production and ensure food security. Consequently, agriculture has intensified, leading to increased decomposition of organic matter and subsequent degradation of soil physical properties [**3]**. Anthropogenic activities, particularly those associated with harsh agro-climatic conditions, such as high temperatures, further exacerbate the issue. High temperatures accelerate the decomposition of soil organic matter, which otherwise serves as a natural soil conditioner, resulting in soil degradation. Biochar is a carbonaceous product obtained by subjecting biomass to high temperatures in the absence or limited presence of oxygen, a process known as pyrolysis. As a consequence, distinctive physical attributes manifest, including remarkable porosity and an expansive surface are**[4]** . Owing to its aromatic configuration and crystalline graphitic layers, biochar exhibits substantial resistance to decomposition, rendering it recalcitrant within the soil over extended durations. This persistence far surpasses that of organic matter, ranging from 10 to 1000 times longer. Biochar's attributes exhibit diversity contingent upon the kind of biomass utilized as feedstock and the precise parameters of the pyrolysis process, encompassing charring duration, speed, and temperature**[3**]. Notably, biochar originating from woody source materials typically displays a coarser texture and greater resistance to degradation, a contrast to the biochar produced

from agronomic residues. Furthermore, biochar produced at higher temperatures tends to have fewer nutrients and higher micro-porosity, whereas biochar produced at lower temperatures contains more nutrients and fewer micro-pores**[5]**. It is essential to recognize that different types of biochar possess distinct properties, and their impact on soil physical properties varies depending on the specific soil type and prevailing climatic conditions **[6]**. Consequently, the effectiveness of a particular biochar in enhancing soil physical properties is influenced by these factors, highlighting the need tailored and context-specific approaches to optimize the use of biochar as a soil amendment.

Effect of Biochar on Soil Properties

Effect of biochar on Soil's porosity

Soil porosity, which represents the ratio of volume of soil sample to the total soil sample volume, is a critical soil attribute that significantly influences plant growth. Three types of pores, namely microspores macro pores, and mesopores, exist in the soil, distinguished by their size. These pores play vital roles in providing aeration, facilitating the movement and retention of nutrients, water, and also serving as habitats for beneficial soil microbes. Utilizing biochar brings about a general augmentation in soil porosity, albeit the degree of this enhancement hinges on the particular biochar variant employed and the specific soil variety into which biochar is introduced **[7]**. The proportional influence of these three categories of pores on the cumulative expansion of soil porosity diverges according to the biochar type and soil type at hand. The rise porosity of soil can be attributed to the abundant porous nature of biochar itself properties**[8]**. However, it is worth noting that some scientists have observed a decrease in soil porosity after biochar application due to the clogging of soil pores by fine biochar particles. The effect of different percentage using in soil and types of biochar application on soil porosity in various soils is illustrated in different study.

Effect of biochar on Soil's Bulk Density

Bulk density serves as a gauge of the compactness with which soil particles are packed together. This metric is computed by dividing the mass of soil that has been dried in an oven by its overall bulk volume, encompassing both the volume occupied by soil particles and the interstitial pore spaces. The bulk density of soil plays a crucial role in determining various soil properties and significantly impacts plant growth.

For instance, high bulk density of soils with (>1.6 Mg cm^-3) have reduced water absorption capacity and create greater penetration resistance for plant roots, ultimately affecting soil characteristics and plant growth**[9]** . The application of biochar results in a decrease in bulk density of soil due to the high porosity of biochar. Incorporating biochar into the soil leads to a notable reduction in bulk density through the augmentation of pore volume, thereby fostering improved soil structure. Furthermore, as noted by **[10]** elevating the rate of biochar application correlates with a substantial reduction in bulk density. This observation underscores the capacity of biochar to enhance soil physical attributes and promote plant growth

Effect of biochar on Soil's aggregation

Soil aggregation is the process by which soil colloidal particles are bound together through net attractive forces. This property is of utmost importance in terms of soil structure. A well-aggregated soil manifests favorable structure, establishing an optimal conduit for the interplay of nutrients and water within the soil matrix, thereby aiding plant absorption **[4]**.The contribution of microorganisms in enhancing soil aggregation holds pivotal importance. Specific polysaccharides released by these microorganisms additionally foster the cohesion of soil colloidal particles**[8]**. Upon biochar incorporation into the soil, it serves as a sanctuary for microorganisms, granting them shelter from predators and safeguarding them against desiccation. In turn, these microorganisms actively contribute to soil aggregation by secreting polysaccharides, thereby fostering a more stable and well-structured soil **[11**]. The application of biochar can significantly influence soil aggregation by creating a favorable environment for beneficial microorganisms,

leading to improved soil structure and overall soil health. This, in turn, positively impacts nutrient and water movement within the soil, ultimately benefiting plant growth and crop productivity.

Effect of biochar on soil water holding capacity

Soil water retention capacity pertains to the utmost volume of water that a soil is capable of containing or retaining, and it is a critical property from both farmers' and plant growth perspectives. Soils with high water retention capacity require less frequent irrigation for crops and promote better plant growth. Biochar application has been shown to significantly enhance the available moisture content of the soil, increasing it by up to 96%, and the saturated moisture content by 55% **[9**]. Studies have demonstrated that soil amended with biochar can retain 15% more moisture compared to untreated soil . The influence of biochar on water retention capacity is dependent on soil texture, as described [**8]**Sandy soils experience a significant increase in water retention capacity with biochar application, while loamy and clay soils may exhibit little to no increase. Experimental findings by **[11]** support the idea that biochar application increases soil moisture retention capacity due to improved soil porosity and the adsorptive nature of biochar. Additionally, **[10]** observed the existence of hydrophilic functional groups both on the exterior surface of the biochar's graphing sheet and within its pores. These elements also play a role in augmenting the soil's water retention capability. Overall, biochar application can be a valuable strategy to improve soil water retention capacity, benefiting agricultural productivity and promoting better plant growth, especially in sandy soils or those with poor water-holding abilities.

Discussion and Suggestion

The index characteristics of the soil were assessed in accordance with the relevant IS Codes. Preliminary geotechnical laboratory assessments were carried out to establish the baseline attributes of the untreated clay employed in the research. Standard geotechnical property evaluations, including Atterberg limits, specific gravity, grain size distribution, unconfined compressive strength, and compaction tests, were conducted to analyze the soil's performance as utilized in this investigation. We undertake a comprehensive review of existing literature to amass and assess data concerning the noteworthy role of biochar in enhancing soil's physical attributes. Biochar exerts a favorable impact on the rigidity of treated specimens. Introducing biochar to clay leads to a decrease in the failure strain of these samples when contrasted with untreated clay. biochar results in heightened water uptake and a decrease in inter-particle pores among clay components, leading to a decline in the soil's maximum dry unit weight and a concurrent rise in its ideal moisture content. Furthermore, we delve into the mechanisms that underpin these enhancements, pinpointing aspects that demand more in-depth exploration. The study is centered on investigating the impact of biochar on the enhancement of soil strength and exploring potential applications of clay stabilized with biochar.

Summary

Indeed, the application of biochar can lead to significant improvements in soil physical properties, but the effectiveness of these improvements depends on several factors. The type of biochar used, which is determined by the pyrolysis conditions and the type of biomass utilized, plays a crucial role in influencing its impact on the soil. Additionally, the specific soil type in which biochar is applied is another critical factor. Different soils have unique characteristics, and the response to biochar application may vary based on their properties and composition. Furthermore, the rate of biochar application is a key consideration. The amount of biochar added to the soil can influence the degree of improvement in soil physical properties. The optimal rate may differ based on soil conditions, crop type, and specific objectives of soil management.

By considering these factors and tailoring the application of biochar accordingly, it is possible to harness its full potential for enhancing soil physical properties, leading to improved soil structure, increased water

retention, better nutrient availability, and ultimately, higher crop yields. Careful selection and application of biochar can significantly contribute to sustainable agricultural practices and soil management strategy.

References

1. Thines, K.R., Abdullah, E.C., and Mubarak, N.M. (2017) Effect of process parameters for production of microporous magnetic biochar derived from agriculture waste biomass. Microporous and Mesoporous Materials, **253**, 29–39.
2. Brassard, P., Godbout, S., Lévesque, V., Palacios, J.H., Raghavan, V., Ahmed, A., Hogue, R., Jeanne, T., and Verma, M. (2019) Biochar for soil amendment, in Char and carbon materials derived from biomass, Elsevier, pp. 109–146.
3. Mona, S., Bhateria, R., Deepak, B., Kiran, B., and Nisha, R. (2019) Biochar for Reclamation of Saline Soils. Microorganisms in Saline Environments: Strategies and Functions, 451–466.
4. Aslam, Z., Khalid, M., and Aon, M. (2014) Impact of biochar on soil physical properties. Scholarly Journal of Agricultural Science, **4** (5), 280–284.
5. De la Rosa, J.M. (2020) Biochar as Soil Amendment: Impact on Soil Properties and Sustainable Resource Management, MDPI.
6. Fu, G., Qiu, X., Xu, X., Chi, Z., and Zhang, W. Effect of Biochar on Desert Soil Wind Erosion Using Sweep Model and Vis-Nir Spectroscopy Technique. Available at SSRN 4112034.
7. Guo, M., Song, W., and Tian, J. (2020) Biochar-facilitated soil remediation: mechanisms and efficacy variations. Frontiers in Environmental Science, 183.
8. Joseph, S.D., Camps-Arbestain, M., Lin, Y., Munroe, P., Chia, C., Hook, J., Van Zwieten, L., Kimber, S., Cowie, A., and Singh, B. (2010) An investigation into the reactions of biochar in soil. Soil Research, **48** (7), 501–515.
9. Lebrun, M., Miard, F., Nandillon, R., Scippa, G.S., Bourgerie, S., and Morabito, D. (2019) Biochar effect associated with compost and iron to promote Pb and As soil stabilization and Salix viminalis L. growth. Chemosphere, **222**, 810–822.
10. Wang, Y., Liu, Y., Zhan, W., Zheng, K., Wang, J., Zhang, C., and Chen, R. (2020) Stabilization of heavy metal-contaminated soils by biochar: Challenges and recommendations. Science of the Total Environment, **729**, 139060.
11. Zhang, L., Jing, Y., Chen, G., Wang, X., and Zhang, R. (2019) Improvement of physical and hydraulic properties of desert soil with amendment of different biochars. Journal of Soils and Sediments, **19**, 2984–2996.

Chapter-18

Optimizing the use of Reclaimed Paving Materials in Granular Sub Base for Road Construction: An Extensive Analysis

Sunil Priyadarshi, Samir Kumar

[1]Assistant Professor, Civil Engineering Department, Swami Vivekananda University

Abstract: Reclaimed Paving Materials offer a promising solution for road construction due to their availability and potential for cost savings. By reusing RPM materials, we can reduce the consumption of fresh aggregates, conserve natural resources, and minimize waste generation. However, the effective utilization of RPM in the granular sub base requires optimization techniques and careful consideration of various factors. The aim of this study is to optimize the use of Reclaimed Paving Materials in granular sub base, providing an open alternative for Indian roads. This approach helps reduce construction costs and ensures the sustainability of raw materials. Road construction is a costly process, involving millions of tons of aggregate. Given the scarcity of fresh aggregate, the present study explores the possibility of using recycled aggregate as a replacement for a portion of the fresh aggregate. This aligns with the government's goal of conserving budgets and promoting environmentally friendly practices through "Green Technology." Therefore, recycling pavements emerges as an efficient solution for road construction and maintenance, offering significant advantages such as cost savings, environmental preservation, and the preservation of virgin materials.

Keywords: Reclaimed Paving Materials (RPM), Granular Sub Base (GSB), Ministry of Road transport and Highway (MoRTH), Road construction Method.

Introduction

Reclaimed Paving Materials (RPM) refer to materials obtained from existing asphalt pavements that have been removed or milled. Now a day's abundant waste available due to resurfacing and up gradation of the existing roads like major district roads, state highway, and national highways. these materials are then recycled and reused in new asphalt mixtures. RPM can include a combination of aged bituminous (asphalt binder), aggregates, and other pavement materials. Recycling RPM helps to reduce the demand for new raw materials and minimizes the amount of waste generated from pavement removal processes. Since the quantities available is more which makes highway and transportation engineers to find solution to reuse the reclaimed paving materials and thereby consuming the waste and conserving the natural resources. It is obtained either by milling or by a full depth recovery method. It may highly useful materials when crushed and screened properly.

The utilization of RPM aggregate remains relatively uncommon in India and other developing nations. Apart from financial investments, the availability of raw materials is a critical factor in road development projects. The Indian Roads Congress, envisioning future road advancements in the country, has indicated a need for 3500 million cubic meters of aggregates in its special publication, 'Road Development Plan VISION: 2021.' As India's road network undergoes modernization and the demand for travel continues to rise, these investments will inevitably escalate. Consequently, India faces a pressing requirement to adopt a sophisticated approach for road construction and maintenance, with the objective of minimizing expenses and decreasing reliance on raw materials.

To achieve this, the integration of recycled aggregate as a substitute material can reduce the demand for

fresh aggregate. In the current study, the RPM aggregate originates from the remains of dismantled roads. By analyzing existing literature and case studies, the research aims to pinpoint the most effective practices and guidelines for maximizing RPM utilization in the granular sub base of rural roads. The findings will contribute to the development of sustainable and cost-effective solutions for road construction, benefiting rural communities, minimizing construction costs, and promoting environmental stewardship.

Literature Review

The primary objective of this review is to conduct a thorough examination of current practices and identify effective strategies for maximizing the utilization of Reclaimed Paving Materials (RPM) in the granular sub base of village roads. The study will extensively analyze various methodologies and techniques used in previous research and projects to gain valuable insights into the performance, durability, and structural integrity of RPM-based granular sub base layers has earned the reputation of being the most recycled material worldwide, finding applications as an aggregate substitute in bituminous mixtures, granular sub-bases, base aggregates, and embankment or fill materials. The material under review for this research is sourced from diverse resources. Some of these resources are directly relevant to the present study, while others are only loosely related but still contribute valuable insights to the topic. The review aims to amalgamate and synthesize this information to provide a comprehensive understanding of the optimization strategies for incorporating Reclaimed Paving Materials in the granular sub base of roads construction. By exploring and evaluating the performance of RPM in previous projects and studies, this review will serve as a valuable resource for engineers, researchers, and policymakers engaged in rural road development projects. The findings will contribute towards developing sustainable road construction and maintenance practices, aiming to minimize costs, reduce dependency on raw materials, and enhance the overall quality and longevity of village roads. Ultimately, this review aims to play a crucial role in advancing the state of knowledge in this field, encouraging the widespread adoption of RPM in granular sub base applications, and fostering more environmentally friendly and economically viable road development practices in India.

History at a Glance

The recycling of bituminous pavements has emerged as an advanced methodology adopted in several countries for the rehabilitation and restoration of pavements. Although the concept was initially introduced in 1915, it gained popularity during the 1970s when there was a significant surge in the price of bituminous materials. The ensuing inflationary pressures compelled theexploration and implementation of recycling techniques as a means to mitigate construction costs and promote sustainability within the industry.
Since then, extensive research and development efforts have been dedicated to studying and refining the recycling process. The performance of these high Reclaimed Paving Materials (RPM) mixtures has been thoroughly examined, and it has been observed that they exhibit comparable performance characteristics to conventional mixes. This finding has provided further impetus for the widespread adoption of recycling practices in pavement construction and maintenance.

Present Scenario

The utilization of Reclaimed Paving Materials (RPM) is an emerging technique in India, holding promising benefits for both the government and contractors in terms of efficiency and cost savings. Although research on RPM in India is still limited, it is extensively employed in the United States and various other countries, offering valuable insights into best practices. To improve mix design and ensure quality control, ongoing advancements are being made in RPM sampling, testing, and material characterization. These efforts are

targeted at supporting contractors and transportation departments in optimizing the utilization of RPM in road construction. Assessments based on regional requirements cover a range of factors, including low-temperature testing, rutting susceptibility, cracking resistance, moisture susceptibility, and mixture stiffness. Evaluating these parameters is critical to guaranteeing the pavement's performance and long-term durability. By continuously refining these techniques and assessments, the industry aims to enhance the effectiveness of RPM integration, leading to more resilient and long-lasting pavements. The bituminous industry continues to strive for an enhanced understanding of the correlation between performance tests and real-world field performance. Ongoing efforts focus on identifying the most effective performance tests that can accurately predict the behavior of RPM mixes under different conditions. This research helps pave the way for informed decision-making and improved quality assurance in RPM utilization.

Studies on Recycling

Kandahl, et. al(1995) [1] The performance of the recycled mixes was evaluated by comparing them with the control mixes using resilient modulus testing. Resilient modulus measures the ability of the pavement material to recover its shape after being subjected to deformation from traffic loads. To assess the resilient modulus, an accelerated aging procedure was employed, which involved subjecting the mixes to alternating freezing and thawing cycles. This accelerated aging process aimed to simulate the harshest moisture conditions that the pavement might experience in its lifetime..

Brown (1984) [2] The study was a combination of field and laboratory evaluation suggested that the use of rejuvenator in recycled bitumen mix would decrease the potential rutting and also increase the life of recycled pavement. By conducting these tests, researchers could determine how well the recycled mixes would withstand the effects of repeated freeze-thaw cycles and assess their overall performance in comparison to the control mixes

Ding et.al (2019)[3] The controlled experiments involved analyzing the blending process of Reclaimed Paving Materials (RPM) with a fresh mixture. Various percentages of screened RPM were mixed with new coarse aggregate. One mixture, which consisted of 20% screened RPM, underwent staged extraction and recovery. The findings from this study revealed that only a minor portion of the aged bituminous in RPM actively took part in the remixing process.

Kennedy et.al (1998)[4] The main aim of this study was to establish guidelines for integrating Reclaimed Paving Materials (RPM) into bituminous mixes, following the SUPERPAVE binder specifications. The study's findings revealed that with an increase in the percentage of RPM binder, the stiffness of the binder also increased. This stiffness change occurred at a consistent rate throughout the entire range of 0-100% RPM binder, or it escalated at lower temperatures. Moreover, the rate of stiffness change either remained constant across the 0-100% RPM range or increased when higher percentages of RPM were added to the blend. These results provide valuable insights into the behavior and characteristics of RPM-based bituminous mixes, guiding engineers in optimizing their usage and ensuring proper pavement performance.

Alawi and chauhan (1998) [5]The study's conclusions indicated that the recycled pavement sections performed well on the test track, even under heavy loading conditions. The positive results suggest that the use of recycled materials in pavement construction can be a viable and effective option, meeting performance requirements and demonstrating their suitability for actual road applications. The data gathered from both the field and laboratory evaluations provided valuable insights into the durability and performance of recycled pavements, contributing to the ongoing efforts to implement sustainable and cost-effective road construction practices.

Sharma et. al. (2021) [6] The objective of the research was to rehabilitate a specific section of the highway. To achieve this, two semi-dense mixtures were created, consisting of maximum aggregate sizes of 12mm and 20mm. These mixtures contained 40% and 60% of Recycled Pavement Material (RPM)

respectively. The properties of these mixtures were then compared to control mixtures that utilized two grades of bitumen, namely penetration grade 60/70.Ultimately, the conclusions drawn from the study were as follows: The impact test results for the laboratory-prepared recycled mixes were satisfactory and comparable to those of the virgin mixes. It was found that an RPM content of 60% could be effectively incorporated into the recycled mixes, provided that proper handling and mix design practices were employed. Furthermore, the analysis of stiffness modulus and indirect tensile strength tests indicated that the performance of the recycled mixes was comparable to that of the virgin mixes.

McGarrah-(2007) [6]This report evaluates previous studies that have investigated the characteristics and behaviors of both 90% RPM mixtures and blends of RPM with virgin aggregates. Several notable findings from this analysis are presented. While a maximum percentage of 50% RPM is commonly used, it does not necessarily indicate the optimal percentage, and it is recommended to restrict it to 27%. RPM is known for its inherent variability, and by ensuring a consistent gradation in the produced RPM, the extent of this variability can be minimized, resulting in more reliable performance outcomes.

Su et.al [7]The research conducted on a specially designed test track aimed to evaluate the effects of incorporating a sub-base layer mixture composed of 50% natural aggregates and 50% Recycled Pavement Material (RPM) on pavement performance. The study's conclusions emphasize the various advantages of RPM recycling, particularly in terms of economic enhancement, transportation infrastructure improvement, and the creation of job opportunities. Furthermore, the utilization of RPM in pavement construction and maintenance promotes labor-based practices, contributing to job creation and fostering overall economic growth. These initial findings suggest that incorporating RPM into pavement projects could have positive economic and social impacts, making it a promising and sustainable option for future infrastructure development and maintenance.

Sharma and Singla,. (2014)[8]the key findings from the laboratory investigation are as follows: To achieve the desired gradation, trials were conducted by incorporating 60% RPM mix, 30% aggregates of 40mm size, and 10% stone dust. The Aggregate Impact Value was determined to be 14.89%, while the Combined Flakiness and Elongation index was found to be 27.64%. These values were below the maximum permissible limits of 30% as specified by MoRTH for the Wet Mix Macadam (WMM) base course, indicating satisfactory material performance. The study measured the specific gravity of the aggregates, which fell within the range of 2.8 to 3.0. Additionally, the water absorption of the aggregates was found to be within the specified limits of 0.3 to 2.0%. These findings demonstrate that the material met the specified requirements, indicating its suitability for the intended use. In summary, the specific gravity and water absorption values of the aggregates were within acceptable ranges, confirming that the material is suitable for the intended application in the study.

Rao et al (2019) [9] This paper provides an overview of the introduction and production process of recycled concrete aggregates (RCA) and delves into their diverse applications in the construction industry. The properties of recycled aggregates are thoroughly examined and compared with those of natural aggregates. The research findings highlight that recycled aggregates offer promising potential for various construction applications. One of the significant applications of recycled aggregates is in aggregate base courses, which play a critical role as a structural foundation for roadway pavements. The study reveals that these untreated recycled aggregates can be effectively utilized in constructing foundations for paving projects, demonstrating their practicality and suitability for such applications. In conclusion, the paper emphasizes the versatility and benefits of using recycled concrete aggregates in construction projects, particularly for aggregate base courses, contributing to sustainable practices and resource conservation in the construction industry.

Singh et.al (2014) [10] For this study, a modified Proctor CBR test was conducted on five different mix batches. Each batch included replacement levels of 0%, 10%, 20%, 30%, 40%, and 50% of fresh aggregate

with recycled aggregate at their respective optimum moisture contents. The results indicate that, up to a 30% replacement level, the maximum dry density of the recycled aggregate matrix is approximately 0.01 g/cc higher compared to the reference mix containing natural aggregate. However, the CBR of the recycled aggregate matrix at the same replacement level is approximately 1% lower than the reference mix with natural aggregate. This reduction in strength could be attributed to the relatively lower strength of the recycled aggregate in comparison to fresh aggregate. These findings suggest that while the maximum dry density of the recycled aggregate matrix slightly increases, there is a slight decrease in the CBR value compared to the reference mix. The lower strength of the recycled aggregate might account for this reduction in strength.

Zaumanis et.al (2021), [11]This practical study demonstrates the significant influence of replacing virgin materials with Reclaimed Paving Materials (RPM) in various road construction applications. The findings indicate that by incorporating 20%, 40%, and 60% RPM into black cotton soil, the California Bearing Ratio (CBR) values increase by 2%, 3.8%, and 6.8%, respectively. This improvement in CBR values suggests that the use of RPM can effectively enhance the sub-grade performance. Moreover, the study reveals substantial savings in virgin materials by utilizing RPM. Specifically, a reduction of 25% in virgin material can be achieved for GSB Grade-II, while a 35% reduction is possible for Wet Mix Macadam (WMM). This demonstrates the potential cost and resource savings associated with incorporating RPM into road construction projects.

He, G., and Wong, W. (2007)[12] In summary, the abundance of R.A.P. generated from road expansion and upgrades presents an opportunity to address both the disposal of industrial waste and the conservation of natural resources. By incorporating R.A.P. materials in the G.S.B., significant cost savings can be achieved, offering a sustainable solution for road construction projects. Incorporating R.A.P. materials in the Granular Sub Base (G.S.B.) also leads to construction cost savings of approximately 25-30%. By analyzing the cost implications, it has been determined that implementing R.A.P. materials in a 5 km stretch can result in savings of up to 35%.

Vasudevan (2007)[13] it is feasible to adopt RPM in various layers, ranging from 20% to 50% of the total mixture. By utilizing RPM, we can effectively reduce the consumption of new asphalt materials while still maintaining the desired performance and structural integrity of the pavement. This approach not only reduces the environmental impact associated with the disposal of old pavement materials but also contributes to the preservation of natural resources. The incorporation of RPM in different layers of flexible pavements is a viable solution that offers economic, environmental, and sustainability benefits. It provides an opportunity to make efficient use of existing materials, reduce construction costs, and minimize the demand for virgin resources.

Singh and Duggal (2015) [14]The findings of this study indicate that incorporating RPM in asphalt mixes can yield comparable or even superior results compared to virgin mixes. again, this study concludes that a 30% RPM content in the mix exhibits similar performance to that of a virgin bituminous mix and outperforms other RPM percentages tested. Additionally, by incorporating 30% RPM mixes in a project, a significant cost reduction of 21% can be achieved. As the utilization of RPM continues to gain traction in India, it holds promise as a sustainable and economically viable solution for the construction industry.

In conclusion of above, the recycling of bituminous pavements has evolved into a well-established and effective methodology for the rehabilitation and construction of pavements. Originating in the early 20th century, the approach gained significant momentum in the 1970s due to rising bituminous prices. Extensive research has demonstrated the comparable performance of high RPM mixtures, affirmed their viability and encouraged the industry to embrace recycling practices. The adoption of recycling not only reduces construction costs but also supports environmental sustainability by conserving resources and minimizing waste generation.

Summary and Conclusion

The percentage of Reclaimed Paving Materials (RPM) used in road construction projects varies depending on the project and the condition of the RPM materials. It has been successfully used up to 70% in certain road projects. It is not advisable to prepare a blending mix with 100% use of RPM. The large size of aggregates in the RPM mix tends to be deficient due to the crushing and aging process. The utilization of recycled aggregate in granular sub base (GSB) for road construction offers both economic advantages and environmental benefits by mitigating mining pollution. The ideal proportion of Reclaimed Paving Materials (RPM) in granular mixes does not have a fixed and universally applicable percentage. Instead, different road projects have successfully employed varying percentages of RPM based on their unique specifications and needs. Recycling aggregates from demolition projects can save costs associated with transporting the material to landfills and disposal.

These conclusions highlight the feasibility and advantages of utilizing RPM in road construction, while also emphasizing the need for careful consideration of factors such as RPM percentage, aggregate size, and strength criteria to ensure the successful implementation of RPM-based granular sub base in village road projects.Overall, the adoption of recycled aggregate in GSB for road construction provides a dual advantage of cost savings and environmental sustainability. By embracing this approach, the industry can contribute to minimizing mining pollution while reaping the economic benefits offered by the utilization of recycled materials.

References

1. Kandahl, P.S., Rao, S.S., Watson, D.E., and Young, B. (1995) Performance of recycled hot mix asphalt mixtures.
2. Brown, E. (1984) Evaluation of properties of recycled asphalt concrete hot mix. International Air Transportation Conference, 1599.
3. Ding, X., Chen, L., Ma, T., Ma, H., Gu, L., Chen, T., and Ma, Y. (2019) Laboratory investigation of the recycled asphalt concrete with stable crumb rubber asphalt binder. Construction and Building Materials, 203, 552–557.
4. Kennedy, T.W., Tam, W.O., and Solaimanian, M. (1998) Effect of reclaimed asphalt pavement on binder properties using the superpave system.
5. Alawi, Y., and Chouhan, R. (2018) Experimental study of construction and demolition waste in flexible pavement. International Journal of Advance Research, Ideas and Innovations in Technology, 4 (2), 2074–2079.
6. McGarrah, E.J. (2007) Evaluation of current practices of reclaimed asphalt pavement/virgin aggregate as base course material.
7. Su, N., Xiao, F., Wang, J., and Amirkhanian, S. (2017) Characterizations of base and subbase layers for Mechanistic-Empirical Pavement Design. Construction and Building Materials, 152, 731–745.
8. Sharma, J., and Singla, S. (2014) Study of recycled concrete aggregates. International Journal of Engineering Trends and Technology, 13 (3), 123–125.
9. Rao, P.A., and Deulkar, V. (2019) Utilization of Reclaimed Asphalt Pavement and Ceramic Waste in Pavement Construction.

10. Singh, V.P., Mishra, V., Harry, N.N., and Bind, Y.K. (2014) Utilization of Recycled Highway Aggregate by Replacing it with Natural Aggregate. Journal of Academia and Industrial Research (JAIR), 3 (6), 263.

11. Zaumanis, M., Loetscher, D., Mazor, S., Stöckli, F., and Poulikakos, L. (2021) Impact of milling machine parameters on the properties of reclaimed asphalt pavement. Construction and Building Materials, 307, 125114.

12. He, G., and Wong, W. (2007) Laboratory study on permanent deformation of foamed asphalt mix incorporating reclaimed asphalt pavement materials. Construction and Building Materials, 21 (8), 1809–1819.

13. Vasudevan, R., Sekar, A.R.C., Sundarakannan, B., and Velkennedy, R. (2012) A technique to dispose waste plastics in an ecofriendly way–Application in construction of flexible pavements. Construction and Building Materials, 28 (1), 311–320.

14. Jaspreet, S., Jashanjot, S., and Duggal, A. (2015) K. A Review Paper on Reclaimed Asphalt Pavement (Rap). Inte. J. Modern trends in engg. and researsh, 2 (08), 454–456.

Chapter 19

Enhancing Power System Reliability: Three-Zone Distance Protection for Transmission Line Contingencies

[1]Suvraujjal Dutta*,[2]Sandip Chanda, [3]Papun Biswas, [4]Sandip Chanda, [5]Abhinandan De

[1]Swami Vivekananda University, Barrackpore
[2]Jis college of Engineering
[3]Ghani Khan Chowdhury Institute of Engineering and Technology
[4]IIEST, Shibpur

Corresponding Author Email: suvraujjal@svu.ac.in

Abstract

In this study, a unique method for pinpointing the location of transmission line faults is presented.The three zone distance protection technique has traditionally been used to identify and isolate problematic sections from the line. A transmission line outage could result in overloading conditions, which could lead to improper operation of the distance relay used in the scheme. A new dz/dt technique has been used in this work in the pursuit of constructing an appropriate distance relay protection scheme of transmission line with contingency resiliance. With the aid of the numerical relay ADR239A, the Matlab Simulink modeling of the distance protection method has been standardised, and some promising findings have been discovered.

Keywords: Matlab simulink, Three zone protection, numerical relay, distance relay, overloading condition, contingency.

Introduction

For power engineers, power system protection has been a difficult area of engineering. Power systems, which consist of a vast network of interconnected devices, contain various power generating, consuming, measuring, and controlling apparatuses that are interconnected. Any anomalous occurrence has the potential to throw off the balance of these devices and bring instability into the system. Therefore, it is crucial to protect the power system from these anomalous circumstances. Additionally, a flaw or improper operation in a tiny area might weaken the capacity of the entire system to maintain equilibrium, which could ultimately lead to cascade failure or systemic collapse. Power experts began creating several security plans for this network as soon as it was being developed. In [1] It can be shown that a study was done on the contribution made by line distance protection zone 3 to voltage instability leading to a significant system outage of a big power network. This is done in an effort to identify the conditions that, in the presence of active distance protection relays in all three zones, could result in voltage collapse. The load flow of the straightforward IEEE14-bus test system is developed and solved as the study's first step. A thorough dynamic simulation of the standard CIGRE Nordic32-bus network, which closely mimics the Swedish network, was conducted in order to generate a scenario that is similar to the actual blackout that occurred in Sweden and Denmark in 2003. PSS/E software was used to identify the crucial lines that caused cascaded tripping.

In [2]The "Numerical Distance Protection Relay Commission and Testing" focuses on setting up, installing, commissioning, and testing a numerical distance protection relay, REL 511*2.3 from ABB Company. The relay can detect phase-to-phase and phase-to-earth faults and responds to all fault types. A new strategy for separating line overloads from true problems is suggested, using line outage distribution factor and generation shift factor-based power flow estimation methods.In [5] Distance and carrier current systems are two important types of transmission line protection that have undergone substantial development to meet requirements. The transmission line demo panel's purpose is to show how to use a distance (impedance) relay to clear a defect from a transmission line. Relay indicates the distance across which a fault has occurred since fault impedance is proportional to the length of the line from the placement of the relay to the fault spot. In [6provides an approach that comprises of a sophisticated real-time tool that integrates the event tree analysis (ETA)-based relay monitoring tool with the neural network-based fault detection and classification (NNFDC) and synchronized sampling-based fault localization (SSFL) algorithms. With its superior performance, the fault analysis tool serves as a benchmark for conventional distance relays, and the relay monitoring tool offers comprehensive local information about the disturbances.In [7]Texas A&M University (TAMU) group earlier introduced a new interactive scheme of system-wide and local monitoring

and control tools for effectively dealing with cascading outages, which is presented in part I of PSerc project S-19: Detection of This project aims to examine data requirements for implementing proposed system-wide and local substation algorithms, transform substation and system-wide data into information for algorithms, and develop an implementation framework for monitoring and control instruments. It uses DIgSILENT program for numerical distance protection relay modeling and simulation on 110 kV transmission lines. Matlab/Simulink software is used for in-depth modeling, and a GUI is created for the developed model. Quadrilateral relay systems and Bergeron model type transmission lines are developed and simulated using PSCAD/EMTDC analysis software. The dz/dt scheme is proposed to address transmission line contingency issues.

Theory

Distance relay and three zone scheme

The operation of a distance relay or impedance relay is extremely straightforward. One voltage element is fed from the system's potential transformer, and the other is supplied by the current transformer. The secondary current of the CT generates the deflecting torque, while the voltage of the potential transformer generates the restoring torque. Deflecting torque is more than restoring torque in typical operating conditions. Relay will therefore not work. However, when something is wrong, the voltage decreases and the current increases significantly. Deflecting torque then exceeds restoring torque, and dynamic components of the relay begin to move as a result, closing the No contact of the relay. Therefore, it is obvious that the distance relay's functioning or working principle depends on the system's voltage to current ratio.

Zone 1 of Protection

1. Phase relays and ground relays are two categories for distance relays.
2. Phase relays (three phase, L-L) and ground relays (S-L-G, L-L-G) are used to safeguard the transmission line from phase faults and ground faults, respectively.
3. A distance relay must serve as both the primary and backup protection, just like an over current relay.
4. The distance relay in the accompanying fig. must offer line AB primary protection and lines BC, BD, and BE backup protection.

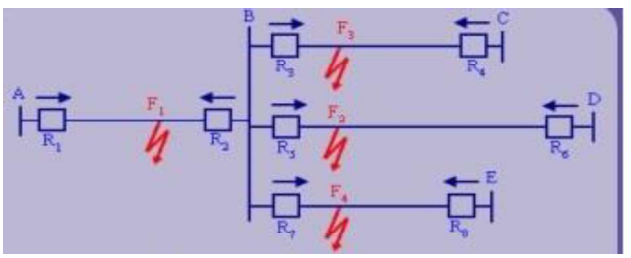

Fig 1: Primary and backup protection

Zone 2 and zone 3 protection

Zone 2 is typically set to 120% of primary line impedance, providing sufficient margin for non-zero fault

impedance and errors in relaying, and also providing backup protection to an adjacent line.

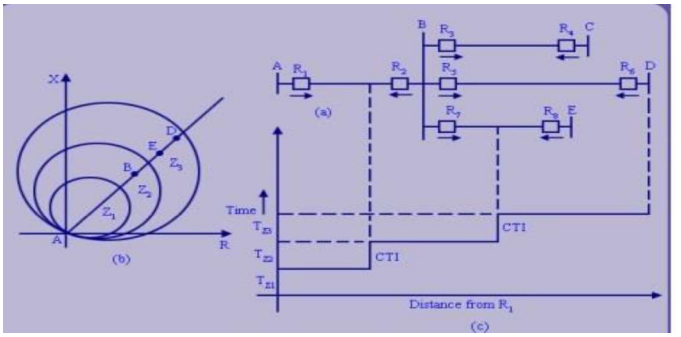

Fig 2:a ,b ,c three zones of protection

Present distance relay protection scheme:

The study uses a Simulink-based model and numerical relay to standardize distance protection problems on a 220 KV transmission line. The model considers a three-line to ground fault and uses relay settings for backup protection. Two backup relays detect faults and take preventative action if not recognized by the instantaneous relay.

a) The three-zone protection plan model that was developed:
The following figure shows the proposed three zone protection. To put this general paradigm into practice, several functional blocks have been created.

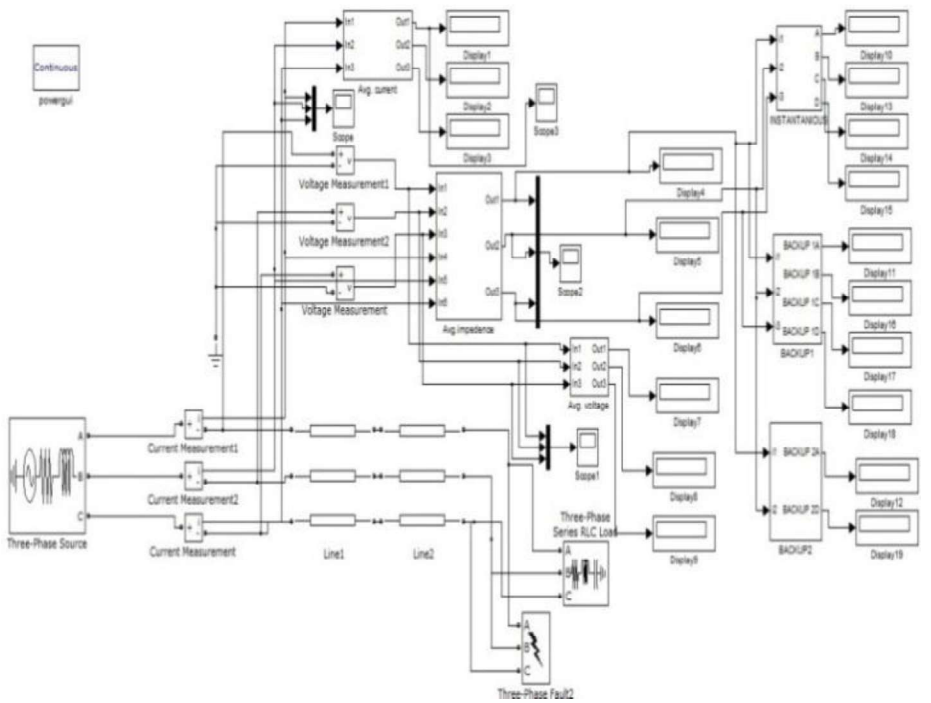

Fig 3: Three Zone protection model

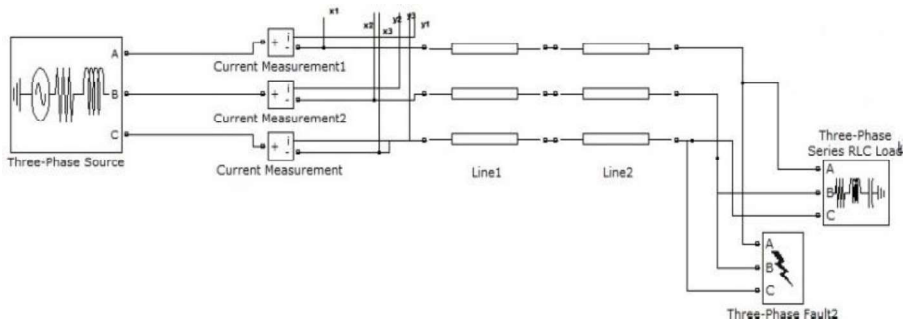

Fig 3.1: 220 KV long transmission line model

Standard parameters of 220kv long transmission line has been deployed in the fig 3.1.

Average current

The average current is determined by taking the RMS value at the outset and then passing it through the discrete mean value block.

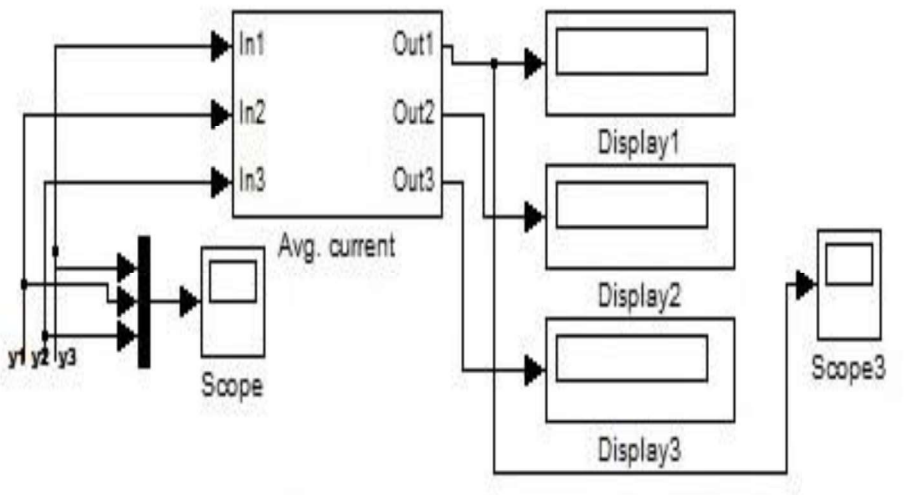

Fig 3.2: Average current block

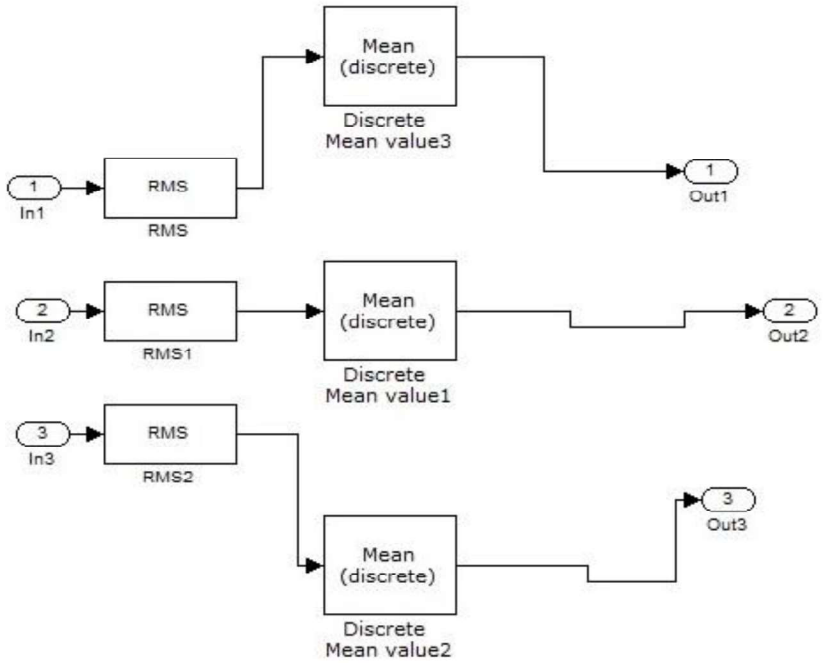

Fig 3.3: Subsystem of Average current

Average voltage

The average voltage is determined by taking the RMS value as shown in Figure 3.4 and passing it through the discrete mean value block.

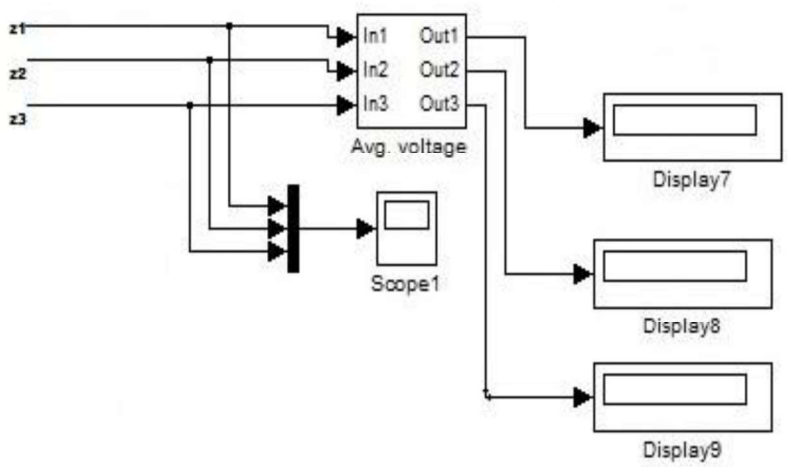

Fig 3.4: Average voltage block

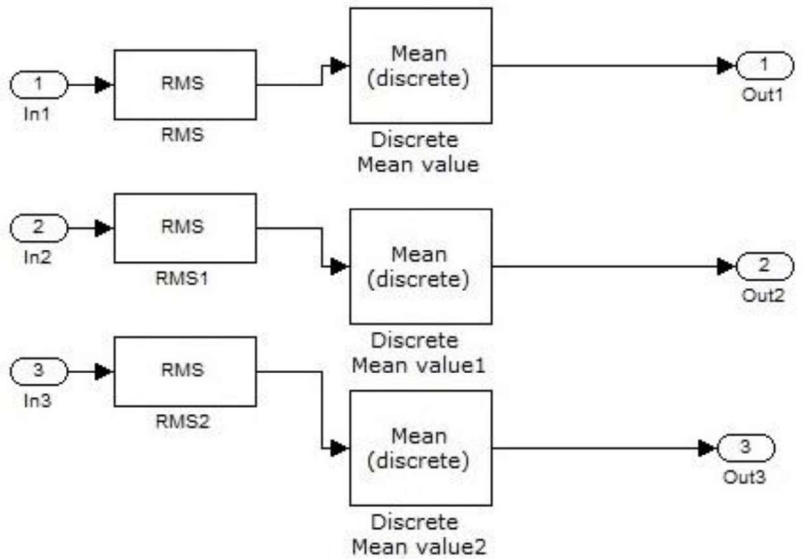

Fig 3.5: Subsystem of average voltage

Average impedance

The average impedance is calculated by dividing the discrete mean voltage by the discrete mean current

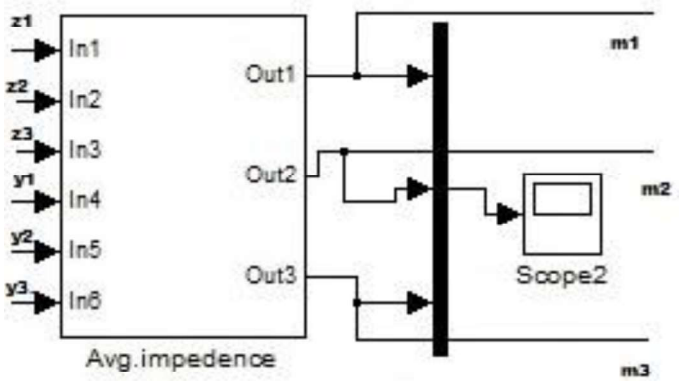

.

Fig 3.6: Average impedance block

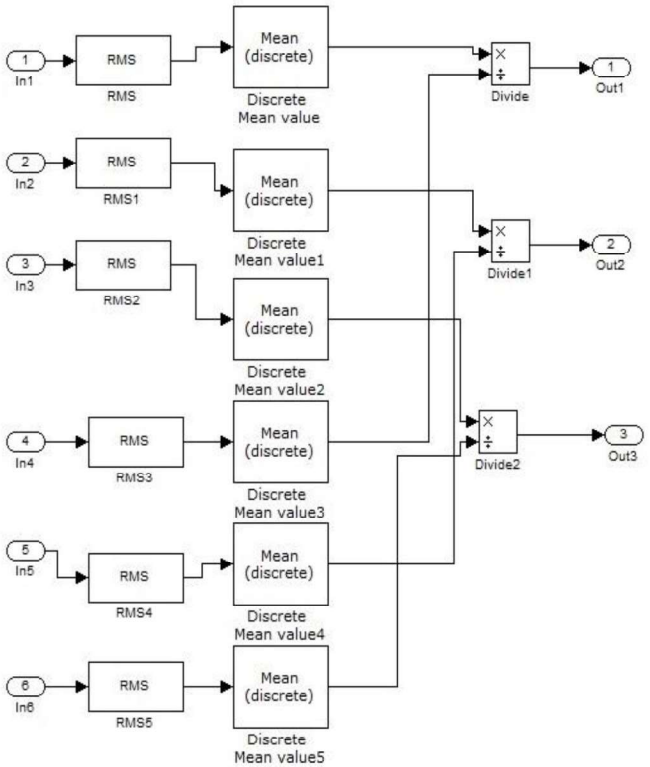

Fig 3.7: Subsystem of Average Impedance

Backup 1

The Backup1 relay's operation relies on comparing the running value with the predefined impedance value, requiring proper relay setting and optimal logical expressions. It must detect fault after a specific time delay.

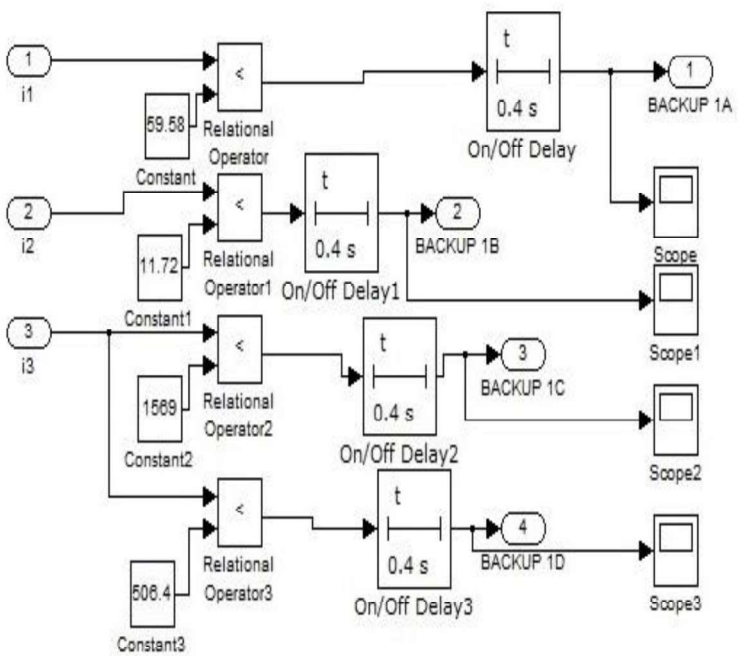

Fig 3.8: Subsystem of Backup1

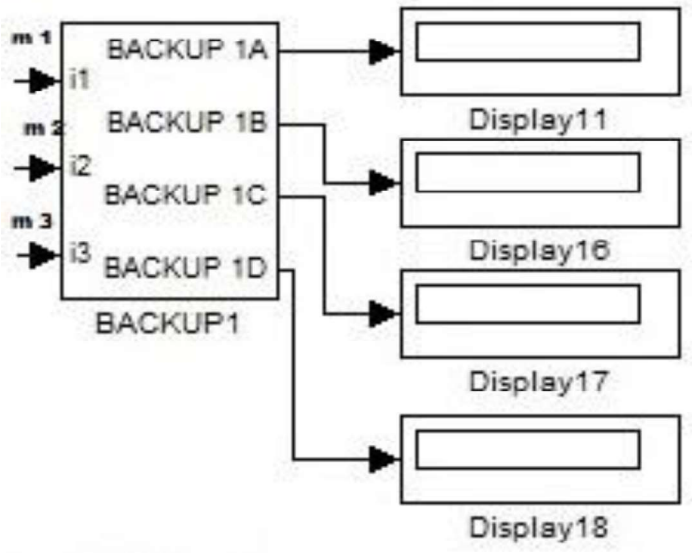

Fig 3.9: Backup1 block

Backup 2

The time delay for backup 2 as shown in fig 3.10 is comparatively longer with respect to backup1. These relays work as secondary protection if the primary protection fails.

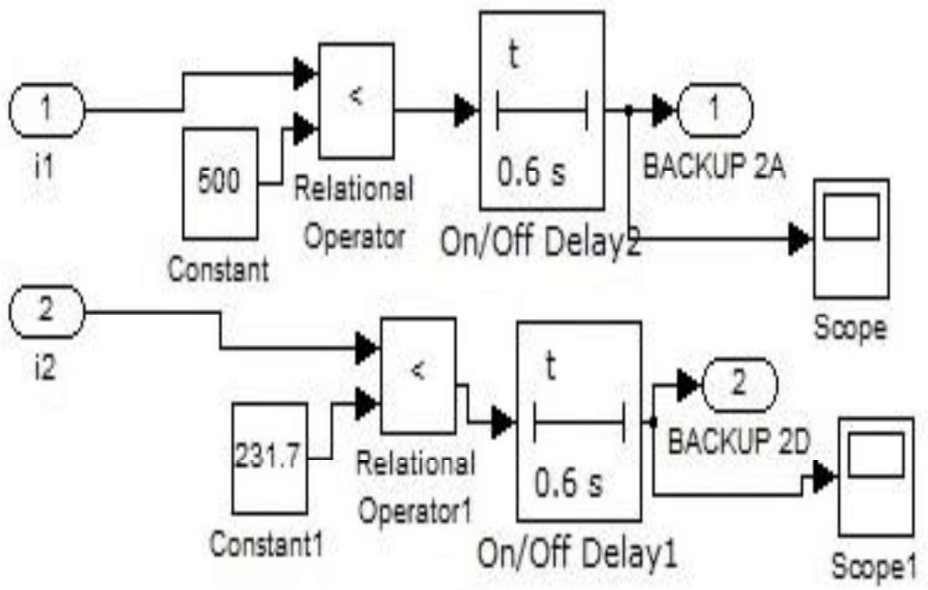

Fig 3.10: Subsystem of Backup2block

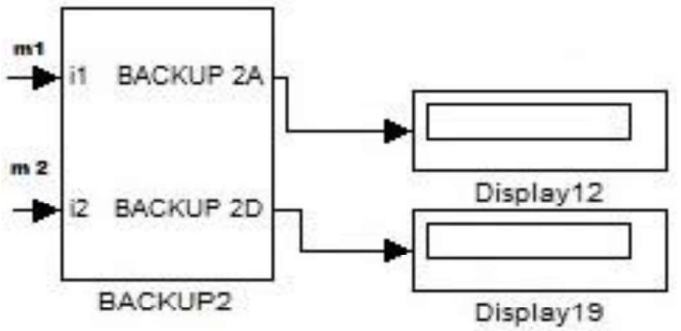

Fig 3.11: Block diagram of Backup2

Instantaneous

The instantaneous relay should operate immediately after a fault if the impedance parameter exceeds the zone's impedance value, without considering time delay, as illustrated in figs 3.12 and 13.

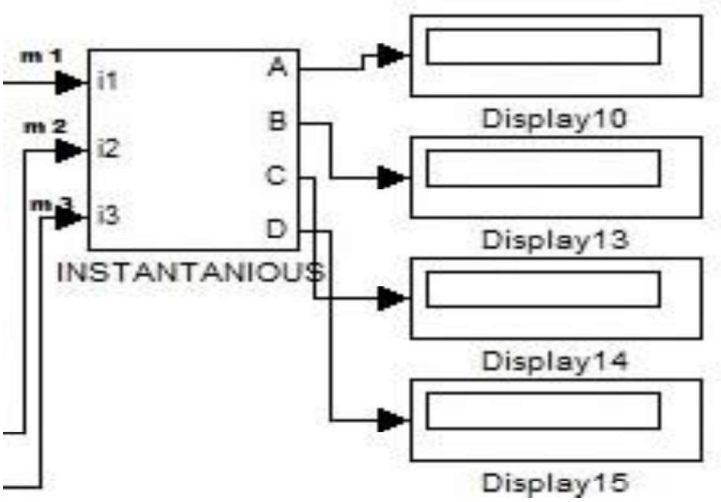

Fig 3.12: Block diagram of instantaneous

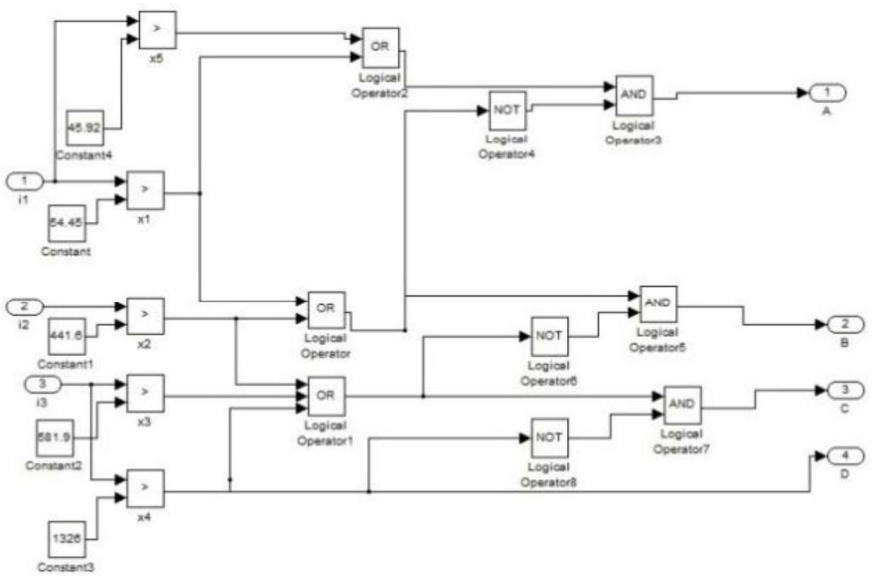

Fig 3.13: Subsystem of Instantaneous block

Algorithm of the development of the scheme:

1. Simulink has been used to construct the fundamental model.
2. A standard numerical relay has been used to calibrate the model.
3. The relay immediate, backup 1, and backup 2 circumstances have been identified and tabulated.
4. Boolean logic has been designed to control each of the aforementioned relays.
5. The model is applied the logics.
6. The model is designed to function in three lines with a ground fault.
7. Phase contingency caused the model's behavior to shift.

The logic based on dz/dt emerged as a result.

Callibration of simulink model with standard numerical relay:

Fig 4: ASHIDA numerical impedance relay

- The numerical relay in fig 4 was used to calculate impedances with and without fault conditions, using the provided readings.
- The impedances were utilized to establish the relay settings for the three zone protection scheme in the simulink model, as discussed in section III.

The readings from table no I were taken to calculate impedances with and without fault conditions.

Case Studies

The standard numerical relay was used to standardize the Simulink model, and the resulting relay settings were then applied to the various zones of the three zone protection.The three zones' instantaneous relays are denoted in the following tables by A, B, C, and D. The backup instantaneous relays are denoted by A1, B, C, and D1, while the backup backup relays are denoted by A2, D2. Each zone is mounted with primary and backup protections, as was detailed in section II. The relays are evaluated against their performance as determined in a typical three zone protection by conducting the subsequent case studies.

a) Testing of three zone protection simulation model

Fault in zone one: The time vs impedance curve in fig 5 shows a reading obtained during a fault in Zone one, indicating that the relay may not reach the steady state.

TABLE I: Calibration of Numerical Distance Relay

	Sample one		
Without fault	ja=000.02	Ua=054.09	Xa=0.000369
	jb=000.01	Ub=055.30	Xb=0.000180
	jc=000.01	Uc=061.86	Xc=0.000161
With fault	ja=002.01	Ua=053.82	Xa=0.408955
	jb=000.20	Ub=055.30	Xb=0.003616
	jc=000.16	Uc=062.02	Xc=0.002579
	Sample two		
Without fault	ja=000.35	Ua=053.98	Xa=0.006483
	jb=002.49	Ub=055.30	Xb=0.04502
	jc=000.21	Uc=061.97	Xc=0.003388
With fault	ja=000.18	Ua=054.13	Xa=0.0033253
	jb=000.11	Ub=055.46	Xb=0.0019834
	jc=000.04	Uc=062.12	Xc=0.0006439
	Sample three		
Without fault	ja=000.35	Ua=054.14	Xa=0.006464
	jb=000.29	Ub=055.56	Xb=0.005219
	jc=002.76	Uc=062.17	Xc=0.044394
With fault	ja=000.34	Ua=054.04	Xa=0.0062916
	jb=000.29	Ub=055.45	Xb=0.0052299
	jc=002.73	Uc=061.99	Xc=0.0440393

TABLE II. Relay Settings at Zone One

Distance of the line(in km)	**Relay settings**										**Time of operation**		
	A	**B**	**C**	**D**	**1A**	**1B**	**1C**	**1D**	**2A**	**2D**	**Instantaneous**	**Backup1**	**Backup 2**
100	1	0	0	0	1	0	1	1	1	0	0.164	0.439	0.630

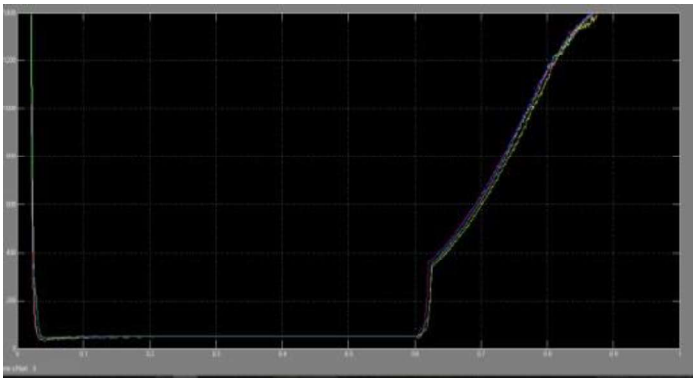

Fig5: Impedance characteristics for the fault in Zone one

Fault in zone two: The following reading has been obtained during the fault in Zone two.

Table III.Relay Settings at Zone Two

Distance of the line(in km)	**Relay settings**										**Time of operation**		
	A	**B**	**C**	**D**	**1 A**	**1 B**	**1 C**	**1 D**	**2 A**	**2D**	**Instantaneous**	**Backup 1**	**Backup 2**
80	1	0	0	0	1	0	1	1	1	0	0.030	0.420	0.620

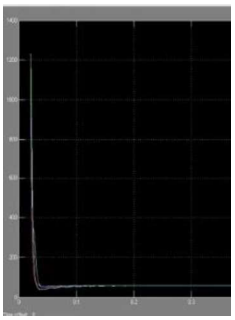

Fig 6: Impedance characteristics for the fault in zone two.

Fault in zone Three:

Table IV and Figure 7 display the fault and subsequent impedance characteristics in zone three.

Table IV.

Distance of the line(in km)	**Relay settings**										**Time of operation**		
	A	**B**	**C**	**D**	**1 A**	**1 B**	**1 C**	**1 D**	**2 A**	**2 D**	**Instantaneous**	**Back up1**	**Back up 2**
200	1	0	0	0	1	0	1	1	1	0	0.055	0.429	0.624

Relay Settings at Zone Three

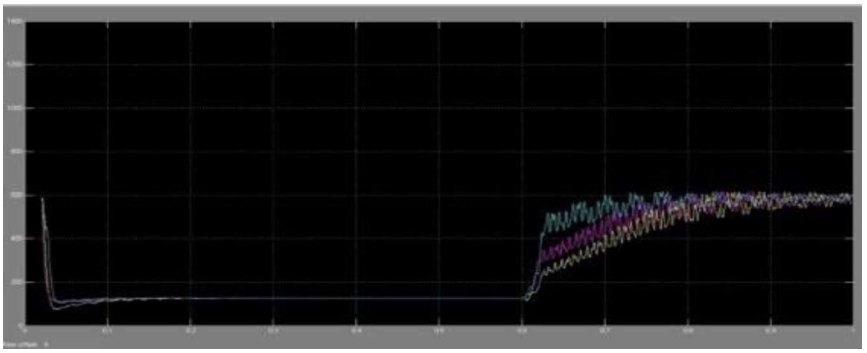

Fig 7: Impedance characteristics for the fault in zone three.

b) Mal operation of the relays in contingency

The study shows relays are operating according to three zone protection requirements, but a special case with an outage revealed that primary relay B operates early and primary relay A is not, indicating the three zone protection Scheme Is Not Reliable In Contingency Cases.

Table V. Discrepancy in Relay Operation Between with Outage and without Outageof a Transmission Line

WITHOUT OUTAGE		**WITH OUTAGE**	
RELAY	TIME	RELAY	TIME
PRIMARY A	0.05	PRIMARY B	0.04
PRIMARY B	0.1	B,C	0.45
B,D	0.44	B,D	0.55
B,C	0.44		

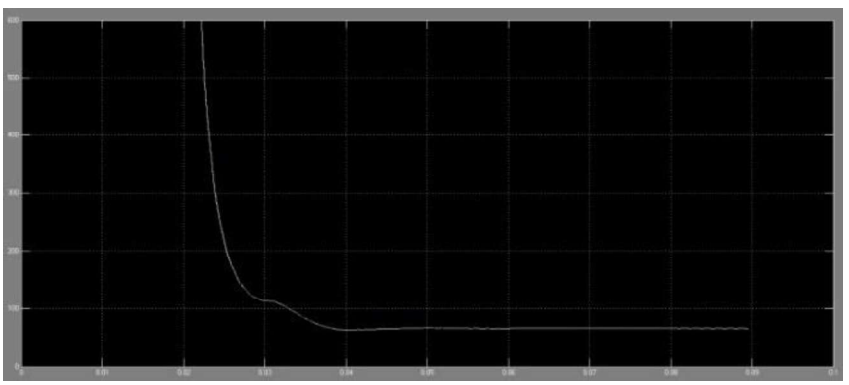

Fig 8: Impedance characteristics with outage

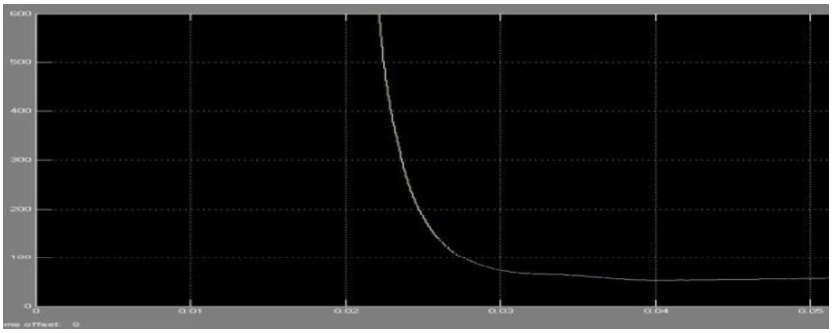

Fig 9: Impedance characteristics without outage

c) Effect of dz/dt technique adopted.

It is clear from the previous two curves that an outage condition causes the impedance to change its value more quickly than it would without one.

Hence, Dz/dt=(600-25)/0.05=19166.67 ohm/sec under no outage conditions.

Dz/dt=(600-115)/0.05=16166.67 ohm/sec when there is an outage.

With this discovery, we suggest that when faults occur in transmission lines covered by a three zone protection scheme, the rate of change of impedance should also be taken into account. Therefore, the relays should function depending on changes in impedance as well as its values. With this in mind, the subsystems have undergone improvements, and an increase in three zone protection's dependability has been seen.

Conclusion

A thorough analysis of the literature found that using numerical distance relays to protect transmission lines in three zones has been a difficult issue for power system engineers during the past ten years, particularly during transmission line contingency. Since their behavioral investigations can only be carried out using simulation for the purpose of extensive real-time monitoring, modeling of these numerical relays with respect to a hardware configuration is therefore of the utmost relevance. Only when all three phases are relevant can the three zone protection with distance relay be used in a three phase to ground fault. Relays could malfunction in the event of a transmission line failure.Thedz/dt protection technique was developed since the classic impedance relay protection scheme fails during line contingency.

References

[1] Mani V. Venkatasubramanian, Project Leader, Washington State University ,Mladen Kezunovic, Texas A&M University, Vijay Vittal, Arizona State University, Detection, Prevention and Mitigation of Cascading Events, Power Systems Engineering Research Center A National Science Foundation Industry/University Cooperative Research Center since 1996.

[2] Mr. Sathaporn Sittiwong, an enhanced performance of distance relay algorithm to prevent undesired zone 3 operation during load encroachment, A thesis submitted in partial fulfillment of the requirements for the degree of master of science in electrical power engineering siridhron international Thai-German graduate school of engineering(TGGS), graduate college king mongkuts , University of technology north Bangkok academic year 2007 copyright of king mongkuts university of technology north Bangkok.

[3] Muhd Hafizi Idris, School of Electrical SystemEngineering University Malaysia Perlis,Kuala Perlis, Malaysia hafiziidris@unimap.edu.my, Surya Hardi School of Electrical System Engineering University

Malaysia Perlis, Kuala Perlis, Malaysia surya@unimap.edu.my, Mohd Zamri Hasan School of Electrical System Engineering University Malaysia Perlis Kuala Perlis, Malaysia zamrihasan@unimap.edu.my, Teaching Distance Relay Using Matlab/Simulink Graphical User Interface.

[4] Harikrishna M, Department of Electrical Engineering, Indian Institute of Technology Roorkee, Roorkee, India, Email: harigpee@iitr.ernet.in,Performance of quadrilateral relay on EHV transmission line protection during various faults, ACEEE International Journal on Control System and Instrumentation, Vol. 1, No. 1, July 2010.

[5] M. Kezunovic and C. Pang are with the Department of Electrical and Computer Engineering, Texas A&M University, College Station, TX 77843-3128, USA (emails: pangchz@neo.tamu.edu, kezunov@ee.tamu.edu), IMPROVED TRANSMISSION LINE PROTECTION DURING CASCADING EVENTS.

[6] D. Ouahdi, R. Ladjeroud, and I. Habi, Reliability of Impedance Relay,World Academy of Science, Engineering and Technology International Journal of Electrical, Computer, Energetic, Electronic and Communication Engineering Vol:2, No:11, 2008.

[7] Xu Yan,State Key Laboratory of Alternate Electrical PowerSystem with Renewable Energy Sources, North China Electric Power University, Baoding,China Xuyan@ncepubd.edu.cn, Han Ping State Key Laboratory of Alternate Electrical PowerSystem with Renewable Energy Sources, North China Electric Power University Baoding, China 357753780@qq.com,Review on Methods of Wide Area BackupProtection in Electrical Power System, International Conference on Mechatronics, Electronic, Industrial and Control Engineering (MEIC 2015).

[8] M.Rambabu1,M.Venkatesh2,J.S.V.SivaKumar3,T.S.L.V.AyyaRao4, 1 2 3 4 Asst Professor, EEE Department, GMRIT, Rajam, A.P,India, Three Zone Protection By Using Distance Relays in SIMULINK/MATLAB, International Research Journal of Engineering and Technology (IRJET) e-ISSN: 2395-0056 Volume: 02 Issue: 05 | Aug-2015 www.irjet.net p-ISSN: 2395-0072.

[9] ASHIDA Numerical Three Phase Distance Relay, ASHIDA ELECTRONICS PVT LTD ASHIDA HOUSE, Plot No. A-308, Road No. 21,Wagle Industrial Estate,Thane (W)-400 604. INDIA.Email:sales@ashidaelectronics.com,Web:www.ashidaelectronics.com,Ref.:ADR239A_V2,Issue: 03 02.11.2010.

[10] Nikolovski, S.; Marić, P. &Prhal, D, NUMERICAL SIMULATION OF DISTANCE PROTECTION ON THREE TERMINAL HIGH VOLTAGE TRANSMISSION LINES ADVANCED ENGINEERING, 3(2009)2, ISSN 1846-5900.

[11] Tushar Yesansure , Nagpur University, Ramdeobaba College of Engineering and Management, Katol Road, Nagpur 440013, Maharashtra, India,tushar.yesansure@gmail.com , International Journal of Science and Research (IJSR), India Online ISSN: 2319-7064.

[12] An Artificial Intelligence-Based Three-Zone Distance Protection Scheme for Transmission Lines by Muhammad Asim Khan, Muhammad Aamir Khan, and Kashif Mehmood, published in IEEE Transactions on Smart Grid in 2023.

[13] A Hybrid Three-Zone Distance Protection Scheme for Transmission Lines with Adaptive Fault Resistance Compensation by Muhammad Irfan, Waqas Ahmad, and Muhammad Usman Qureshi, published in IEEE Transactions on Power Delivery in 2022.

[14] A Novel Three-Zone Distance Protection Scheme for Transmission Lines Considering Fault Resistance and Load Encroachment by Muhammad Rizwan, Muhammad Usman Qureshi, and Waqas Ahmad, published in the IEEE Access journal in 2022.

[15] A Three-Zone Distance Protection Scheme for Transmission Lines with Improved Accuracy and Reliability by Muhammad Awais, Muhammad Usman Qureshi, and Waqas Ahmad, published in the IEEE Transactions on Industrial Electronics journal in 2022.

[16] A Three-Zone Distance Protection Scheme for Transmission Lines with Enhanced Performance under Power Swing Conditions by Muhammad Salman, Muhammad Usman Qureshi, and Waqas Ahmad, published in the Journal of Power Engineering in 2022.

[17] A Three-Zone Distance Protection Scheme for Transmission Lines with Adaptive Reach Setting by Muhammad Sohail, Muhammad Usman Qureshi, and Waqas Ahmad, published in the IEEE Transactions on Power Systems journal in 2022.

Chapter 20

Optimal PMU Placement Methods in Power Systems: A Review of Phasor Measurement Unit Integration

Suvraujjal Dutta*, Titas Kumar Nag, Promit Kumar Saha, Susmita Dhar Mukharjee
Swami Vivekananda University Barrackpore, West Bengal
Corresponding Author Email: suvraujjal@svu.ac.in

Abstract

The Phasor Measurement Unit (PMU) is a crucial component for keeping track of, safeguarding, and managing the current power system. PMUs provide synchronized measurements of real-time data for voltage, current, and frequency for the present power systems. From an economic and huge data handling perspective, placing PMUs in each bus to monitor the system is not practical. Therefore, in order to achieve the maximum power system observation, it is imperative that the number of PMUs in the bus system be reduced. From the past to the present, various methods have been used to tackle this optimum PMU placement (OPP) problem, including heuristic methods and mathematical programming. From the past to the present, various methods have been used to tackle this optimum PMU placement (OPP) problem, including heuristic methods and mathematical programming. A rapid, experience-based way for tackling optimization problems is the heuristic approach. In this work, various optimization techniques for handling OPP problems are reviewed.

Keywords: Phasor Measurement Unit (PMU), Global Positioning System (GPS), Optimal Placement of PMU (OPP), State Estimation (SE), Supervisory Control and Data Acquisition (SCADA), Heuristic algorithm.

Introduction

There are no alternatives to careful observation and secure control of the power system given its dynamic properties. Major disruptions and contingencies in recent years have led to significant blackouts all around the world. The operating values of the system may fluctuate from the threshold points due to disturbances such as single- or three-phase line faults, generator losses, load changes, etc. In this situation, a system state monitoring and precise measuring instrument is necessary for the proper and steady operation of the power system. The Supervisory Control and Data Acquisition (SCADA) system is the most used tool for measuring system data [1]. Timestamped synchronized signals within 1 ms were originally introduced in the 1990s as phasor measurement units (PMUs) [2]. Linear state estimation is used for the measurements in PMU measuring techniquesPMU provides quicker sampling rates than SCADA/EMS system and high-speed voltage control [4]. When a PMU is inserted in a bus, it offers more information than only the voltage phase of thenot just the present phasor of that bus, but also all of the lines that are attached to and close to it [5]. Adequate SE measurements are needed to completely observe the power system, which raises the issue of ideal placement. In a real-world scenario, a nation's electrical infrastructure may contain hundreds of thousands of buses. Therefore, installing PMUs in each bus to make the system fully and immediately visible is neither practical nor cost-

effective.

The OPP problem is thus proposed as a significant difficulty to achieve the ideal number of PMUs and their arrangement in the system [6]. For years, various optimization methods have been put out to address this optimization issue [6]. This essay provides a survey of previous, present, and ongoing research in the area of OPP in power systems. The traditional and heuristic optimization techniques are the main areas of focus. Section II describes the introduction of PMU, while Section III continues with the formulation of the problem. In Section IV, various approaches of solving the OPP problem are covered. The conclusion for this work is found in Section V.

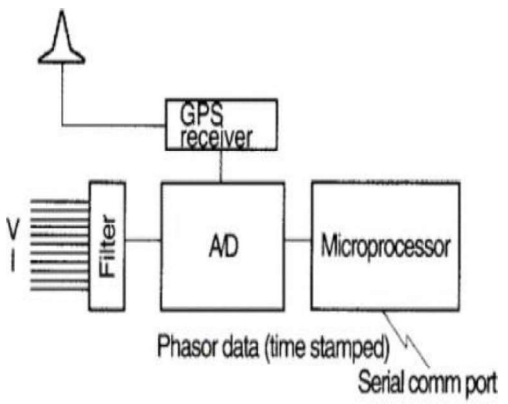

Fig1. Featured Component of PMUs [7]

Phasor Measurement Unit

What is Phasor Measurement Unit

The Phasor Measurement Unit (PMU) synchronizes with a local or global time source to measure the voltage, current, and frequency phasors from the electric grid. It is now possible to measure time synchronized real-time measurements data from far-off measurement locations on the grid because of this time synchronized characteristic. The measurement technique in question is called a synchrophasor. PMUs are currently the primary measuring tools for both existing and upcoming power systems [7].

Major Component of PMU

1) GPS receiver: This receiver outputs a signal at 1 pulses per second (pps) with a time stamp. The primary characteristic of this time tag is that it includes UTC as well as local time information for seconds, minutes, days, and years.

2) Microprocessor: Phasors are managed by a microprocessor using a recursive method. By taking into account the data obtained from the GPS timing message at the very beginning, it may determine the sample number. Modems can be used for remote sensing.

3) Phase-locked oscillator: Divide the 1 pps into the desired number of pulses/second in order to sample the acquired signal. A standard PMU samples at a rate of 30-48 cycles per second.

4) Surge Filtering: These filters give the same phase shift and attenuation of the secondary output of current and voltage transformers.

Formulation of Optimal PMU Placement Problem

PMU can gather information about the phase voltage from its mounting point. It can also measure the branch currents from associated buses. Figure 2 depicts how standard PMUs are connected to a system. The measured signal that PMUs are transmitting from various sites is being collected by PDCs. The PDC collects and arranges the phasor readings while the signal processor transforms data from PMUs into information that can be displayed on the Human Machine Interface (HMI) State [8].The two primary approaches for system observability analysis are topological and numerical observability techniques. Numerical analysis is currently extensively used since it has recently been subjected to high matrix calculation analysis.

1. Direct measurement:

   The PMU detects the phase voltage of the PMU-installed bus and the linked brunch current from all joint lines to it using the direct measurement approach (Figure 3a).

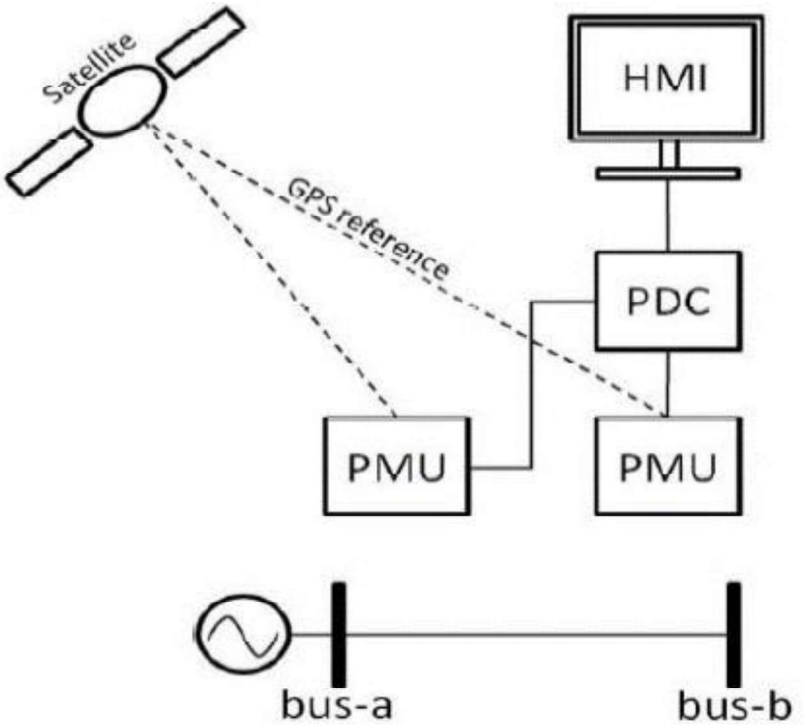

Fig 2. Outline of PMU with GPS reference signals [8]

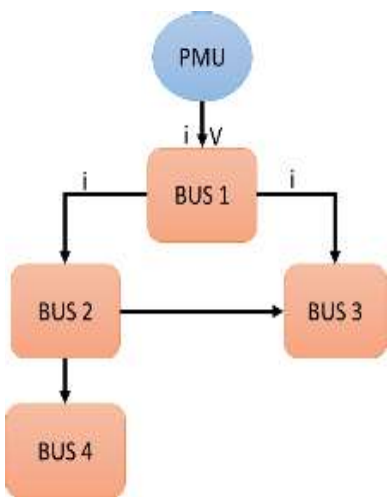

(a)

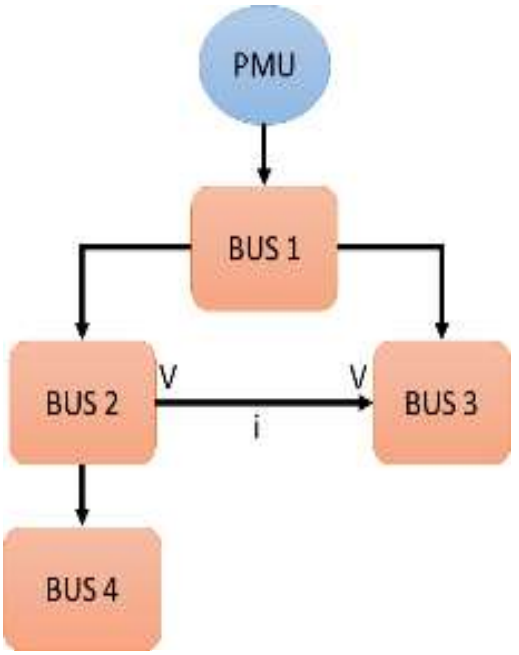

(b)

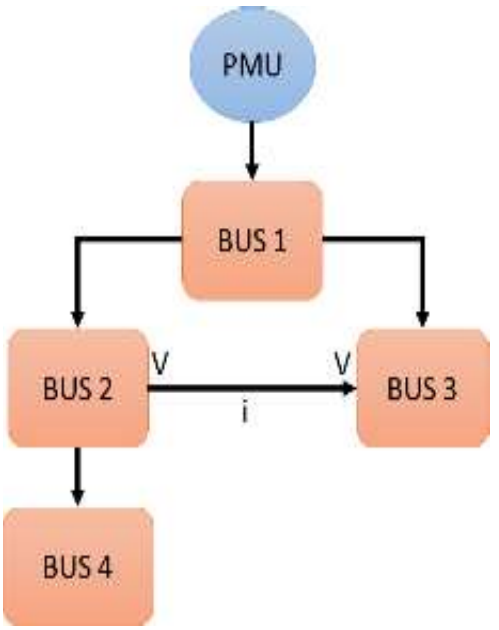

(c)

Fig 3.(a) Direct Measurement (b) Pseudo Measurement (c) Pseudo Measurement considering line current.

1) Pseudo Measurement:

The voltage and current of the PMU-installed bus, as well as the line current of the associated buses, are known in this measuring technique. Additionally, the other buses' voltage may be abnormal.

Using this rule, it is possible to observe the relationship between Buses 1 and 2 (Figure 3b). If the voltage of the two connected buses is known, this rule can also be used. In that situation, it would be simple to determine the current between them (Figure 3c).

2) Zero-Injection Bus Measurement

Numerous factors are considered if a zero injection bus is present in the system.

a) The voltages at every junction line are known.

b) The voltage of the zero-injection bus is unknown, although all other adjunct bus voltages are known. For the current measurement for those joint lines in the first case, Kirchhoff's current law offers a simple solution (Figure 4a). In the second instance, it will be easy to determine the known parameters from figure 4b using the node equation. The voltage law and Kirchhoff's current equation both provide simple calculations for determining the unidentified power system parameter.

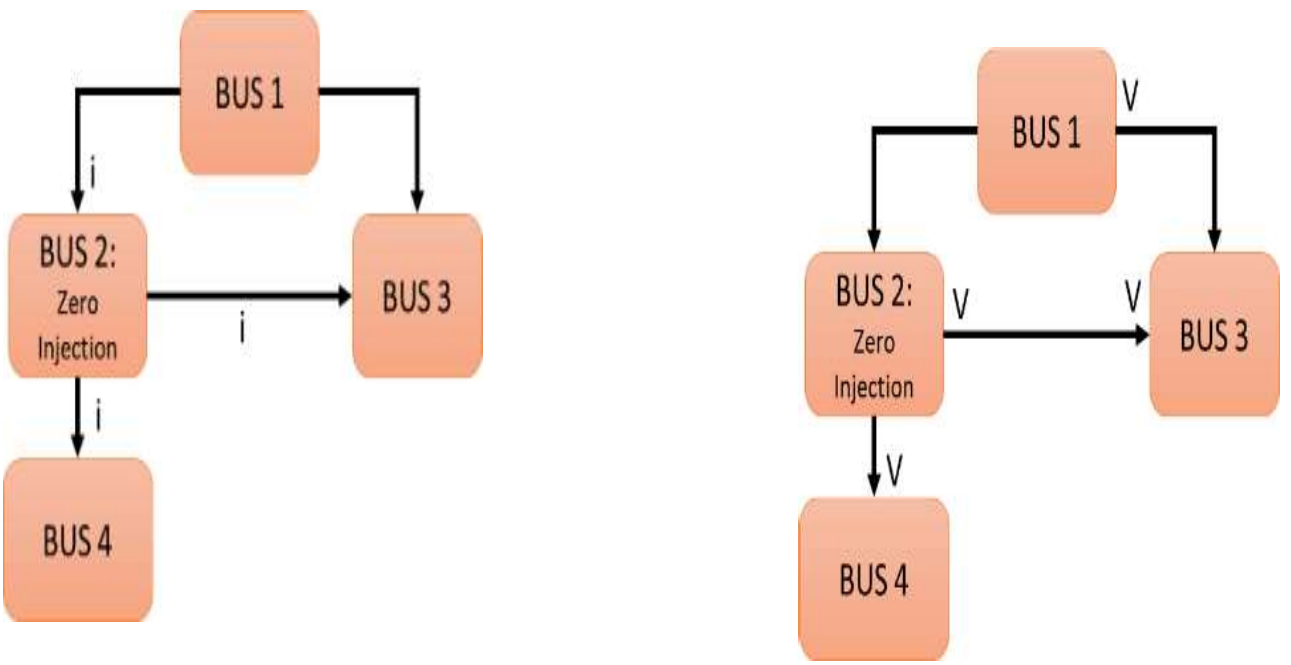

(a) (b)

Fig 4. Zero-Injection Bus Measurement Techniques applying KCL and KVL theories.

The main purpose of the OPP problem is to define the least number of PMUs in the system and also validate the full system observability.

Optimum PMU Placement Methods

A. Conventional Methods

B. Integer Quadratic Programming (IQP): The connection matrix, which represents network topology, is used to describe the OPP problem. The linear constrained and variable integer value will be taken into account when optimizing the quadratic objective function. Through providing a full system observability in both normal and outage conditions, this technique will lower the number of PMUs.

C. Integer Linear Programming (ILP): ILP approaches, particularly Binary integer programming, take into account the system's injection and power calculations as well as the computation of PMU failure error through state estimation. ILP formulation is based on eigenvectors derived from the adjacency matrix of the spanning tree. After decomposition, the PMUs are positioned appropriately in the sub to reduce the installation rate.

D. Heuristic Methods

It is crucial to use various placement approaches that will enable full system observability because installing PMUs at every bus to evaluate and control the defective area is not cost-effective. Several heuristic techniques are available at the moment.

In a tabular format, a brief summary of numerous heuristic techniques is provided.

No	Methods Name	Description	Benefits
1	Genetic Algorithm (GA)	Providing a complete visible power system with few PMU units and a map of their distribution [9]. It considers the connection between current phasors and PMU units.	This approach has the major benefit of offering the best Pareto-optimal option rather than a single answer.
2	Simulated Annealing (SA)	This technique uses genetic probabilistic meta heuristics. Its major goal is to identify a somewhat reasonable solution within a given time frame, regardless of the best option. To determine the parameter sensitivities of each bus, a practical sensitivity analysis method is used [10]. In order to place the initial PMUs for the system observability, incidence matrix approaches are being used.	This approach offers simultaneous full power system observability and important dynamic data measurement from the power systems.
3	Particle Swarm Optimization (PSO)	A population-based stochastic optimization method is called particle swarm optimization (PSO) [11]. By using these strategies, the configuration criteria and data loss modeling can be mapped.	provides several solutions rather than a single one for data loss at the designated PMUs.

4	Tabu Search(TS)	A meta heuristic local search algorithm is Tabu Search (TS) [12]. By monitoring and directing the search, this approach is used to tackle problems involving combination optimization. The Tabu Search (TS) method and an augmented incidence matrix are both used in the TS.	faster computing times with more accurate results.
5	Artificial Neural Network (ANN)	A rough functional link between voltage stability indices and system parameters can be created using ANNs [13].	various solutions based on computer models are offered.
6	Immune Genetic Algorithm (IGA)	It is based on the principles of genetic algorithms, and this process is used to protect living things from germs and viruses [14].	Large-scale systems can easily benefit from significant process speed.
7	Differential Evaluation (DE)	Differential Evolution (DE) is another meta heuristic technique that creates potential solutions by iteratively optimizing a problem utilizing both the Pareto Non-Dominated Sorting algorithm and Differential Evolution [15].	Finding the number of Pareto-optimal solutions that provide accurate solutions and full observability is simple and rapid.
8	Matrix Reduction	Using a preprocessing technique, this method reduces the amount of PMUs [16]. and resolve the OPP problem using mathematical techniques like Lagrangian relaxation, matrix reduction algorithm, or virtual data elimination preprocessing.	For full ob-servability, computation time will be reduced and made simple to implement in large-scale power systems.
9	Mutual Information	By using a notion from information theory called mutual information, uncertainty modeling, to reduce the number of PMUs [6].	Uncertainty in the system is easily modifiable.
10	Ant Colony Optimization	It is a traditional probabilistic method that makes use of graphs to simplify computational issues.[13]	Reduce the complexity of the computations.

11	Iterated local search	It is a combination of page rank placement algorithm (PPA) and ILS.[16]	Easy understanding and implementing.

Table I: Various Optimal PMU Placement methods

Table II: Comparison between different OPP Methods Based on The above-mentioned OPP methods characteristics and benefits, a comparison studies are being presented in the Table II.

No.	Characteristics	Programming Based Algorithm		Heuristic Methods		
		Integer Quadratic Programming	Integer linear Programming	Genetic Algorithm	Matrix Reduction	Particle swarm optimization
1	Computational Efficiency	Moderate	High	Moderate	Moderate	High
2	System Observability	High	High	High	High	High
3	Computation Time	Moderate	High	Moderate	Less	Moderate
4	System Complexity	High	Low	Moderate	Low	High
5	PMU Requirement	High	Moderate	Low	Low	High

Conclusion

Many different techniques have been used to examine the situation and choose the best place to implant the PMUs. The ideal PMU placement is now an intelligent instrument for power system stability and control. Here, a sizable

The examination of the optimization strategies used in this

for PMU placement, it will provide a platform for academics to classify these methods and determine the best solution.serve as a guide and aid in the discovery of the optimization criteria for emerging trends.

References

[1] [D. J. Gaushell, H. T. Darlington, "Supervisory control and data acquisition",Proc. IEEE, vol. 75, no. 12, pp. 1645-1658, 1987.

[2] G. Phadke, "Synchronized phasor measurements in power systems", IEEEComput. App. Power, vol. 6, no. 2, pp. 10-15, Apr. 1993.

[3] [S.M. Mazhari, H. Monsef, H. Lesani, A. Fereidunian, A multi-objectivePMU placement method considering measurement redundancy and observabilityvalue under contingencies, IEEE Trans. Power Syst. 28 (2013)2136–2146
[4] Wu L., Xia L. (2012) Research on Data Compatibility of PMU/SCADAMixed Measurement State Estimation. In: Zhao M., Sha J. (eds) Communicationsand Information Processing. Communications in Computer andInformation Science, vol 288. Springer, Berlin, Heidelberg.
[5] EPRI Final Report (1997), Assessment of Applications and Benefitsof Phasor Measurement Technology in Power Systems, GE Power Syst.Engineering.
[6] M. Nazari-Heris, B. Mohammadi-Ivatloo Application of heuristic algorithmsto optimal PMU placement in electric power systems: an updatedreview Renew Sustain Energy Rev, 50 (2015), pp. 214-228.
[7] Phadke AG. Synchronized Phasor measurements. IEEE Computer Applicationsin Power, 1993 Apr.
[8] R. Shewale, B. Kethineni, U. Balaraju, S. Bhil, P. More, Optimalpacement of phasormeasurement units for power system observabilityby heuristic search method, International Journal of Advanced Technologyand Engineering Research 2 (2) (2012) 128–133.
[9] F. J. Martin, F. Garcia-Lagos, G. Joya, F. Sandoval, "Genetic algorithmsfor optimal placement of phasor measurement units in electrical networks",IEE Electronic Letters, vol. 39, june 2003.
[10] Hong-ShanZ, YingL, Zeng-Qiang M, Lei Y. Sensitivity constrainedPMU placement for complete observability of power systems . In: Transmissionand distribution conference and exhibition : Asia and Pacific, 2005IEEE/PES: IEEE; 2005.p.1–5.
[11] Huang J,WiNE.Fault-tolerant placement of phasor measurement unitsbased on control reconfigurability. Control Eng Pract2013;21:1–11.
[12] Peng J,SunY,Wang.Optimal PMU placement for full network observabilityusing tabu search algorithm. Int J Electr Power Energy Syst 2006;28: 223–31.
[13] Sreenivasa Reddy PS, Chowdhury S. PMU placement-a comparativesurvey and review. In: Proceedings of 10th IET international conferenceon developments in power system protection (DPSP); 2010.
[14] Optimal placement of phasor measurement units using immunity geneticalgorithm FAminifar, C Lucas, A Khodaei, M Fotuhi-Firuzabad– IEEETransactions on power delivery, 2009.
[15] C.Peng, H. Sun, and J. Guo, "Multi-objective optimal PMU placementusing a non-dominated sorting differential evolution algorithm", InternationalJournal of Electrical Power & Energy Systems, vol. 32, pp. 886-892,Oct. 2010.
[16] Zhou M,Centeno VA, Phadke AG, Hu Y, Novosel D,Volskis HA.Apreprocessing method for effective PMU placement studies.In:Thirdinternational conference on electric utility deregulation and restructuringand power technologies, 2008 (DRPT2008): IEEE; 2008. p. 2862–7.
[17] A. K. Panigrahi, S. R. Pradhan, and S. K. Panda, "Optimal PMU placement in power systems using topology transformation method," in 2016 IEEE Power and Energy Society General Meeting (PESGM), Boston, MA, USA, 2016, pp. 1-5.
[18] M. S. Almalawi and M. A. Abu-Seada, "An optimal PMU placement method for power system observability," in 2011 IEEE/PES Power Systems Conference and Exposition, Phoenix, AZ, USA, 2011, pp. 1-7.
[19] S. K. Biswas and S. N. Mahanty, "PMU placement based on power system characteristics," in 2019 IEEE International Conference on Electrical, Communication, and Computer Engineering (ICECCE), Jakarta, Indonesia, 2019, pp. 1-6.
[20] M. Shahidehpour, Y. Wang, Z. Huang, and Z. Li, State estimation and monitoring of electric power systems. IEEE press, 2004.

[21] A. K. Panigrahi, et al., "Optimal PMU placement in power systems using topology transformation method," in 2016 IEEE Power and Energy Society General Meeting (PESGM), Boston, MA, USA, 2016, pp. 1-5.
[22] M. S. Almalawi and M. A. Abu-Seada, "An optimal PMU placement method for power system observability," in 2011 IEEE/PES Power Systems Conference and Exposition, Phoenix, AZ, USA, 2011, pp. 1-7.
[23] S. K. Biswas and S. N. Mahanty, "PMU placement based on power system characteristics," in 2019 IEEE International Conference on Electrical, Communication, and Computer Engineering (ICECCE), Jakarta, Indonesia, 2019, pp. 1-6.
[24] M. Shahidehpour, et al., State estimation and monitoring of electric power systems. IEEE press, 2004.

Chapter 21

HVDC Protection Strategies: An In-Depth Survey and Analysis

Suvraujjal Dutta*, Avik Datta, Rituparna Mitra, Rituparna Mukharjee
Swami Vivekananda University, Barrackpore, North 24 Parganas, Kolkata – 700121,West Bengal, India.

*Corresponding Author Email: suvraujjal@svu.ac.in

Abstract

This paper provides a brief overview of the UHVDC transmission technology, which is popular for long-distance and large-capacity transmission. The environment is retrieved by the perplexingly long distances of DC lines. The HVDC system defect with the highest level of legal liability. a bipolar system capable of performing polarities on both poles. These numerous UHVDC approaches include the hardware implementation loop, ANN, and Wavelet. High-Voltage Direct Current (HVDC) protection systems are essential components of modern power systems that use HVDC transmission technology. HVDC transmission is used to transmit electrical power over long distances with reduced losses compared to traditional alternating current (AC) transmission. Protecting these HVDC systems is crucial to ensure the reliability and stability of the overall power grid.

Keywords: UHVDC, Bipolar, Travelling Wave, ANN, Wavelets, large-capacity transmission

Introduction

Long-distance transmission of both AC and DC electricity using ultra-high voltage electrical transmission. The preferred DC voltage level for use in UHVDC transmission is in the 800kv range. High stresses were accommodated for in the equipment built for UHVDC transmission [5,83]. The UHVDC transmission line in a bipolar system is made for DC rectifier stations with continuous ratings. The performance and redundancy of the system determine how well a DC harmonic filter works in a UHVDC system. Dimensioning was based on switching impulse level. The fundamental protection scheme that relays power serves as the foundation for the traveling wave [34, 88].

The fundamental modifications to the way the electric power system is built and run call for integrated disturbance propagation. UHVDC transmission is economically appealing for long-distance bulk power transfer [16]. It is more difficult to detect high resistance faults and safeguard the pole range of the lines from genuine waves. It is challenging for UHVDC systems to tolerate high lightning impulse levels in oil-insulated reactors. As a result, the UHVDC system may utilize air core reactors [15, 43]. Long creep is necessary for station design to have a significant impact. UHVDC are excessively long due to non-linear in-air clearance and switching overvoltage [63, 64, 65]. The UHVDC transmission line has clear benefits in terms of system capability enhancement and cost reduction. The uses and control of hybrid cascade multilevel converters have been covered in numerous works [69]. An HVDC system that transfers electrostatic electricity produced by

capacitance and AC grids is integrated with the inertia of wind turbines [70]. Instability in the power grid that causes substantial financial losses when issues with HVDC transmission happen [51, 74].

Due to advantages like increased distance, rapid, and HVDC has been used frequently in contemporary power systems due to its flexible control [82], reduced losses [92], increased power transmission capabilities [79], and vital role in asynchronous networks.

Here's an evaluation of HVDC protection systems in modern power systems:

1. Overview of HVDC Systems:

- HVDC systems are used for long-distance power transmission, often underwater or across challenging terrains.

- They involve the conversion of AC to DC at the sending station, transmission through DC lines, and reconversion to AC at the receiving station.

- HVDC systems use power electronic devices, such as thyristors or IGBTs (Insulated Gate Bipolar Transistors), for conversion.

2. Protection Requirements:

- HVDC systems require specialized protection schemes due to the unique characteristics of DC transmission.

- Key protection requirements include fault detection, fault clearance, and coordination with the AC protection system.

3. HVDC Protection Elements:

- Converter Protection: Protects the converter station from various faults, such as overvoltage, over current, and voltage imbalance.

- DC Line Protection: Detects and clears faults on the DC transmission line, such as short circuits and line faults.

- AC Filter Protection: Protects AC filters and components from disturbances and harmonics.

- Control and Monitoring: Provides real-time monitoring of system parameters and communicates with the control system for rapid intervention during faults.

4. Fault Detection and Clearing:

- HVDC protection systems use various techniques for fault detection, such as current differential

relays, impedance relays, and rate-of-rise of voltage/current (RoCoF) protection.

- Fault clearing involves isolating the faulted section and blocking converter operation if necessary to prevent further damage.

5. Redundancy and Reliability:

- HVDC systems often incorporate redundancy in protection elements to ensure reliability and fault tolerance.

- Redundancy can include duplicate relays and communication channels to minimize the risk of false trips or system failures.

6. Communication and Coordination:

- HVDC protection systems communicate with the broader SCADA (Supervisory Control and Data Acquisition) system for remote monitoring and control.

- Coordination with AC protection systems is critical to ensure that faults on the DC side do not propagate to the AC grid.

7. Cyber security:

- Modern HVDC protection systems need robust cyber security measures to safeguard against cyber attacks that can disrupt system operation.

8. Testing and Maintenance:

- Regular testing and maintenance of protection relays and devices are essential to ensure their proper functioning during fault conditions.

9. Advanced Technologies:

- Some modern HVDC protection systems may incorporate advanced technologies like synchrophasors and data analytics for real-time condition monitoring and predictive maintenance.

10. Standards and Regulations:

- HVDC protection systems must comply with international standards and regulations to ensure interoperability and safety.

HVDC protection systems are a critical component of modern power systems that use HVDC transmission technology. These systems are designed to detect and clear faults, ensure system reliability, and coordinate with the AC protection system. To meet the evolving needs of the power grid, ongoing research and

development are essential to improve the performance, reliability, and cyber security of HVDC protection systems.

Bipolar Transmission for UHVDC System

The list of existing installations and the most significant current control and modeling techniques for VSC-based HVDC power transmission systems are also provided in [59,60]. Two conductors, one positive and the other negative on Earth, make up a bipolar link. At each terminal station, electrode lines connect the midpoints of the converters to the earth. Two times as much voltage as there is between any two conductors and groups exists between the conductors. The bipolar's schematic is shown in Fig. 1.

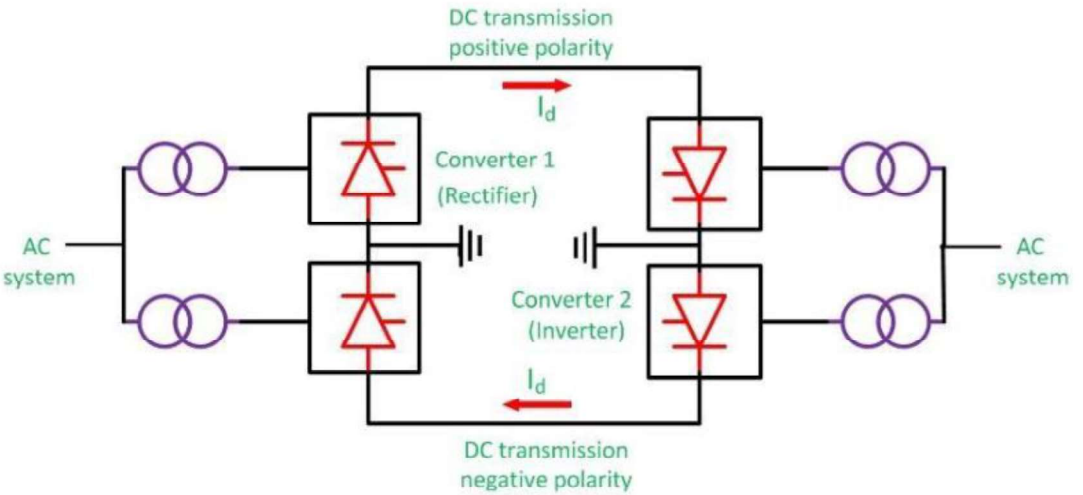

Fig.1. Schematic diagram of a bipolar system

The majority of HVDC power systems use them. It regulates steady current and advances the supply of half-rated power [40]. The DC transmission line's midpoint can be used to set a bipolar fault [72]. Therefore, a bipolar system is separated into two separate modal networks, a pole network and a field network.

A ground-mode network and a mode network. The protective mechanism uses these modal voltages and currents rather than the real values [22]. As a result, a bipolar system is separated into two separate modal networks, referred to as a pole mode network and a ground mode network [25]. Although the structure of the bi-polar and mono-polar high-voltage direct current systems are similar, there are several key distinctions between them, such as the mutual coupling effect between the pole lines and the opposite voltage polarity.

Principle of Travelling Wave Protection

The specific HVDC line protections are traveling wave protection, DC under voltage protection, differential protection, AC-DC wire-touched protection, and metal wire loop protection. Of all the above protections, traveling wave protection is regarded as the primary protection, with the others being used as a backup [61, 62]. The principal protection for HVDC transmission lines is often voltage-derivative protection and traveling-wave-based protection [80,91]. The amounts e and Zi are referred to as characteristics and have a direct impact on the forward and backward propagating waves [1-3]. Traveling wave protection serves as the primary HVDC transmission protection technique, while background protection is provided via derivative and differential protection. A traveling wave is produced at the place of a fault on a DC line to be sufficient along the DC line

and to imitate between converter station equipment.

A. Travelling Wave Theory

The resistances of the line conductor and the insulation brought on by skin and corona effects would deform the shape of waves moving in homogeneous lines [30]. They serve as a reflection of the surge impedance lines that alter current and voltage. Signal processing is a result of the voltage and current's enormous shift. The traveling waves are then created [11,13].

B. Fault in Travelling Wave

Even though the fault deviates from the transmission line, it still generates travelling wave voltage and current that spread throughout the system in the opposite direction. The magnitude of the superimposed voltage and current varies at the discontinuity as a result [23,24]. Traveling wave fault locators are fairly simple to commission because they don't require knowledge of the line or source parameters [12]. To determine the internal and external protection zone, the fault point is calculated [71,75]. Due to electromagnetic coupling, the positive and negative poles can be seen on both ends [73].

C. Direction of Travelling Wave

The immediate polarity of the traveling wave is required to determine the direction of the fault by comparing the travelling wave's direction. When there is a forward fault, the voltage and current traveling wave from the bus bar to the transmission line is going in the opposite direction and has the opposite sign. In a reverse fault, the arriving voltage and current traveling wave's sign is unaltered. The frequency spectrum of traveling waves ranges from 10 to 100 kHz [19].

Models for lossless transmission that take into account the moving wave's direction perform best [84–86]. It examines the angle of zero crossing and discusses single phase losses, describing the constraints and lack of sensitivity [31]. Both faults that detect faults to shut down relay locations and faults that evolve are detected.

Techniques involved in UHVDC

A. Wavelet

Orthogonal at each side and oscillatory that decay the value of zero are the dominant and necessary conditions for wavelets [35–39]. The simplest technique to identify direct local changes in its sign is by this effective method of signal processing [4, 6].Similar to the Fourier transform, the wavelet linear transformation allows for the time localization of different frequency components within a given signal [81, 87].The wavelet packet affects the UHVDC shunt reactors, which conduct current protection [26–29]. They basically divided functions into three categories: phase selection, classification, and discrimination [89,90]. It responds well to medium frequencies while taking the error fault into account for responses in the short time domain [7-9]. Any power level and projects utilizing cables or overhead lines can use it. As a result of the HVDC converter's use of series

capacitors, no switched capacitor banks are needed to compensate for the hybrid system, reducing the size and complexity of the power circuit [20]. The can transmit wave signal information at the proper moment [41, 42].

B. Artificial Neural Network (ANN)

The majority of the time, they are arranged in accordance with input that is multiplied by weights and calculated using an algorithm that takes into account neuron activity [67]. They are practically inspired computer techniques that will lead to significant advancements in the computing field. They calculate the core properties and loss of magnetic transformers, which stabilize the iron loss compression of built transformers [68]. The primary function of ANN is to categorize and distribute various fault kinds [78]. The scenario is reversed when the fault is external to the unit [17,18].

C. FPGA (Field-Programmable Gate Array)

FPGA stands for Field-Programmable Gate Array. It is a type of integrated circuit (IC) that can be programmed or configured after manufacturing to perform a wide range of digital functions. Unlike traditional application-specific integrated circuits (ASICs), which are custom-designed for a specific purpose and cannot be reconfigured, FPGAs offer flexibility and reprogrammability.

Here are some key characteristics and uses of FPGAs:

1. Configurability: FPGAs consist of an array of configurable logic blocks (CLBs) and interconnects that can be programmed to implement custom digital circuits. You can configure an FPGA to perform tasks ranging from simple logical operations to complex digital signal processing.

2. Parallel Processing: FPGAs excel at parallel processing because they can implement multiple functions simultaneously. This makes them suitable for applications like real-time video processing, cryptography, and scientific computing.

3. Rapid Prototyping: FPGAs are often used in the early stages of hardware development to prototype and test digital designs before committing to ASIC fabrication. This allows engineers to iterate quickly and save time and costs.

4. High Performance: FPGAs can offer high performance for specific tasks because their hardware can be optimized for a particular application. This makes them valuable for tasks where performance is critical, such as in aerospace, telecommunications, and high-frequency trading.

5. Reconfigurability: FPGAs can be reprogrammed as needed, making them adaptable to changing requirements and allowing for upgrades without replacing hardware.

6. Hardware Acceleration: FPGAs are commonly used to accelerate specific functions in computing systems. For example, they can accelerate machine learning inference, database operations, and encryption/decryption.

7. Signal Processing: FPGAs are well-suited for digital signal processing (DSP) applications, such as audio and

video processing, radar, and wireless communications.

8. Low-Power Options: Some FPGAs are designed for low-power applications, making them suitable for battery-powered devices and IoT (Internet of Things) applications.

To program or configure an FPGA, developers use hardware description languages (HDLs) like Verilog or VHDL, or high-level synthesis tools that can generate FPGA configurations from high-level code. Once programmed, the FPGA functions as a custom digital circuit.

Overall, FPGAs are a versatile tool in the world of digital hardware design and offer a balance between the flexibility of software and the performance of dedicated hardware. They are used in various industries and applications where customization and rapid development are essential.

D. Lighting Unit

Lightning can cause non-fault transients but not back-flashover when it strikes a line or a tower. It is sufficient to distinguish between faults and non-faults. The input is frequently added at the fault location by the dc line fault. Non-fault lightning, in addition to lightning injection, frequently occurs close to steady state.

Table I. Contributions and Techniques in UHVDC

Techniques	**Contribution**
1.WAVELET	A wavelet coefficient-based method is described for distinguishing between load change and fault scenario using a DC line. (2016).
2.ANN	minimizing voltage deviation while coordinating the voltage control system (2014).
3.FPGA	This approach is used to evaluate the effectiveness of cost-effective hardware and real-time protection schemes (2011).
4.FUZZY	This technique is used to locate ground faults that are either simple line-to-ground faults or line-to-line faults, which are the most challenging to locate using the standard deterministic methodology (1995).
5.EMTP	a novel method of investigation of the modally decomposable transmission line model.
6.S–transform	It is employed to extract temporary intelligence from faults.Under various circumstances, the projected algorithm performs satisfactorily (2010).
7.SCADA	This concept of hybrid online networking modeling using CIM technology on a live SCADA system was proposed in 2009.

The techniques and contributions in UHVDC are shown in table 1. For each technique, a contribution is included along with the year. These contributions include lengthy transmission,

reduced losses, and increased power transmission capability.

Conclusion

Transmission with UHVDC is crucial for long transmission distances and high capacity. This essay examines the system for protecting the electrical grid. As a result, this study also featured a discussion of UHVDC transmission, including its benefits, as well as transmission-related techniques including ANN, wavelets, HIL, lightning stroke, and boundary units.

References

[1] K. Snelson, “Propagation of Travelling Waves on Transmission Lines- Frequency Dependent Parameters,” International journal of Hydro- Electric Power Commission of Ontario, Vol.91, Issue.1, pp.85-91, May 1971.

[2] A. Semlyen and A. Dabuleanu, “Fast and Accurate Switching Transient Calculations on Transmission Lines with Ground Return Using Recursive Convolutions,” International journal of IEEETransactions on Power Apparatus and System, Vol.94, No.2, pp.561-571, April 1975.

[3] G. Bianchi, G.Luoni and A.Morello, "High Voltage DC Cable for Bulk Power Transmission,” International journal of IEEE Transactions on Power Apparatus and Systems, Vol.99, No.6, pp.2311-2317,December 1980.

[4] J.R.Marti, “Accurate Modelling of Frequency-Dependent Transmission Lines in Electromagnetic Transient Simulations,” International journal of IEEE Transactions on Power Apparatus and Systems, Vol.101, No. 1,pp.147-157,January 1982.

[5] Alessandro Ferrero, Silvia Sangiovanni and Ennio Zappitell,“A Fuzzy- Seat Approach Fault-Typed Notification in Digital Relaying,” International journal of IEEE Transactions on Power Delivery, Vol.10, No. 1, pp.169-175, January 1995.

[6] R.Yacamini and J.W. Resende,“High-Voltage DC Transmission,” International journal of IEE Proc, Gener. Transm, Distrib, Vol. 143, No. 1, pp.66-74, January 1996.

[7] Christian Dufour and Hoang Le-Huy, “Highly Accurate Modeling of Frequency-Dependent Balanced Transmission Lines”, International journal of IEEE Transactions on Power Delivery, Vol. 15, No. 2, pp.610-615, April 2000.

[8] L.J.Xiao and L.Zhang, “Harmonic Cancellation for HVDC Systems using a Notch-Filter Controlled Active DC Filter,” International conference on IEEE Proc, International conference on Gener, transm,distrib., Vol.147, No.3,pp.176-179 ,March 2000.

[9] L. Shang, G. Herold, J. Jaeger, R. Krebs, and A. Kumar,“Analysis and Identification of HVDC System Faults using Wavelet Modulus Maxima,” International Conference on AC-DC Power Transmission, London, UK, Nov 2001

[10] L. Shang, G. Herold, J. Jaeger, R. Krebs, and A.Kumar, "High-Speed Fault Identification and Protection for HVDC Line Using Wavelet Technique," International conference on IEEE Porto Power Tech Conference, Porto, Portugal September 2001.

[11] P.F.Gale, P.V.Taylor, P.Naidoo, C.Hitchin and D.Clowes, "Travelling Wave Fault Locator Experience On Eskom S Transmission Network," International conference on Developments in Power System Protection, Amsterdam, Netherlands, May 2001.

[12] Ha Hengxu and Zhang Baohui, "Study on Identification of Fault and Lightening Strokes in Boundary Protection for EHV Transmission Lines," International Conference on Power System Technology Kunming, China 2002.

[13] John O'reilly, Alan R. Wood, and Chris M. Osauskas, "FrequencyDomain Based Control Design for an HVDC Converter Connected to aWeak AC Network", International journal of IEEE Transactions on [32] S. Mishr, C. N. Bhende, and B. K. Panigrahi, "Detection andPower Delivery, Vol. 18, No. 3, pp.1028-1033, July 2003.

[14] Wei Chen, O. P. Malik, Xianggen Yin, Deshu Chen, and Zhe Zhang,Classification of Power," International journal of IEEE Transactions on Power Delivery, Vol. 23, No. 1, pp.280-287, January 2008."Study of wavelet-Based Ultra High Speed Directional Transmission

[15] Dipankar Chanda, N. K. Kishore,Avinash and K. Sinha, "A WaveletTransmission Line Voltage Traveling Wave Protection Based on Wavelet Transform," International Conference on High Voltage Engineering and Application, Chongqing, China, November 2008.bMultiresolution-Based Analysis for Location of the Point of Strike of a

[16] A Halinka and M Szewczyk, "Ann Based Detection of Electrical Faults

[17] Yu-PingLu, L.L. Lal and Guo-Qing Tang, "Neural Network Based Generator-Transformer Protection," Third International Conference on Machine Learning and Cybernetics, Shanghai, August 2004.

[18] D.Naidoo and N.M. Ijumba, "HVDC Line Protection for the Proposed HVDC Systems,"International Conference on Power System Technology, Singapore, November 2004."Transmission Expansion Planning in Electricity Markets," International journal of IEEE Transactions on Power Systems, Vol. 23, No.1, pp.238-248, February 2008.

[19] Bjarne R. Andersen andLie Xu, "Hybrid HVDC System for Power

[20] Tomasz Tarasiuk, "Hybrid Wavelet-Fourier Spectrum Analysis,"

[21] D. Naidoo and N.M. Ijumba," A Protection System For Long HVDC Transmission Lines," International Conference on Inaugural IEEE, Conference and Exposition in Africa Durban, South Africa,April 2005.

[22] Guobing Song, JialeSuonan, Qingqiang Xu, Ping Chen, and Yaozhong Ge, "Parallel Transmission Lines Fault Location Algorithm Based on Differential Component Net," International journal of IEEEWave/Boundary Protection for Monopolar HVDC Line Quality Disturbances Using S-Transform and Probabilistic Neural Network," International journal of IEEE Transactions on Power Delivery, Vol. 24, No. 2, pp.569-578, April 2009.

[23] Xu Wenhao, Liao Zhiwei, Huang Shaoxian and Wang Gang, "A Model of HVDC Control System Based on Hybrid Petri Net," International conference on IEEE Transmission and Distribution Conference &

Exhibition: Asia and Pacific Dalian, China,March 2005

[24] D. Naidoo and N.M. Ijumba, “A Protection System for Long HVDC Transmission Lines,”International conference on Inaugural IEEE Conference vand Exposition in an Africa Durbun, South Africa,july 2005.

[25] Peter Riedel, “Harmonic Voltage and Current Transfer, and AC- and DC-Side Impedances of HVDC Converters,” International journal of IEEE Transactions on Power Delivery, Vol. 20, No. 3, pp. 2095- 2099, July 2005.

[26] U Astrom, L. Weimers, V. Lescale and G. Aspl “Power Transmission with HVDC at Voltages Above 600 KV,” International conference on IEEE Transmission and Distribution. Conference & Exhibition: Asia and Pacific, Dalian, China, July 2005.

[27] Xu Yan, Liu Haof and Wang Zengping, “Research on the Application of Wave packet Decompostion Based Non-Unit Protection on The EHV Lines with Shunt Reactors,” International Conference on Power System Technology, Chongqing, China, Oct 2006.

[28] M. O. FaruqueYuyan Zhang, and Venkata Dinavahi, “Detailed Modeling of Cigré HVDC Benchmark System Using PSCAD/EMTDC and PSB/Simulink,” International journal of IEEE Transactions on Power Delivery, Vol. 21, No. 1, pp.378-387, January 2006.

[29] Ernesto Vázquez, Jorge Castruita, Oscar L. Chacón, and Arturo Conde, “A New Approach Traveling-Wave Distance Protection—Part I: Algorithm,” International journal of IEEE Transactions on Power Delivery, Vol. 22, No. 2, pp.795-800, April 2007.

[30] Carlos Aguilera, Eduardo Orduña, and Giuseppe Rattá, “Directional Traveling-Wave Protection Based on Slope Change Analysis,” International journal of IEEE Transactions on Power Delivery, Vol. 22, No. 4, pp. 2025- 2033, October 2007.

[31] Willis Long and Stig Nilsson “HVDC Transmission Yesterday and Today,” International journal of IEEE Power and Energy Magazine,Vol. 5, Issue 2, pp.22-31, April, 2007.Zeming Yang, “Study on The Dynamic Performance Characteristics of HVDC Control and Protections for The HVDC Line Fault,” International conference on EHV Power Transmission Company of China Southern Grid, Xingy, March 2009.

[33] Li Zhen -Qiang and Lv Yan-Ping, “A Novel Scheme of HVDCLine Protection,” International journal of IEEE Transactions on PowerDelivery, Vol. 18, No. 4, pp.1134-1139, October 2003.

[34] Rashmi A.Keswani, “Identification Of Fault in HVDC ConvertersLightning Overvoltage on a Transmission Line,” International journal ofIEEE Transactions on Power Delivery, Vol. 19, No. 4, pp.1727-1733, October 2004.Using Wavelet Based Multi-ResolutionAnalysis,” First International Conference on Emerging Trends in Engineering and Technology, Nagpur, Maharashtra, India, July 2008.

[35] Sebastián De La Torre, Antonio J. Conejo, and Javier Contreras, in Generator-Transformer Units,” International conference onDevelopments in Power System ProtectionAmsterdam, Netherlands,April 2004

[36] P. Naidoo and N.M. Ijumba, “A Novel Approach to Providing on Route Power Supplies to Rural and UrbanCommunities in Close Proximity to the Extra High Voltage DC Transmission Line,” International conference on Power and Energy Society General Meeting - Conversion and Delivery of Electrical Energy in the 21st Century, Pittsburgh, PA, USA, July 2008.

[37] Xinzhou Dong, Wei Kong, and Tao Cui,” Fault Classification andTransmission to Island Networks,”

International journal of IEEE Transactions on Power Delivery, Vol. 19, No.4, pp.1884-1890, October 2004.Faulted-Phase Selection Based on The Initial Current Traveling Wave," International journal of IEEE Transactions on Power Delivery, Vol. 24, No. 2, pp. 552-559, April 2009.

[38]Xiaolei Liu, A. H. Osman, and O. P. Malik, "Hybrid TravelingInternational journal of IEEE Transactions on Power Delivery, Vol. 19, No. 3, pp.957-964, July 2004.

[39] You Min, Zhang Bao-Hui and Bo Zhi-Qian, "Study of Non-Unit Transient-Based Protection for HVDC Transmission Lines," International conference on Power and Energy Engineering, Wuhan, China, March 2009.Transactions on Power Delivery, Vol. 20, No. 4, pp.2396-2406, [40] Aimin Li, Zexiang Cai, Qizhen Sun, Xiaohua Li, DayongRen andOctober 2005.

[41] Cailiang Gao, Zhiwei Liao, Shaoxian Huang, "Fault Diagnosis of Commutation Failures in The HVDC System Based on Wavelet Singular Value and Support Vector Machine," International conference on Power and Energy Engineering, Wuhan, China,November 2009.

[42] Xiaolei Liu, A.H. Osman, and O.P. Malik, "Hybrid Traveling Wave/Boundary Protection for Bipolar HVDC Line," International conference on Power & Energy Society General Meeting,Calgary,Canada ,April 2009.

[43] Antonis Paramania and Goran Andersson, "Coordinated Expansion Planning Based on a Cost Benefit Analysis," International conference on the European Energy Market Leuven, Belgium, January 2009.

[44] S. P. Teeuwsen, C. Rasmussen and H. Abildgaard, "Dynamic Performance of The New 400 KV Storebaelt HVDC Project," International conference on Power Systems Conference and Exposition, Seattle, WA, USA, March, 2009.

[45] K. Nakayama, G. Fujita and R. Yokoyama, "Load Frequency Control for Utility Interaction of Wide-Area Power System Interconnection," International conference on Transmission & Distribution Conference &Exposition , Seoul, South Korea, October 2009.

[46] U. Astrom, V. F. Lescale, D. Menzies, Ma Weimin and Liu Zehong," The Xiangjiaba-Shanghai 800 Kv UHVDC Project, Status and Special Aspects,"International Conference on Power System Technology, Hangzhou, China,October 2010.

[47] PeymaJafarian and Majid Sanaye-Pasand, "A Traveling-Wave- Based Protection Technique Using Wavelet/PCA Analysis," International journal of IEEE Transactions on Power Delivery, Vol. 25, No. 2, pp.588-599, April 2010.

[48] JialeSuonan, Shuping Gao, Guobing Song, ZaibinJiao,andXiaoning

Kang, "A Novel Fault-Location Method for HVDC TransmissionLines,"International journal of IEEE Transactions on PowerDelivery,Vol. 25,No.2,pp.1203-1209, April 2010.

[49] S. Zhang, B. H. Zhang, M. You, and Z. Q. Bo,"Realization of The Transient-Based Boundary Protection for HVDC Transmission Lines Based on High Frequency Energy Criteria,"International Conference on Power System Technology, March 2010.

[50] VahidMadani, DamirNovosel, Stan Horowitz, Mark Adamiak, Javier Amantegui, Daniel Karlsson, Shinichi Imai, and Alexander Apostolov, "IEEE PSRC Report on Global Industry Experience, with System Integrity Protection Schemes (Sips)," International journal of IEEE Transactions on Power Delivery, Vol. 25,

No.4, pp.2143-2155, October 2010.

[51] S.P. Teeuwsen and R. Rösse, "Dynamic Performance of the 1000 MW Britned HVDC Interconnector Project," International conference on Power and Energy Society General MeetingProvidence, RI, USA,July 2010.

[52] K. De Kerf, K. Srivastava,M. Reza, D. Bekaer, S. Cole, D. Van Hertem and R. Belmans, "Wavelet-Based Protection Strategy For DC Faults in Multi-Terminal VSC HVDC Systems," International journal of IET Generation, Transmission & Distribution, Vol. 5, Issue. 4, pp. 496–503, January 2011.

[53] Xiaolei Liu, Ahmed H. Osman, and Om P. Malik, "Real-Time Implementation of a Hybrid Protection Scheme for Bipolar HVDC Line using FPGA," International journal of IEEE Transactions on Power Delivery, Vol. 26, No. 1, January 2011.

[54] Ying Zhang, NenglingTai and Bin Xu, "Fault Analysis and Traveling-Wave Protection Scheme for Bipolar HVDC Lines," International journal of IEEE Transactions on Power Delivery, Vol. 27, No. 3, pp.1583-1591, July 2012.

[55] Til Kristian Vrana, Daniel Huertas-Hernando, and Olav BjarteFosso,"Benefits of Asymmetric HVDC Links for Large Scale Offshore Wind Integration,"International conference on Power and Energy Society General Meeting, San Diego, CA, USA, July 2012.

[56] Zheng Xiao-Dong, Taineng-Ling, James S. Thorp, and Yang Guang-Liang, "A Transient Harmonic Current Protection Scheme for HVDC Transmission Line," International journal of IEEE Transactions on Power Delivery, Vol. 27, No. 4, pp.2278-2285, October 2012.

[57] Nikolas Flourentzou, and Vassilios G. Agelidis, "Multimodule HVDC System Using She-PWM with DC Capacitor Voltage Equalization," International journal of IEEE Transactions on Power Delivery, Vol. 27, No. 1, pp.79-86, January 2012.

[58] Kezhen Liu, JilaiYu,Hongchun Shu and Zhiyu Chen, "Study On Electrical Transient Protection For ±800kv UHVDC Transmission Lines," International conference on Power and Energy Engineering ConferenceShanghai, China, March 2012.

[59] Rajat Majumder, Carsten Bartzsch and Peter Kohnstam "High- Voltage Dc on the New Power Transmission Highway," International journal of IEEE Power and Energy Magazine,Vol.10, Issue.6,pp.39-49,December 2012.

[60] Therese Uzochukwuamaka Okeke and RamyGeorgiousZaher, "Flexible AC Transmission Systems (Facts)," International Conference onNew Concepts in Smart Cities: Fostering Public and Private Alliances, Gijon, Spain December 2013.

[61] JialeSuonan, Jiankang Zhang, Zaibin Jiao, Liming Yang, And Guobing Song, "Distance Protection for HVDC Transmission Lines Considering Frequency-Dependent Parameters," International journal of IEEE Transactions on Power Delivery, Vol. 28, No. 2, pp.723-732, April 2013.

[62] JialeSuonan, Jiankang Zhang, Zaibin Jia, Liming Yang, And Guobing Song, "Distance Protection for HVDC Transmission Lines Considering Frequency-Dependent Parameters," International journal of Transactions on Power Delivery, Vol. 28, No. 2, pp.29-34, April 2013.

[63] Anders Bergman, Johann Meisner, and Stefan Svensson,"Enabling DC-Side Metering in HVDC

Stations," International journal of IEEE Transactions on Power Delivery, Vol 29, No.1, pp.370-377,February 2014.

[64] Reena R. Moon andR.K. Dhatrak, "Extraction of Features to

Discriminate and Detect Transformer Inrush Current and FaultyCondition using ANN," International Conference on Magnetics,Machines & Drives, Kottayam, India, July 2014.

[65] Ms. Sonali, B. Maind and Ms. Priyanka Wankar , " Research Paper on Basic of Artificial Neural Network,"International Journal on Recent and Innovation Trends in Computing and Communication ,Vol. 2 Issue.1,pp.96-100,January 2014.

[66] Zhong Chen, Zhihui Wang and Mengnan Li, "A Hybird Cascade H- Bridge Seven-Level Converter for Active Power Filter,"International conference on Industrial Electronics Society, Dallas, TX, USA ,Nov 2014.

[67] Oluwole D. Adeuyi, Marc Cheah-Mane and Yanan Wu, "Frequency Support from Modular Multilevel Converter Based Multi-Terminal HVDC Schemes," International conference on Power & Energy Society, Denver, CO, USA, July 2015.

[68] FirouzBadrkhaniAjaei and Reza Iravani,Cable Surge Arrester Operation Due to Transient Over Voltages Under DC-Side Faults in the MM-HVDC Link," International Journal on IEEE Transactions on Power Delivery, Vol. 31, Issue.3, pp.1213-1222, June 2016.

[69] H. D. Mehta and Rajesh M. Patel, "A Review on Transformer Design Optimization and Performance Analysis using Artificial Intelligence Techniques," International Journal of Science and Research, Vol.3, Issue. 9, pp.726-733, September 2014.

[70] Zhao Li, Guibin Zou, Bingbing Tong, Houlei Gao and Qian Feng, "Novel Traveling Wave Protection Method for Hig h Voltage DC Transmission Line," International conference on Power & Energy Society General MeetingDenver, CO, USA, July 2015,

[71] Sherin Tom, Jaimol Thomas and Ganesh M,"A Novel Algorithm for Fault Location and Identification in HVDC Transmission Lines Based on Transients," International Conference on Emerging Research in Electronics, Computer Science, and Technology,Mandya, India,Dec 2015.

[72] Pu Zhao, Qing Chen, Luhua Xing, "DC Fault Analysis of VSC- HVDC and DC Cable Protection Principle," International conference on Power and Energy Engineering Conference, Brisbane, QLD, Australia, November 2015.

[73] Ahmed R. Adly1, Ragab A. El Sehiemy, Almoataz Youssef Abdelaziz, Nabil M.A. Ayad1, "Critical Aspects on Wavelet Transforms Based Fault Identification Procedures in HVDC Transmission Line,"International journal of IET Gener. Transm. Distrib., Vol.10, Issue. 2, pp. 508-517 2015.

[74] S. Sumathi and Bansilal,"Artificial Neural Network for Coordinated Control of Statcom, Generator Excitation and Tap Changing Transformer," International journal of Electrical Power and Energy Systems,Vol.64,pp.536–541 2015.

[75] Sul Ademi, DimitriosTzelepis, Adam Dy´Sko, Sankara Subramanian and HengxuHa,"Fault Current Characterisation in VSC-Based HVDC Systems," International Conference onDevelopment in Power System Protection, Edinburgh, UK,March 2016.

[76] Song, Zhibin Ma and XingfuJin, “Novel Pilot Protection Principle for High-Voltage Direct Current Transmission Lines Based on Fault Component Current Characteristics,” International journal of IET Generation, Transmission &Distribution,Vol. 9, Issue.5,pp.468- 474,April 2015.

[77] Jian Liu, Nengling Tai, Chunju Fan and WentaoHuang,“Protection Scheme for High-Voltage Direct current Transmission Lines Based on Transient AC Current,” International Journal of Emerging and Selected Topics in Power Electronics International journal of IET Gener,Transm,Distrib.,Vol.9,Issue.16,pp.2633-2643,July 2015.

[78] Jing Lyu, Xu Cai, and Marta Molinas, “Frequency Domain Stability Analysis of MMC-Based HVDC For Wind Farm Integration,”International journal of Emerging and Selected Topics in Power Electronics,vol.4, Issue.1,pp.141-151, March 2016 .

[79] Nagesh Geddada, Yew Ming Yea and AbhisekUkil, “Fault and Load Change Differentiation in High Voltage Direct Current (HVDC) System,” International Conference onPower Electronics, Drives and Energy Systems , Trivandrum, India,December 2016

[80] Peter Mohaupt andPeter Derks, “Challenges in High Voltage and Ultra High Voltage AC and DC Field Testing,” International Conference onReliability Of Transmission And Distribution Networks,London,UK,November 2016.

[81] Ashwini.K, Khairnar and Dr.P.J.Shah,“Study of Various Types of Faults in HVDC Transmission System,” International Conference onGlobal Trends in Signal Processing, Information Computing and Communication, Jalgaon, December 2016.

[82] Lei Wang, Qing Chen and Chuanxin Xi, “Study on the Traveling Wave Differential Protection and the Improvement Scheme for VSC- HVDC Transmission Lines,” International Conference onPower and Energy Engineering,Xi'an, China December 2016.

[83] Tian Wu, Bin Xiao, Kai Liu, Ting Liu, Yong Peng, Ziming Su, Pan Tang and Xinglie Lei,” Study on Overhead Transmission Line Magnetic Field Harmonics of VSC-HVDC,” International Conference onHigh Voltage Engineering and Application ,Chengdu, China, September 2016.

[84] Jenny ZhengZhou, Aniruddha and M. Gole, “Rationalisation and Validation of DC Power Transfer Limits for Voltage Sourced Converter Based High Voltage DC Transmission,” International journal of IET Gener., Transm., Distrib., Vol.10,Issue.6,pp.1327- 1335,May 2016.

[85] Y.ManjuSree, G.Ravi Kumar, M.Vaidehi and G.VamsiPriya, “Wavelet Approach for Transient Current Based Multi Terminal Transmission System Protection Scheme in the Presence of SVC,” International Conference on Electrical, Electronics and Optimization Techniques, Chennai, India, March 2016.

[86] Fei Kong, Zhiguo Hao, and Baohui Zhang, “A Novel Traveling Wave Based Main Protection Scheme for ±800 KV UHVDC Bipolar Transmission Lines,” International journal of IEEE Transactions on Power Delivery, Vol. 31, Issue.5,pp.2159-2168, May 2016.

[87] Swathi S B and Nisha G Poothullil, “Analysis of Active Power Control of HVDC in Damping Power Oscillations,” International Conference on Next Generation Intelligent Systems, Kottayam, India, September 2016.

[88] Karthi, R. Radhakrishnan, Jm. Baskaran and Louis Sam Titus, “Performance Analysis on Various

Controllers of VSC - HVDC Transmission Systems," International Conference onComputational Intelligence and Computing Research, Chennai, India,December 2016.

[89] Jian Liu,Nenglng Tai and Chunju Fan, "Transient Voltage Based Protection Scheme for DC Line Fault in Multi Terminal VSC-HVDC System," International journal of IEEE Transactions on Power Delivery,Vol.32, Issue.3, pp.1483 - 1494,September 2016.

[90] Yu Ze, Wen Jun, Wang Ling, Kong Weibo and Zhao Xiaobin, "The Study on Advanced Three-Pulse Harmonic Model of Twelve-Pulse Converter," International Conference on Power and Renewable Energy, Shanghai, China, October 2016.

[91] H. Huang and V. Ramaswami, "Design of UHVDC Converter Station," International conference on Transmission and Distribution Conference and Exhibition,Dalian, China, August 2005.

[92] FatihÜnal and Sami Ekici, "A Fault Location Technique for HVDC Transmission Lines Using Extreme Learning Machines," International conference on smart Grid and Cities Congress and Fair, Istanbul, Turkey,April 2017.

Chapter 22

Ensemble Security Predictor based Power System Dynamic Security State Predictor

Rituparna Mukherjee* , Susmita Dhar Mukherjee , Avik Datta, Rituparna Mitra
Department of Electrical Engineering, Swami Vivekananda University, Barrackpore, North 24 Parganas, Kolkata – 700121,West Bengal, India.

Corresponding Author Email: rituparnamukherjee@svu.ac.in

Abstract

Real-time assessment and prediction of dynamic security is critical in power system operation and control. Analysis of the current operational condition and forecast of possible future vulnerability is critical for real-time decision-making and implementation of appropriate operation and control measures to ensure the secure running of bulk power systems. Online security evaluation necessitates a minimal level of complexity and computational time. Because of their high processing complexity and extended analysis time, existing approaches for assessing dynamic security of electric power networks are insufficient for online and real-time situations. The implementation of pattern recognition and machine learning technologies to map the underlying relationship between system operating conditions and the dynamic security status of the system can, however, provide an effective solution to this problem. This paper proposes an advanced pattern recognition approach to dynamic security analysis of large and complex power systems based on ensemble decision tree, a recently introduced pattern recognition tool capable of forming reliable decision rules for fast and accurate prediction of power system operating states in a real-time and on-line environment, even when applied to very large systems. An Ensemble Security Predictor (ENSP) has been designed and trained to operate as a 'dynamic security state predictor', predicting and classifying the operating states of a power system into secure, insecure, and intermediate transitional classes. When implemented in an IEEE 118-bus standard system, the created ENSP outperformed other analogous classifiers such as the method of least squares (MLS), neural network (NN), vector quantization (VQ), and support vector machine (SVM).

Keywords: Power system transient stability, dynamic security, pattern recognition, classification, prediction, feature extraction, feature selection, ensemble decision tree.

Introduction

Secure operation of large interconnected electric power systems is arguably the biggest challenge against maintenance of uninterrupted supply of electricity to consumers. Power systems recurrently experience disturbances like outage of generating units and other power supply equipment (contingencies), short-circuits in power transmission lines (faults) and combination of these events, which have the potential to alter the

configuration of a power system and sometimes, also to change the operating state of the power system. Security refers to the 'degree of risk' that a power system poses in surviving against likely occurrence of these disturbances without major interruption in power supply to consumers, at any point of time. Security analysis is therefore imperative to assess, how robust a system is, relative to large variety of severe, yet plausible disturbances [1]. Power system security studies can be broadly categorized as: static security analysis (SSA) and dynamic security analysis (DSA). Since, change in operating condition (state) is imminent after any major contingency, it is important that the system finally settles to a new state of operation, which is stable. In SSA, transition to new stable operating state is presumably accomplished and the analysis is only focused on assessment of whether any physical and/or security constraints were violated in the post-contingency steady-state operating condition [2]. However, a quick shift to a new steady-state operating point in the event of a significant disturbance is impractical. As a result, the system may operate in a quasi-stable state for an extended period of time, which may cause relays and other system isolation and protection mechanisms to operate unintentionally. This frequently causes cascaded tripping and system outages, which ultimately jeopardize the security of the system. The size and complexity of modern power grids, as well as the continual operation of power supply equipment at or near its capacity limits as a result of power market competition, have all contributed to an increase in the danger of insecurity. For modern power systems, both the change in operating state and the intermediate quasi-stable operational phase itself are of relevance, dynamic security analysis [3], [4] has consequently become crucial. One of the most precise techniques for dynamic security analysis under significant shocks (transient stability) is nonlinear time domain simulation (TDS) [5]. A set of nonlinear time-domain differential/algebraic equations must be used to mathematically model a power system in order to capture the dynamic behavior of the generators and other power system components. The dynamic behavior of a system is then evaluated under plausible sets of disturbances, and it is determined if transient stability would be preserved or lost for each disturbance by solving these equations using numerical integration methods. The main complaint against TDS is that it necessitates lengthy numerical integrations that are resource- and time-intensive, making it unsuitable for online applications [6]. TDS's inability to evaluate relative stability is another flaw [7].The direct method is an alternative approach to transient stability analysis that uses the transient energy function [8] to determine the stability of a power system's post-contingency operating point. The direct method is less computationally demanding than the numerical integration approach, but it does not achieve the same level of accuracy because it normally uses reduced order modeling of the post-contingency system, making it impractical for large-scale power systems. A review of existing methods for assessing the dynamic security of electric power networks finds that none of these standard approaches can be effectively implemented in online and real-time situations due to their computational complexity. The problem's complexity is exacerbated by the fact that most critical pre-emergency states of the electric power system, which can potentially lead to large-scale blackouts, are unique, and there is no single algorithm that can effectively reveal such conditions in real-time security assessment. As a result, there is an urgent need to establish a quick and dependable approach for real-time security monitoring and assessment of large power systems' present security level. Some pioneering research works from the late 1980s [9, 10] demonstrated that an effective solution to this problem can be found by using artificial intelligence (AI) and machine learning approaches. AI techniques, as well as machine learning and data mining approaches, have been tried to develop'very fast' and 'intelligent' DSA systems [11], [12], with promising results. This was attributed to their general skill of fast detection of 'patterns' and ability to 'learn from examples,' which are unique abilities that may be efficiently used to recognise the current working state of a power system. These AI techniques attempt to map the intrinsic link between system operating conditions (input) and the system's dynamic security state (output). They can thus identify and trace.

This work uses the ensemble method of classification to present an advanced AI-based solution to security

analysis of big and complex power systems [13]. Even when applied to very large systems, the ensemble technique may develop solid decision rules for fast and accurate prediction of power system operating states in real-time and on-line environments. The single most important goal of using pattern recognition methods was to reduce the computing overhead to a bare minimum so that it could be used online. The underlying offline analysis, on the other hand, was made as comprehensive as feasible by training the pattern classifier off-line using findings from the most painstaking and accurate computations. As a result, a well-trained classifier should be capable of obtaining accuracy comparable to that produced by. To put it simply, the task of pattern recognition entails creating a pattern vector V, the elements of which contain adequate and accurate information about the stability of the power system, allowing a predictor to determine the system stability solely based on V in the event of an emergency. The power system's pre-contingency operational points are then all evaluated using this vector in order to produce a comprehensive training data set.

The Concept of Ensemble Decision Tree Based Dynamic Security State Prediction and Classification

The goal of developing a security predictor is to anticipate and categorise the operational circumstances of a power system prior to a contingency by evaluating its ability to temporarily destabilise the system in the case of credible contingencies and outages. An Ensemble Security Predictor (ENSP) has been trained to function as a dynamic security classifier for this purpose. It is possible for the proposed ENSP to categorise the dynamic states of a system into secure, insecure, or even some intermediate transitional classes by presenting it with any given pre-contingency operational condition. A secure class is made up of all pre-contingency operational states of a power system where there is "zero" chance that critical line faults, which could lead to instability, could exist. On the other hand, an insecure class refers to pre-contingency operating states that feature one or more "critical line faults" that have the potential to lead to instability. Therefore, it is necessary to establish a "critical line fault" for this purpose. A 3-phase line fault or, in some cases, any other asymmetrical fault that could cause transitory instability in at least one of the system's generators is known as a critical line fault. A reliable and thorough parameter to evaluate the criticality of a line fault is the critical clearance time (tcr) associated with the fault. More specifically, it can be used as a gauge of the line's vulnerability (criticality) following the occurrence of the fault [14], [15]. If the fault is not fixed within tcr, instability (i.e., one or more machines becoming unstable) is likely for each fault. As a result, each defect must have its own unique critical energy (Vcr), which must be determined in order to compute the tcr. Because Vcr differs for each failure, figuring it out can be time-consuming and difficult computationally. Off-line determination of Vcr and subsequent computation of tcr were performed using the Potential Energy Boundary Surface (PEBS) approach [16].

The next step is to classify each line according to whether or not its tcr is smaller than the minimum fault clearing time that can be achieved after the values of tcr for each line have been computed offline. Since such high-speed fault clearance is rarely possible, every tcr 80mS (about 4 cycles for a 50 Hz system) has been regarded as extremely essential. Since it is simple to produce an 8-cycle fault clearing time, the tcr of 160 mS has been deemed non-critical. Therefore, it is possible to think of the 80 mS to 160 mS (48 cycles in a 50 Hz system) range as the transitional or intermediate range for dynamic security.

Offline training is required for the proposed ENSP in order to teach them how to relate pre-emergency operating circumstances to post-emergency criticality (insecurity). The proposed ENSP can successfully be used to identify any credible pre-contingency operating condition of a power system (including unanticipated operating conditions) in an online environment and predict the likelihood that the condition would result in future post-contingency dynamic insecurity.

Ensemble Decision Tree Predictor model

Ensemble Decision Tree (DT) is a collaborative assembly of individual decision trees, where each single tree structure is built on classification or regression models [17]. A decision tree may be perceived as a method of dissecting data sets into more minute subsets with increase in the depth of a hypothetical tree. A tree usually comprises of 'decision nodes' and 'leaf nodes' where numerous branches may fall on each decision node. A classification or decision is represented by a leaf node. The node corresponding to the best predictor is termed as the root node. A single decision tree can however rarely generalize the data it was not trained on. Combining the predictions of large number of decision trees however result very accurate predictions. Such method of combining individual decision trees is known as an 'ensemble method'. Mathematically speaking, a decision tree has low bias and high variance. Ensemble of many decision trees reduces the variance while maintaining the same low bias. The ensemble approach can therefore be viewed as an extension of the bagging idea [18].

Bagging tries to implement parallel learning of similar learners on small sample populations and then takes a mean of all the predictions. A collective decision is finally obtained by using an elementary 'committee' method which classifies an object according to the decision of most of the base learners. One of the progressive bagging-based approaches is the method called Random Forest [19]. 'Boosting' is another popular technique [20] for improving the accuracy of a predictor by applying the prediction repeatedly in a series and then combining the weighted output of each predictor, so that the total error of the prediction is minimized. In many cases, the prediction accuracy of such a series greatly exceeds the accuracy of the base predictor used alone. The Tree Boost algorithm [21] is used for improving the accuracy of models built on decision trees. Research [22] has shown that models built using Tree Boost are among the most accurate of any known decision tree models. The Tree Boost algorithm is functionally similar to 'Decision Tree Forests' [23] because it creates a tree ensemble, and it uses randomization during the tree creations. However, a random forest builds the trees in parallel and they 'vote' on the prediction, whereas Tree Boost creates a series of trees, and the prediction receives incremental improvement by each tree in the series.

Off-Line Simulation of The TEST SYSTEM

The IEEE 118-bus benchmark system, representing the American Electric Power (AEP) system in the U.S. Midwest as of December 1962 was chosen as an appropriate case for all off-line studies, considering its large dimension and topological spread, as well as intricacy. The IEEE 118-bus system contains 54 generators including 35 synchronous condensers, 186 lines, 9 transformers and 91 load buses. A schematic single line diagram of the system is presented in the Appendix-I.

Simulation of Pre-Contingency Operating Conditions for Training the ENSP

The success of the ENSP largely depends on adequacy of training, both in terms of 'quality' as well as 'quantity' of training exemplars. 'Quality' refers to consideration of diverse and well dispersed pre-contingency operating points. These operating points must effectively represent the whole operating space of power system, keeping in mid the fact that the machine learning approaches are usually more efficient in interpolation rather than extrapolation of data. 'Quantity' on the other hand refers to the total number of observations or number of samples used for training, where each observed sample corresponds to a unique pre-contingency operating condition. Though, there is no guideline regarding how many observations should be considered 'adequate' for a given problem, the rule of thumb is to start with sample size, at least 10 times the number of features present in the data, and update the sample size incrementally, if the training accuracy is not

up to the expectation.

Creation of large number of diverse and well dispersed pre-contingency steady-state operating points was achieved by multiple load-flow simulations in the IEEE 118-bus test system with variable initial starting conditions such as generation and load variations, as well as with changed network topologies like generator and line outages and their combinations. With the objective to simulate the most practical operating scenarios, simultaneous load variations were considered in about 14% of the total number of system load buses at a time. Out of the total 91 load buses, any arbitrary 13 buses were randomly selected at a time as candidates for load variation in 5 steps (0.5, 0.75, 1.0, 1.25 & 1.5 p.u. of the base load of the buses). The process was then repeated for the next 13 arbitrary buses (but not common with any of the previously selected buses) and so on, until all the system buses were covered (that is a total of 7 times). This generated 5×7=35 distinct, well dispersed and yet highly probable loading (and corresponding generation) scenarios. Each of the above 35 loading conditions were them combined with single-generator outage conditions. Considering 54 number generators in the IEEE 118 bus system, and 'no generator outage' as yet another scenario, a total of 35×55=1925 unique load-generation-generator outage scenarios were simulated. Multiple generator outages were not considered, as this would massively proliferate those operating conditions, which are far less credible in real-time operation and hence having large representation of such operating conditions, as training exemplars would be hardly beneficial. Following the same principle, only single line-outage cases were considered as another form of assortment. Considering 186 number of lines in the test system, and taking 'no line-outage' as one more condition, combining 186 single line-outage cases with 35 load-generation patterns, 187×35=6545 mutually exclusive load-generation-line outage combinations were simulated. Thus, all together 1925+6545=8470 unique yet credible initial steady-state operating points were simulated for a broad representation of the complete operational space of the IEEE 118-bus test system. However, out of these 8470 cases, 3735 load-generation-outage combinations caused generator and line lodability limit (static security criteria) violations during load-flow analysis, and hence they were disregarded as credible steady-state pre-contingency operating points. Finally, the 4735 remaining acceptable initial operating points were used as the training exemplars for the ENSP. Newton-Raphson load flow (NRLF) analysis were performed, starting with each of these 4735 initial conditions and in each case the 780 steady state pre-contingency operating variables shown in Table-I were obtained as solutions of the load-flow program. After the pre-contingency operating variables were computed and archived, 3-phase line faults were simulated in each of the 186 lines of the test system and critical fault clearing time (t_{cr}) of each line were calculated using the PEBS method described in section-II to determine the criticality of a particular line fault under a given pre-contingency operating condition. These pre-contingency operating variables and t_{cr} combinations were then finally used as training exemplars for the ENSP.

Selection of Primary Variables and Primary Pattern Vector

Choice of input information plays a crucial role in training the ENSP. The preliminary selection of input information for training the ENSP began with pre-selection of operating variables, termed as 'primary variables', which are presumably representative of the dynamic characteristic of the system and somehow correlated with post-contingency system security. This usually refers to a set of initial pre-contingent conditions (such as: load-generation level, line flows, bus-voltage magnitudes etc.); network topology and connectivity at pre-contingency (such as: generator and line outages); and the type of contingency. It's worth mentioning, that in real-time power system operation, only static features are readily available or measurable through SCADA. It was therefore prudent to consider only pre-contingency static features, given their availability in real-time condition and simplicity. The dynamic features, though could provide important information about post-contingency dynamic changes in the system leading to potential instability, were avoided only for the reason

that they could be derived only through intensive (and impractical) calculations. Bus voltage angles and generator load angles, though carry important information, were not chosen as primary variables, as these are measurable through PMU's only, whose availability many be uncertain in many dated power systems. Table-I shows the 780 initial pre-selected primary variables for the IEEE 118-bus test system. These variables then constitute the 'primary pattern vector'. A primary pattern vector can be expressed as: $X_P = [P_{Gi}, Q_{Gi}, P_{Lj}\ Q_{Lj}, V_{Bk}\ , P_{Lin\ x\text{-}y}, Q_{Lin\ x\text{-}y}, F_{Gi}, F_{Linx\text{-}y}]$ where the suffix i stands for the i^{th} system generator, j stands for the j^{th} load bus, $Lin_{x\text{-}y}$ refers to the transmission line connecting bus x and bus y. F_G and F_{Lin} are the two 'contingency flags' representing single generator and single line-outage conditions. X_P needs to be calculated at 4715 representative operating points to generate an exhaustive set of pattern vectors, which are then passed on to a feature selection algorithm for screening before finally feeding the ENSP.

Table I The Initial Pre-Selected Primary System Variables

Primary System Variables	Symbol used	Number of variables
Active generation	P_G	54
Reactive generation	Q_G	54
Active load power	P_L	91
Reactive load power	Q_L	91
Bus voltage magnitude	V_B	118
Line active power flow	P_{Lin}	186
Line reactive power flow	Q_{Lin}	186
Total		780

Selection of dominant variables or features

Choice of input information plays a crucial role in machine learning. While precise and pertinent information improves the efficiency and predictive power of machine learning algorithms, noisy, irrelevant and redundant information are likely to deteriorate their performance. Therefore, selection of input information is one important task to be performed in every machine learning exercise. The term 'feature' refers to the distinctive attributes which can broadly represent a system. The idea behind feature selection is that the data contains some features that are either redundant or irrelevant, and can therefore be discarded without any significant loss of information. Redundant and irrelevant are however, two distinct concepts. Even a relevant feature may turn redundant in the presence of another relevant feature of similar kind, with which it has a 'strong correlation'. A feature selection algorithm can therefore be perceived as an intelligent search technique which can recommend or generate new feature subsets, based on some evaluation metric to differentiate the feature subsets qualitatively. In the context of 'power system security prediction', feature selection should be focused on choosing the attributes that will help in developing a more accurate predictive model while requiring less data [24]. The features may be the original power system attributes or operating variables like voltage, current, power etc., or sometimes new features may also be created combining some of these attributes. The feature selection technique will identify and remove the irrelevant and redundant attributes from data that do not contribute to the accuracy of the security prediction model (or may even decrease the accuracy of the model). Fewer attributes is always desirable as it cuts computation time and resource and also reduces complexity of the prediction model. Feature selection is not same as dimensionality reduction. Though the objective of both the

methods is to decrease the final number of attributes in the data, a dimensionality reduction method, such as 'Principal Component Analysis (PCA)' [25] attempts to create new combinations of attributes. A feature selection method, such as 'Relief' [26], on the other hand tries to filter the irrelevant and redundant attributes present in the data without any modification of the attributes. In the context of power system security analysis, the later approach is more suitable, as it helps in retention of the power system variables in their original form for future traceability and analysis (white box model). While large variety of feature selection methods and algorithms are available [27], [28], [29], when using Decision Tree (DT) learning model, usually 'Gini Index' method [30] is the most preferred feature selection method, which is used as the splitting criteria in most DT algorithms. Fig 1 depicts the sequence of steps implemented in this research work for effective feature selection.

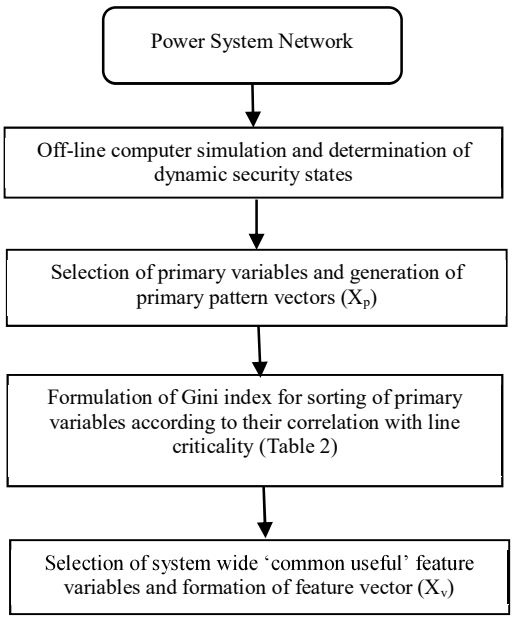

Fig. 1. The sequence of steps implemented for Feature Selection

Gini Index based Feature Selection

The 'Gini Index' in Decision Tree is an 'index of impurity', which is used to filter and select the attributes with less 'impurity'. Smaller the impurity is, more useful is the attribute in distinguishing between the classes. The method examines the decrease of impurity when using a chosen feature. It is a correlation-based criterion, which attempts to estimate a feature's ability to aid classification. It was originally proposed by Breiman, Friedman, Olshen and Stone in 1984 [31] and was widely used in many decision tree algorithms as a splitting rule. In 2007, Shang et al. [32] developed a novel feature selection algorithm for text categorization based on Gini index. In Gini method, the features and splitting variables are chosen by the split criterion that produces the highest impurity reduction for the next split. The Gini index formulation can be described as:

$$\mathrm{Gini}(t_K) = \sum_i P(\frac{t_k}{C_i})^2 . P(\frac{C_i}{k})^2$$

Where $P\left(\frac{t_k}{C_i}\right)$is the probability that the feature t_k occurs in category C_i and $P(\frac{C_i}{k})$ refers to the conditional probability that the feature t_k belongs to the category C_i when the feature $t_k$occurs.

Using Gini index, all the 780 operating variables (described in Table 1) were sorted in descending order of their

correlation with the criticality (t_{cr}) of a line. This way, sorting of variables was done for each of the 186 individual lines. Table 2 shows the sorted variables for 4 randomly chosen lines (lines connecting bus pair: 68-81, 11-13, 17-18 and 101-102) with the highest correlated variable scaled to 100% in each case. For space constraint only the top 15 variables are depicted in the Table 2.

Table 2: Operating Variables Sorted in Descending Order of Correlation with Line Criticality (t_{cr})

Line $_{68-81}$		Line $_{13-11}$		Line $_{17-18}$		Line $_{101-102}$	
Variable	Corr with t_{cr} in %	Variable	Corr with t_{cr} in %	Variable	Corr with t_{cr} in %	Variable	Corr with t_{cr} in %
P_{G69}	100	P_{G15}	100	P_{G18}	100	P_{G91}	100
P_{G80}	94	P_{G4}	97	P_{G113}	95	P_{G92}	92
P_{G116}	95	Q_{G15}	93	P_{G19}	91	P_{G100}	87
$P_{LIN69-70}$	92	P_{G6}	91	Q_{G18}	90	P_{G103}	82
$P_{LIN80-79}$	90	P_{LIN6-7}	85	$P_{LIN18-19}$	89	P_{G111}	81
Q_{G69}	88	P_{LIN4-5}	83	Q_{G113}	87	$P_{LIN91-92}$	79
Q_{G116}	85	Q_{G6}	81	Q_{G19}	86	$P_{LIN100-103}$	76
$Q_{LIN69-70}$	81	P_{G12}	79	P_{G15}	84	Q_{G91}	72
$P_{LIN116-65}$	78	$P_{LIN12-3}$	77	Q_{G15}	82	$Q_{LIN91-92}$	70
$Q_{LIN116-65}$	73	$Q_{LIN12-3}$	75	$P_{LIN17-16}$	77	$P_{LIN102-93}$	64
V_{B99}	70	Q_{LIN4-5}	71	$P_{LIN18-15}$	72	$P_{LIN101-100}$	61
V_{B76}	64	Q_{LIN6-7}	65	$Q_{LIN18-15}$	61	$Q_{LIN102-93}$	59
$Q_{LIN80-79}$	60	Q_{G4}	62	$Q_{LIN18-19}$	52	Q_{G92}	51
V_{B80}	55	V_{B15}	60	V_{B15}	41	Q_{G100}	49
V_{B69}	50	V_{B4}	485	V_{B18}	35	V_{B91}	44

It's interesting to note that the correlation of variables with t_{cr} varies from one line to another. As such it's impossible to find a common set of variables having same degree of correlation with t_{cr} for every line. However, for training the ENSP, all feature vectors must have common set of feature elements. An acceptable solution to this dilemma was arrived by computing the 'average correlation' of all the 780 variables with the t_{cr} of the 186 individual lines. Finally, the feature vector was formed with a minimal set of 15 numbers system-wide variables, which can be perceived as the 'common useful features' with high average correlation with all the 186 t_{cr}'s. The average correlation of these final 15 feature variables is depicted in Fig. 2. The final feature vector Xv has the structure: $X_V = [P_{G69}, P_{G18}, P_{LIN69-70}, P_{G91}, P_{G80}, Q_{G15}, P_{LIN6-7}, P_{G15}, P_{LIN18-19}, Q_{G69}, Q_{G6}, Q_{LIN69-70}, Q_{LIN18-19}, V_{B15}, V_{B69}]$

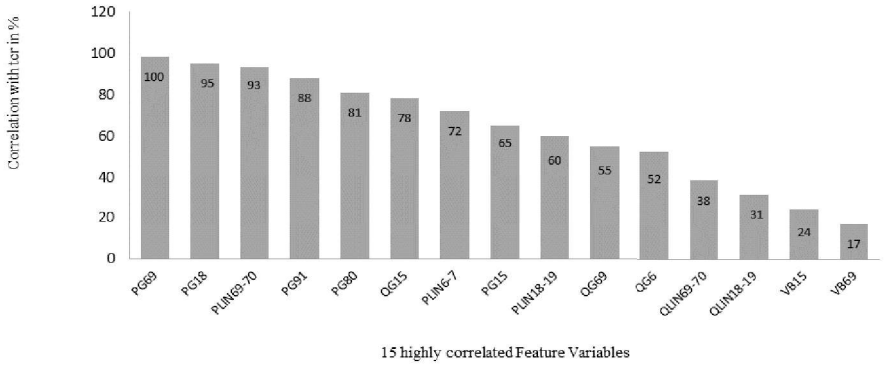

Fig. 2. Final 15 feature variables with their correlations with t_{cr}

Offline Training of ENSP and Classification of Training Samples

The Ensemble DT based security predictor enabled reliable prediction and decision rule creation for the post-contingency dynamic security states of the IEEE 118-bus benchmark system. The ensemble DT models were trained off-line using cross-validation with t_{cr}. Out of the 4735 pre-contingency operating conditions created in section: V, randomly chosen 3157 ones (approximately 2/3rd of total data) were used to form the learning set. Remaining 1578 cases (approximately 1/3rd of total data) were preserved as the test samples. Table 3 depicts the 3157 random training exemplars used in training the ENSP along with the remaining 1578 test samples.

Table 3:Training and Test Data for the ENSP

Security level				No. of credible pre-contingency operating conditions	
Criticality Class	No. of non-critical lines: A (t_{cr}> 160 mS)	No. of moderately critical lines: B (80 > t_{cr} > 160 mS)	No. of highly critical lines: C (t_{cr} < 80 mS)	Training Samples	Test Samples
0	A=186	B=0	C=0	0	0
1	185 ≥ A ≥ 124	1 ≤ B ≤ 62	C=0	318	159
2	124 ≥ A ≥ 62	62 ≤B ≤ 124	C=0	474	236
3	0 ≤ A ≤ 62	B ≥ 124	C=0	1102	550
4	0 ≤A ≤ 185	B=(185-A)	C=1	788	394
5	0 ≤A ≤183	B=(186-C-A)	2 ≤ C ≤3	315	159
6	0 ≤A ≤182	B=(186-C-A)	C > 3	160	80
Total:				3157	1578

The individual decision trees (DTs) in the ensemble model were trained by sub-sampling of the training data using the bagging and boosting principles. Optimal model for the ensemble DT was derived by assembling those candidate models, which have the highest prediction accuracies of the post-contingency dynamic security states.

TABLE 4: Prediction accuracy of the ENSP over 3143 random training cases

Criticality Class	No. of credible operating cases	No. of cases with correct security prediction	Accuracy of Prediction in %
0	0	--	--
1	318	309	97.2
2	474	457	96.4
3	1102	1051	95.4
4	788	753	95.6
5	315	304	96.5
6	160	154	97
All Security Classes	3157	3028	95.91

The final decision on the predicted security states was taken by principle of majority voting. The accuracy achieved for different security classes (at different criticality levels) as well as the overall prediction accuracy for the 3157 training samples is depicted in Table 4, where prediction accuracy is defined as:

$$\text{Prediction Accuracy} = \frac{\text{number of correct security state predictions}}{\text{total number of security state predictions}} \times 100$$

Prediction and Classification of Test Samples

The performance and prediction accuracy of the ENSP was tested over 1572 random cases. Performance of different DT-based techniques were tested and compared with the objective to finally elect the best prediction model for the intended dynamic security states prediction in the IEEE 118-bus benchmark system. Among the 'boosting-DT' models [33], the 'Stochastic Gradient Boosting (SGB)' [34] was tested where in each iteration a sub-sample of the training data is drawn at random from the full dataset without replacement. The randomly selected sub-sample is then used to train the individual base learners [35]. In the 'Adaptive Boosting-DT' category, the 'Ada Boost (AB)' [36] model was tested, which is an ensemble model that attempts to create a 'strong classifier' from a number of 'weak classifiers' [37]. In the "bagging" [38] category, 'Random Forest (RF)' was tested, which is a decision tree model in which individual trees have structural similarities, but the algorithm trains the sub-trees in a manner that reduces the correlation between the prediction results of the individual sub-trees, resulting better overall prediction accuracy. The prediction accuracy for each DT model was verified using cross-validation with t_{cr} value for each individual test case and the results are presented in Table 5.

TABLE 5: Prediction Accuracy of the ENSP for 1578 Random Test Cases

Degree of Criticality	No. of Credible Cases	No. of Cases Where Security	Accuracy of Security Class

	Considered	Class was Correctly Predicted	Prediction in %
1	159	152	95.6
2	236	223	94.5
3	550	519	94.4
4	394	379	96.2
5	159	148	93.1
6	80	76	95.0
All Security Classes	1578	1497	94.86

To compare the prediction accuracy of the ensemble approach against 'single learner' approach, popular single learner techniques, such as Support Vector Machine (SVM) [39], Method of Least Squares (MLS) [40], Learning Vector Quantization (LVQ) [41], Probabilistic Neural Network (PNN) [42] and Kohonen's Neural Network (KNN) [43] were used. The performance of each classification method is presented in Table 6.

TABLE 6: Prediction Accuracy of Different Ensemble and Single Learner Methods

Metrics	Ensemble methods			Single Learner methods				
	RF	AB	SGB	MLS	KNN	LVQ	PNN	SVM
Accuracy %	.4	.5	.5	.2	.1	.8	.4	.7
Kappa %	95.5	94.3	91.2	81.6	85.7	87.6	86.6	90.9

The results indicate that ensemble-DT models in general have better accuracy when compared with the single learner ones. Among the various ensemble approaches, the Random Forest and Ada Boost models were found to be the better performing ones to detect the dynamic security states in the IEEE 118-bus test system.

Conclusion

This work presented a 'pattern-recognition' and 'machine learning' approach to real-time online dynamic security evaluation of power system networks. An efficient ensemble decision tree (DT) based security predictor (ENSP) was developed to predict and classify power system dynamic operating states into secure, insecure and intermediate transitional classes under wide range of operating scenarios and credible set of contingencies. The objective behind the use of pattern recognition method was to reduce the computational overhead to a minimum, to make it suitable for on-line usage. The underlying offline analysis however was made as extensive as possible by training the ENSP off-line, using results obtained from the most tedious and accurate dynamic security calculations. Since selection of input information is important in machine learning exercise, intelligent search for optimal features was performed to discard the redundant and irrelevant features without any significant loss of information. 'Gini-Index' based feature selection was identified as a suitable method for extracting the optimal feature sets, relevant in the context of dynamic security prediction, which focused on choosing the 'high quality' attributes that helped in developing a more accurate security prediction

model while requiring less data. Efficacy of different classifiers were also tested and Ensemble Decision Tree (DT) was found to be more accurate compared to other equivalent classifiers built upon method of least square (MLS), neural network (NN), vector quantisation (VQ) and support vector machine (SVM) techniques, when implemented in large power systems like an IEEE 118-bus system, reducing the chances of failure of appropriate control actions in the events of potential dynamic insecurity.

References

1. Z. Buxiang & T. Fusheng, "The Distributed Monitor System for Security and Stability in the Complicated Power Systems", Power System Technology, Proceedings. POWERCON '98. International Conference on 18-21 Aug. 1998.
2. S. Kalyani, K. S. Swarup, "Design of pattern recognition system for static security assessment and classification, Pattern Analysis and Applications" August 2012, Volume 15, Issue 3, pp 299–311.
3. M. J. Laufenberg & M. A. Pai, "A New Approach to Dynamic Security Assessment Using Trajectory Sensitivities", IEEE Transactions on Power Systems, Vol. 13, No. 3, August 1998.
4. G. Istemihan, D. Ruisheng, V. Vijay, K. Sharma, & S. Mandal, "Decision Tree-Based Preventive and Corrective Control Applications for Dynamic Security Enhancement in Power Systems", IEEE transactions on power systems, vol. 25, no. 3, August 2010.
5. M. A. El-Sharkawi & R. Atteri, "Static Security Assessment of Power System Using Kohonen Neural Network", Proceedings of the Second International Forum on Applications of Neural Networks to Power Systems, 19-22 April 1992.
6. P. Kumkratug & P. Laohachai, "Time domain simulation technique of a power system transient with VSC based facts devices", First Asia International Conference on Modelling & Simulation (AMS'07) 27-30 March 2007
7. P Sekhar & Prof. S Mohanty "Power system contingency ranking using Newton Raphson load flow method", Annual IEEE India Conference (INDICON), 2013.
8. M. F. Bedrinana, V. L. Paucar & C. A. Castro "Transient Stability using Energy Function Method in Power Systems Close to Voltage Collapse", Large Engineering Systems Conference on Power Engineering, 10-12 Oct. 2007.
9. M. Shukla&M. Abdelrahman "Artificial neural networks based steady state security analysis of power systems", Thirty-Sixth South eastern Symposium Conference on System Theory, 16-16 March 2004.
10. G. Chicco, R. Napoli&F. Piglione, "Fast contingency analysis by means of a progressive learning neural network", Power Tech Budapest 99. Abstract Records. (Cat. No.99EX376), 29 Aug.-2 Sept. 1999.
11. X. Yan, Z. Y. Dong, J. H. Zhao, P. Zhang & K. P. Wong," A Reliable Intelligent System for Real-Time Dynamic Security Assessment of Power Systems", IEEE transactions on power systems, VOL. 27, NO. 3, AUGUST 2012.
12. D. Utyamishev & I. P. Vaisband, "Real-Time Detection of Power Analysis Attacks by Machine Learning of Power Supply Variations On-Chip", IEEE Transactions on Computer-Aided Design of Integrated Circuits and Systems, 29 November 2018, Pp 1 – 1.

13. C. W. Wang, "New Ensemble Machine Learning Method for Classification and Prediction on Gene Expression Data", International Conference of the IEEE Engineering in Medicine and Biology Society, 30 Aug.-3 Sept. 2006.
14. L. Pisica, G. Taylor, "Classification of operating states for decision making in power systems control with feature selection based on mutual information", 9th International Conference on Fuzzy Systems and Knowledge Discovery (FSKD) 2012.
15. L. Y. Ren, F. Tian, J. F. Yan, Z. H. Yu, F. Su, T. Wu, "Online Application and Fast Solving Method for Critical Clearing Time of Three-Phase Short Circuit in Power System", International Journal of Smart Grid and Clean Energy, ISSN: 2315-4462, vol. 2, no. 1, January 2013, Pp 93–99.
16. H. D. Chiang, F. F. Wu and P. P. Varaiya, "Foundations of the potential energy boundary surface method for power system transient stability analysis", IEEE Transactions on Circuits and Systems, Volume: 35 , Issue: 6 , Jun 1988, Pp 712 – 728.
17. C. Kamath, E. Cantu-Paz, "Creating Ensembles of Decision Trees through Sampling", 2001, International Conference on Machine Learning, Williams College, MA, June 28- July 1, 2001.
18. Zhukov, N. Tomin , V. Kurbatsky , D. Sidorov , D. Panasetsky , & A. Foley, "Ensemble methods of classification for power systems security Assessment", ScienceDirect, Volume 15, Issue 1, January 2019, Pp 45-53.
19. E. A. Freeman, G. G. Moisen, J. W. Coulston, and B. T. Wilson, "Random forests and stochastic gradient boosting for predicting tree canopy cover: comparing tuning processes and model performance", Canadian Journal of Forest Research, 2016, vol 3, Pp 323-339,
20. L.V. de Souza , A.T.R. Pozo , A.C. Neto & J.M.C. da Rosa, "An Empirical Study of Time Series Forecasting Using Boosting Technique with Correlation Coefficient", Seventh International Conference on Intelligent Systems Design and Applications (ISDA), 20-24 Oct. 2007
21. N. Chaudhari , T. Hinge and S. Dambhare, "Dynamic security analysis for voltage security using Decision Trees", IEEE Region 10 Conference (TENCON), 22-25 Nov. 2016.
22. M. Wozniak, "Experiments with Boosted Decision Tree Classifiers", Eighth International Conference on Intelligent Systems Design and Applications, 26-28 Nov. 2008.
23. B. Nassif , M. Azzeh , L. F. Capretz & D. Ho, "A comparison between decision trees and decision tree forest models for software development effort estimation", Third International Conference on Communications and Information Technology (ICCIT), 19-21 June 2013.
24. Zhang, Y. Li, Z. Yu & F. Tian, "A weighted random forest approach to improve predictive performance for power system transient stability assessment", IEEE PES Asia-Pacific Power and Energy Engineering Conference (APPEEC), 25-28 Oct. 2016.
25. T. Zhang, & B. Yang, "Big Data Dimension Reduction using PCA", IEEE International Conference on Smart Cloud, 2016.
26. F. Wenbing, W. Quanquan and Z. Hui, "Feature Selection Method Based on Adaptive Relief Algorithm", 2010 3rd International Conference on Computer and Electrical Engineering (ICCEE), IPCSIT vol. 53 IACSIT Press, Singapore, 2010.
27. J. Yang, Z. Qu, and Z. Liu, "Improved Feature-Selection Method Considering the Imbalance Problem in Text Categorization", the Scientific World Journal, Volume 2014, Article ID 625342.
28. W. Shang, H. Huang, H. Zhu, Y. Lin, Y. Qu, & Z. Wang, "A novel feature selection algorithm for text categorization", Expert Systems with Applications, vol 33, Pp 1–5, 2007.

29. A. Abbas, M. S. Morsy, H. E. A. Talaat & M. E. El-Hawary, "A Generator Tripping Emergency Control Strategy for Dynamic Security Enhancement Using Rule Based Fuzzy Assessment", IEE MELECON Cairo , EGYPT, May 7-9, 2002.
30. L. Haoyue, Z. MengChu, S. L. Xiaoyu & Y. Cynthia, "Weighted Gini Index Feature Selection Method for Imbalanced Data", IEEE 15th International Conference on Networking, Sensing and Control (ICNSC), 2018.
31. S. B. Yang & S. I. Yang, "New decision tree based on genetic algorithm", International Symposium on Computer, Communication, Control and Automation (3CA), 5-7 May 2010.
32. S. Sivagama Sundhari, "A knowledge discovery using decision tree by Gini coefficient", International Conference on Business, Engineering and Industrial Applications, 5-7 June, 2011.
33. H. Cui, D. Huang, Y. Fang , L. Liu & C. Huang, "Webshell Detection Based on Random Forest–Gradient Boosting Decision Tree Algorithm", IEEE Third International Conference on Data Science in Cyberspace (DSC), 18-21 June, 2018.
34. H. Ding , G. Li , X. Dong & ; Y. Lin, "Prediction of Pillar Stability for Underground Mines Using the Stochastic Gradient Boosting Technique", IEEE Access (Volume: 6) Pp: 69253 – 69264.
35. S. Pathical & G. Serpen, "Hybridization of Base Classifiers of Random Subsample Ensembles for Enhanced Performance in High Dimensional Feature Spaces", Ninth International Conference on Machine Learning and Applications, 12-14 Dec. 2010.

36. D. Tian , G. He , J. Wu , H. Chen & Y. Jiang, “An accurate eye pupil localization approach based on adaptive gradient boosting decision tree”, Visual Communications and Image Processing (VCIP), 27-30 Nov, 2016.
37. A. Othman, M. Tahir, R. E. Shatshat, & K. Shaban, Application of Ensemble Classification Method for Power Transformers Condition Assessment, IEEE 30th Canadian Conference on Electrical and Computer Engineering (CCECE), 2017.
38. P. Li , J. Huang , K. Zhang & T. Bi, “Imbalance data classification method based on cluster boundary sampling RF-Bagging”, International Conference on Software Intelligence Technologies and Applications & International Conference on Frontiers of Internet of Things 2014, 4-6 Dec, 2014.
39. G. S. Hu & J. Xie ; F. F. Zhu, “Classification of power quality disturbances using wavelet and fuzzy support vector machines”, International Conference on Machine Learning and Cybernetics, 18-21 Aug, 2005.
40. S. D. Kim & K. W. Lim, “An iterative least-square training method for classification-based motion adaptive temporal filtering”, Digest of Technical Papers International Conference on Consumer Electronics (ICCE), 9-13 Jan, 2010.
41. P. Tse ; D.D. Wang ; D. Atherton, “Improving learning vector quantization classifier in machine fault diagnosis by adding consistency”, Proceedings of ICNN'95 - International Conference on Neural Networks, 27 Nov.-1 Dec, 1995.
42. Lockheed Palo Alto Res. Lab., CA, USA, “Probabilistic neural networks for classification, mapping, or associative memory” IEEE International Conference on Neural Networks 24-27 July, 1988.
43. M. R. Aghamohammadi, F. Mahdavizadeh & R. Bagheri, “Power System Dynamic Security Classification Using Kohenen Neural Networks”, IEEE/PES Power Systems Conference and Exposition, 15-18 March, 2009.

Chapter 23

Power System Transient Stability Analysis using Kohonen Neural Network Security Classifier - a Case Study on the IEEE 57-Bus System

Rituparna Mukherjee*, Susmita Dhar Mukherjee, Titas Kumar Nag, Promit Kumar Saha
Swami Vivekananda University, Department of Electrical Engineering
Corresponding Author Email: rituparnamukherjee@svu.ac.in

Abstract

This paper presents an approach to power system dynamic security assessment using Kohonen's Neural Network (KNN) based pattern classifier. A standard pattern recognition framework, has been followed in order to ensure that real-time implementation of the proposed framework is feasible. With the aim of recognizing the vulnerability associated with various pre-contingency operational circumstances, the Security Classifier (SC) was created and trained with operational data obtained from developed computer model of the power system. The proposed SC was successfully tested on IEEE 57-bus benchmark system to recognize and classify wide variety of operating conditions based on their vulnerability to dynamic insecurity post major contingencies.

Keywords: Classification, Kohonen's Neural Network (KNN), Dynamic Security, Power System Stability.

Introduction

Electrical power systems are complex networks designed to produce and supply electrical power reliably and economically to the consumers. In recent years, there has been increasing competition among the power utilities to deliver quality electrical power at affordable rates. De-regulation [1] in electrical power market has further intensified such competition and forced all the three major entities, namely the generation, transmission and distribution system operators to utilize their resources to the maximum possible extent. While this has led the power generators to push the operation of synchronous generators close to their stability limits, the transmission utilities have been compelled to exploit the network capacities to highest possible extent. Operating such overstressed power systems are technically challenging, as any major perturbation can lead to catastrophic consequences, including equipment failure, system collapses and complete black outs. These overstressed power systems have therefore raised serious concerns about operational reliability and have posed new challenges to power system security. A power system network often experiences severe disturbances like equipment outages, such as outage of some of the generating units, transformers, and transmission lines etc., commonly termed as the contingencies. Such contingencies often result due to unintended operation and mal-operation of the system protection devices, such as the relays. The relays are generally intended to protect major power equipment like alternators, transformers and transmission lines from a variety of plausible power system faults. When a fault occurs, the relay dedicated to protect a particular equipment is supposed to operate and isolate the faulty equipment selectively, from healthy part of the system. However, faulty operation of a relay such as a relay mal-tripping may lead to isolation of much larger section of a power system than it is actually necessary to isolate the faulty equipment. The consequences are the sudden loss generators, transformers and important transmission lines, which may challenge power system security. A power system can be called operationally secure if there is little possibility of a wide-scale system outage or complete black out consequent to any major perturbations, which can result temporary suspension of system operation and interruption of power supply to consumers.

It is imperative that operation of a power system must be secure under all conditions. The design of a power system should therefore be robust to absorb the consequences of major contingencies, without much impact on system security. It is also important to follow certain operational practices, which are critical for maintaining system security, even when some critical equipment is unavailable due to contingencies. Power system security analysis is therefore considered one among the most important studies in power system operation and research, which is meant to evaluate the resilience of a power system

network against variety of contingencies which a power network may experience in day to day operation. The power system contingencies, can therefore be viewed as the adverse events which can result undesirable circumstances and operating conditions, which are plausible, but not always predictable with high degree of certainty. Power system security analysis includes: static security analysis (SSA) [2] and dynamic security analysis (DSA) [3]. After a severe disturbance and contingency, power system usually undergoes a change of state. It is desirable that a power system restores back to normal or stable state post such contingencies. SSA assumes that stable operation is restored post disturbance and the analysis mainly focuses on whether any kind of limit violation or any compromise with system's physical or security parameters occurred in order to reach post-contingency new steady state operating point [4].In the event of a severe contingency, quick transition to new steady-state operating point is often infeasible and the system may continue to operate in a quasi-stable state for a considerably long duration of time [5]. Unlike in SSA, dynamic security analysis (DSA) [6], [7] involves study of the operating state transition post contingencies. Thus, the quasi-stable operating state, referred earlier is of greater significance in DSA. There exist several methods for dynamic security assessment of power system. Time domain simulation (TDS) is considered a relatively accurate method for DSA for studying large disturbances rotor angle stability analysis, also known as transient stability analysis (TSA) [3]. TDS requires representation a power system by a set of non-linear time domain equations to model the dynamic characteristic of every power system equipment. These equations are then solved by numerical integration methods in order to assess dynamic behavior of the system post contingency and TSA then analyses whether a disturbance may lead to loss of stability. The major hindrance in performing TSA is the heavy computational overhead, which makes the analysis both time and resource consuming and usually slow. This renders many of the existing DSA techniques unsuitable for real-time application [8]. Direct method of TSA, which utilizes transient energy function is a viable alternative approach to TDS for determining post contingency operating condition of a power system [9]. However, the direct method uses reduced order modeling of a contingent system, and therefore, usually lacks the high levels of accuracy which TDS offers. It is worth mentioning that, the vulnerable pre-contingency operating states of a power system, which can result potential instability and system outages are often unique. As such, almost no exclusive method to reveal such vulnerable operating conditions, fast enough, to be usable in real-time security assessment hardly exists. It is, therefore imperative, that developing a powerful and robust online security monitoring system is of pivotal importance in order to assess the current security level of a power system and to make the power system operator aware of possible security issues. When a security issue is detected, it is also necessary to take appropriate preventive and control actions to avert any possible future system outage and to regain system security.

Power system security analysis has been a major focus area of power system research for long. The review of existing literature reveals that, researchers [10],[8] considered time domain simulation (TDS) as one of the most accurate methods for dynamic security analysis (DSA) under large perturbations, which is more commonly termed as transient stability analysis (TSA) [3]. The TDS method relies on developed mathematical model of a power system network in the form of nonlinear time-domain differential and/or algebraic equations. These equations can presumably represent the dynamic behaviour of generators, loads and other dynamic components present in the power system. Numerical integration is usually performed to

solve these equations to obtain the dynamic behaviour of a power system under perturbed conditions. However, these numerical integrations are highly time and resource consuming, and therefore real-time application of TDS in TSA is mostly unsuccessful, as the analysis has to performed very fast, within short time-frame of few tens of milliseconds. The research work in [4] however revealed a novel method to quickly analyse transient stability using TDS.

Other than the TDS method, another viable approach to TSA is the direct method, which uses transient energy function [11], [12] to ascertain stability of a power system at its new post-contingency operating point. The direct method is computationally less intensive compared to the numerical integrations performed in TDS. However, the direct method is also less accurate than TDS [13] as it involves reduced order modelling of the post-contingency system and uses several simplifying assumptions and hypotheses. A new method proposed in [14] generalized the concept of energy function and extended the traditional energy function method to develop a more general Lyapunov functions family (LFF) in order to overcome some of the limitations of the classical energy function method. Direct method was traditionally considered impractical for performing TSA in large-scale power system networks. However, a recent research work [15] reported use of direct method in real-time dynamic security assessment of a very large-scale power system. The case-study reported in this paper used a power system comprising of 14,500 number of system buses and 3000 synchronous generators. The lack of availability of any effective computational method for fast and accurate real-time DSA, stimulated early adoption of Machine Learning (ML) and Pattern Recognition (PR) methods by the research community involved in power system security studies. A number of novel researches in the late 1980 [16]-[17] attempted ML/PR approach to map the relationship between a power system's pre-contingency operating condition and the post-contingency dynamic security state. Once such underlying correlations could be successfully recognized, the dynamic stability state for the operating cases involving unforeseen contingencies could also be predicted with minimum computational efforts. Even, the pre-contingency operating conditions, which may have led to these dynamic insecure conditions, could also be predicted by the ML/PR based techniques. A pioneering research work in [16] proposed a framework to deal with the power system transient-stability problem online. The authors proposed an inductive inference approach, to develop rules correlating a power system's stability with the relevant system parameters.

The large pool of above-mentioned research works reveal that applications of AI and ML can be effective to ease the computational burden involved in the analysis of power system security and therefore, they can be effective in the development of fast, real-time dynamic security assessment (DSA) methods. [19][20]

In this paper, a novel PR approach towards transient stability-based security evaluation of power system networks in real-time environments was presented. An efficient Kohonen's Neural Network (KNN) based Security Classifier (KNNSC) was developed in the research work to predict and classify power system's dynamic operating states into secure and insecure classes under wide range of operating scenarios and credible contingencies. Use of the efficient Kohonen's Neural Network (KNN) (DT) based pattern classification in this research work significantly reduced the computational overhead, making the proposed method suitable for real-time usage. Relevant system attributes (features) were screened, discarding the redundant and irrelevant features without significant loss of information. Gini-Index based feature selection was identified as a suitable method for identification of critical attributes, which were relevant in the context of dynamic security state prediction. An illustrative case study was presented in the paper, which demonstrated the development and implementation of the proposed KNNSC for dynamic security state classification in the IEEE 57-bus power system. The proposed method delivered encouraging results and outperformed the other popular classification methods, such as: Support Vector Machine (SVM), Method of Least Squares (MLS), Learning Vector Quantization (LVQ) and Probabilistic Neural Network (PNN) based classifiers in terms of accuracy and development/ implementation time.

The Kohonen's Neural Network (KNN) Based Security Classifier (KNNSC)

The purpose for development of a security classifier is to classify a power system's pre-contingency operating conditions by evaluating its vulnerability to transient instability in the events of major contingency or equipment outage. For this purpose, a Kohonen's Neural Network (KNN) Security Classifier, termed as KNNSC, has been developed as a dynamic security assessment (DSA)-tool to offer real-time power system dynamic security state prediction and classification. The KNNSC was designed to use real-time power system operating data, obtained through Supervisory Control and Data Acquisition (SCADA). The output of the KNNSC is the predicted post-contingency dynamic state of the system, which is either secure, or insecure. Such security assessments were carried out under wide variety of severe, but credible contingencies. A secure class refers to those pre-contingency operating states of a power system, in which there is zero feasibility of existence of any critical line-faults (faults which can cause potential instability). An insecure class, on the other hand, refers to those pre-contingency operating states, which have at least one (or more) critical line-fault existing, which may result potential instability in the future. The index of criticality of a pre-contingency operating condition was assessed by the number of critical line-faults that may exist under the given operating condition. The KNNSC was developed and trained off-line with the objective to recognize the degree of criticality which are associated with different pre-contingency operating conditions. The KNNSC was successfully implemented in a simulated environment to recognize a power system's unforeseen operating conditions and predict their vulnerability to post-contingency dynamic insecurity.

Dynamic Security State Classification by KNNSC – a Case Study on IEEE 57-bus system

An illustrative case study showing development and implementation of the proposed Kohonen's Neural Network (KNN) Security Classifier (KNNSC) for dynamic security state classification in the IEEE 57-bus power system has been presented in this case study. The IEEE 57 Bus Test Case represents a portion of the American Electric Power System (in the Midwestern US) as it was in the early 1960's which contains of 57 buses, 7 generators and 42 loads. The schematic diagram shown in fig 1

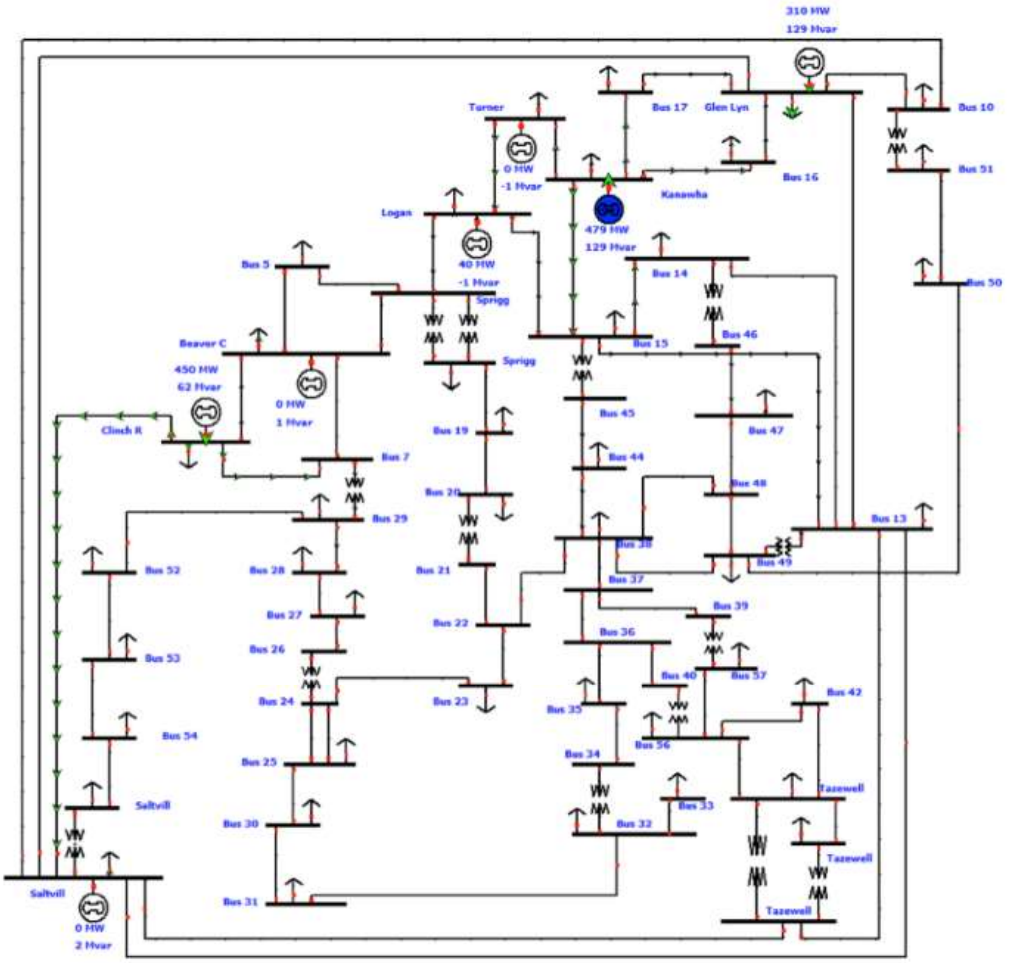

Fig 1: Schematic Diagram of IEEE 57 bus test syste Offline Simulation of the IEEE 118 bus test system in MATLAB Power System Analysis Toolbox (PSAT)

A dynamic model of the IEEE 118-bus system was created in MATLAB based Power System Analysis Toolbox (PSAT) [4.13] for the present study. The power flow and time domain simulation (TDS) functions, which are available in the Power System Analysis Toolbox (PSAT), were used in this case study and the TDS function was suitably extended for the calculation of transient stability.

All simulations were performed on a desktop PC running on Intel Core i7 3.4 GHz CPU with 8GB of RAM. Data files containing power system model-data and contingency information were created to serve as input to the TDS program. The time domain simulations were initialized by the power flow results. Each time domain simulation (TDS) was run over a chosen time-horizon of 200mS (10 cycles), unless the simulation got automatically terminated as a result of singularity arising due to plausible transient instability. Transient instability happened in several cases following major disturbances, such as faults, when the faults were not cleared within tcr. Critical clearing time (tcr) of each line fault was determined by running TDS recurrently, by varying fault clearing time values in the range of 80ms ~ 180ms in steps of 10ms. The computed values of tcr were later used to assess the security state of the IEEE 57-bus system.

Simulation of Pre-Contingency Operating Conditions for Training the KNNSC

In the present research work, large numbers of diverse and well-spread pre-contingency operating conditions (OCs) were simulated by multiple power-flow simulations of the test system. Variable initial starting conditions, such as: diffident load-generation scenarios, changed network topologies arising out of

generator, transformer and line outages and their combinations were considered while performing such multiple power-flow simulations. To simulate well-dispersed pre-contingency OCs following variations in operating conditions were simulated. Load variations in random sets of 6 buses were considered at a time. The loads were varied in 5 discrete steps of 0.5, 0.75, 1.0, 1.25 & 1.5 p.u. of the base load of these selected buses. This procedure was then recursively followed for next 6 randomly chosen buses, not common with any one of the previously selected buses. The process was repeated a total of 7 times to cover all the 42 load buses. Generation scenarios also changed in accordance with the load changes and were reflected in the power-flow solutions. The above-mentioned procedure produced 5×6=30 unique, yet credible load-generation scenarios. Each of the above 6 loading conditions was them combined with single-generator outage conditions. Considering 7 number generators in the IEEE 57 bus system and 'no generator outage' as yet another scenario, a total of 30×8=240 unique load- generation-generator outage scenarios were simulated. Multiple generator outages were not considered, as this would massively prolife rate those operating conditions, which are far less credible in real-time operation and hence having large representation of such operating conditions, as training exemplars would be hardly beneficial. Following the same principle, single line-outage cases were considered as another form of variation in OC. Considering 80 number of lines in the test system, and taking 'no line-outage' as one more condition, combining 80 single line-outage cases with 100 load-generation patterns, 81×30=2430 mutually exclusive load- generation-line outage combinations were simulated. Thus, all together 240+2430 = 2670 unique yet credible initial steady-state OCs were simulated for a broad representation of the complete operational space of the IEEE 57-bus test system.

Offline Building and Training of the Kohonen's Neural Network (KNN) Security Classifier

The Kohonen's Neural Network (KNN) Security Classifier (KNNSC) was developed in Python, scikit-learn platform on a desktop PC running on Intel Core i7 3.4 GHz CPU with 8 GB of RAM. The Classification and Regression Tree (CART) model was used to develop the Kohonen's Neural Network (KNN) classifier. The KNNSC was trained using the training set comprised of the operating cases (OCs) created earlier. The KNNSC was meant to classify the OC's into secure and in-secure classes. Out of the 2670 OCs simulated, 1780 randomly chosen OCs (approximately 2/3rd of total OCs) were used for training the KNNSC. Remaining 890 cases (approximately 1/3rd of total OCs) were used later as test OCs. Table 3 depicts the distribution of training and test OCs for the KNNSC. Both training and test data comprised of 59% secure OCs (shaded with green colour in Table 3) and 41% insecure OCs (shaded with red colour in Table 3).

Table 3 Distribution of training and test data for the KNNSC

Security Conditions				**No. of credible pre-contingency operating conditions**	
Security State	**No. of non-critical lines: A (t_{cr}> 160 mS)**	**No. of moderately critical lines: B (80 > t_{cr} > 160 mS)**	**No. of highly critical lines: C (t_{cr} < 80 mS)**	**Training Samples**	**Test Samples**
Secure (59%)	A=186	B=0	C=0	0	0
	79 ≥ A ≥ 55	1 ≤ B ≤ 34	C=0	180	90

	55 ≥ A ≥ 34	34 ≤B ≤ 55	C=0	280	140
	0 ≤ A ≤ 34	B ≥ 55	C=0	570	285
Insecure (41%)	0 ≤A ≤ 79	B=(79-A)	C=1	450	225
	0 ≤A ≤77	B=(79-C-A)	2 ≤ C ≤3	220	110
	0 ≤A ≤71	B=(186-C-A)	C > 3	80	40
Total:				**1780**	**890**

Estimation of KNNSC-building and Training time

With the top-15 highly correlated feature variable in as attributes/nodes, a desktop PC running on Intel Core i7 3.4 GHz CPU with 8GB of RAM accomplished KNNSC building and training in just over 4.5 hours with only 1203 iteration. The DT-building and training time in such case exceeded 37 hours with average training cycle time of 49.15 Sec. Thus, KNNSC building and training time dropped by more than 87% when using reduced number of feature variables.

Training Accuracy of the developed KNNSC

The training accuracy of the KNNSC was evaluated and is depicted in the form of confusion matrix of Table 4. The training accuracy was found to be encouraging for a large power network like the IEEE 57-bus system considered in this case-study.

In the training data-set, 96 insecure OCs out of 653 originally insecure OC were misclassified as secure OCs. However, the rest 557 insecure OCs were correctly classified as insecure OCs.

- On the contrary, 35 OCs out of 1127 originally secure OCs were misclassified as insecure OCs, whilethe rest 1092 secure OCs were correctly identified as secure OCs.

Where as

- TP (True Positive): when an OC is classified as secure when it is truly secure.
- FP (False Positive): an OC is classified as insecure when it is truly secure
- TN (True Negative): an OC is classified as insecure when it is truly insecure
- FN (False Negative): an OC is classified as secure when it is truly insecure
- N: Total number of OCs used = TP + FP + TN + FN

Table 4 Confusion Matrix of the KNNSC for 1780 training cases

		Predicted as		
		Secure	**Insecure**	
Actual	**Secure**	**TP**= 1092	**FP = 35**	**TP + FP =** 1127
	Insecure	**FN = 96**	**TN**= 557	**FN + TN =** 653

	TP + FN = 1188	**FP + TN = 592**	**N = 1780**

A number of metrics were developed and employed to evaluate the performance of the proposed KNNSC as under using the terminologies explained:

$$\text{Classification Accuracy (CA)} = (\text{TP} + \text{TN})/\text{N} \quad (1)$$

$$\text{Composite Misclassification Rate (CMR)} = (1 - \text{CA}) \quad (2)$$

$$\text{Secure Misclassification Rate } (\mathbf{SMR}) = \text{FP}/(\text{TP} + \text{FP}) \quad (3)$$

$$\text{Insecure Misclassification Rate } (\mathbf{IMR}) = \text{FN}/(\text{TN} + \text{FN}) \quad (4)$$

Table 5 depicts the performance of KNNSC on 3143-training OCs in terms of the performance metrics defined in equation (1) – (4).

Table 5 Classification performance of KNNSC for the 3143 training cases

Performance Metric	**Ratio of Cases**	**% value**
Classification Accuracy (CA)	1649/1780	92.64
Composite Misclassification Rate (CMR)	(1-0.926)	0.074
Secure Misclassification Rate (SMR)	35/1127	0.031
Insecure Misclassification Rate (IMR)	96/653	8.24

Performance of the KNNSC in classifying unseen Test Operating Cases

After the KNNSC was successfully built and trained, its classification performance was evaluated using 890 numbers of unseen test OCs. Confusion matrix in Table. 6 depicts the security state classification results of the KNNSC for the 890 unseen test OCs. The KNNSC could capably classify the unseen cases with only 60-instances of insecure OC misclassifications and 70-instances of secure OC misclassifications, which results Secure Misclassification Rate (SMR) of 10.2% and Insecure Misclassification Rate (SMR) of 10%.

Table 6 Confusion matrix depicting performance of KNNSC on 1572 unseen test OCs

		Predicted as		
		Secure	**Insecure**	
Actual	**Secure**	TP = 440	FP = 50	**TP + FP = 490**
	Insecure	FN = 40	TN = 360	**FN + TN = 400**
		TP + FN = 480	**FP + TN = 410**	**N = 890**

Classification performance of KNNSC for unseen test operating conditions was evaluated in the way similar to what was done previously for the training cases. The performance metrics defined in equation (1) – (4) were used for a comprehensive assessment of the KNNSC's classification efficacy. The results are presented in Table 7.

Table 7 Classification performance of KNNSC for unseen test cases

Performance Metric	**Ratio of Cases**	**% value**
Classification Accuracy (CA)	800/890	89.9
Composite Misclassification Rate (CMR)	1-0.9	0.1
Secure Misclassification Rate (SMR)	50/490	0.102
Insecure Misclassification Rate (IMR)	40/400	0.1

In the context of power system security classification misclassification of secure OCs is less hazardous, as this can only trigger false alarm, which will generally not affect the normal operation of the system. However, misclassification of insecure OCs can have severe consequences, as the same is likely to result lack of remedial actions, which may lead to instability and system outages. It is, therefore, imperative that a robust power system security classifier should have IMR as low as possible. The developed KNNSC satisfied this vital criterion.

Comparison of Classification Performance of KNNSC with other Classifiers

The classification performance of KNNSC was also compared against other popular classification algorithms, such as: the Support Vector Machine (SVM) [21], Method of Least Squares (MLS) [22], Learning Vector Quantization (LVQ) [23], and Probabilistic Neural Network (PNN) [24]. The results of comparison are depicted in Table 8 and Table 9. It is evident from the results depicted in Table 8 that KNNSC offered more accurate and reliable DSA results compared to KNNSC. The classification performance of KNNSC was also found to be superior than other tested classification methods like SVM, MLS, LVQ and PNN.

Table 8 Comparison of performance of different classification methods

Classifier	**Classifier Performance Metrics**			
	CA (%)	**CMR (%)**	**SMR (%)**	**IMR (%)**

KNN	**89.9**	**10**	**10.2**	**10**
DT	81.04	18.96	21.16	15.79
SVM	79.9	20.1	28.2	17.1
MLS	76.3	23.7	32.3	18.6
LVQ	74.2	25.8	35.5	22.3
PNN	72.6	27.4	39.4	26.21

The results presented in Table 9 on the other hand reveal that the KNNSC is computationally lighter and more efficient than KNN, SVM, MLS, LVQ and PNN with shorter training and execution times.

Table 9 Comparison of training and execution time of different classifiers

Classification Method	Classifier Training Time	Execution Time
KNN	**4.5 hour**	**180 ms**
DT	8.7 hour	221 ms
SVM	8.2 hour	372 ms
MLS	8.5 hour	585 ms
LVQ	9.1 hour	781 ms
PNN	9.3 hour	819

4 Conclusion

This paper presented another novel method for real-time dynamic security assessment (DSA) of electrical power systems based on pattern-recognition (PR) approach. An efficient Kohonen Neural Network Security Classifier (KNNSC) was developed to evaluate and classify power system's dynamic operating states into secure and insecure classes under large variety of operating conditions and credible contingencies. Use of efficient Kohonen's Neural Network (KNN) based pattern classification reduced the computational overhead to a minimum, making the proposed method suitable for real-time usage. Only relevant system attributes (features) were screened, discarding the redundant and irrelevant features without significant loss of information. Gini-Index for feature screening was identified as an efficient method for identification of critical attributes, which are relevant in the context of dynamic security state prediction. An illustrative case-study on IEEE 57-bus power system has been presented in this paper which demonstrated the development and implementation of the proposed KNNSC for real-time DSA. It outperformed other popular classification methods, such as: SVM, MLS, LVQ and PNN, offering shorter training and execution times.

Reference

[1]. C. K. Woo, M. King, A. Tishler, and L. C. H Chow, Costs of electricity deregulation, Energy, Vol. 31, No. 6–7, PP: 747-768, May–June 2006.

[2]. L. Wehenkel, Machine Learning Approaches to Power System Security Assessment, IEEE Intelligent Systems Magazine, Vol 12, No 5, pp: 60 -- 72, October 1997.

[3]. P. Kundur, Power System Stability and Control, McGraw-Hill Education, 1994.

[4]. R. Zhang, Y. Xu, Z. Y. Dong, and K. P. Wong, Post-disturbance transient stability assessment of power systems by a self-adaptive intelligent system, IET Generation, Transmission and Distribution, Vol. 9, No. 3, pp 296–305, 2015.

[5]. M. J. Laufenberg and M. A. Pai, A new approach to dynamic security assessment using trajectory sensitivities, in IEEE Transactions on Power Systems, vol. 13, no. 3, pp. 953-958, Aug. 1998.

[6]. Z. Y. Dong, Y. Xu, P. Zhang and K. P. Wong, Using IS to Assess an Electric Power System's Real-Time Stability, in IEEE Intelligent Systems, vol. 28, no. 4, pp. 60-66, July-Aug. 2013

[7]. K. Sun, S. Likhate, V. Vittal, V. S. Kolluri and S. Mandal, An Online Dynamic Security Assessment Scheme Using Phasor Measurements and Kohonen's Neural Network (KNN) s, in IEEE Transactions on Power Systems, vol. 22, no. 4, pp. 1935-1943, Nov. 2007.

[8]. J. Q. James, D. J. Hill, A. Y.S. Lam, J. Gu, and V. O.K. Li, Intelligent time-adaptive transient stability assessment system, IEEE Transactions on Power Systems, Vol. 33, No. 1, pp 1049-1058, 2017.

[9]. H. D. Chang, C. C. Chu, and G. Cauley, Direct stability analysis of electric power systems using energy functions: Theory, applications, and perspective, Proc. IEEE, Vol. 83, No. 11, pp 1497–1529, Nov 1995.

[10]. S. Morteza, N. Eva Wu, and John S. Bay. Transient stability assessment of large lossy power systems. IET Generation, Transmission & Distribution, Vol. 12, No. 8, pp. 1822-1830, 2018.

[11]. F. A. Rahimi, M. G. Lauby, J. N. Wrubel and K. L. Lee, Evaluation of the transient energy function method for on-line dynamic security analysis, in IEEE Transactions on Power Systems, vol. 8, no. 2, pp. 497-507, May 1993.

[12]. T. Long Vu and K. Turitsyn, Lyapunov Functions Family Approach to Transient Stability Assessment, IEEE Transactions on Power Systems, Vol. 31, No. 2, pp 1269–1277, 2015.

[13]. H. D. Chiang, H Li, and J. Tong, On-Line Transient Stability Screening of a Practical 14,500-Bus Power system: Methodology and Evaluations, High Performance Computing in Power and Energy Systems, pp 335-358, 2013.

[14]. L. Y. Ren, F. Tian, J. F. Yan, Z. H. Yu, F. Su, and T. Wu, Online Application and Fast Solving Method for Critical Clearing Time of Three-Phase Short Circuit in Power System, International journal of Smart grid and Clean Energy, Vol 2, No 1, 2013.

[15]. L. Wehenkel, T. Van Cutsem, and M. Ribbens-Pavella, An artificial intelligence framework for on-line transient stability assessment of power systems, IEEE Power Eng. Rev., Vol. 9, No. 5, pp. 77–78, 1989.

[16]. A. A. Fouad, S. Vekataraman, and J. A. Davis, An expert system for security trend analysis of a stability-limited power system, IEEE Trans. Power Syst., Vol. 6, No. 3, pp. 1077–1084, Aug. 1991.

[17]. M. A. El Sharkawi. Vulnerability Assessment and Control of Power System, IEEE/PES Transmission and Distribution Conference & Exhibition: Asian Pacific, pp 656-660, 2005.

[18]. M. R. Aghamohammadi, F. Mahdavizadeh and R. Bagheri, Power System Dynamic Security Classification Using Kohenen Neural Networks, IEEE/PES Power Systems Conference and Exposition Date of Conference, 2009

[19]. R. Mukherjee and A. De, Development of an Ensemble Kohonen's Neural Network (KNN) -Based Power System Dynamic Security State Predictor, in IEEE Systems Journal, vol. 14, no. 3, pp. 3836-3843, Sept. 2020, doi: 10.1109/JSYST.2020.2978504.

[20]. R. Mukherjee and A. De, Real-time Dynamic Security Analysis of Power Systems using Strategic PMU Measurements and Kohonen's Neural Network (KNN) Classification, Electrical Engineering, Springer, DOI: 10.1007/s00202-020-01118-z, October 2020, Impact Factor: 1.128

[21]. F. Gomez, A. Rajapakse, U. Annakkage, and I. Fernando, Support Vector Machine-Based Algorithm for Post-Fault Transient Stability Status Prediction Using Synchronized Measurements, IEEE Trans. Power Syst., Vol. 26, No. 3, pp. 1474–1483, Aug. 2011.

[22]. I. Kamwa, S. Samantaray, and G. Joos, On the accuracy versus transparency trade-off of data-mining models for fast-response PMU based catastrophe predictors, IEEE Trans. Smart Grid, Vol. 3, No. 1, pp. 152–161, Mar. 2012.

[23]. James, J. Q., et al. Intelligent time-adaptive transient stability assessment system. IEEE Transactions on Power Systems Vol 33, No 1, pp 1049-1058, 2018.

[24]. M. He, J. Zhang, and V. Vittal, A data mining framework for online dynamic security assessment: Kohonen's Neural Network (KNN) s, boosting, and complexity analysis, in Proc. IEEE PES Innovative Smart Grid Technologies, ISGT 2012.

Chapter 24

A Literature Review on High Gain dc-dc Boost Converter

Promit Kumar Saha*, Rituparna Mukherjee , Rituparna Mitra, Suvraujjal Dutta, Susmita Dhar Mukherjee, Aritras Chakraborty

Department of Electrical Engineering, Swami Vivekananda University, Barrackpore, West Bengal

Abstract

The usage of industrial fuels like coal, diesel, nuclear energy, etc. has grown recently. The traditional sources might disappear in the upcoming years. Engineers and researchers are increasingly focusing their attention on non-conventional sources including solar power, fuel cells, batteries, wind power, etc. However, the majority of these sources have an issue with delivering very low and unstable voltage, making them unsuitable for commercial usage. Therefore, connecting the supply to the grid is necessary in order to use these non-traditional sources. PV applications frequently employ dc-dc converters. Numerous researchers published advances in dc-dc converter topologies. This study offers a thorough analysis of current DC-DC converter topologies.

Keywords: High voltage gain dc-dc boost converters, boost converters, magnetic coupling, switched inductors, multi-level, multistage, switched capacitors, and voltage multiplier cells.

Introduction

Today's industries demand dc-dc converters in large quantities. Industrial applications perform better with variable dc sources. For competing power conversion applications, a variety of dc-dc boost converters are offered. These dc-dc converters are well known in unconventional sources and are also widely used in fields like medicine, physics, and the military, among others. In general, boost converters are in great demand in situations where a high dc voltage is needed [1]. This study discusses many methods for attaining greater gain than typically obtained by boost converters based on these requirements. The electrical power magnitude is increased by unconventional energy sources. Power converter topologies are particularly helpful for the next step of power generation since solid fuel produces pollutants. The output voltage of the PV panels ranges from 20 to 60 volts. Dc-dc boost converters are frequently used as an interface between PV panels, an inverter, and a load. For voltage gain in PV panels, a large boost up is needed. About 380 volts are needed for the input of a full bridge inverter [2].

This template, modified in MS Word 2007 and saved as a “Word 97-2003 Document” for the PC, provides authors with most of the formatting specifications needed for preparing electronic versions of their papers. All standard paper components have been specified for three reasons: (1) ease of use when formatting individual papers, (2) automatic compliance to electronic requirements that facilitate the concurrent or later production of electronic products, and (3) conformity of style throughout a conference proceedings. Margins, column widths, line spacing, and type styles are built-in; examples of the type styles are provided throughout this document and are identified in italic type, within parentheses, following the example. Some components, such as multi-leveled equations, graphics, and tables are not prescribed, although the various table text styles are provided. The formatter will need to create these components, incorporating the applicable criteria that follow.

Voltage Boosting Techniques

There are several voltage boosting methods accessible today. These many voltage boosting methods, along with their benefits, drawbacks, and applications, are discussed in this work.

Multistage technique

This method makes use of different converter stages combined in various connections. This approach combines multilayer converter, cascaded, and interleaved approaches. Depending on the underlying approach, the voltage gain of these methods grows exponentially or linearly.

1. Cascaded Converters

Dc-dc converters must have the capacity to flow power in both directions. Regenerative energy may be absorbed and stored in the energy storage system as a result of this characteristic. Additionally, certain applications need an input-output voltage limit that overlaps. When using a cascaded buck-boost converter, a middle inductor is used. In fig. 1, this topology is depicted. An interface inductor is employed in this method between the input and output stages [3].

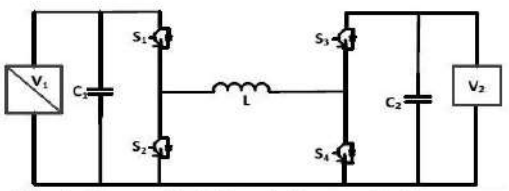

Fig.1 Cascaded Buck Boost Inductor

In electrically powered automobiles, the battery voltage is often substantially lower than the DC bus voltage with a high voltage stage. However, depending on the properties of the battery and the system's architecture, there may be overlap between the battery voltage and the dc bus voltage. The converter must be able to transport the voltage of the output side and the input side with the range of overlap, which is another major issue of the researcher.

System instability during operation may result from the cascaded proportional integral control. Therefore, Mukherjee et al. [4] used a series linked dc-dc topology to preserve the system's stability.

In the literature, the cascaded converters are often divided into three types:

a. Batteries [5–10], fuel cells, and super capacitors [11–12] are a few types of sources used in converters.
b. Many sources, including standalone photovoltaic systems with batteries and solar/wind hybrid energy systems [13]–[16].
c. Variable operating conditions at the same kind of sources in converters can be caused by solar panels that are partially shaded in various ways [17]–[18].

In order to accomplish input voltage sharing (IVS) and output voltage sharing (OVS) for an input series output series (ISOS) converter, Wei et al. [19] introduced the duty cycle-based model predictive control (DC-MPC) approach. Wei et al. also suggested an input series output series type converter using a discrete time optimized model, and the optimized duty cycles for input voltage sharing and output voltage sharing are predicted with a cost function. The suggested method was contrasted with the traditional proportional

integral (PI) controller-based method. The findings show that the suggested duty cycle based MPC approach is superior for input and output voltage sharing because it is easier to use, less expensive, and has better dynamic performance.

The hybrid cascaded dc-dc converter's schematic diagram is shown in Figure 2. A poly phase converter is seen in Fig. 2 with switches and an energy storage device being used to produce each phase, each of which is controlled by a configurable switch. With the aid of switches, the energy storage devices are able to store a little amount of energy from one dc side to the other. The adjustment of single-phase switching action to a poly phase arrangement solves the issue of energy flow interruption [20].

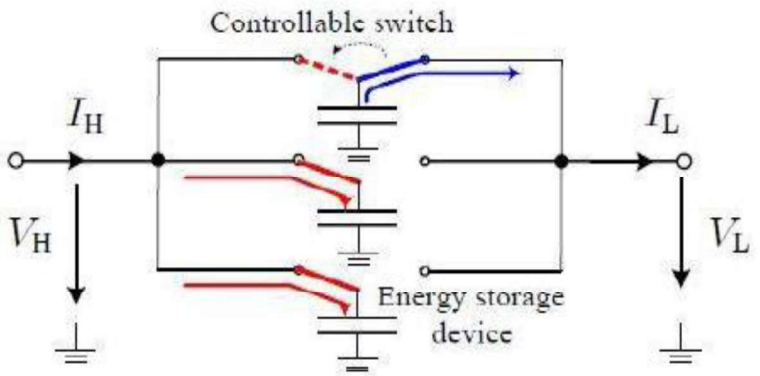

Fig.2HCDC

2. Interleaved Converter

The conventional bidirectional buck-boost (CBB) converter is non-isolated, inexpensive, and of straightforward design. A architecture made up of a linked inductor and a bidirectional buck-boost converter was presented by Chen et al. [21]. The family of soft switching bidirectional converters with high ZVS range was proposed by Mohammadi et al. [22]. Bidirectional dc-dc converters that are not isolated have been covered in [23] through [25].

A revolutionary method was put out by Bahrami.H [26] et al. that reduces ripple current when running high current inductors with soft switching and high VGR on the battery side. This design combines the DAHB converter with interleaved cascaded buck-boost converters. The voltage stress on main switches is lessened and voltage gain is improved in a series connection.

Xuefenget.al [27] describes a High Gain Input-Parallel Output-Series DC/DC Converter with Dual Coupled-Inductors. The voltage multiplier module is another component of this design. For the purpose of splitting the input current and minimizing input current ripple, the main windings of two linked inductors are parallel connected. On the other hand, this converter has all the benefits of interleaved series linked output capacitors, which result in a higher output voltage, fewer output voltage ripples, and reduced switch voltage stress. In order to raise the output voltage, the secondary sides of two linked inductors are additionally connected in series with a regenerative capacitor and a diode. Due to leakage inductance caused by the connected inductors, the active switches turn ONN at zero current, which worsens the diode's reverse recovery issue. Leakage inductance energy may be regenerated in this converter. Hu et al.'s isolated ultra-high step-up dc-dc converter in matrix transformer topology was proposed [28] as a method to increase power and improve fault tolerance utilizing a flyback converter. This enables the capacity for fault tolerance to be increased. Reduced voltage stress on the switching element and transformer size is now easily achievable thanks to technology.

Prabhala et al. [29] suggested a high voltage gain dc-dc converter with two input boost stages. It's based on a Dickson Charge Pump [20]. Voltage multiplier cells are used to boost voltage gain. The voltage gain is determined by the number of stages and the input stage's duty cycle.

Zhang et al. [30] suggested a bidirectional interleaved switching capacitor dc-dc converter with a broad voltage range for energy storage systems. In this method, an interleaved structure is applied to the LV side to reduce current ripples. Similarly, a series-connected arrangement is used on the HV side of the converter to achieve voltage gain. These converters are also quite efficient.

3. Multilevel Converter

The voltage source converter-based high voltage direct current system is gaining popularity as the HVDC system grows in popularity. When compared to thyristor-based HVDC systems, voltage source converter-based HVDC offers greater advantages. It has active and reactive power control, a black start converter, a high output voltage and current with no ripple, and a high output voltage and current with no ripple. These converters also have several drawbacks, like as switching losses and a lower fault tolerant capability to dc side faults. Multilevel converters have been proposed to address all of these issues [31-37]. Because of its low dv/dt, low harmonics, scalability, and flexibility, the modular multilevel converter is gaining popularity among these converters. It has reduced switching losses as well.

Because fault tolerant capability is more significant in converters, fault tolerant multilevel converters for HVDC applications have received a lot of attention. These topologies employ a complete bridge submodule. As a result, this architecture makes extensive use of semiconductor switches. Mathew et al. [38] provide a generalised cross-connected submodule with fewer switches that has the same properties as the FBSM depicted in Fig.3.

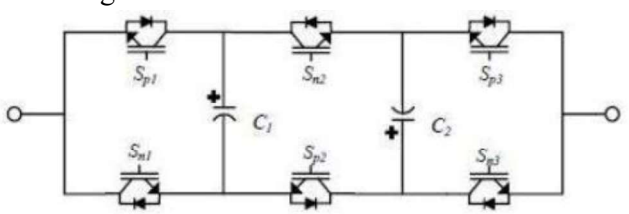

Fig.3 5 level X-SM structure

4. Switched Capacitor (Charge pump)

Non-conventional sources, such as solar and fuel cells, prefer a low voltage range for operation, whereas grid-tied systems require a high voltage range. These high voltage ranges have an effect on efficiency. To address the poor efficiency issue, Das et al [39] suggested a unique high voltage gain with high efficiency dc-dc converter based on a linked inductor, intermediate capacitor, and leaky energy recovery mechanism. To reduce losses, the converter's input energy is losslessly stored in a linked inductor and intermediate capacitor.

As the name (n/m) X converter, a variation Dickson converter is offered [40]. This arrangement can provide the desired voltage gain while being very efficient.

Many more advantages and disadvantages of switched capacitor-based converters have been described in [41-43]. Dickson-based converters outperform switched capacitor-based converters in terms of performance [44].

Figure 4 depicts the (n/m) X converter, which is developed from a common structure of (k/m) X. This converter has n arms and n legs, resulting in a total of 2n limbs. Each arm is equipped with a series combination of two capacitors [45].

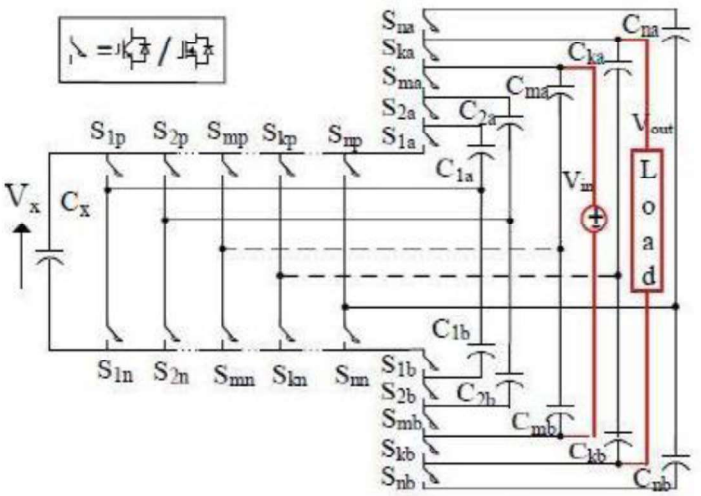

Fig.4 A generic (k/m) X Converter

5. Voltage Multiplier technique

400 V DC supply systems are becoming increasingly common due to their superior efficiency, greater dependability, and lower cost as compared to alternating current supply systems [46]-[49]. The finest examples of dc distribution systems are telecommunications, data communications, commercial and residential [50]-[52]. The most difficult task in dc supply systems or dc distribution systems is dc-dc converters for 400 V systems. PV panels have a DC voltage range of 20 to 40 volts. A large duty ratio is necessary to increase these voltages, which leads in severe voltage stress on components, voltage ripples, and low efficiency.

To address these issues, [53]-[56] suggested topologies for dc-dc boost converters followed by voltage multiplier cells. Table I compares several converters based on the number of components, voltage gain, and voltage stress on switches using this approach.

Bin et al. [53] suggested a hybrid converter with good voltage gain but low output voltage as compared to its own VM circuit. It also has a significant ripple in the input current. Table 1 compares various converters based on voltage gain and components employed. The table was created by combining topologies from the literatures [53]-[56].

Table 1: Comparison of different converters

Topology	[53]	[54]	[55]	[56]
No of Switches	1	1	2	2
No of Inductors	1	1	2	2
No of Capacitors	4	3	3	3
No of Diodes	4	3	3	4
Vout/Vin	$\frac{3-D}{1-D}$	$\frac{2}{1-D}$	$\frac{3+D}{1-D}$	$\frac{1}{D(1-D}$
Vswitch/vout	$\frac{1}{3-D}$	$\frac{1}{2}$	$\frac{1}{3+D}$	(1-D)D
Input Current	Discontinuous	Continuous	Discontinuous	Continuous

Gang et al. [54] presented switching capacitor-based converters that enhance low voltage in relation to component count. YU et al. [55] propose a switched capacitor base converter that generates ripples. Input current is presented in a discontinuous fashion. Rosas-Caroet al. [56] developed a transformer-less converter that provides continuous input current but causes excessive stress in switches with voltages more than two-thirds of the voltage. Baddipadiga et al. [57] developed a novel converter topology with a two-phase interleaved boost converter on the input side and a 400 Dickson charge pump-based voltage multiplier on the output side.

This converter is best suited for a 400 V dc bus. This converter can also extract electricity from a single source as well as two separate sources. Because of the low voltage rating of VM capacitors, the size of these converters is reduced.

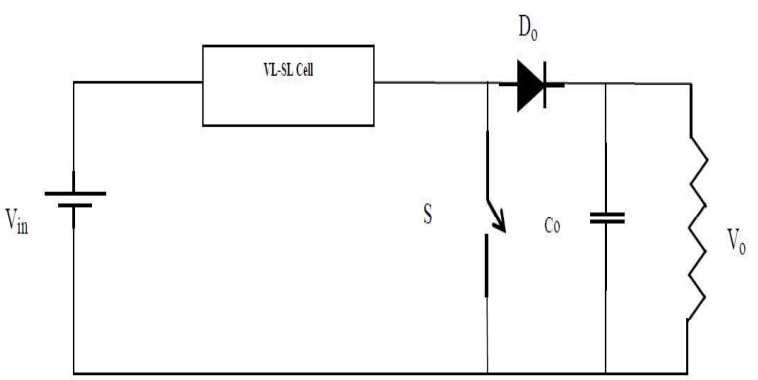

Fig.5 Voltage Lift Technique

6. Switched Inductor and Voltage Lift technique

Voltage lift is one of the better and accepted methods or techniques for boosting the output voltage in a dc-dc boost converter. In this approach, a capacitor is charged to a specific value by the source voltage. Following that, the output voltage is increased by the voltage of the charged capacitor. The voltage level may be boosted further by adding additional capacitors. When two capacitors are employed, the method is known as re-lift; when three capacitors are used, it is known as triple lift; and similarly, quadruple-lift technique [58]. Based on this technology, Luo et al [59] presented various boost converters. Voltage Lift method has been utilised with Zeta, Cuk, and SEPIC converters [60]. Figure 5 depicts the basic basis of the VL method.

7. Magnetic Coupling

Magnetic coupling is the most often used boosting technique. It may function as a non-isolated or isolated dc-dc converter. Some coupled-inductor based dc-dc converters have been devised to provide independence from the switch duty cycle complexity [61]-[68]. High voltage spikes arise on the device as a result of linked inductor leakage inductance.

It also causes significant energy losses. RCD snubbers can be used to manage voltage fluctuation, current, and clamp voltage overshoot. RCD snubbers are made up of a resistor, a capacitor, and a diode. In this instance, leakage energy is still squandered, hence these converters are also proposed [65]-[66]. In this situation, the number of switches grows, increasing the circuit's complexity. Wai and colleagues [67] presented a passive regenerating snubber. This converter has a larger voltage gain than other coupled inductor converters. Khalizadeh et al. developed a converter with a single switch employing a three-winding coupled inductor in the same channel. The inductor's leakage energy may be utilised in this converter, and the diode's reverse recovery difficulty can be alleviated. This converter is intended for maximum voltage gain while maintaining a high-power density and efficiency. It is made up of one switch and two voltage multiplier cells. It also has two regenerative snubbers for high voltage conversion, recycling stray inductance energy, and decreasing voltage spikes.

3 Comparison of Different Techniques

Voltage Boosting Technique	**Advantages**	**Disadvantages**	**Appropriate applications**
Switched Capacitor (Charge Pump)	Cheap, Light weight, Small size, high power density and Fast response.	Comparatively complicated modulation, Sensitive to the ESR of capacitors and Lack of output voltage regulation.	Energy accumulation, Mobile displays (AMOLED), Automotive and vehicular applications and High gain dc-dc applications.
Voltage Multiplier	High voltage capability topology, Cell based structure, and also it can be integrated to various converters.	High voltage stress on components, and need several cells for high voltage applications.	X-ray, laser, Military, plasma research and particle accelerator.

Switched Inductor and Voltage Lift	High boost ability, and biddable in many converters.	Need more passive elements, and not suitable for high power applications.	Mid-range dc-dc converters and High gain dc-dc applications.
Magnetic Coupling	High design freedom, Versatile in boost ability due to tunable, turns ratio of magnetic coupling, Switch can be implemented at the low voltage side help to reduce conduction losses and High efficiency in soft switched type.	Negative effects of leakage inductance, High voltage spike, and Relatively bulky.	High power/voltage DC supply, High voltage applications (military, physics), DC micro grids, Telecommunication and data centers, Bidirectional (FC, PV, UPS, P-EV, H-EV, V2G), Regenerative (elevator, tram/trolleybus), and Avionic and space.

Conclusion

This work includes a literature review of several dc-dc converter topologies that have been studied in major international publications such as IEEE, IET, SCI, and many more. These converters were investigated in order to gain a better grasp of converter techniques and uses. This research also reveals the optimal converter topology for high voltage gain, low ripples, and good efficiency. These converters are used in solar PV, electric vehicles, and other applications. Many of these converters have been evaluated using real-time and hardware simulators. These are also being tried with applications such as solar and electric vehicles.

References

[1] M. Forouzesh, Y. P. Siwakoti, S. A. Gorji, F. Blaabjerg and B. Lehman, "A survey on voltage boosting techniques for step-up DC-DC converters," 2016 IEEE Energy Conversion Congress and Exposition (ECCE), Milwaukee, WI, 2016, pp. 1-8.

[2] Revathi, B. S., &Prabhakar, M. (2016). Non isolated high gain DC-DC converter topologies for PV applications–A comprehensive review. Renewable and Sustainable Energy Reviews, 66, 920-933.

[3] A Ahmed, M. A. Khan, M. Badawy, Y. Sozer and I. Husain, "Performance analysis of bi-directional DC-DC converters for electric vehicles and charging infrastructure," 2013 IEEE Energy Conversion Congress and Exposition, Denver, CO, 2013, pp. 1401-1408.

[4] N. Mukherjee and D. Strickland, "Control of Cascaded DC–DC Converter-Based Hybrid Battery Energy Storage Systems—Part I: Stability Issue," in IEEE Transactions on Industrial Electronics, vol. 63, no. 4, pp. 2340-2349, April 2016.

[5] Kanchanaharuthai, A.; Chankong, V.; Loparo, K.A., "Transient Stability and Voltage Regulation in Multimachine Power Systems Vis-à-Vis STATCOM and Battery Energy Storage," IEEE Trans. Power Syst., vol.30, no.5, pp.2404-2416, Sept. 2015.

[6] Serban, I.; Teodorescu, R.; Marinescu, C., "Energy storage systems impact on the short-term frequency stability of distributed autonomous microgrids, an analysis using aggregate models," IET Renew. Power Gener, vol.7, no.5, pp.531-539, Sept. 2013.

[7] Mithulananthan, N.; Shah, R.; Lee, K.Y., "Small-Disturbance Angle Stability Control With High Penetration of Renewable Generations," IEEE Trans. Power Syst., vol.29, no.3, pp.1463-1472, May 2014

[8] Ortega, A.; Milano, F., "Generalized Model of VSC-Based Energy Storage Systems for Transient Stability Analysis," IEEE Trans. Power Syst., vol. PP, no.99, pp.1-12, 2015 (in Press).

[9] Bazargan, D.; Filizadeh, S.; Gole, A.M., "Stability Analysis of Converter-Connected Battery Energy Storage Systems in the Grid," IEEE Trans. Sustain. Energy, vol.5, no.4, pp.1204-1212, Oct. 2014.

[10] Lu, X.; Sun, K.; Guerrero, J.M.; Vasquez, J.C.; Huang, L., "State-of-Charge Balance Using Adaptive Droop Control for Distributed Energy Storage Systems in DC Microgrid Applications," IEEE Trans. Ind. Electron., vol.61, no.6, pp.2804-2815, June 2014.

[11] Inthamoussou, F.A.; Pegueroles-Queralt, J.; Bianchi, F.D., "Control of a Supercapacitor Energy Storage System for Microgrid Applications," IEEE Trans. Energy Convers., vol.28, no.3, pp.690-697, Sept. 2013.

[12] Bostrom, A.; von Jouanne, A.; Brekken, T.K.A.; Yokochi, A., "Supercapacitor energy storage systems for voltage and power flow stabilization," in Proc. 1st IEEE Conf. on Technologies for Sustainability (SusTech), vol., no., pp.230-237, 1-2 Aug. 2013.

[13] Wandhare, R.G.; Agarwal, V., "Novel Stability Enhancing Control Strategy for Centralized PV-Grid Systems for Smart Grid Applications," IEEE Trans. Smart Grid., vol.5, no.3, pp.1389-1396, May 2014.

[14] Kamel, R.M.; Chaouachi, A.; Nagasaka, K., "Three Control Strategies to Improve the Microgrid Transient Dynamic Response During Isolated Mode: A Comparative Study," IEEE Trans. Ind. Electron., vol.60, no.4, pp.1314-1322, April 2013.

[15] Massing, J.R.; Stefanello, M.; Grundling, H.A.; Pinheiro, H., "Adaptive Current Control for Grid-Connected Converters WithLCL Filter," IEEE Trans. Ind. Electron., vol.59, no.12, pp.4681-4693, Dec. 2012.

[16] Mohamed, Y. A -R I, "Mitigation of Converter-Grid Resonance, Grid-Induced Distortion, and Parametric Instabilities in Converter-Based Distributed Generation," IEEE Trans. Power Electron., vol.26, no.3, pp.983-996, March 2011.

[17] Walker, G.R.; Sernia, P.C., "Cascaded DC-DC converter connection of photovoltaic modules," IEEE Trans. Power Electron., vol.19, no.4, pp.1130-1139, July 2004

[18] Bratcu, A.I.; Munteanu, I.; Bacha, S.; Picault, D.; Raison, B., "Cascaded DC–DC Converter Photovoltaic Systems: Power Optimization Issues," IEEE Trans. Ind. Electron., vol.58, no.2, pp.403-411, Feb. 2011.

[19] Q. Wei, B. Wu, D. Xu and N. R. Zargari, "Model Predictive Control of Capacitor Voltage Balancing for Cascaded Modular DC–DC Converters," in IEEE Transactions on Power Electronics, vol. 32, no. 1, pp. 752-761, Jan. 2017.

[20] J Yang, Z. He, H. Pang and G. Tang, "The Hybrid-Cascaded DC–DC Converters Suitable for HVdc Applications," in IEEE Transactions on Power Electronics, vol. 30, no. 10, pp. 5358-5363, Oct. 2015.

[21] G Chen, Y. Deng, L.Chen, Y.Hu, L.Jiang, X. He, and Yousheng Wang, ―A Family of Zero-Voltage-Switching Magnetic Coupling Non-isolated Bidirectional DC-DC Converters, ― IEEE Trans. Ind. Electron., vol. 64, no. 8, pp. 6223 - 6233, Aug. 2017.

[22] M R. Mohammadi , and H. Farzanehfard ,‖ Family of Soft Switching Bidirectional Converters with Extended ZVS Range,― IEEE Trans. Ind. Electron., vol. 64, no. 9, pp. 7000-7008, Sept. 2017.

[23] C c. Lin , L. s. Yang , and G.W. Wu ,‖ Study of a non-isolated bidirectional DC-DC converter,― IET. Power Electron., vol. 6, no. 1, pp. 1755-4535, Jan. 2013.

[24] H Ardi , R. R. Ahrabi , and S. N. Ravadanegh , ― Non-isolated bidirectional DC–DC converter analysis and implementation, ― IET. Power Electron., vol. 7, no. 12, pp. 3033 - 3044, Dec. 2014.

[25] H Ardi , A. Ajami , F. Kardan , and S. N. Avilagh ,‖Analysis and Implementation of a Nonisolated Bidirectional DC–DC Converter With High Voltage Gain, ― IEEE Trans. Ind. Electron., vol. 63, no. 8, pp. 4878 - 4888, Aug. 2016.

[26] H Bahrami, S. Farhangi, H. Iman-Eini and E. Adib, "A New Interleaved Coupled-Inductor Nonisolated Soft-Switching Bidirectional DC–DC Converter With High Voltage Gain Ratio," in IEEE Transactions on Industrial Electronics, vol. 65, no. 7, pp. 5529-5538, July 2018

[27] X Hu and C. Gong, "A High Gain Input-Parallel Output-Series DC/DC Converter With Dual Coupled Inductors," in IEEE Transactions on Power Electronics, vol. 30, no. 3, pp. 1306-1317, March 2015.

[28] Y Hu, R. Zeng, W. Cao, J. Zhang and S. J. Finney, "Design of a Modular, High Step-Up Ratio DC–DC Converter for HVDC Applications Integrating Offshore Wind Power," in IEEE

[29] V. A. K. Prabhala, P. Fajri, V. S. P. Gouribhatla, B. P. Baddipadiga and M. Ferdowsi, "A DC–DC Converter With High Voltage Gain and Two Input Boost Stages," in IEEE Transactions on Power Electronics, vol. 31, no. 6, pp. 4206-4215, June 2016.

[30] Y. Zhang, Y. Gao, J. Li and M. Sumner, "Interleaved Switched-Capacitor Bidirectional DC-DC Converter With Wide Voltage-Gain Range for Energy Storage Systems," in IEEE Transactions on Power Electronics, vol. 33, no. 5, pp. 3852-3869, May 2018.

[31] M. Bahrman and B. Johnson, ―The ABCs of HVDC transmission technologies,‖ IEEE Power and Energy Magazine, vol. 5, no. 2, pp. 32–44, 2007.

[32] N. Flourentzou, V. Agelidis, and G. Demetriades, ―VSC-based HVDC power transmission systems: an overview,‖ IEEE Trans. on Power Electron., vol. 24, no. 3, pp. 592–602, 2009.

[33] B. Gemmell, J. Dorn, D. Retzmann, and D. Soerangr, ―Prospects of multilevel VSC technologies for power transmission,‖ in Proc. IEEE Transmission and Distribution Conf. and Expo., pp. 1–16, 2008.

[34] S. Kouro, M. Malinowski, K. Gopakumar, J. Pou, L. Franquelo, B. Wu, J. Rodriguez, M. Perez, and J. Leon, ―Recent advances and industrial applications of multilevel converters,‖ IEEE Trans. on Ind. Electron., vol. 57, no. 8, pp. 2553–2580, 2010.

[35] J. Candelaria and J.-D. Park, ―VSC-HVDC system protection: a review of current methods,‖ in Proc. IEEE Power Systems Conf. and Expo.,pp. 1–7, 2011.

[36] J. Yang, J. Zheng, G. Tang, and Z. He, ―Characteristics and recovery performance of VSC-HVDC transmission line fault,‖ in Proc. Asia Pacific Power and Energy Eng. Conf., pp. 1–4, 2010.

[37] A. Lesnicar and R. Marquardt, ―An innovative modular multilevel converter topology suitable for a wide power range,‖ in Proc. IEEE Power Tech Conference, vol. 3, June 2003.

[38] E. C. Mathew, M. B. Ghat and A. Shukla, "A Generalized Cross-Connected Submodule Structure for Hybrid Multilevel Converters," in IEEE Transactions on Industry Applications, vol. 52, no. 4, pp. 3159-3170, July-Aug. 2016.

[39] M. Das and V. Agarwal, "Design and Analysis of a High-Efficiency DC–DC Converter With Soft Switching Capability for Renewable Energy Applications Requiring High Voltage Gain," in IEEE Transactions on Industrial Electronics, vol. 63, no. 5, pp. 2936-2944, May 2016.

[40] Singer, Z.; Emanuel, A.; Erlicki, M.S., "Power regulation by means of a switched capacitor," in Electrical Engineers, Proceedings of the Institution of , vol.119, no.2, pp.149-152, February 1972

[41] Singer, Z.; Emanuel, A.; Erlicki, M.S., "Power regulation by means of a switched capacitor," in Electrical Engineers, Proceedings of the Institution of , vol.119, no.2, pp.149-152, February 1972

[42] Tse, C.K.; Wong, S.C.; Chow, M.H.L., "On lossless switched-capacitor power converters," in Power Electronics, IEEE Transactions on , vol.10, no.3, pp.286-291, May 1995

[43] Makowski, M.S.; Maksimovic, D., "Performance limits of switched-capacitor DC-DC converters," in Power Electronics Specialists Conference, 1995. PESC '95 Record., 26th Annual IEEE , vol.2, no., pp.1215-1221 vol.2, 18-22 Jun 1995

[44] M. D. Seeman and S. R. Sanders, "Analysis and Optimization of Switched-Capacitor DC-DC Converters," Computers in Power Electronics, 2006. COMPEL '06. IEEE Workshops on, Troy, NY, 2006, pp. 216-224.

[45] [45] D. Gunasekaran, L. Qin, U. Karki, Y. Li and F. Z. Peng, "A Variable (n/m)X Switched Capacitor DC–DC Converter," in IEEE Transactions on Power Electronics, vol. 32, no. 8, pp. 6219-6235, Aug. 2017.

[46] V. A. K. Prabhala, B. P. Baddipadiga, and M. Ferdowsi, "DC distribution systems - An overview," in Renewable Energy Research and Application (ICRERA), 2014 International Conference on, 2014, pp. 307-312.

[47] G. AlLee and W. Tschudi, "Edison Redux: 380 Vdc Brings Reliability and Efficiency to Sustainable Data Centers,"Power and Energy Magazine, IEEE, vol. 10, pp. 50-59, 2012.

[48] V. Sithimolada and P. W. Sauer, "Facility-level DC vs. typical ac distribution for data centers: A comparative reliability study," in TENCON 2010 - 2010 IEEE Region 10 Conference, 2010, pp. 2102-2107.

[49] S. M. Lisy, B. J. Sonnenberg, and J. Dolan, "Case study of deployment of 400V DC power with 400V/-48VDC conversion," in Telecommunications Energy Conference (INTELEC), 2014 IEEE 36th International, 2014, pp. 1-6.

[50] A. Fukui, T. Takeda, K. Hirose, and M. Yamasaki, "HVDC power distribution systems for telecom sites and data centers," in Power Electronics Conference (IPEC), 2010 International, 2010, pp. 874-880.

[51] D. J. Becker and B. J. Sonnenberg, "DC microgrids in buildings and data centers," in Telecommunications Energy Conference (INTELEC), 2011 IEEE 33rd International, 2011, pp. 1-7.

[52] E. Rodriguez-Diaz, M. Savaghebi, J. C. Vasquez, and J. M. Guerrero, "An overview of low voltage DC distribution systems for residential applications," in Consumer Electronics - Berlin (ICCE-Berlin), 2015 IEEE 5th International Conference on, 2015, pp. 318-322.

[53] W. Bin, L. Shouxiang, L. Yao, and K. M. Smedley, "A New Hybrid Boosting Converter for Renewable Energy Applications," Power Electronics, IEEE Transactions on, vol. 31, pp. 1203-1215, 2016.

[54] W. Gang, R. Xinbo, and Y. Zhihong, "Nonisolated High Step-Up DC-DC Converters Adopting Switched-Capacitor Cell," Industrial Electronics, IEEE Transactions on, vol. 62, pp. 383-393, 2015.

[55] T. Yu, W. Ting, and H. Yaohua, "A Switched-Capacitor-Based Active-Network Converter With High Voltage Gain," Power Electronics, IEEE Transactions on, vol. 29, pp. 2959-2968, 2014.

[56] J. C. Rosas-Caro, F. Mancilla-David, J. C. Mayo-Maldonado, J. M. Gonzalez-Lopez, H. L. Torres-Espinosa, and J. E. Valdez-Resendiz, "A Transformer-less High-Gain Boost Converter With Input Current Ripple Cancelation at a Selectable Duty Cycle," Industrial Electronics, IEEE Transactions on, vol. 60, pp. 4492-4499, 2013.

[57] B. P. Baddipadiga and M. Ferdowsi, "A high-voltage-gain dc-dc converter based on modified dickson charge pump voltage multiplier," in IEEE Transactions on Power Electronics, vol. 32, no. 10, pp. 7707-7715, Oct. 2017.

[58] F. L. Luo and H. Ye, Advanced DC-DC Converters: crc Press, 2003.

[59] L. Fang Lin, "Luo-converters, voltage lift technique," in Proc. IEEE PESC, 1998, pp. 1783-1789 vol.2.

[60] E. H. Ismail, M. A. Al-Saffar, A. J. Sabzali, and A. A. Fardoun, "A family of single-switch PWM converters with high step-up conversion ratio," IEEE Trans. Cir. and Sys. I: Reg. Papers, vol. 55, pp. 1159-1171, 2008.

[61] W. H. Li and X. N. He, ― Review of non-isolated high step-up DC/DC converters in photovoltaic grid-connected applications,‖ IEEE Trans. Ind. Electron., vol. 58, no. 4, pp. 1239–1250, Apr. 2011.

[62] Y. P. Hsieh, J. F. Chen, T. J. Liang, and L. S. Yang, ―Analysis and implementation of a novel single-switch high step-up DC-DC converter,‖ IET Power Electronics, vol. 5, lss. 1, pp. 11-21, Jan. 2012.

[63] Tseng, Kuo-Ching, Jang-Ting Lin, and Chi-Chih Huang. "High step-up converter with three-winding coupled inductor for fuel cell energy

[64] source applications." IEEE Transactions on Power Electronics, vol 30, no. 2: 574-581, 2015.

[65] X.F.Hu, G.R.Dai, L.Wang, C.Y.Gong, ―A Three-state switching boost converter mixed with magnetic coupling and voltage multiplier techniques for high gain conversion,‖ IEEE Transactions on Power Electronics, vol 31, no. 4: 2991-3001,2016.

[66] T. F. Wu, Y. S. Lai, J. C. Hung, and Y. M. Chen, ―Boost converter with coupled inductors and buck–boost type of active clamp,‖ IEEE Trans. Ind. Electron., vol. 55, no. 1, pp. 154-162, Jan. 2008.

[67] Y. Zhao, W. H. Li, and X. N. He, ―Single-phase improved active clamp coupled-inductor-based converter with extended voltage doubler cell,‖ IEEE Trans. Power Electron., vol. 27, no. 6, pp.2869-2878. Jun. 2012.

[68] R. J. Wai, and R. Y. Duan, ―High step-up converter with coupled-inductor,‖ IEEE Trans. Power Electron., vol. 20, no. 5, pp. 1025-1035, Sep. 2005.

[69] Mohammad Khalilzadeh, KarimAbbaszadeh, ―Non-isolated high step-up DC–DC converter based on coupled inductor with reduced voltage stress,‖ IET Power Electronics. Vol. 8, Iss. 11, pp. 2184–2194, May.2015.

Chapter 25

A Review on Application of Solar Energy in Agriculture Sector

Promit Kumar Saha*, Rituparna Mukherjee , Suvraujjal Dutta, Rituparna Mitra, Avik Datta Titas Kumar Nag
Department of Electrical Engineering, Swami Vivekananda University, Barrackpore, West Bengal

Abstract
In nations like India, solar energy that strikes the earth is wasted. The world's future energy requirements are expected to be met if 1% of the solar radiation that is received can be converted into energy. In addition to solar radiation, India's extensive agricultural sector provides food for the majority of people on the planet. The Indian government has taken steps to encourage the use of solar energy while minimizing the use of non-renewable resources. The current study investigates several developments in solar energy utilization in Indian agriculture, which may be used to minimize the use of power from non-conventional sources, which is both expensive and environmentally destructive. The current study indicates that more investigation is required to increase the applicability and efficacy of solar power consumption for long-term use**.**

Keywords: Agriculture, Farmers, India, Renewable, Solar Energy

Introduction

The primary means of human nutrition is agriculture. However, the destruction of the environment has been brought about by the use of various energy production sources, including coal power plants, vehicles, and agricultural practises such stubble burning and fertiliser use. It has been anticipated that non-renewable resources may run out soon, forcing the creation of ecologically friendly renewable resources. A significant amount of power is also required by agricultural fields in order to irrigate, run tractors, and complete other crop-related tasks[1].

Solar energy is the greatest of the renewable energy sources since it can be used for a range of agricultural applications. Other renewable energy sources include wind, hydro, tidal, geothermal, and biomass energy. The use of renewable energy sources is supported by several academics and scientists fighting climate change and global warming, and they are striving to raise awareness of them. The burning of fossil fuels and other activities that cause pollution are a factor in climate change and global warming. These energy sources generate greenhouse gases, which can absorb solar radiation and raise the earth's temperature. Energy generation poses a number of challenges for developing countries like India. In India, there are more than 50% of families without access to electricity. More individuals are becoming aware of the advantages of using solar energy to do their daily duties as the population of the globe increases and global temperatures rise. Power consumption is increasing while power production is declining.

In the next years, more energy will be needed to irrigate the crops. Many fields have dried up as a result of low ground water levels and a lack of electricity to pump underground water. The dependence on the monsoon is increasing, but this is because of the delays in precipitation brought on by climate change and global warming. Agriculture generally uses electricity for irrigation purposes. In dry places that depend mostly on rainfall, solar panels might help enhance production[2–6].

2 Benefits of Solar Energy

The best and most abundant source of energy is the sun. Solar energy is a source of clean, renewable energy that derives from the sun and is discharged as heat and light. Modern technology makes it possible to use solar energy. Solar energy may be captured via solar panels, solar photovoltaic, solar heating, and solar cooking. The use of solar energy in agriculture might contribute to the growth of sustainable farming. In order to increase agricultural output, several countries are currently integrating solar energy into their farming practises. The Indian government has started a number of initiatives, including the Rooftop PV and Small Solar Power Generation Programme (RPSSGP) for farmers and the Jawaharlal Nehru National Solar Mission (JNNSM). However, these programmes are unknown to Indian farmers [5]. The majority of equipment is now fuelled by solar energy rather than traditional fuels like diesel, petrol or oil in many countries. Here is a quick explanation of a few of the technologies:

A. Pumps for Water

Diesel-powered water pumps are used by farmers in India to irrigate their crops. They use water pumps that are driven by diesel, petrol or oil to pump water from wells or open dams for a range of agricultural uses. Different irrigation techniques are being used by nations including the United States, Europe, France, Germany, China, Finland, Canada, and India. Different solar water pumping systems include motor pumps, switches, solar panels, and tracking systems. These solar pumps are more affordable, consume less energy, and emit less greenhouse gases. The KUSUM programme was started by the Rajasthan government in India, and it proposed that these fields produce power for $3.14 per kWh. According to the World Bank, solar power is preferable in certain countries in terms of operation, finances, and environmental considerations, while some nations are yet ignorant of the benefits given by solar power.

B. Dryers Solar

Dehydrators powered by petrol or diesel are used by farmers to dry their harvests before packing and transporting them to storage facilities. A few farmers dry their crops using solar energy, which is economical and good for the environment. A solar energy collector, drying tracks, and a shelter make up a solar dryer. Farmers dry their crops by blowing hot air that circulates over a solar-powered fan.

C. Solar Mower

Many farmers use solar-powered mowers to cut grass or crops in the same manner they would with traditional mowers. Mowers fuelled by diesel are more environmentally damaging than those driven by solar energy. Electric circuits, DC motors, blades, and three wheels are all components of solar lawn mowers, along with a solar panel that charges the battery.

D. Solar Tractors

Tractors are crucial agricultural equipment that may be found on practically every farm. Tractors are generally fuelled by diesel or petrol; however, some scientists and researchers have mounted solar panels on the roofs of tractors to allow these panels to get the maximum sunlight, allowing these massive tractors to run on solar power. The combination of solar panels and lithium batteries is transforming agriculture. These tractors can

be powered directly or indirectly by solar energy; some run-on lithium batteries that are charged by solar panels, while others have top-mounted solar panels that can either drive the tractor or charge the batteries while it is operating.

E. Solar Greenhouses

Greenhouses are used in a number of areas, and the crops grown in them require heat. Solar panels installed on these residences provide enough heat to benefit crops and boost output. These green structures are used in the winter to allow crops to be grown despite the harsh weather. The sun powers these solar greenhouses, which also incorporate solar energy heaters for illumination and warmth. These greenhouses help farmers grow fruits and vegetables out of season by maintaining a pleasant temperature.

F. Solar Water and Space Heaters

Farmers use space and water heaters to maintain the animals at a suitable temperature. In these heaters, solar power is employed to convert sunlight into heat energy. The poultry and pig sectors have several hurdles in terms of delivering heat and food while also preserving animal earnings. These solar water and space warmers are needed to replace the detrimental dust and hazardous gases that are emitted by crops and plants. These heaters may also sterilise and disinfect many sorts of equipment.

G. Solar Electric Fences

Crops and flora are ravaged by animals such as cows, elephants, and buffalos. Farmers all across the world use various forms of fencing to secure their crops. A solar-powered fence is constructed up of solar panels that give electricity to the wires, and any animal or creature that comes into touch with the barrier receives an electric shock, avoiding crop damage.

H. Solar Pumping System

Photovoltaic (PV) panels are used to irrigate agricultural fields since they only need a little quantity of energy to carry out different operations. The energy generated by the PV panels may be used for a variety of different tasks, such as storing crops, fruits, and vegetables, or spraying pesticides. PV systems are not suitable for sectors that need a high level of power input, such as rice mills or agricultural operations. Solar panels, submersible pumps, solar charge controllers, and batteries make up simple solar pumping systems.

I. Solar Panel

Solar panels are made up of semiconductor-based solar cells. The fundamental function of these solar cells is to convert the solar energy that falls on them into direct current (DC) electrical power. Both the number of cells and the load rating are directly related. The number of solar cells must be raised as the load increases. One of the most major drawbacks of solar panels is that they must be oriented to the sun's angle in order to

produce the optimum amount of energy.

J. Submersible Pump

It is a type of pump that is sunk deep inside the well, either up to the groundwater level or where a natural stream of water exists. The size and power of the pump are determined by the depth of the well as well as the available ground water level.

Importance of Renewal Energy for Agricultural Farm

Several studies in the literature have demonstrated the significance of mixing renewable energy with agricultural productivity. As solar energy technology applications, crop and grain drying, room and heating systems, greenhouse heating, photovoltaic solar systems, and irrigation water pumps were all examined. The solar panel/photovoltaic (PV) system has been considered as the best alternative in agricultural operations, particularly in remote rural areas, because it is inexpensive to maintain, has minimal environmental impact, and can be used for a number of applications. This claim was supported by Qoaider and Steinbrecht, who investigated the economic feasibility of PV technologies in providing irrigation energy requirements in remote agricultural communities in rural desert areas with the goal of allowing farmers to reduce the high cost of generating electricity from diesel. This innovative energy technology strategy will be critical in steering the region's long-term growth. It is constructed hypothetically, giving estimates of the life cycle cost (LCC) of a PV device capable of meeting the entire community's energy demands. This solar panel generator can pump around 111,000 m^3 of lake water each day, enough to irrigate 1,260 hectares of land and power the neighbouring residents' houses. By comparing the efficiency of a solar panel system generator to that of a diesel generator [7].

Litterature Review

Bardi et al. investigated if farmers might move from fossil fuels to renewable green energy sources, which could improve the quality and quantity of food processed on a variety of farms. It may also supply power for agricultural equipment such as road hauling and field research. Only a few agricultural equipment operators are now aware of the issues posed by fossil fuel depletion and global warming. This is the source of the climate change problem. Unless farmers' views change, the problem will intensify. Growers should also use energy-saving equipment and the PV system to optimise land since it is cost-effective and can be utilised for a number of purposes [8].

Dupraz and colleagues explored the most effective strategies for transforming solar radiation into energy and agriculture. It is sometimes referred to as photovoltaic (PV) or agro-photovoltaic (APV) farming, and it is a natural solution to agriculture's lack of renewable energy. By lifting the solar panels to a height of 2 metres above the ground, this technique was designed to increase the crops' mild shadow. Climate, water availability, and energy supply are all factors that impact agricultural expansion. As a result, in order to maximise agricultural output and enhance land utilisation, modern technology must be paired with creative economic efficiency farming practises and the optimal use of limited land resources with little environmental damage. The DC energy from the solar panel is transmitted to the battery. This DC electricity from the battery is received by the converter and converted to AC power. AC electricity is used to power the ventilation systems in the greenhouse, which create heat or regulate temperature [9].

To maintain the indoor greenhouse, Maher et al. suggested a greenhouse model with a fuzzy-based management system. 2021 Copyright. Publications based on cutting-edge research. All rights are reserved. Induction motors, heating systems, and other components are used in the environment for ventilation, heating, humidification, and dehumidification applications for long-term greenhouse agricultural production with effective climate management for higher output. According to their findings, both the fuzzy controller and the PV generator may be employed in greenhouses to conserve energy and reduce the cost of agricultural output[10].

Discussion

The solar panel system produces low-cost renewable energy and is appropriate for long-distance agricultural operations such as irrigation water pumping. In contrast, the functioning of a solar panel technology system necessitates adequate energy, a solar panel, a pump controller, a motor pump, water sources, and a water tank. The solar panel is made up of several silicon cells or solar cells. The solar cell is the smallest component of the panel. Solar cells gather energy when the sun shines on the solar sheet. Solar energy is converted to direct current (DC) by semiconductors, then to alternating current (AC) by the alternator in the pump regulator and supplied to the water pump, which drains and stores water from the water resource.

A. Factors affecting performance of Solar Power

Several variables impact solar panel production efficiency, including:
1. Load Resistance

The voltage at which the panel can work is determined. Because the panel's performance is governed by the load's strength, a control system that monitors the maximum power point must guarantee that the load's voltage and current operating needs are matched.
2. Cell Temperature

The panel operates less effectively and the voltage declines when the cell temperature increases over the standard production temperature of 25 ° C. As a result, heat may be seen as a response to electron mobility. A panel at 80-90 C loses 0.5 percent of its efficiency for every degree increase in temperature. As a result, airflow above and beneath the panel is essential for the mounting scheme's design to dissipate heat.

PV panel shadowing frequently resulted in a considerable drop in output. Factors like as sun irradiance and cell temperature impact the ability of a solar panel device. In addition to these, additional contributing elements such as the durability of other components and other environmental circumstances impact its efficiency. The term "local ecosystem" refers to the environment that has been modified by human activity, such as the urban environment, plant varieties, and weather patterns. All of these variables will have a technical influence on the efficiency of the solar panel, resulting in a 2-50 percent decline in power production in various places.

Conclusion

This study proposes that solar energy might provide a long-term solution to many of the world's present problems, such as climate change, energy shortages, atmospheric conservation, and drought. According to the literature, farmers in the United States, the European Union, and Asian countries are in the forefront of adopting solar energy. Despite the fact that this technology has various benefits, as proven in this article,

most African farmers are less receptive of solar systems for agriculture. The African continent benefits from increased solar radiation as well, since it contains 60% of the world's fertile land. Solar energy is appropriate for agricultural applications such as electrical shielding, threshing, aerating, grinding, drainage, and purifying.

Despite this, farmers feel that the initial cost of solar water pump systems is more than that of a diesel water recirculating pump, but neither method takes production or maintenance costs into account. One of the most important characteristics is the PV collection of solar water pump systems, which may be used to create electricity if irrigation is not necessary. Solar water pumping equipment can effectively satisfy the irrigation water demands of marginal farmers in the landholding system. Pump sets are constructed every year in India as a result of rising fuel costs. The solar water pump technology allows for more efficient usage, lowering fuel consumption. It contends that the periodicity of the energy market and thermal power plants imposes specific costs on society and the environment. Based on the foregoing, we believe that solar pumping is a more viable option for watering India's crops than diesel engine pumping. Solar water pumps are not more expensive economically if solar energy is used continually, but their capital costs are significant.

References

[1] Jacobson MZ, Delucchi MA, Bauer ZAF, Goodman SC, Chapman WE, Cameron MA, et al. 100% Clean and Renewable Wind, Water, and Sunlight All-Sector Energy Roadmaps for 139 Countries of the World. Joule. 2017;

[2] Pirasteh G, Saidur R, Rahman SMA, Rahim NA. A review on development of solar drying applications. Renewable and Sustainable Energy Reviews. 2014.

[3] Escobar-Ochoa M, Cuervo-Andrade S, Rincon-Prat S. Methodology for the design of a thermal energy storage module for asolar tunnel dryer using phase change materials (PCM). Rev UIS inn. 2018;

[4] Husain MI, Lee GH. Utilization of Solar Energy in Agricultural Machinery Engineering: A Review. J Biosyst Eng. 2015;

[5] Chow TT, Tiwari GN, Menezo C. Hybrid solar: A review on photovoltaic and thermal power integration. International Journal of Photo energy. 2012.

[6] Xu Y, Li J, Tan Q, Peters AL, Yang C. Global status of recycling waste solar panels: A review. Waste Management. 2018.

[7] Qoaider L, Steinbrecht D. Photovoltaic systems: A cost competitive option to supply energy to off-grid agricultural communities in arid regions. Apply Energy. 2010;

[8] Bardi U, El Asmar T, Lavacchi A. Turning electricity into food: The role of renewable energy in the future of agriculture. J Clean Prod. 2013;

[9] Dupraz C, Marrou H, Talbot G, Dufour L, Nogier A, Ferard Y. Combining solar photovoltaic panels and food crops for optimising land use: Towards new agrivoltaic schemes. Renew Energy. 2011;

[10] Maher A, Kamel E, Enrico F, Atif I, Abdelkader M. An intelligent system for the climate control and energy savings in agricultural greenhouses.Energy Effect. 2016;

Chapter 26

Review of the growth prospects for renewable energy in several countries

Susmita Dhar Mukherjee*, Rituparna Mukherjee, Suvraujjal Dutta
Department of Electrical Engineering, Swami Vivekananda University, Barrackpore, West Bengal
Corresponding Author Email: susmitadm@svu.ac.in

Abstract

The use of renewable energy is now crucial to addressing environmental issues. The advancement in this area has the potential to increase energy efficiency and lessen the greenhouse effect. This essay highlights the state of renewable energy development in several nations. Analysis has been done of the rising renewable energy development trend. The energy market must be changed, and the rationality of policymaking must be maintained, in order to support the development of renewable energy sources. The energy industry benefits from a good educational system and awareness of renewable energy in the event of development. This study revealed that a significant amount of research is being done on renewable energy. This essay has informed readers about numerous uses for renewable energy as well as how those uses have changed across different countries.

Keywords: Renewable Energy, Solar energy, Wind energy, Hydro energy, coal energy, nuclear energy, natural gas, geothermal energy, Biomass energy, international development.

Introduction

Energy efficiency improvements and greenhouse gas reduction are challenging tasks in the modern world [1, 2]. The best alternative solution to this issue is renewable energy. Additionally, it significantly contributes to raising employment levels across nations and enhancing environmental preservation. For the creation of the next generation of energy technologies, many nations used renewable energy [3, 4]. Experience in low-carbon development is crucial as national policies develop and renewable energy technologies enter their middle age. [5]. Numerous studies have examined how renewable energy is developing. Pazheri et al. [6] assessed the state of renewable energy and discussed the most recent developments in bringing down the price of renewable energy. [7]. The development of renewable energy was explored by Zhang et al. [8] together with China's energy structure. Increases in the capacity of renewable energy sources and the proportion of electricity used for energy consumption are both required to reduce carbon emissions. Wang et al. predicted China's condition of sustainable energy development and examined energy-saving policies [9]. Even though several studies on various forms of renewable energy have already been conducted, there are very few systematic comparisons and analyses of these studies in the literature. Furthermore, they could contain partial statistics or missing data; as a result, it's important to undertake a thorough and systematic examination of global renewable energy using study findings made public by reputable institutes.

Development state of renewable energy:

According to statistics, even though the amount of primary energy consumed globally has decreased yearly, throughout the last two years the pace of global energy consumption has been steadily increasing. Similar to this, the growth in fossil fuel usage over the last ten years has only totaled 16.90% [10,15]. Coal consumption is continuing to decline at a lower rate. Comparing the data from 2017, for instance, we can

see that the growth rate was only responsible for around one-third of the increase in primary energy useThe total amount of nuclear energy used worldwide has been steadily declining due to safety concerns. When compared to the level from ten years ago, nuclear power usage has been steadily declining for two years [11]. On the other hand, the use of natural gas is also growing quickly during the past three years and will reach its peak in ten years. Other renewable energy sources had growth at a rate of up to 16.64%, or approximately. The consumption of fossil energy is growing at a rate that is 11 times faster than average [12]. Various renewable energy sources, including wind, solar, biomass, geothermal, hydrogen energy, and other sources, have different development structures depending on the country. There is still a lot of space for development in China's renewable energy [13].

Renewable Energy Evolution in European Union

In the European Union, the energy revolution began much earlier. The biggest carbon emissions trading scheme in the world was originally introduced in 2003, and it also produced impressive results. They have policies and goals for short-, medium-, and long-term development as well as support mechanisms and sustainability requirements. EU Leads the World in Energy Structural Transformation. They consume 2.5 times as much coal, nuclear, and non-hydro renewable energy than the typical country worldwide [13]. In 2030, renewable energy generation in the EU is predicted to increase by 50% compared to the current scenario, according to various reports [14,15]. Electricity demand has increased along with energy efficiency. The EU will likely need to make additional efforts to meet its renewable energy objective, according to the current scenario [16].

Renewable Energy Evolution in US, Australia, and Brazil

Australia now ranks tenth in the world in terms of energy production, and it is one of the three OECD countries that export energy on a net basis. However, the overall energy structure is still being developed, and the share of renewable energy is rather marginal [20]. Brazil is a global leader in the usage of renewable energy. Brazil was the first nation to use biomass fuels, and it is also the greatest producer and consumer of this fue Energy usage ongoing expansion and an increase in the proportion of renewable energy. Brazil, which ranks seventh in the world for installed capacity, has significant wind energy potential. Brazil, which became a pioneer in liquid biofuels, was likewise committed to creating alternative fuels [15]. The United States becomes the world's leading producer and exporter of wood pellets and biomass power in this situation. The state of renewable energy development is favourable. According to the EIA research, industry will consume much more energy and electricity, and correspondingly, the rate at which renewable energy is consumed will also continue to rise [15].

C. **Renewable Energy Evolution in India**

The second-most populous nation in the world is India. Here, there is a clear imbalance between the supply and demand of energy, and there is also a high need for renewable energy. India experiences energy shortages, external energy reliance, and energy security challenges, all of which are progressively becoming more important as a result of economic expansion and energy consumption. Since the demand for renewable energy is always rising, the supply must also rise in line with this trend. While coal has long been above 50% of India's energy mix, fossil fuels continue to hold the absolute top spot. Compared to the corresponding consumption rate, less coal, oil, and natural gas have been produced. It is necessary to preserve India's rapid development as a result of renewable energy Renewable energy is developing quickly and has a lot of potential. India is the seventh-largest hydropower producer, with a big hydropower installed capacity of 45.29 GW in 2017 [17–19], according to the sources. India has abundant biomass resources thanks to its favorable geography. The research states that in 2017, 8.4 GW of electricity were

produced by biomass generating, gasification, and combined heat and powerIn India, however, there is not enough of a spread of renewable energy. On the other hand, given the quick rise in global energy consumption, renewable energy production needs to be bolstered in comparison to traditional energy, which is still growing significantly [20]. In 2050, India will produce 75% of its energy from renewable sources, according to a prediction by Bloomberg New Energy Finance (BNEF)

References

[1] S. Keles , S. Bilgen , Renewableenergysources inTurkeyforclimatechange mitiga- tion and energy sustainability, Renew Sustain EnergyRev 16 (2012) 5199–5206 .

[2] K. Kaygusuz , Energy for sustainable development: a case ofdevelopingcountries,RenewSustainEnergyRev16(2012)1116–1126.

[3] S.Sen,S.Ganguly,Opportunities,barriersandissueswithrenewableenergy devel- opment-A discussion, Renewable and SustainableEnergy Reviews 69 (2017 Mar 1) 1170–1181.

[4] E. Martinot , C. Dienst , L. Weiliang , C Qimin , Renewable energyfutures: tar- gets,scenarios, and pathways, Annu Rev Environ Resour32 (1) (2007) 205–239 .

[5] Y. He , Y. Xu , Y. Pang , H. Tian , R Wu , A regulatory policy topromote renewable energy consumption in China: review and futureevolutionary path, Renew Energy 89 (2016 Apr 1) 695–705 .

[6] S. Kankam , E. Boon , Energy delivery and utilization for ruraldevelopment:lessonsfromNorthernGhana,EnergySustainDev13(3)(2009) 212–218.

[7] E. Nfah , J. Ngundam , R Tchinda , Modelling of solar/diesel/batteryhybrid power systems for far-north Cameroon, Renew Energy 32 (5)(2007) 832–844 .

[8] D. Dizdaroglu , The role of indicator-based sustainability assessmentin policy and the decision-making process: a review and outlook,Sustainability 9 (6) (2017 Jun) 1018 .

[9] F.R. Pazheri , M.F. Othman , N.H Malik , A review on globalrenewable electricity scenario, Renew Sustain Energy Rev 31 (2014)835–845 .

[10] D. Zhang , J. Wang , Y. Lin , Y. Si , C. Huang , J. Yang , B. Huang ,W Li , Present situation and future prospect of renewable energy inChina, Renew Sustain Energy Rev 76 (2017) 865–871 .

[11] J.Wang,L.Li,Sustainableenergydevelopmentscenarioforecastingand energy sav- ing policy analysis of China, Renew Sustain EnergyRev 58 (2016) 718–724 .

[12] B. Hillring , National strategies for stimulating the use of bio-energy:policy instru- ments in Sweden, Biomass Bioenergy 14 (1988) 45e .

[13] Davis A. Graham , Brandon Owens , Optimizing the level ofrenewable electric R&D expenditures: using real options analysis,Energy Policy 31 (2003) 1589 .

[14] Martine A. Uyterlinde , Martin Junginger , Hage J. de Vries , et al. ,Implications of technological learning on the prospects for renewableenergy technologies in Europe, Energy Policy 35 (2007) 4072e4087 .

[15] BP, Statistical Review of World Energy –all data 1965-2019,December 2020, https://www.bp.com/ .

[16] Eurostat, online database, Energy intensity (nrg_ind_ei), May 23,2019, https://ec.europa.eu/eurostat/data/database .

[17] Eurostat, Greenhouse gas emissions intensity of energy consumption(SDG_13_20), June 12, 2019, https://ec.europa.eu/eurostat/data/database.

[18] Eurostat, Greenhouse gas emissions, base year 1990 (t2020_30), June12, 2019, https://ec.europa.eu/eurostat/data/database .

[19] Agora-Energiewende,DataAttachment-TheEuropeanPowerSec-torin 2017, January 30, 2018, https://www.agora-energiewende.de/en/publications/data-attachment-the-european-power-sectorin-2017/

Chapter 27

A Comparative Review of the Use, Difficulties, and Future of Renewable Energy

Susmita Dhar Mukherjee* , Rituparna Mukherjee, Rituparna Mitra
Department of Electrical Engineering, Swami Vivekananda University Barrackpore, West Bengal
Corresponding Author Email: susmitadm@svu.ac.in

Abstract

The population rise has led to a substantial increase in energy demand. Aside from this, increased energy use is required for economic and technological advancement. However, the world's precious energies are finite. Additionally, it is crucial to increase the usage of traditional energy sources because they produce significant amounts of greenhouse gases that harm the planet's ecology. However, our civilization cannot really advance without energy. So, in order to rescue the earth, we must choose some other energy sources. That sustainable and renewable sources of energy should be used. A variety of renewable energy sources can be found around the world in various regions. The key benefits of renewable energy are its minimal impact on the ecology, its ability to be produced even in inclement weather, and its overall effectiveness as a weapon against environmental pollution. It significantly affects economic expansion, employment development, and energy security. However, there are certain issues with the storage of renewable energy. Scientists and investors are working nonstop to find a solution. The installation of a renewable energy system might occasionally be complicated by public opposition. Opportunities for employment and some facilities lessen opposition to the use of clean energy. The public's knowledge of renewable energy and its benefits aids policymakers in their decision-making. An extensive experiment on sustainable energy is currently underway, according to a study of review publications on the subject. This work has produced a concept regarding various applications of renewable energy, their application challenges, and their resolution. Additionally, it has been noted that in the coming years, the use of renewable energy will increase dramatically due to improved technology and storage arrangements, growing government initiatives to minimize carbon emissions for economic growth, and other factors.

Keywords: Renewable Energy, Solar energy, Wind energy, Hydro energy, Tidal energy, Geothermal energy, Biomass energy, Utilization, Future Prospect.

Introduction

In the past several years, there has been a substantial change in the world economy. Because to industrialization, there is a daily rise in energy demand. Fossil fuels continue to be the world's primary energy source, yet they are a finite resource. The fact that fossil fuels will run out in a few years poses a threat to mankind. In addition to this, there are numerous other ways that the usage of traditional energy sources pollutes the environment. We must find an alternative energy source to prevent these issues. We can consider sustainable energy at this point. The sustainable energies are eco- friendly and economic. The proper use of renewable energy may undoubtedly replace the use of conventional source of energy. Environmental pollution can be easily controlled by the use of sustainable energy. We can obtain and use this renewable energy almost anywhere in the world and throughout the year without endangering the environment. [1]. It is possible to find endless amounts of unconventional energies in this globe. Utilizing sustainable energy contributes to a reduction in the amount of carbon in the atmosphere. In the future, it lessens the worry about an energy catastrophe. Utilizing renewable energy sources can promote economic development and advance the green revolution [2].Some nations today are battling a lack of energy supplies.

Some nations in Asia and Africa are also experiencing economic lags as a result of the energy crisis. This is the cause of the widespread loss of a decent level of living. These issues can be resolved by making significant use of renewable energy. While some developing nations are lucky to have non-conventional energy resources, their usage processes still need to be improved. If they are successful in utilizing their renewable energy resources, their entire economic, lifestyle, and power-generation scenario will alter [3]. Significant eco-system indicators include the greenhouse effect and weather changes. Because of this, various nations are working to create new technologies that utilize renewable energy sources and have also made the decision to lessen carbon emissions into the atmosphere. Their initiative to develop novel technology in the area of unconventional energy is a sign of the use of sustainable energy. [4]. Reduced atmospheric carbon emissions are necessary to protect our planet from the greenhouse effect. We need to stop using traditional energy sources in order to create an eco-friendly environment. We must make use of renewable energy sources. This will contribute to a better environment. Long-term energy needs will also be met with the aid of sustainable energy. [5]. In order to use energy effectively and achieve feasible evolution, alternative sources of energy are crucial. Mankind has a challenge to reduce the carbon discharge in the atmosphere. But in spite of this challenge the world economy is still depending on conventional energy resources. Increasing requirement of natural gas is an indication of less green house gas out flow and it is also a symbol of non-conventional energy utilization[6]. One of the most important factors in the development of renewable energy is financing for sustainable energy. Investors are drawn to funding for renewable energy sources. Investors are also considering their responsibilities in relation to this kind of investing. Regarding this, they are considering concerns pertaining to politics, society, technology, the economy, and the environment [7]. Competent authorities are working to implement new strategies for the use of renewable energy in an effort to stop climate change. Along with creating new automation, this project also improves employment opportunities. Making use of unconventional energy also helps humanity save money [8].The general public is crucial to the development of renewable energy. They respond to renewable energy in different ways. Researchers and decision-makers keep tabs on how the public feels about renewable energy. Their acceptance of unconventional energy enables the responsible authority to select a strategy for utilizing various energy sources. [9].Natural treasures that are found almost everywhere and all year round are unconventional energies. These energy resources are easily usable thanks to various mechanisms. Our ecosystem is not negatively impacted. The answer to the coming energy dilemma is renewable energy sources. These renewable energies are accessible to us with just one investment. We must accept these energies on a global scale if we want a secure environment. Solar, wind, hydropower, tidal, geothermal, and biomass energy are the most efficient renewable energy sources. [1,2,3].

Solar Energy

The most widely used source of reliable, safe, and secure power is solar energy. A small portion of this enormous source is what we are using. Both active and passive solar energy can be classified as solar energy. [10, 11]. J. Li and J. Huang[12]It has been found that solar energy is a somewhat superior choice for sustainable energy. It is a crucial energy source for creating a greener planet. They observed that there are several barriers to using solar energy as a replacement for conventional energy. To address these issues, the policymaker needs to take some action. O.A. Al-Shahri, F.B. Ismail, M.A. Hannan, and other authors.[13] observed that using sustainable energy helps to lower power supply costs and greenhouse effect. They discovered that the key challenge to enhancing energy preservation performance is the improvement of many functional factors of solar energy. They used a variety of improvement strategies to increase the deployment of solar energy's effectiveness. Solar energy was described by J. Zhang et al. [14] as a solution to the world's future energy needs. Unused solar energy can be successfully transformed into electrical energy. Numerous semiconductors have developed over time and are crucial for the use of solar energy. Due to its excellent optical or electrical properties and suitable band distance, Cadmium Sulfide (CdS) is most effective in this context. According to J.S. Roy et al. [15], the proper use of solar energy in accordance

with general need is a crucial issue. They designed an extremely concentrated solar energy delivery system (ECoSEnDS) to use for day illumination and waste water cooling. The aforementioned gadget can be used to treat wastewater using solar energy in addition to providing day lighting with the aid of suitable semiconductor micro photo catalysts.With the aid of a finned solar collector filled with paraffin, Bo Xu et al [16] investigated solar collectors with energy storage. They discovered that as air movement increases, heat absorption efficiency does as well. In their observations, they noted the average paraffin temperature, the temperature of the exit air, and the efficiency of heat absorption with various types of air circulation.. They also observed that under unfavorable conditions, the efficiency of heat absorbing drops and energy collection duration increases.They came to the conclusion that a solar collector and energy storage enable to fully utilize solar energy, which is good for the environment. According to Laibao Liu et al. [17], as the solar/wind adequacy factor increases, so does the purchasing power of a single source of energy. The differences between a hybrid wind/solar system and a single wind/solar system are smaller for large areas. They advised local cooperation since it lowers production costs, lessens solar/wind energy generation fluctuations, and improves the system as a whole. Malik, S.A., and Ayop, A.R.[18] noted that a key factor in a society's willingness to accept new technologies is the level of education available to its citizens. They suggested that a project for the disadvantaged community to generate their own solar electricity might be useful to defend their predicament.Because their economic situation and educational level are crucial for the adoption of solar PV technology, policymakers find it easier to establish such projects among the less educated people. They also came to the conclusion that appropriate education and understanding of new technology are crucial for economic development. According to Tervo et al. [19], an appropriate storage system is required for the continuous supply of sustainable energy..In this regard, thermal storage is a better means of sustaining solar power. They suggested a solid-state heat engine replacement for solar-thermal conversion made up of a photovoltaic cell, thermal radiation cell, and solar absorber. They discovered a limited solar restoration effectiveness of 45% for one sun with absorber and single-junction cells in the same region and 85% for solely intense sunlight.

Wind Energy

Another sustainable energy source is wind energy. The key perk of this energy use is that it continues to function in inclement weather. The placements of the wind turbines are particularly important to achieve maximum efficiency since they improve the system's efficiency. The recommended altitude for wind turbines is roughly 30 meters, and this is where they are typically installed In relation to the blade diameter, the wind turbines are spaced 5–15 times apart. A windmill with a horizontal axis and one with a vertical axis performs equally well. Air flow is a crucial factor in how well a windmill performs. It performs ineffectively when the air flow is less than 13 km/h and performs optimally when the air flow is around 22 km/h. Three-bladed horizontal axis windmills with a power output capacity of 50 to 350 kW have become more common recently. The global green movement has a weapon in this energy producing system, and it also offers a solution to the coming energy crisis. [1].Wind energy is a sustainable and pollution-free source of energy, according to Hui Liu et al. [20]. A lot of work has been done recently to maximize the use of wind energy. They discussed many upgrade techniques to improve prediction efficiencies in various ways. According to Sneh Deep et al. [21], of all non-conventional energy sources, wind energy has grown to be the most prosperous sustainable energy supply. When calculating wind energy using data from wind flow statistics, they discovered that the actual wind energy is overestimated. Depending on where it located geographically, this error varies. They indicated that two variables needed to be accurately estimated in order to determine wind power using the two parameter Weibull model. The accessibility option can be determined using this way. To determine the available wind power, they also suggested using the Weibull model with three parameters. Sustainable energy sources have been found to be crucial for a nation's development, according to P. Borawski et al. [22]. They used a variety of academic articles and statistical data to track the development of wind energy in the EU. They discovered the maximum average wind

speed. Accordingly, Germany, Spain, the United Kingdom, and France all used energy. They were also aware of this development in nearly all of the EU's member states. The use of wind energy has increased significantly during the past few years, according to Y. Gao et al. [23] who evaluated China's wind energy future. They saw that the Qinghai Tibet Plateau, Hexi Corridor, and Eastern Inner Mongolia all have access to favorable and acceptable wind energy. Utilizing this energy is a simple way to substitute using traditional energy sources. A reliable mechanism for preserving the collected energy is needed in order to use this enormous amount of energy. It also requires a considerable upfront investment for large-scale storage arrangements. For the next generation's preservation of wind energy, they indicated that battery energy storage stations would be a preferable alternative. They came to the conclusion that this recommendation might be used everywhere. According to D.L. Bessette and S.B. Mills [24], wind energy is the primary sustainable energy substitute in the US at the moment. The future of wind energy depends on enough resources, electricity supply methods, and public awareness. The use of wind energy helps to strengthen the economy and provides a solution to any potential energy crises. To educate the public about wind energy is a significant problem for scientists and policymakers. The public's perception of wind energy influences where to put new wind turbines. They found that installing production-related equipment, expanding employment opportunities, and providing some community facilities lessen community opposition to the use of wind energy. They suggested that this policy would be useful to the decision-maker for the installation of a wind turbine.

Tidal Energy

Our planet's surface is covered in water to a significant extent. This enormous body of water serves as a sustainable energy source. India has thousands of kilometers of coastline as a result of its location. The water stream offers many chances for use. The water stream can be converted into electrical power. The energy solidity at a suitable location by the sea is roughly 65 MV/mile. This energy can be partially transformed into wave-driven electrical energy. During a natural disaster, there are various challenges with collecting or using tidal energy.[1].Some European nations are making an effort to increase their use of renewable energy sources, according to N. Isaksson et al. [29]. One of these is tidal energy. Tidal energy equipment has a negative impact on marine wildlife despite its significance in the green energy revolution. The author offered several suggested methods for calculating the effects of tidal energy devices on seabirds. According to C.J. Mejia-Olivares et al. [30], the entire region of Latin America is beginning to understand the significance of the green energy revolution. The enormous tidal energy is unknown to the nations of Latin America. An enormous tidal range is present in Mexico, to the north of the Gulf of California. Because of this, it might be a good place to use tidal energy. They conduct their experiment by using tide level forecasts from a depth-averaged bar tropic hydrodynamic model. In addition, they used a 0-D function modeling to determine the power that might be produced from a particular area. Their research demonstrates that the range of annual power production is 20 to 50 kWh/m2. H.-B. Goh, et al. [31] discovered that the cape is a crucial location for capturing tidal energy. In their experiment, they used the numerical model for Tg Tuan Cape. Evaluation of tidal power utilization's potential and effects was done close to the cape. The results of the experiment showed that the pointy portion of the cape would be a good location for tidal energy production. They found an inverse link between velocity changes and depth after making more observations about the effects of depth and stream velocity on eight different variables. The competent authorities should benefit from their observations when choosing a location to harness tidal energy.

Geothermal Energy

Geothermal energy is the name for the heat energy that our earth has stored. This energy is usable as renewable energy and is free of pollution. Magma, scorching rock on the surface, and heated water or

streams are the sources of this heat energy. This heat can be used by using a heat pump. Homes can be heated or cooled using geothermal energy. [1,32].Y. Wang et al. [33] clarified that geothermal energy is unquestionably reliable for the production of renewable energy. The green world benefits from it. It is abundantly present in nature and requires a minimal installation fee. Geothermal energy is abundant in China. By using this energy, they can balance the demand for natural energy in eastern and western China. China has just started to gradually deploy geo thermal energy. The writers focused on the current state of geothermal energy use in China while taking into account all the challenges related to economic, political, technical, and the environment. They made several recommendations for the development of geothermal energy in China. Geothermal energy is becoming more and more popular, which may influence China's future development. S. Di Fraia, et al. [34] identified a number of issues with the Island's use of conventional energy for waste water treatment. It costs more, and the system encounters several challenges. They recommended a geothermal energy system for energy production, sludge management, and waste water treatment because of this. Utilizing the Engineering Equation Solver environment, an exergoeconomic analysis is used to analyze this design. The results of the reactivity test show that the heat from geothermal resources has a significant impact on how well the system works and how much it costs to operate. To cut down on exergoeconomic costs, they also offered other improvement techniques. The overall hourly exergoeconomic cost of the system products drops to its lowest level when the temperature of the geothermal resource reaches roughly 110 °C and 58.91% of the drying agent flow is recycled. According to Taghizadeh- Hesary et al. [35], Japan's power consumption has altered significantly since the Fukushima nuclear accident. In an effort to increase the usage of renewable energy, they turned back to conventional energy. The writers looked into Japan's lack of attention to geothermal energy. They looked at the problems from a social, legal, financial, economic, and technical standpoint. Data from 1974 to 2017 were used in the analysis, which was done using a Vector Error Correction Model (VECM). The results show that there is still a relationship between the parameters, public opinion, installation costs, and levy plans. In terms of producing geothermal energy, the last one is more crucial. In this situation, a grant may prompt a range of responses. The opposition to geothermal energy was also mentioned, along with ecological issues and public outcry.

Biomass Energy

Energy derived from living things is called biomass. A society's future can be altered through the wise use of biomass energy. There is a vast supply of biomass naturally available in India. Biodegradable garbage can be used to generate this energy. The term "biomass energy" refers to combustibles made from plant and animal waste. A portion of the biomass is organic. In biomass, the solar energy has been chemically conserved. During chemical reactions, this energy is released. [1[36] Z. Wang et al. noted that there is disagreement over the impact of biomass application. Few investigations focused on the outcome of using biomass for energy. Some event had a negative impact.. The authors looked into the benefits of biomass energy spending in the BRICS nations between 1990 and 2015. They can assess the challenges posed by cross-sectional dependence and slope heterogeneity by using economic methodology.

Conclusion

The earth's traditional energy resources are depleting quickly. As a result, fossil fuel must be replaced. We should utilize less conventional energy in order to preserve the planet for future generations. The best options to a potential energy crisis are renewable energies. Utilizing sustainable energy in the right ways is a step toward a worldwide green revolution. The availability of renewable energy is abundant around the planet. The challenges of implementing sustainable energy are continuously being addressed by scientists, academics, and decision-makers. The need for new methods to use renewable energy is a challenge to technologists. In addition to this, a key factor in the use of unconventional energy is the general public's awareness of renewable energy. The various applications of renewable energy and their application challenges have been established in this study. According to this study, the use of renewable energy will increase dramatically over the next few years due to increased government policies restricting carbon

emissions for economic growth and proper storage arrangements.

References

[1] Alrikabi,N.K.M.A."Renewableenergytypes."JournalofCleanEnergyTechnologies 2, no. 1 (2014): 61-64.

[2] M.Boulakhbara,B.Lebrouhib,T. Kousksou,S. Smouhd,A. Jamild,M.Maaroufib, M. Zazia, Journal of Energy Storage 32 (2020) 101806.

[3] A. Daniel, D. Jianguo, R. O. Darko, K. B. Boamah, and A. Emmanuel."Investigatingthestateofrenewableenergyandconceptofpumpasturbinefor energy generation development." Energy Reports 6 (2020): 60-66.

[4] C. Yuanyuan, and X. Yao. "Carbon intensity reduction assessment ofrenewableenergytechnologyinnovationinChina:Apaneldata modelwithcross-section dependence and slope heterogeneity." Renewable andSustainable Energy Reviews 135 (2021): 110157.

[5] Abdelmigeed,MaiO.,EslamG.Al-Sakkari,MahmoudS.Hefney,Fatma M. Ismail, Amr Abdelghany, Tamer S. Ahmed, and Ibrahim M. Ismail."Magnetized ZIF-8 impregnated withsodiumhydroxideasaheterogeneouscatalyst for high-quality biodiesel production." Renewable Energy 165(2021):405-419..

[6] N. Sarah, and K. Matsumoto. "Does renewable energy substitute LNGinternational trade in the energy transition?." Energy Economics 92 (2020):104964.

[7] H. Ali, Y. Ju, S. M. H. Bamakan, and H. P. Le. "Renewable energyinvestment risk assessment in belt and road initiative countries underuncertainty conditions." Energy 214 (2021): 118923.

[8] D. Joris, K. Schumacher, and W. Fichtner. "Topic Modeling UncoversShifts in Media Framing of the German Renewable Energy Act." Patterns(2020):100169.https://doi.org/10.1016/j.patter.2020.100169.

[9] O. Sydney, P. Lal, A. Susaeta, and N. Vedwan. "Assessment of publicawareness, acceptance and attitudes towards renewable energy in Kenya."Scientific African 9 (2020): e00512.

[10] Ashokverghese,"NewandRenewableEnergyResources,"ProceedingsofInternationalconferenceonAlternateEnergyresources,AsianInstituteofTechnology, Thailand, pp. 403 –410,1998.

[11] Cline, William R. The economics of global warming. Institute forInternational Economics, 1992, pp. 45-55,.

[12] J. Li and J. Huang, Renewable and Sustainable Energy Reviews 132(2020)110002.

[13] A.Omar,A.F.B.Ismail,M.A.Hannan,M.S.HossainLipu,AliQ.Al-Shetwi, R.A. Begum, Nizar F.O. Al-Muhsen, Ebrahim Soujeri, Journal ofCleaner Production 284 (2021) 125465.

[14] J. Zhang, X. Yuana, M. Si, L. Jianga, H. Yu, Advances in Colloid andInterface Science 282 (2020) 102209.

[15] R.J.Sankar,S.Morency,G.Dugas,andY.Messaddeq."Developmentof an extremely concentrated solar energy delivery system using silicaoptical fiber bundle for deployment of solar energy: Daylighting tophotocatalytic wastewater treatment." Solar Energy 214 (2021): 93-100

[16] "Optimizingwind/solarcombinationsatfinerscalesto mitigate renewable energy variability in China." Renewable andSustainable Energy Reviews 132 (2020): 110151.Syed A., and A. R. Ayop. "Solar energy technology: Knowledge,awareness, and acceptance of B40 households in one district of Malaysiatowards governmentinitiatives." Technologyin Society63(2020):101416.

[17] Tervo,EricJ.,WilliamA.Callahan,EricS.Toberer,Myles A.Steiner,and Andrew J. Ferguson. "Solar Thermoradiative-Photovoltaic EnergyConversion." Cell Reports Physical Science 1, no. 12 (2020): 100258.https://doi.org/10.1016/j.xcrp.2020.100258.

[18] L.Hui, Y. Li, Z. Duan, and C. Chen. "A review on multi-objectiveoptimization framework in wind energy forecasting techniques andapplications." Energy Conversion and Management 224 (2020): 113324.

[19] S. Deep, A. Sarkar, M. Ghawat, M. K. Rajak, Renewable Energy 161(2020)319e339.
[20] B. Piotr, A. Bełdycka-Bórawska, KJ. Jankowski, B. Dubis, and J. W.Dunn. "Development of wind energy market in the European Union."Renewable Energy 161 (2020): 691-700.
[21] G.Yang, S. Ma, T. Wang, T. Wang, Y. Gong, F. Peng, and A.Tsunekawa."Assessingthewindenergypotentialof Chinainconsideringitsvariability/intermittency."EnergyConversionandManagement226(2020):113580.
[22] Bessette, Douglas L., and Sarah B. Mills. "Farmers vs. lakers:Agriculture, amenity, and community in predicting opposition to UnitedStates wind energy development."Energy Research & Social Science 72:101873.
[23] J. Jakub, A. Kies, and P. Zajac. "Synergetic operation of photovoltaicand hydro power stations on a day-ahead energy market." Energy 212(2020):118686.
[24] I.Youssef,M.R.Soliman,andM.Kahil."Recoveringenergybyhydro-turbines application in water transmission pipelines: A case study west ofSaudi Arabia." Energy 211 (2020): 118613.
[25] C. Hao, H. Wang, R. Li, Y. Zhang, and X. He. "Thermo-dynamic andeconomicanalysisofsanovelnear-isothermalpumpedhydrocompressedairenergy storage system." Journal of Energy Storage 30 (2020): 101487.
[26] C.Cheng,A.Blakers,M.Stocks,B.Lu,GlobalEnergyInterconnection,Volume 2 Number 5 October 2019. (386 -392).
[27] I. Natalie, Elizabeth A. Masden, Benjamin J. Williamson, Melissa M.Costagliola-Ray,J.Slingsby,J.DRHoughton,andJ.Wilson."Assessingtheeffects of tidal stream marine renewable energy on seabirds: A conceptualframework." Marine Pollution Bulletin 157 (2020): 111314.
[28] C. J. M.O., Ivan D. Haigh , A. Angeloudis , Matt J. Lewis, Simon P.Neill, Renewable Energy 155 (2020) 469- 483.
[29] G.Hooi-Bein,SH.Lai,M.Jameel,HMTeh,andRJ.Chin."Feasibilityassessment of tidal energy extraction at the Tg Tuan coastal headland: Anumerical simulation study." Sustainable Energy Technologies andAssessments 38 (2020): 100633.
[30] Narjes, F. Balali, A. Nasiri, H. Seifoddini, and W. Otieno. "Waterwithdrawal and consumption reduction for electrical energy generationsystems." Applied Energy 248 (2019): 196-206.
[31] Yuqing,Y.Liu,J.Dou,M.Li,andM.Zeng."GeothermalenergyinChina:Status,challenges, andpolicyrecommendations."Utilities Policy64(2020):101020.
[32] F.Simona,A.Macaluso,N.Massarotti,andL.Vanoli."Geothermalenergyfor wastewater and sludgetreatment: An exergoeconomicanalysis."Energy Conversion and Management 224 (2020): 113180.
[33] Farhad, A. Mortha, H. F.Asl, T. Sarker, A. Chapman, Y.Shigetomi, and T. Fraser. "Role of energy finance in geothermal powerdevelopment in Japan." International Review of Economics & Finance 70(2020):398-412.
[34] Zhaohua,Q.Bui,andB.Zhang."Therelationshipbetweenbiomassenergy consumption and human development: Empirical evidence fromBRICS countries." Energy 194 (2020): 116906.
[35] Farhad, A. Mortha, H. F.Asl, T. Sarker, A. Chapman, Y.Shigetomi, and T. Fraser. "Role of energy finance in geothermal powerdevelopment in Japan." International Review of Economics & Finance 70(2020):398-412.
[36] "Therelationshipbetweenbiomassenergy consumption and human development: Empirical evidence fromBRICS countries." Energy 194 (2020): 116906.